



*A National Center of Excellence in Advanced Technology Applications*

ISSN 1520-295X

---

# Seismic Fragility of Suspended Ceiling Systems

by

Hiram Badillo-Almaraz, Andrew S. Whittaker,  
Andrei M. Reinhorn and Gian Paolo Cimellaro

University at Buffalo, State University of New York  
Department of Civil, Structural and Environmental Engineering  
Ketter Hall  
Buffalo, New York 14260

Technical Report MCEER-06-0001

February 4, 2006

This research was conducted at the University at Buffalo, State University of New York and was supported primarily by the Earthquake Engineering Research Centers Program of the National Science Foundation under award number EEC-9701471.

## NOTICE

This report was prepared by the University at Buffalo, State University of New York as a result of research sponsored by the Multidisciplinary Center for Earthquake Engineering Research (MCEER) through a grant from the Earthquake Engineering Research Centers Program of the National Science Foundation under NSF award number EEC-9701471 and other sponsors. Neither MCEER, associates of MCEER, its sponsors, the University at Buffalo, State University of New York, nor any person acting on their behalf:

- a. makes any warranty, express or implied, with respect to the use of any information, apparatus, method, or process disclosed in this report or that such use may not infringe upon privately owned rights; or
- b. assumes any liabilities of whatsoever kind with respect to the use of, or the damage resulting from the use of, any information, apparatus, method, or process disclosed in this report.

Any opinions, findings, and conclusions or recommendations expressed in this publication are those of the author(s) and do not necessarily reflect the views of MCEER, the National Science Foundation, or other sponsors.

Report Documentation Page 50272-101	1. Report No. MCEER-06-0001	2.	3. Recipient's Accession No.
4. Title and Subtitle Seismic Fragility of Suspended Ceiling Systems		5. Report Date 2/3/2006	
		6.	
7. Authors H. Badillo-Almaraz, A.S. Whittaker, A.M. Reinhorn, G.P. Cimellaro		8. Performing Organization Report No.	
		10. Project / Task / Work Unit No. 042005	
9. Performing Organization Name and Address Department of Civil, Structural and Environmental Engineering State University of New York at Buffalo Buffalo, NY 14260		11. Contract (C) or Grant (G) No. (C) EEC-9701471	
		(G)	
12. Sponsoring Organization Name and Address Multidisciplinary Center for Earthquake Engineering Research State University of New York at Buffalo Red Jacket Quadrangle Buffalo, NY 14261		13. Type of Report / Period Covered Technical Report	
		14.	
15. Supplementary Notes This research was conducted at the University at Buffalo, State University of New York and was supported primarily by the Earthquake Engineering Research Centers Program of the National Science Foundation.			
16. Abstract (limit 200 Words) The failure of suspended ceiling systems has been one of the most widely reported types of nonstructural damage in building structures in past earthquakes. Despite repeated damage to such systems, there has been no systematic study of their seismic behavior beyond qualification studies for selected manufacturers. This report reveals fragility method findings of full-scale experimental testing on an earthquake simulator of six ceiling systems. The following variables are the basis for comparison: size and weight of tiles, use of retainer clips, use of compression posts, and physical condition of grid components. A literature review, figures, and references are included.			
17. Document Analysis a. Descriptors Earthquake Engineering. Fragility methods. Suspended ceiling systems. Failure. Structural performance. Nonstructural damage. Systematic studies. Vulnerability. Structural analyses. Seismic fragility curves. Seismic performance. Limit states. Performance levels. Tiles. Retainer clips. Compression posts. Grid components.			
b. Identifiers/Open-Ended Terms c. COSATI Field/Group			
18. Availability Statement Release Unlimited.		19. Security Class (This Report) Unclassified	21. No. of Pages 225
		20. Security Class (This Page) Unclassified	22. Price 35.00





---

# Seismic Fragility of Suspended Ceiling Systems

by

Hiram Badillo-Almaraz<sup>1</sup>, Andrew S. Whittaker<sup>2</sup>,  
Andrei M. Reinhorn<sup>3</sup> and Gian Paolo Cimellaro<sup>4</sup>

Publication Date: February 4, 2006

Submittal Date: August 18, 2003

Technical Report MCEER-06-0001

Task Number 042005

NSF Master Contract Number EEC 9701471

- 1 Graduate Research Assistant, Department of Civil, Structural and Environmental Engineering, University at Buffalo, State University of New York
- 2 Professor, Department of Civil, Structural and Environmental Engineering, University at Buffalo, State University of New York
- 3 Clifford C. Furnas Professor, Department of Civil, Structural and Environmental Engineering, University at Buffalo, State University of New York

MULTIDISCIPLINARY CENTER FOR EARTHQUAKE ENGINEERING RESEARCH  
University at Buffalo, State University of New York  
Red Jacket Quadrangle, Buffalo, NY 14261

---



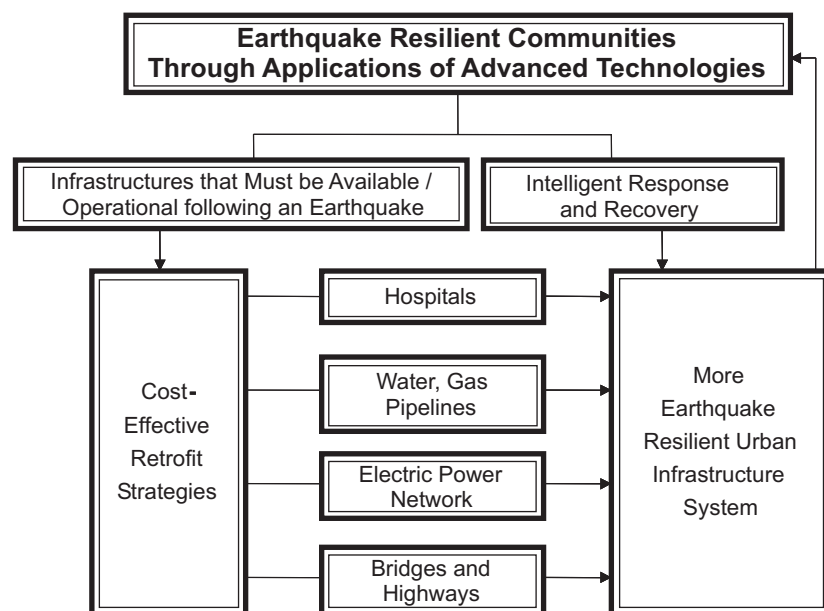
## Preface

The Multidisciplinary Center for Earthquake Engineering Research (MCEER) is a national center of excellence in advanced technology applications that is dedicated to the reduction of earthquake losses nationwide. Headquartered at the University at Buffalo, State University of New York, the Center was originally established by the National Science Foundation in 1986, as the National Center for Earthquake Engineering Research (NCEER).

Comprising a consortium of researchers from numerous disciplines and institutions throughout the United States, the Center's mission is to reduce earthquake losses through research and the application of advanced technologies that improve engineering, pre-earthquake planning and post-earthquake recovery strategies. Toward this end, the Center coordinates a nationwide program of multidisciplinary team research, education and outreach activities.

MCEER's research is conducted under the sponsorship of two major federal agencies: the National Science Foundation (NSF) and the Federal Highway Administration (FHWA), and the State of New York. Significant support is derived from the Federal Emergency Management Agency (FEMA), other state governments, academic institutions, foreign governments and private industry.

MCEER's NSF-sponsored research objectives are twofold: to increase resilience by developing seismic evaluation and rehabilitation strategies for the post-disaster facilities and systems (hospitals, electrical and water lifelines, and bridges and highways) that society expects to be operational following an earthquake; and to further enhance resilience by developing improved emergency management capabilities to ensure an effective response and recovery following the earthquake (see the figure below).



A cross-program activity focuses on the establishment of an effective experimental and analytical network to facilitate the exchange of information between researchers located in various institutions across the country. These are complemented by, and integrated with, other MCEER activities in education, outreach, technology transfer, and industry partnerships.

*The failure of suspended ceiling systems has been one of the most widely reported types of nonstructural damage in building structures during past earthquakes. This report presents the results of research to address this problem. The main objectives were to study the performance of suspended ceiling systems commonly installed in the United States; evaluate improvements in response offered by the use of retainer clips that secure the ceiling panels (tiles) to a suspension system; investigate the effectiveness of including a vertical strut (or compression post) as seismic reinforcement in ceiling systems; and evaluate the effect of different boundary conditions on the entire ceiling system during earthquake shaking. Four variables that affect the seismic performance of suspended ceiling systems were investigated: (1) the size and weight of tiles, (2) the use of retainer clips, (3) the use of compression posts, and (4) the physical condition of grid components. A total of six ceiling system configurations were studied using different combinations of these variables: undersized tiles, undersized tiles with retainer clips, undersized tiles with recycled grid components, normal sized tiles, normal sized tiles with retainer clips, and normal sized tiles without the compression post. Results are reported using damage states and fragility curves. The fragility curves provide a decision-making tool for performance assessment of suspended ceiling systems.*



## **ABSTRACT**

The failure of suspended ceiling systems has been one of the most widely reported types of nonstructural damage in building structures in past earthquakes. Despite repeated damage to such systems, there has been no systematic study of their seismic behavior beyond qualification studies for selected manufacturers.

Fragility methods are used herein to characterize the behavior and vulnerability of suspended ceiling systems. Since suspended ceiling systems are not amenable to traditional structural analysis, full-scale experimental testing on an earthquake simulator was performed to obtain fragility data. The results from the full-scale testing are presented as seismic fragility curves. Four variables that affect the seismic performance of suspended ceiling systems were investigated: (1) the size and weight of tiles, (2) the use of retainer clips, (3) the use of compression posts, and (4) the physical condition of grid components. A total of six ceiling system configurations were studied using different combinations of these variables: (1) undersized tiles, (2) undersized tiles with retainer clips, (3) undersized tiles with recycled grid components, (4) normal sized tiles, (5) normal sized tiles with retainer clips, and (6) normal sized tiles without the compression post.

Four limit states of response that cover most of the performance levels described in the codes and guidelines for the seismic performance of nonstructural components were defined using physical definitions of damage. Data were obtained for every limit state to compare the effect of each variable on the response of suspended ceiling systems.



## ACKNOWLEDGEMENTS

Armstrong World Industries Inc. provided all of the ceiling system components for the fragility testing program. This support is gratefully acknowledged. Special thanks are due to Messrs. Paul Hough and Thomas Fritz of Armstrong World Industries, and Mark Pitman, Scot Weinreber and Duane Koslowski of the Department of Civil, Structural and Environmental Engineering at University at Buffalo for their technical support at different times over the course of this study.

The first author would like to thank the *National Council of Science and Technology of Mexico* (CONACYT) and the *General Direction of International Relations of the Public Bureau of Education of Mexico* (Dirección General de Relaciones Internacionales de la SEP) for their financial support during his studies at the State University of New York at Buffalo. Partial support for the work described in this report was provided by the Multidisciplinary Center for Earthquake Engineering Research through grants from the Earthquake Engineering Centers Program of the National Science Foundation (Award Number EEC-9701471) and the State of New York. This support is also acknowledged.



# TABLE OF CONTENTS

SECTION	TITLE	PAGE
<b>1</b>	<b>INTRODUCTION</b>	<b>1</b>
1.1	General	1
1.2	Goal and Objectives	2
1.3	Report Organization	3
<b>2</b>	<b>LITERATURE REVIEW</b>	<b>5</b>
2.1	Introduction to Seismic Fragility	5
2.2	Previous Studies on Fragility Analysis	6
2.3	Previous Studies on Suspended Ceiling Systems	8
<b>3</b>	<b>EXPERIMENTAL FACILITIES AND TEST SPECIMENS</b>	<b>11</b>
3.1	Earthquake Simulator	11
3.2	Test Frame	12
3.3	Specimen Descriptions	19
3.3.1	Introduction	19
3.3.2	Suspension System	19
3.3.3	Tiles	22
3.3.4	Retention Clips	24
3.4	Instrumentation	25
<b>4</b>	<b>DYNAMIC CHARACTERISTICS OF THE TEST FRAME</b>	<b>33</b>
4.1	Introduction	33
4.2	Snap-Back Test	33
4.2.1	Horizontal Direction	33
4.2.2	Vertical Direction	35
4.2.3	Procedure to Obtain Periods and Damping Ratios	37

## TABLE OF CONTENTS (cont'd)

SECTION	TITLE	PAGE
4.3	Frequency Sweep	40
4.4	White Noise	45
4.5	Summary	48
<b>5</b>	<b>SEISMIC QUALIFICATION AND FRAGILITY TESTING</b>	<b>49</b>
5.1	Introduction	49
5.2	Testing of Ceiling Systems	49
5.2.1	ICBO Requirements for Testing and Qualification	49
5.2.2	Horizontal and Vertical Spectra for Qualification and Fragility Testing	50
5.3	Description of the Testing Protocol for Fragility Testing	53
5.4	Dynamic Excitations	55
5.4.1	White Noise	55
5.4.2	Earthquake Histories	57
<b>6</b>	<b>SIMULATOR TESTING OF SUSPENDED CEILING SYSTEMS</b>	<b>77</b>
6.1	Introduction	77
6.2	Descriptions of Ceiling Systems	77
6.2.1	Configuration 1: Undersized Tiles	78
6.2.2	Configuration 2: Undersized Tiles with Retainer Clips	78
6.2.3	Configuration 3: Undersized Tiles with Recycled Grid Components	79
6.2.4	Configuration 4: Normal Sized Tiles	79
6.2.5	Configuration 5: Normal Sized Tiles with Retainer Clips	80
6.2.6	Configuration 6: Normal Sized Tiles without Compression Post	80

## TABLE OF CONTENTS (cont'd)

SECTION	TITLE	PAGE
6.3	Experimental Results	81
6.3.1	Introduction	81
6.3.2	Configuration 1: Undersized Tiles	82
6.3.3	Configuration 2: Undersized Tiles with Retainer Clips	85
6.3.4	Configuration 3: Undersized Tiles with Recycled Grid Components	88
6.3.5	Configuration 4: Normal Sized Tiles	90
6.3.6	Configuration 5: Normal Sized Tiles with Retainer Clips	94
6.3.7	Configuration 6: Normal Sized Tiles without Compression Post	97
6.3.8	Observations	101
6.4	Spectral Accelerations of the Test Frame	101
<b>7</b>	<b>FRAGILITY ANALYSIS AND DATA EVALUATION</b>	<b>153</b>
7.1	Introduction	153
7.2	Limit States	154
7.2.1	Limit State 1: Minor Damage	154
7.2.2	Limit State 2: Moderate Damage	154
7.2.3	Limit State 3: Major Damage	155
7.2.4	Limit State 4: Grid Failure	155
7.3	Demand Parameters	155
7.4	Generation of Fragility Curves	156
7.5	Ceiling System Fragility Data and Interpretation	163
<b>8</b>	<b>SUMMARY AND CONCLUSIONS</b>	<b>195</b>
8.1	Summary	195
8.2	Conclusions	196
<b>9</b>	<b>REFERENCES</b>	<b>199</b>





## LIST OF ILLUSTRATIONS

FIGURE	TITLE	PAGE
3-1	Plan view of the base of the frame	12
3-2	Plan view of the top of the frame	13
3-3	Elevation of the East side of the frame	14
3-4	Detail A-A', frontal view of frame	15
3-5	Detail B, connection of corner of the frame	15
3-6	Detail C, connection of the roof with main beams	16
3-7	Detail D, roof framing connection in the East-West direction	16
3-8	Test frame mounted on the simulator at the University at Buffalo	17
3-9	Roof connection to the main beams on the North side of the frame	18
3-10	Roof connection to the main beams on the West side of the frame	18
3-11	Drawing of the ceiling suspension grid	21
3-12	Ceiling suspension grid	22
3-13	Tile Dune Humigard Plus (Armstrong item no. 1774)	23
3-14	Retention clips	24
3-15	Array of clips attached to the 1.22 m (4 ft) cross runners	25
3-16	Accelerometers on the test frame	26
3-17	Accelerometers monitoring the response of the test assembly	28
3-18	Displacement transducers in the test frame	29
3-19	Displacement transducers mounted on the test frame	30
4-1	Configuration of the snap-back test in the horizontal direction	34
4-2	Acceleration history of free vibration in the horizontal direction	35
4-3	Configuration of the snap-back test in the vertical direction	36
4-4	Acceleration history of free vibration in the vertical direction	36
4-5	Fourier amplitude spectra for the horizontal snap-back test	38

## LIST OF ILLUSTRATIONS (cont'd)

FIGURE	TITLE	PAGE
4-6	First mode free vibration decay in the horizontal direction	38
4-7	Fourier amplitude spectra for the vertical snap-back test	39
4-8	First mode free vibration decay in the vertical direction	39
4-9	Acceleration history used for the sweep of frequencies (first 90 seconds)	41
4-10	Filtered frequency domain records of the simulator input and the frame response output for the horizontal direction using the frequency sweep	43
4-11	Transfer function for the horizontal direction using the frequency sweep	43
4-12	Filtered frequency domain records of the simulator input and the frame response output for the vertical direction using the frequency sweep	44
4-13	Transfer function for the vertical direction using the frequency sweep	44
4-14	Filtered frequency domain records of the simulator input and the frame response output for the horizontal direction using white noise	46
4-15	Transfer function for the horizontal direction using white noise	46
4-16	Filtered frequency domain records of the simulator input and the frame response output for the vertical direction using white noise	47
4-17	Transfer function for the vertical direction using white noise	47
5-1	ICBO Required Response Spectra for horizontal and vertical shaking	50
5-2	RRS for horizontal and vertical shaking for $S_S = 1.0g$	52
5-3	Relationship between MCE NEHRP spectra and target qualification spectrum ( $S_S = 1.0g$ , $S_I = 0.4g$ )	53
5-4	White noise records and Fourier amplitude spectra for the horizontal and vertical motions	56
5-5	Earthquake histories and response spectra before and after applying the RSPM for $S_S = 1.0g$	60

## LIST OF ILLUSTRATIONS (cont'd)

FIGURE	TITLE	PAGE
5-6	Velocity history derived from the acceleration history of figure 5-5b ( $S_S = 1.0g$ )	61
5-7	Displacement history derived from the acceleration history of figure 5-5b ( $S_S = 1.0g$ )	61
5-8	Rectangular modulating function applied to remove the low frequency content in the acceleration history corresponding to $S_S = 1.0g$ ( $f_c = 0.4$ Hz)	61
5-9	Filtered acceleration history corresponding to $S_S = 1.0g$ ( $f_c = 0.4$ Hz)	62
5-10	Velocity history derived from the acceleration history of figure 5-9	62
5-11	Displacement history derived from the acceleration history of figure 5-9	62
5-12	Filtered velocity history ( $f_c = 0.4$ Hz)	63
5-13	Displacement history derived from the velocity history of figure 5-12	63
5-14	Acceleration history derived from the velocity history of figure 5-12	63
5-15	Fourier amplitude spectra for the acceleration history corresponding to a short period mapped spectral acceleration, $S_S = 1.0g$	64
5-16	Earthquake histories and spectra for test A025	66
5-17	Earthquake histories and spectra for test A050	67
5-18	Earthquake histories and spectra for test A075	68
5-19	Earthquake histories and spectra for test A100	69
5-20	Earthquake histories and spectra for test A125	70
5-21	Earthquake histories and spectra for test A150	71
5-22	Earthquake histories and spectra for test A175	72
5-23	Earthquake histories and spectra for test A200	73
5-24	Earthquake histories and spectra for test A225	74
5-25	Earthquake histories and spectra for test A250	75
6-1	Configuration 1 installation, undersized tiles	78

## LIST OF ILLUSTRATIONS (cont'd)

FIGURE	TITLE	PAGE
6-2	Configuration 2 installation, undersized tiles with retainer clips	79
6-3	Configuration 4 installation, normal sized tiles	80
6-4	Configuration 6 installation, normal sized tiles without compression post	81
6-5	Tile rotating before falling, configuration 1	83
6-6	Tile of figure 6-5 falling from the suspension grid, configuration 1	83
6-7	Damage to the cross tees installed in the East-West direction, configuration 2	87
6-8	Damage to the latches on the cross tees in configuration 2	87
6-9	Damage to the East-West cross tees in configuration 4	93
6-10	Damage to the East-West cross tees in configuration 4	93
6-11	Failure of grid and tiles in configuration 5	96
6-12	Failure of tiles in configuration 6	100
6-13	Rivets on the South side wall molding destroyed during shaking	102
6-14	Connection between two main beams	102
6-15	Response spectra corresponding to $S_S = 1.0g$ , undersized tiles	110
6-16	Response spectra corresponding to $S_S = 1.25g$ , undersized tiles	111
6-17	Response spectra corresponding to $S_S = 1.5g$ , undersized tiles	112
6-18	Response spectra corresponding to $S_S = 1.75g$ , undersized tiles	113
6-19	Response spectra corresponding to $S_S = 2.0g$ , undersized tiles	114
6-20	Response spectra corresponding to $S_S = 2.25g$ , undersized tiles	115
6-21	Response spectra corresponding to $S_S = 2.5g$ , undersized tiles	116
6-22	Response spectra corresponding to $S_S = 1.0g$ , undersized tiles with clips	117
6-23	Response spectra corresponding to $S_S = 1.25g$ , undersized tiles with clips	118
6-24	Response spectra corresponding to $S_S = 1.5g$ , undersized tiles with clips	119

## LIST OF ILLUSTRATIONS (cont'd)

FIGURE	TITLE	PAGE
6-25	Response spectra corresponding to $S_S = 1.75\text{g}$ , undersized tiles with clips	120
6-26	Response spectra corresponding to $S_S = 2.0\text{g}$ , undersized tiles with clips	121
6-27	Response spectra corresponding to $S_S = 2.25\text{g}$ , undersized tiles with clips	122
6-28	Response spectra corresponding to $S_S = 2.5\text{g}$ , undersized tiles with clips	123
6-29	Response spectra corresponding to $S_S = 1.0\text{g}$ , undersized tiles with recycled grid	124
6-30	Response spectra corresponding to $S_S = 1.25\text{g}$ , undersized tiles with recycled grid	125
6-31	Response spectra corresponding to $S_S = 1.5\text{g}$ , undersized tiles with recycled grid	126
6-32	Response spectra corresponding to $S_S = 1.75\text{g}$ , undersized tiles with recycled grid	127
6-33	Response spectra corresponding to $S_S = 2.0\text{g}$ , undersized tiles with recycled grid	128
6-34	Response spectra corresponding to $S_S = 2.25\text{g}$ , undersized tiles with recycled grid	129
6-35	Response spectra corresponding to $S_S = 2.5\text{g}$ , undersized tiles with recycled grid	130
6-36	Response spectra corresponding to $S_S = 1.5\text{g}$ , normal sized tiles	131
6-37	Response spectra corresponding to $S_S = 1.75\text{g}$ , normal sized tiles	132
6-38	Response spectra corresponding to $S_S = 2.0\text{g}$ , normal sized tiles	133
6-39	Response spectra corresponding to $S_S = 2.25\text{g}$ , normal sized tiles	134
6-40	Response spectra corresponding to $S_S = 2.5\text{g}$ , normal sized tiles	135

## LIST OF ILLUSTRATIONS (cont'd)

FIGURE	TITLE	PAGE
6-41	Response spectra corresponding to $S_S = 1.5\text{g}$ , normal sized tile with clips	136
6-42	Response spectra corresponding to $S_S = 1.75\text{g}$ , normal sized tiles with clips	137
6-43	Response spectra corresponding to $S_S = 2.0\text{g}$ , normal sized tiles with clips	138
6-44	Response spectra corresponding to $S_S = 2.25\text{g}$ , normal sized tiles with clips	139
6-45	Response spectra corresponding to $S_S = 2.5\text{g}$ , normal sized tiles with clips	140
6-46	Response spectra corresponding to $S_S = 1.5\text{g}$ , normal sized tiles without post	141
6-47	Response spectra corresponding to $S_S = 1.75\text{g}$ , normal sized tiles without post	142
6-48	Response spectra corresponding to $S_S = 2.0\text{g}$ , normal sized tiles without post	143
6-49	Response spectra corresponding to $S_S = 2.25\text{g}$ , normal sized tiles without post	144
6-50	Response spectra corresponding to $S_S = 2.5\text{g}$ , normal sized tiles without post	145
6-51	Mean response spectra at selected locations, undersized tiles	146
6-52	Mean response spectra at selected locations, undersized tiles with clips	147
6-53	Mean response spectra at selected locations, undersized tiles with recycled grid	148
6-54	Mean response spectra at selected locations, normal sized tiles	149
6-55	Mean response spectra at selected locations, normal sized tiles with clips	150

## LIST OF ILLUSTRATIONS (cont'd)

FIGURE	TITLE	PAGE
6-56	Mean response spectra at selected locations, normal sized tiles without post	151
7-1	Schematic representation of a story of typical building and the test fixture	157
7-2	Illustration of part of the procedure to develop fragility curves, configuration 4: normal sized tiles	159
7-3	Fragility curves for 1.5-second spectral acceleration based on different accelerometer histories, configuration 1: undersized tiles	161
7-4	Fragility curves for 1.5-second spectral acceleration for different limit states, configuration 1: undersized tiles	162
7-5	Fragility curves for peak ground acceleration, configuration 1: undersized tiles	165
7-6	Fragility curves for spectral acceleration at 0.2 second, configuration 1: undersized tiles	165
7-7	Fragility curves for spectral acceleration at 0.5 second, configuration 1: undersized tiles	166
7-8	Fragility curves for spectral acceleration at 1.0 second, configuration 1: undersized tiles	166
7-9	Fragility curves for spectral acceleration at 1.5 seconds, configuration 1: undersized tiles	167
7-10	Fragility curves for spectral acceleration at 2.0 seconds, configuration 1: undersized tiles	167
7-11	Fragility curves for peak ground acceleration, configuration 2: undersized tiles with clips	168
7-12	Fragility curves for spectral acceleration at 0.2 second, configuration 2: undersized tiles with clips	168

## LIST OF ILLUSTRATIONS (cont'd)

FIGURE	TITLE	PAGE
7-13	Fragility curves for spectral acceleration at 0.5 second, configuration 2: undersized tiles with clips	169
7-14	Fragility curves for spectral acceleration at 1.0 second, configuration 2: undersized tiles with clips	169
7-15	Fragility curves for spectral acceleration at 1.5 seconds, configuration 2: undersized tiles with clips	170
7-16	Fragility curves for spectral acceleration at 2.0 seconds, configuration 2: undersized tiles with clips	170
7-17	Fragility curves for peak ground acceleration, configuration 3: undersized tiles with recycled grid	171
7-18	Fragility curves for spectral acceleration at 0.2 second, configuration 3: undersized tiles with recycled grid	171
7-19	Fragility curves for spectral acceleration at 0.5 second, configuration 3: undersized tiles with recycled grid	172
7-20	Fragility curves for spectral acceleration at 1.0 second, configuration 3: undersized tiles with recycled grid	172
7-21	Fragility curves for spectral acceleration at 1.5 seconds, configuration 3: undersized tiles with recycled grid	173
7-22	Fragility curves for spectral acceleration at 2.0 seconds, configuration 3: undersized tiles with recycled grid	173
7-23	Fragility curves for peak ground acceleration, configuration 4: normal sized tiles	174
7-24	Fragility curves for spectral acceleration at 0.2 second, configuration 4: normal sized tiles	174
7-25	Fragility curves for spectral acceleration at 0.5 second, configuration 4: normal sized tiles	175



## LIST OF ILLUSTRATIONS (cont'd)

FIGURE	TITLE	PAGE
7-26	Fragility curves for spectral acceleration at 1.0 second, configuration 4: normal sized tiles	175
7-27	Fragility curves for spectral acceleration at 1.5 seconds, configuration 4: normal sized tiles	176
7-28	Fragility curves for spectral acceleration at 2.0 seconds, configuration 4: normal sized tiles	176
7-29	Fragility curves for peak ground acceleration, configuration 5: normal sized tiles with clips	177
7-30	Fragility curves for spectral acceleration at 0.2 second, configuration 5: normal sized tiles with clips	177
7-31	Fragility curves for spectral acceleration at 0.5 second, configuration 5: normal sized tiles with clips	178
7-32	Fragility curves for spectral acceleration at 1.0 second, configuration 5: normal sized tiles with clips	178
7-33	Fragility curves for spectral acceleration at 1.5 seconds, configuration 5: normal sized tiles with clips	179
7-34	Fragility curves for spectral acceleration at 2.0 seconds, configuration 5: normal sized tiles with clips	179
7-35	Fragility curves for peak ground acceleration, configuration 6: normal sized tiles without post	180
7-36	Fragility curves for spectral acceleration at 0.2 second, configuration 6: normal sized tiles without post	180
7-37	Fragility curves for spectral acceleration at 0.5 second, configuration 6: normal sized tiles without post	181
7-38	Fragility curves for spectral acceleration at 1.0 second, configuration 6: normal sized tiles without post	181

## LIST OF ILLUSTRATIONS (cont'd)

FIGURE	TITLE	PAGE
7-39	Fragility curves for spectral acceleration at 1.5 seconds, configuration 6: normal sized tiles without post	182
7-40	Fragility curves for spectral acceleration at 2.0 seconds, configuration 6: normal sized tiles without post	182
7-41	Fragility curves for peak ground acceleration, limit state 1: minor damage	183
7-42	Fragility curves for peak ground acceleration, limit state 2: moderate damage	183
7-43	Fragility curves for peak ground acceleration, limit state 3: major damage	184
7-44	Fragility curves for peak ground acceleration, limit state 4: grid failure	184
7-45	Fragility curves for spectral acceleration at 0.2 second, limit state 1: minor damage	185
7-46	Fragility curves for spectral acceleration at 0.2 second, limit state 2: moderate damage	185
7-47	Fragility curves for spectral acceleration at 0.2 second, limit state 3: major damage	186
7-48	Fragility curves for spectral acceleration at 0.2 second, limit state 4: grid failure	186
7-49	Fragility curves for spectral acceleration at 0.5 second, limit state 1: minor damage	187
7-50	Fragility curves for spectral acceleration at 0.5 second, limit state 2: moderate damage	187
7-51	Fragility curves for spectral acceleration at 0.5 second, limit state 3: major damage	188

## LIST OF ILLUSTRATIONS (cont'd)

FIGURE	TITLE	PAGE
7-52	Fragility curves for spectral acceleration at 0.5 second, limit state 4: grid failure	188
7-53	Fragility curves for spectral acceleration at 1.0 second, limit state 1: minor damage	189
7-54	Fragility curves for spectral acceleration at 1.0 second, limit state 2: moderate damage	189
7-55	Fragility curves for spectral acceleration at 1.0 second, limit state 3: major damage	190
7-56	Fragility curves for spectral acceleration at 1.0 second, limit state 4: grid failure	190
7-57	Fragility curves for spectral acceleration at 1.5 seconds, limit state 1: minor damage	191
7-58	Fragility curves for spectral acceleration at 1.5 seconds, limit state 2: moderate damage	191
7-59	Fragility curves for spectral acceleration at 1.5 seconds, limit state 3: major damage	192
7-60	Fragility curves for spectral acceleration at 1.5 seconds, limit state 4: grid failure	192
7-61	Fragility curves for spectral acceleration at 2.0 seconds, limit state 1: minor damage	193
7-62	Fragility curves for spectral acceleration at 2.0 seconds, limit state 2: moderate damage	193
7-63	Fragility curves for spectral acceleration at 2.0 seconds, limit state 3: major damage	194
7-64	Fragility curves for spectral acceleration at 2.0 seconds, limit state 4: grid failure	194



## LIST OF TABLES

TABLE	TITLE	PAGE
3-1	Summary information on components of the ceiling suspension system	20
3-2	Summary information on the ceiling tiles	23
3-3	Transducers used for the fragility testing program	31
4-1	Frequencies obtained with the three testing methods	48
4-2	Damping ratios obtained with the three testing methods	48
5-1	Test sequence (series A)	54
5-2	Parameters to calculate the horizontal RRS ( $z/h = 1.0$ )	55
5-3	Cut-off frequencies and maximum acceleration, velocity and displacement before and after eliminating the low-frequency content	65
6-1	Results for undersized tiles, series A-D	84
6-2	Results for undersized tiles with retainer clips, series E-G	86
6-3	Results for undersized tiles with recycled grid components, series H-J	89
6-4	Results for normal sized tiles, series L-O, Q, R and BB	91
6-5	Results for normal sized tiles with retainer clips, series P and S-U	95
6-6	Results for normal sized tiles without compression post, series V-AA	98
6-7	Mean spectral accelerations at selected periods, undersized tiles	104
6-8	Mean spectral accelerations at selected periods, undersized tiles with clips	105
6-9	Mean spectral accelerations at selected periods, undersized tiles with recycled grid	106
6-10	Mean spectral accelerations at selected periods, normal sized tiles	107
6-11	Mean spectral accelerations at selected periods, normal sized tiles with clips	108
6-12	Mean spectral accelerations at selected periods, normal sized tiles without post	109



# CHAPTER 1

## INTRODUCTION

### 1.1 General

The response of nonstructural components can significantly affect the functionality of a building after an earthquake, even when the structural components are undamaged. Poor performance of nonstructural components in past earthquakes has led to the evacuation of buildings, to substantial economic losses due to business interruption and in extreme cases to the loss of life.

One of the most widely reported types of nonstructural damage in past earthquakes is the failure of suspended ceiling systems. The performance of suspended ceiling systems during earthquakes can be a critical issue depending on the occupancy of the building. Reconnaissance following past earthquakes has shown that failures of ceiling systems during earthquakes have caused significant losses and disruption in important or critical facilities. For example, in the 1971 San Fernando earthquake, a collapsed ceiling system obstructed the control room operations in an electrical power plant (Sharpe et al., 1973). In the 1989 Loma Prieta earthquake, massive failure of a suspended ceiling system caused the evacuation of the San Francisco International Airport (Benuska, 1990). In the 1993 Guam earthquake, considerable damage to a ceiling suspension system in the blood bank of a major hospital caused a serious disruption to service.

The failure of ceiling systems creates a falling debris hazard. The loss of light fixtures that are often attached to a ceiling system results in the loss of both interior light and the continued function of a building. Also, the failure of ceiling systems may hinder evacuation and rescue efforts after an earthquake and can render a building unusable until the fixtures are replaced (Yao, 2000).

Earthquake-history testing has been used recently for qualification and fragility testing of structural and nonstructural components. Seismic qualification is intended to demonstrate through experimentation that a component in a structure is able to function during and after an earthquake. In contrast to qualification testing, the objective of fragility testing is to establish a

relationship between limit states of response and a representative excitation parameter for a component.

Fragility curves can be used to assess the vulnerability of a structural system and directly account for sources of uncertainty. The development of fragility curves involves the use of both mathematical modeling and physical observations. In the case of suspended ceiling systems, mathematical analysis is difficult due to uncertainties in the physical behavior of elements and components of the system once installed in the ceiling system. Further, the complexity of the mathematical model and the highly nonlinear behavior of the components once tiles are dislodged make robust structural analysis of suspended ceiling systems unrealistic.

Since analytical methods are generally not applicable to the study of suspended ceiling systems and data collected following past earthquakes are not suitable for fragility characterization, experimental methods represent the best and most reliable technique to obtain fragility curves for suspended ceiling systems.

## **1.2 Goal and Objectives**

The main goal of this study was to develop fragility curves of suspended ceiling systems subjected to the action of earthquake shaking. Fragility curves were obtained by experimental testing of suspended ceiling systems on an earthquake simulator. The specific objectives of the research program were: (1) to study the performance of suspended ceiling systems commonly installed in the United States; (2) to evaluate improvements in response offered by the use of retainer clips that secure the ceiling panels (tiles) to a suspension system; (3) to investigate the effectiveness of including a vertical strut (or compression post) as seismic reinforcement in ceiling systems; and (4) to evaluate the effect of different boundary conditions on the entire ceiling system during earthquake shaking.



### **1.3 Report Organization**

This report contains eight chapters and a list of references. Chapter Two provides an introduction to seismic fragility and presents a review of previous studies on fragility analysis and suspended ceiling systems. Chapter Three provides general information the Structural Engineering and Earthquake Simulation Laboratory of the Department of Civil, Structural and Environmental Engineering at the University at Buffalo, the test frame, the instrumentation used to record the responses of both the simulator and the ceiling system testing, and specifications for the test specimens used in this research project. Chapter Four presents the dynamic characteristics of the test frame. Chapter Five presents the procedure used to generate the ground-motion histories used for fragility testing. Experimental results for the different configurations studied in this research project are presented in Chapter Six. Chapter Seven provides an interpretation of the data obtained from the experimental program in the form of fragility curves linked to various states of damage. Chapter Eight describes the main findings and conclusions of this study. References are listed immediately following Chapter Eight.



## **CHAPTER 2**

### **LITERATURE REVIEW**

#### **2.1 Introduction to Seismic Fragility**

Seismic fragility has been defined as the conditional probability of failure of a system for a given intensity of a ground motion. In performance based seismic design, failure is said to have occurred when the structure fails to satisfy the requirements of a prescribed performance level. If the intensity of the ground motion is expressed as a single variable (e.g., the peak ground acceleration or the mapped maximum earthquake spectral acceleration at short periods, etc.), the conditional probability of failure expressed as a function of the ground motion intensity is called a seismic fragility curve (Sasani and Der Kiureghian, 2001).

Ideally, the assessment of fragility should employ as much objective information as possible. Such information is gained from fundamental laws of nature (e.g. laws of mechanics) and from laboratory and field observations. However, such information is often shrouded in uncertainties that arise from imperfections in the mathematical models, from measurement errors, and from the finite size of observed samples. Several mathematical tools or techniques have been developed (e.g., Monte Carlo simulation, Bayesian parameter estimation) to prepare probabilistic models and the assessment of fragility when the available information is incomplete or insufficient. Such techniques are capable of incorporate all types of information and properly account for uncertainties (Der Kiureghian, 1999).

Fragility curves can be generated empirically or analytically. Empirical fragility curves can be developed with the use of data from damage recorded in previous earthquakes or with the use of experimental data obtained from laboratory tests (i.e., scale model testing). Analytical fragility curves can be developed with the use of statistical data obtained with the use of accurate mathematical models that represent certain physical phenomenon. In statistical terms, a fragility curve describes the probability of reaching or exceeding a damage state at a specified ground motion level. Thus a fragility curve for a particular damage state is obtained by computing the

conditional probabilities of reaching or exceeding that damage state at various levels of ground motion.

Fragility curves can be used to present vulnerability data for both structural and nonstructural components systems on buildings. Fragility curves can also be used to compare different seismic rehabilitation techniques and to optimize the seismic design of structures (Shinozuka et al., 2000a). Previous studies using fragility techniques are discussed in the following subsection.

## **2.2 Previous Studies on Fragility Analysis**

Studies on concrete dams, pier bridges, structural walls of reinforced concrete, wood frame housing, etc., have been performed in recent years using fragility analysis as the main tool to assess seismic vulnerability. A summary description and the main findings of studies performed using fragility analysis that were considered useful in the development of the work presented in this report are presented in the following paragraphs.

Singhal and Kiremidjian (1996) developed fragility curves for damage in reinforced concrete frames using Monte Carlo simulation. The authors of this paper considered that the development of fragility curves requires the characterization of the ground motion and the identification of the different degrees of structural damage. Earthquake ground motion amplitude, frequency content, and strong motion duration were considered important characteristics that affect structural response and damage, so they were included in the generation of the fragility curves. The fragility curves obtained considered the nonlinearity of the structure properties and nonstationary characteristics of the ground motions for the purpose of developing the most consistent set of fragility curves possible so they could be used to estimate damage states for a wide range of reinforced concrete frames. Characterization of damage in the concrete frames was made using the Park-Ang global damage indices (Park and Ang, 1985a, 1985b). Structural damage was quantified by five discrete damage states. The authors pointed out that it was desirable to obtain fragility curves for all structural classes because the damage estimates so obtained can be used for cost-benefit analysis to judge retrofit decisions and for the evaluation of potential losses in concrete frames over an entire region.

Reinhorn et al. (2002) presented an approach for assessing seismic fragility of structures. The structural response in terms of probability was evaluated from the inelastic response spectra, the spectral capacity curves, and from consistent relationships that provide the probability distribution function of spectral ordinates.

Shinozuka et. al. (2000b) developed empirical and analytical fragility curves using statistical analysis. According to Shinozuka et. al. the development of vulnerability information in the form of fragility curves is a widely practiced approach when the information is to be developed accounting for a multitude of uncertainties, for example, in the estimation of seismic hazard, structural characteristics, soil-structure interaction, and site conditions. Shinozuka noted that the development of fragility curves required the synergistic use of professional judgment, quasi-static and design-code consistent analysis, utilization of damage data associated with past earthquakes, and numerical simulation of the seismic response of structures based on dynamic analysis. Empirical fragility curves were developed utilizing bridge damage data obtained from the 1995 Hyogo-ken Nanbu (Kobe) earthquake. Analytical fragility curves were then developed for typical bridges in the Memphis area on the basis of a nonlinear dynamic analysis. Two-parameter lognormal distribution functions were used to represent the fragility curves with the two parameters estimated by the maximum likelihood method. Statistical procedures were presented to test the goodness-of-fit hypothesis for these fragility curves and to estimate the confidence intervals of the two parameters of the lognormal distribution.

Sasani and Der Kiureghian (2001) developed probabilistic displacement capacity and demand models of reinforced concrete structural walls for a life-safety performance level using the Bayesian parameter estimation technique<sup>1</sup>. Experimental data were used to develop the capacity model and nonlinear dynamic analysis was employed to develop the demand model. The probabilistic models were used to assess the seismic fragility of a sample reinforced concrete structural wall with two values of the flexural reinforcement ratio in the boundary elements. The

---

<sup>1</sup> The Bayesian parameter estimation technique provides an effective tool for the development of probabilistic models and assessment of fragility when available statistical information is shrouded by uncertainties that arise from imperfections in the mathematical models, from measurement errors and from the finite size of observed samples. Details of the Bayesian technique can be found in the literature (e.g., Box and Tiao, 1992; Der Kiureghian, 1999).

models created represented accurately the behavior of structural walls with medium to large aspect ratio that are properly designed to prevent shear or bond failures.

Ellingwood and Tekie (2001) studied the performance of concrete gravity dams using fragility methods. This study addresses fragility modeling as a tool for risk-based policy development and management of concrete gravity dams and presents quantitative methods that can be used to evaluate failure probabilities of concrete gravity dams due to extreme postulated hydrologic events. The databases required to support the fragility assessment of dams are identified using basic fragility concepts. Fragility analysis provided a tool for rational safety assessment and decision making by using a probabilistic framework to manage the various sources of uncertainty that affected the performance of the dam.

### **2.3 Previous Studies on Suspended Ceiling Systems**

Although several studies have indicated that some improvement in the seismic capacity of suspended ceiling systems has been made in recent years, there exists no robust fragility data for suspended ceiling systems and no proven strategies to increase the seismic strength of suspended ceiling systems. A summary description and main findings of studies performed on suspended ceiling systems in recent years are presented in the following paragraphs.

In 1983, ANCO Engineers Inc. (ANCO, 1983) conducted an experiment on the seismic performance of a 3.6 x 8.5 m suspended ceiling system with intermediate-duty runners and lay-in tiles. The excitation used for the experiment was the 1953 Taft earthquake ground motion. The major finding of this experiment was that the most common locations for damage in suspended ceiling systems were around the perimeter of a room at the intersection of the walls and ceilings, where the runners buckle or detach from the wall angle. Other significant observations included the ineffectiveness of vertical struts and that pop rivets were more effective than sway wires in preventing or reducing damage in suspended ceiling systems subjected to earthquake shaking.

Rihal and Granneman (1984) performed a study of a 3.66 x 4.88 m suspended ceiling system subjected to sinusoidal dynamic loading. The major findings of this study were that vertical

struts reduced the vertical displacement response of the ceiling system and that sway wires were effective in reducing of the dynamic response of the suspended ceiling systems.

In 1993, Armstrong World Industries Inc. undertook a series of earthquake tests of suspended ceiling systems. These tests were performed by ANCO Engineers Inc. (ANCO, 1993) on one 7.31 x 4.26 m (24 x 14 ft) ceiling system using ground-motion histories that were representative of Seismic Zones 2A, 3 and 4 of the 1988 and later versions of the Uniform Building Code (UBC, 1991). A 30-second long earthquake history was developed to represent the expected motions of the third and sixth floors of a six-story moment-resisting steel frame structure located on a soft soil site. Test amplitudes were then scaled up or down so that response spectra computed from measured test input motions enveloped the in-structure floor response spectra for Zones 2A, 3, and 4 for non-structural components supported within critical facilities. The main conclusion drawn from those studies was that the Armstrong ceiling systems tested on the earthquake simulator met the UBC Zone 4 design requirements for nonstructural components in essential facilities.

The vibration characteristics and seismic capacity of a set of 1.2 x 4.0 m suspended ceiling systems were investigated by Yao (2000) using experimental and analytical methods. The main purpose of this study was to distinguish the effects of installing sway wires in the suspended ceiling system. Laboratory tests performed in this study revealed that including 45° sway wires in each direction, as recommended by Ceiling and Interior System Contractors (CISCA, 1992), did not produce a discernable increase in the seismic capacity of the ceiling system. From collection of data from field trips, it was found that systems with adequate edge connectivity (such as those with added pop rivets) increased the seismic capacity of suspended ceiling systems. Similar results were obtained when edge hanger wires were added to the suspended ceiling systems. Adding a constraint transverse to the direction of excitation also influenced the behavior of the suspended ceiling system.

From 2001 through late 2005, Armstrong World Industries Inc. undertook an extensive series of earthquake tests on suspended ceiling systems. The series of tests were performed at the Structural Engineering and Earthquake Simulation Laboratory (SEESL) of the State University

of New York at Buffalo (e.g., Badillo et. al., 2002, Kusumastuti et. al., 2002 and Badillo et. al., 2003a, 2003b). A 4.88 x 4.88 m (16 x 16 ft) square steel frame was constructed to test the different types of ceiling systems. Each of the ceiling systems was subjected to a set of combined horizontal and vertical earthquake excitations for the purpose of qualification. The procedures to qualify the ceiling system were those of the ICBO-AC156 “Acceptance Criteria for Seismic Qualification Testing of Nonstructural Components” (ICBO, 2000). Two performance limit states were defined for the seismic qualification work performed in this study: (1) loss of tiles and (2) failure of the suspension system. The intensity of the earthquake shaking was characterized by the NEHRP maximum considered earthquake short period spectral acceleration,  $S_S$  (FEMA, 2000). The target values of  $S_S$  ranged between 0.25g and 1.75g. Several conclusions were drawn from these series of studies and specific details about the performance of each system tested were given. Among the most important findings were that more failures occurred for the performance limit state of loss of tiles than for the performance limit state of failure of the suspension system. Another important conclusion was that the addition of retention clips was a feasible and cost-effective strategy to improve the performance of ceiling systems, even under very intense earthquake shaking.



## **CHAPTER 3**

### **EXPERIMENTAL FACILITIES AND TEST SPECIMENS**

#### **3.1 Earthquake Simulator**

The earthquake simulator in the Structural Engineering and Earthquake Simulation Laboratory (SEESL) of the State University of New York at Buffalo was used to evaluate and qualify the Armstrong ceiling systems. The 3.66 x 3.66 m (12 x 12 ft) earthquake simulator, or shaking table, has five controlled degrees of freedom (excluding the transverse translational movement), a maximum payload of 489 kN (110 kips) and a working frequency range of 0 to 50 Hz. A composite reinforced concrete testing platform of plan dimensions 6.1 x 3.05 m (20 x 10 ft) extends the useful testing area of the simulator but limits the payload to 378 kN (85 kips). The testing platform includes holes on a 30.5 cm (one-foot) square grid for attaching test specimens. The table is capable of testing a variety of specimens up to a height of 6.7 m (22 ft). The longitudinal (horizontal), vertical and roll degrees of freedom are programmable with feedback control to simultaneously control displacement, velocity, and acceleration. The performance envelope of the table is  $\pm 152$  mm (6 in.) displacement,  $\pm 762$  mm/sec (30 in./sec) velocity and 1.15g acceleration at a payload of 197 kN (44 kips) in the horizontal direction, and  $\pm 76$  mm (3 in.) displacement,  $\pm 508$  mm/sec (20 in./sec) velocity, and 2.30g acceleration in the vertical direction. For a payload of 489 kN (110 kips), the maximum platform accelerations are 0.55g and 1.1g in the horizontal and vertical directions, respectively.

The frequency limit of the simulator system is determined by the natural frequency of the table and the supporting actuator oil columns, both of which have a natural frequency of approximately 60 Hz. This facilitates operation of the simulator over a wide band of frequencies with small error. Input or command signals to the table can be of the following types: harmonic motions (sinusoidal, square, triangular), random motions, and any recorded earthquake history. Additional software is available for the collection and processing of data. Frequency and time-domain analysis of data are routinely performed. Data can also be rapidly transferred via the Internet to other computers within the University computing systems or to outside systems.

### 3.2 Test Frame

A 4.88 x 4.88 m (16 x 16 ft) square frame of ASTM Grade 50 steel was constructed to test the ceiling systems. Figures 3-1 to 3-10 present detailed information of the frame. Figure 3-1 is a plan view of the base of the frame. The frame was attached to the simulator platform using 1 in. diameter bolts in the beams that were oriented in the East-West direction. Details of the configuration of the top of the frame are presented in figure 3-2. Two 10.2 x 10.2 cm (4 x 4 in.) tubular sections connected at each corner served as main columns of the frame as shown in figures 3-3 and 3-5. A 3.8 x 3.8 cm (1-1/2 x 1-1/2 in.) angle was welded around the perimeter of the test frame.

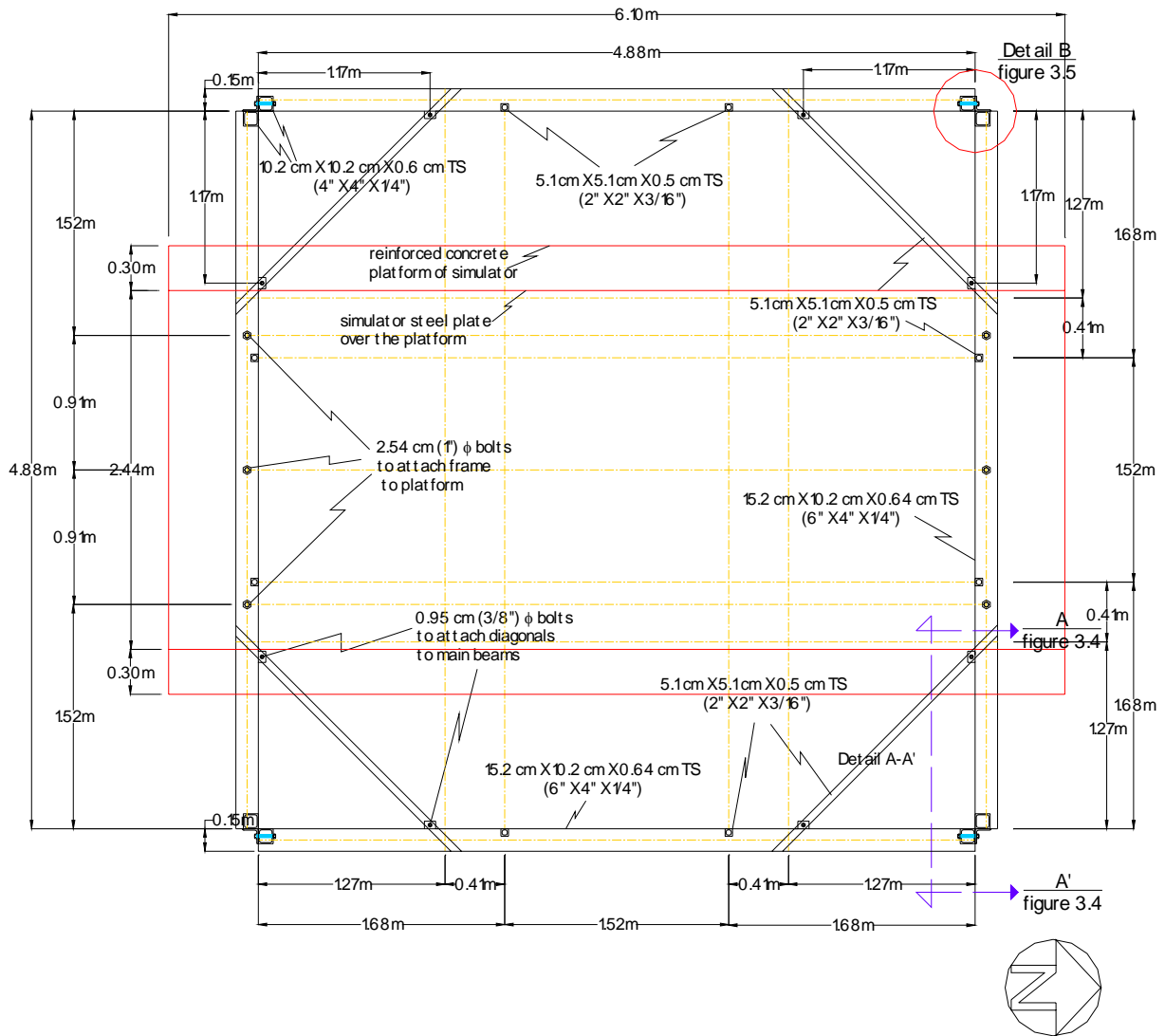


**FIGURE 3-1 Plan view of the base of the frame**

A 5.1 x 15.2 cm (2 x 6 in.) timber ledger was attached to the angle as shown in figures 3-3 and 3-4. The perimeter timber ledger served as a “stud wall” and anchored the ceiling system. To facilitate rapid disassembly, the top of the frame was divided along the East-West axis into two equal parts. Both halves of the roof were connected with 9.5 mm (3/8 in.) diameter bolts as seen in figures 3-2 and 3-7. The top of the frame was connected to the perimeter beams with 9.5 mm (3/8 in.) diameter bolts as shown in figures 3-6, 3-9 and 3-10.

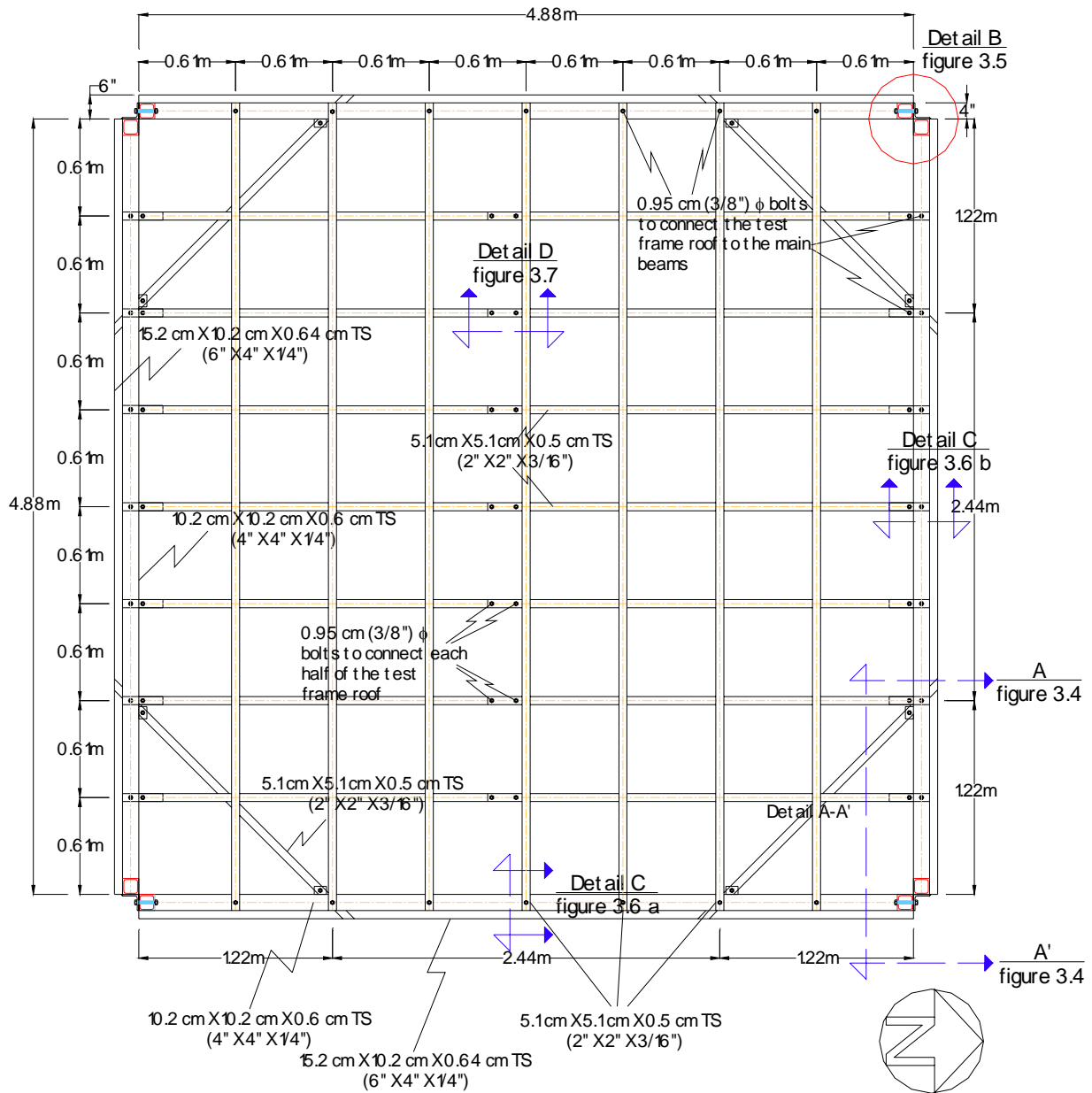


**FIGURE 3-2 Plan view of the top of the frame**

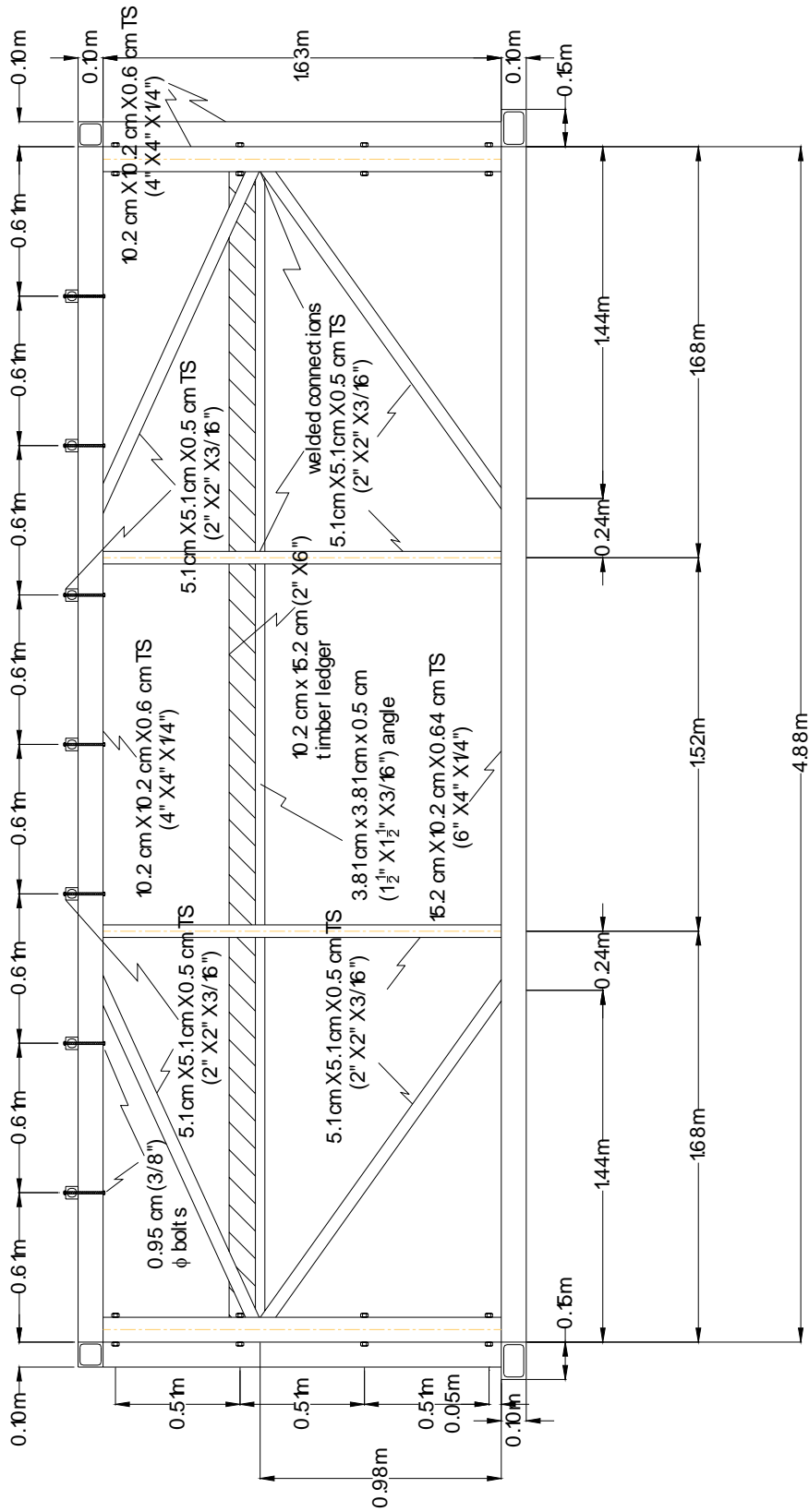


**FIGURE 3-3 Elevation of the East side of the frame**

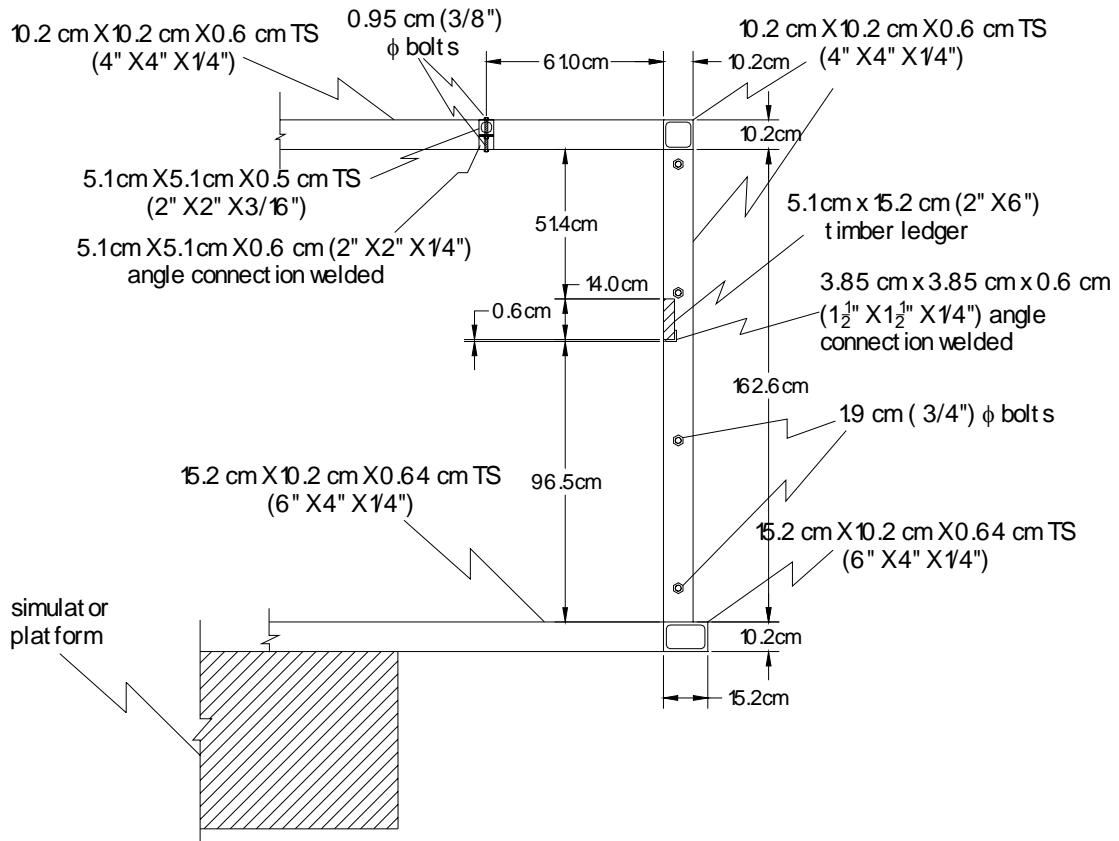


**FIGURE 3-4 Detail A-A', frontal view of frame**

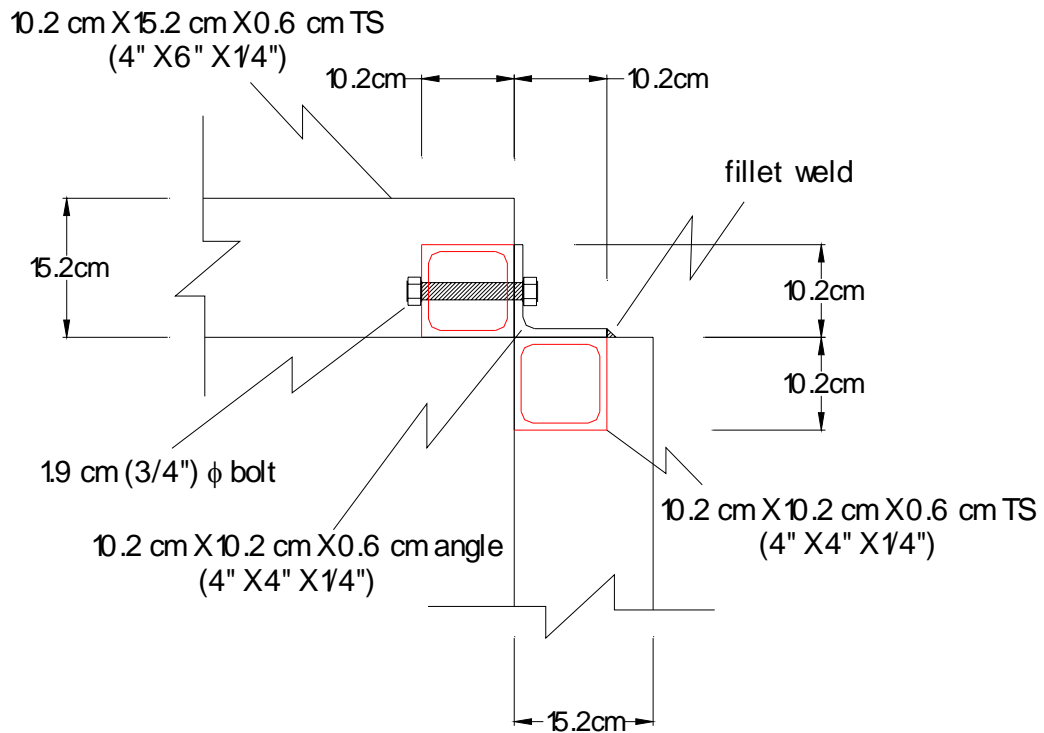
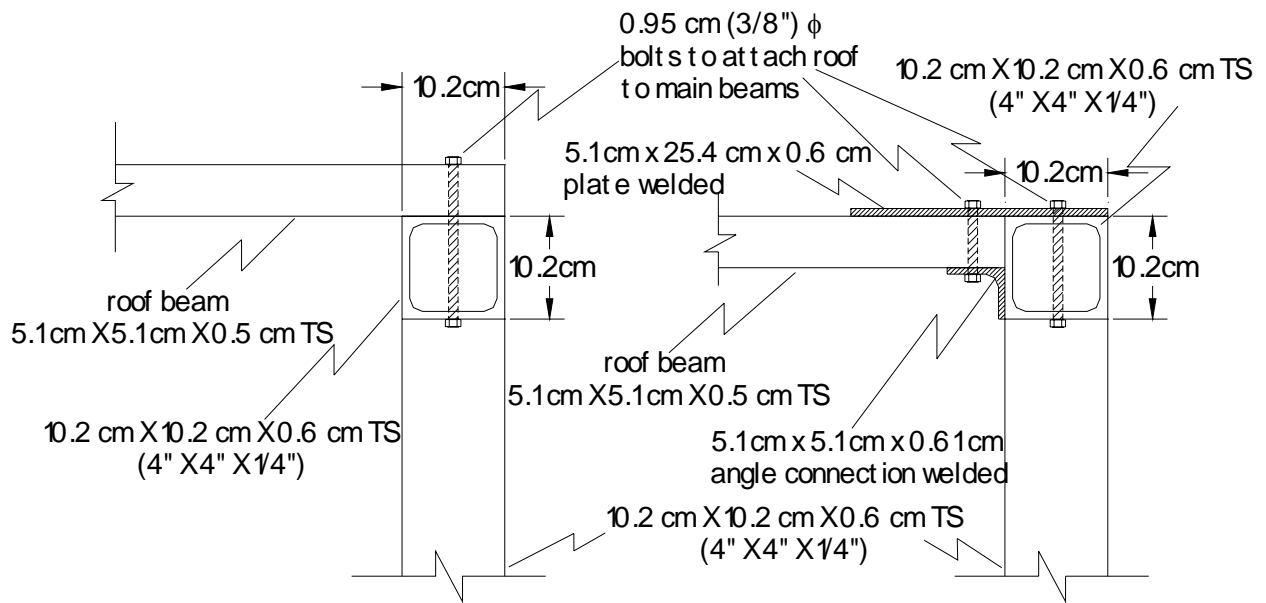


**FIGURE 3-5 Detail B, connection of corner of the frame**



a) connection in the East-West direction      b) connection in the North-South direction

**FIGURE 3-6 Detail C, connection of the roof with main beams**

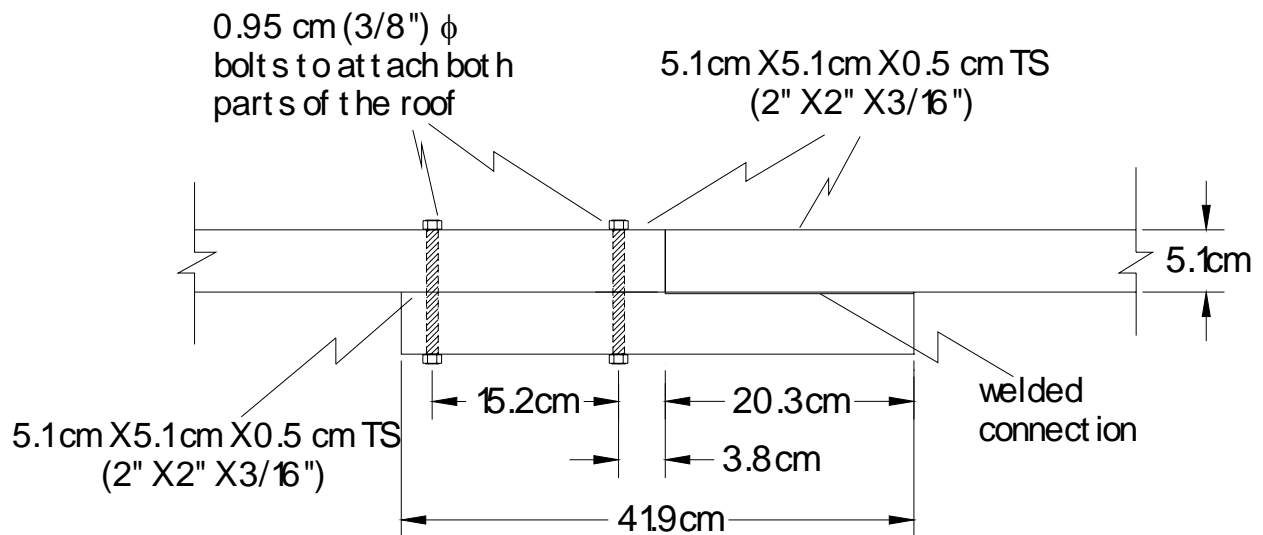


**FIGURE 3-7 Detail D, roof framing connection in the East-West direction**

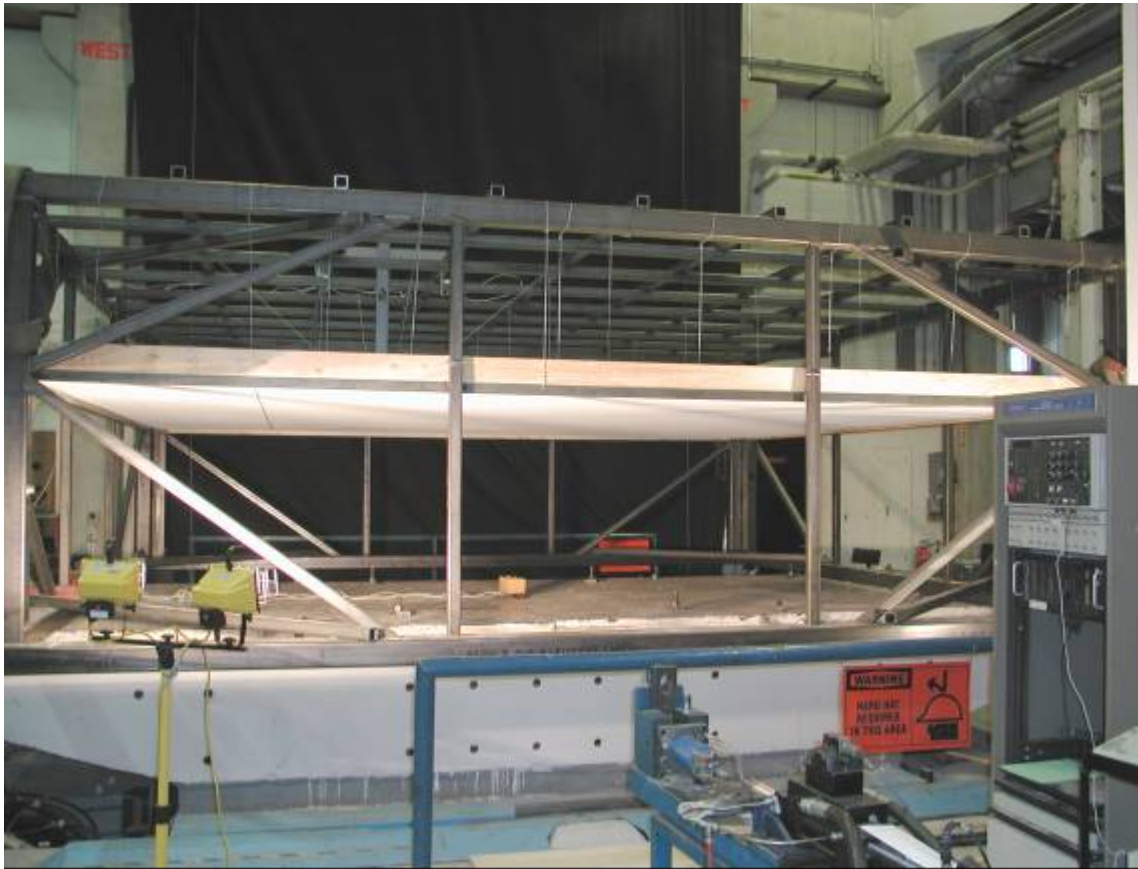


**FIGURE 3-8 Test frame mounted on the simulator at the University at Buffalo**



**FIGURE 3-9** Roof connection to the main beams on the North side of the frame

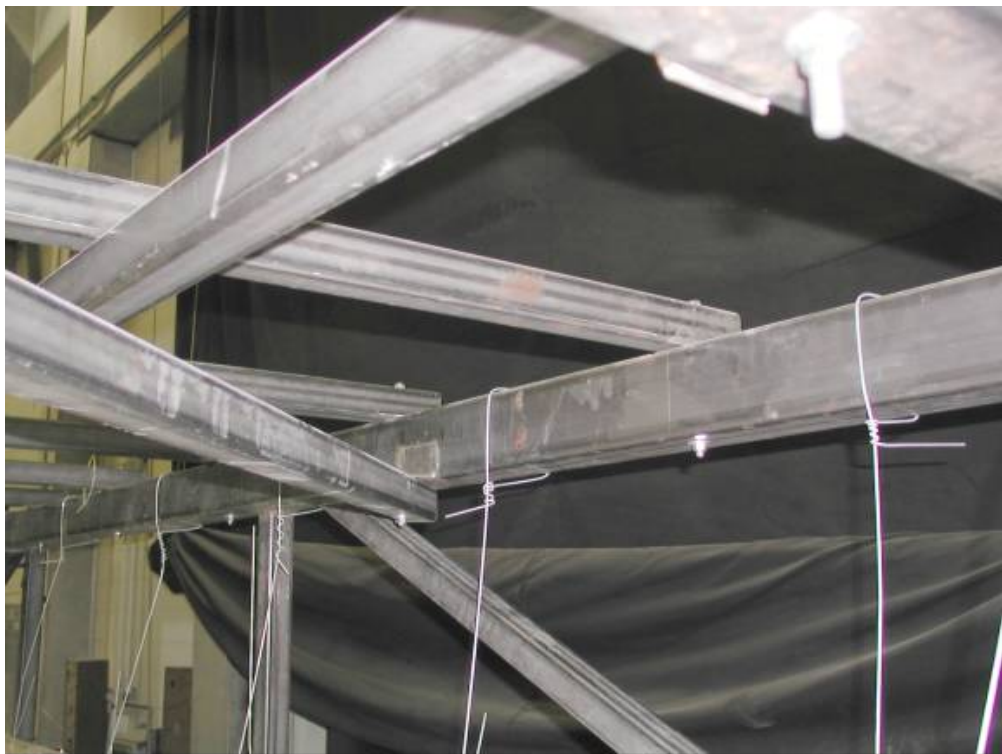


**FIGURE 3-10** Roof connection to the main beams on the West side of the frame



### **3.3 Specimen Descriptions**

#### **3.3.1 Introduction**

Each ceiling system consisted of two key parts: a suspension system, and tiles. In some configurations retention clips were added to the ceiling systems. All the specimens used in the development of this study (grid components, tiles and retention clips) were manufactured and provided by Armstrong World Industries Inc.

#### **3.3.2 Suspension System**

The ceiling systems were installed in a grid that was hung with suspension wires from the top of the test frame. The grid was constructed with the Armstrong PRELUDE XL 23.8 mm (15/16 in.) exposed tee system.

The ceiling suspension system was installed in the test frame per ASTM E580-00 (ASTM, 2000). A 5.1-cm (2-in.) wall molding was attached to the perimeter timber ledger. The main runners and cross runners were attached to the wall molding with rivets on the South and West sides of the frame, while the runners on the North and East sides floated free. The main runners were installed in the North-South direction at spacing of 1.22 m (48 in.) on center. The 1.22 m (4 ft) cross runners were installed in the East-West direction at spacing of 61 cm (24 in.) on center, whereas the 61cm (2 ft) cross runners were installed in the North-South directions at a spacing of 1.22 m (48 in.) on center. The ends of main runners and cross members were tied together using stabilizer bars located within 20.3 cm (8 in.) of each wall molding. Table 3-1 presents summary information of each of the components of the ceiling support grid.

**TABLE 3-1 Summary information on components of the ceiling suspension system**

<i>Component</i>	<i>Item no.</i>	<i>Description</i>	<i>Dimensions (cm)</i>	<i>Comments</i>
Main beams	7301	3.66 m (12 ft) long heavy duty main beam	366 x 2.4 x 4.3	Double web with peaked roof top bulb and bottom flange with pre-finished steel capping
122 cm (4 ft) cross tees	XL7348	1.22 m long cross tee	122 x 2.4 x 3.5	Double web with peaked roof top bulb, bottom flange with pre-finished steel cap and override at each end
61 cm (2 ft) cross tees	XL7328	61 cm long cross tee	61 x 2.4 x 3.5	Double web with peaked roof top bulb, bottom flange with pre-finished steel cap and override at each end
Wall molding	7810	3.05 m (10 ft) long hemmed angle molding	305 x 5.1 x 5.1	5.1-cm (2-in) hemmed angle molding with pre-finished exposed flanges
Stabilizer bars	7425	61 cm (2 ft) long stabilizer bar	61 x 0.95	C-channel shape with notches at 61 cm and with locking tabs at the notches

Suspension (hanger) wires of soft annealed galvanized #12 gage steel were spaced at 1.22 m (48 in.) on center. All hanger wires were attached to the ceiling suspension member and to the roof of support frame with a minimum of 3 turns within 3 inches of the connection. The terminal end of all cross runners and main runners were independently supported with #12 gage hanger wire within 20.3 cm (8 in.) of all walls. Figure 3-11 presents a diagram of the suspension grid.

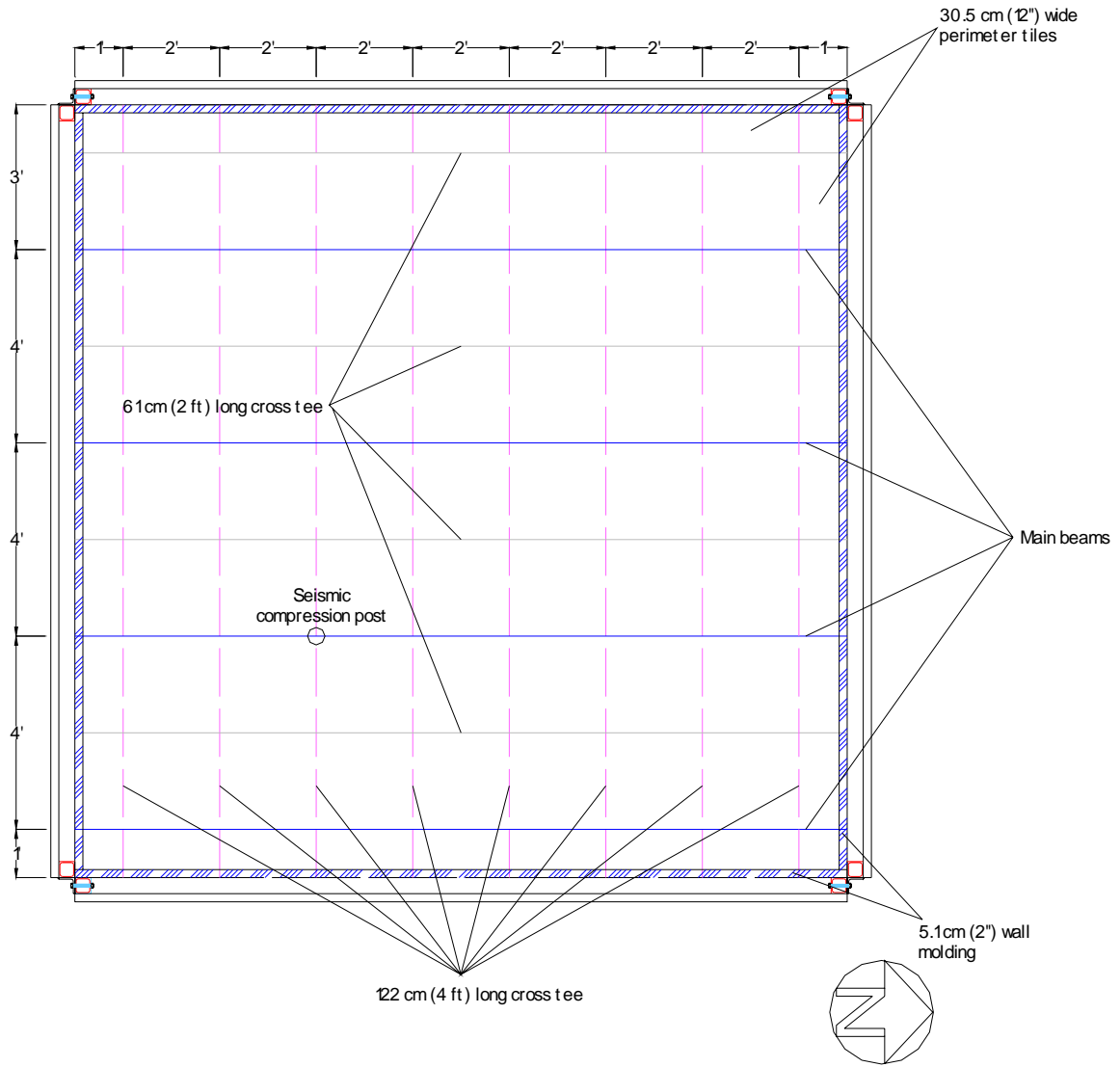


**FIGURE 3-11 Drawing of the ceiling suspension grid**

A compression post was placed 1.52 m (5 ft) away from the South and the East sides of the frame (see figures 3-11 and 3-12). The compression post was fastened to the main runner located in this position and extended up to the structural frame using 45° diagonal cables as shown in figure 3-12. The diagonal restraints were installed using four #12 gage wires secured to the main runner within 2 inches of the cross runner and were splayed 90° from each other at an angle less than 45° from the plane of the ceiling.

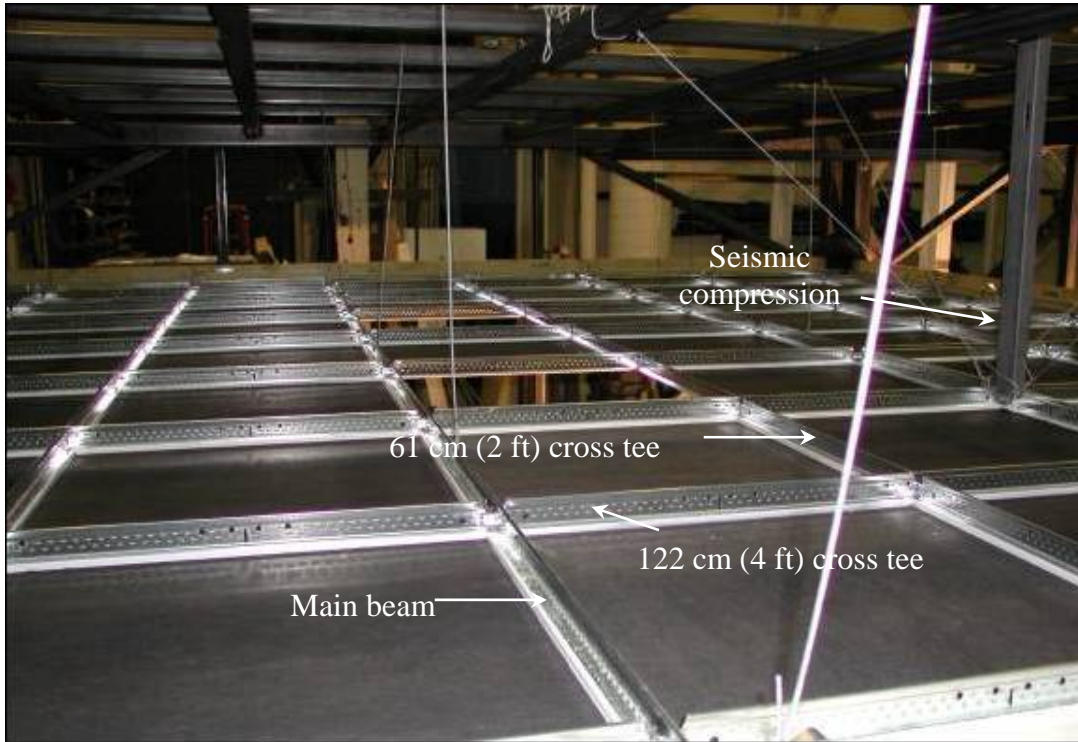


**FIGURE 3-12 Ceiling suspension grid**

### 3.3.3 Tiles

Since the actual size of the tiles may differ from the nominal size depending on quality control in the manufacturing process, two types of tiles were used for fragility testing in this study. Based on personal communication with practicing engineers and manufacturers, ceiling tiles are considered to be of *normal* size if their plan dimensions are not smaller than the nominal dimensions by more than 6.4 mm (1/4 in.) If the tiles are smaller, they are considered to be *undersized*. The tiles were measured in size and weight prior to testing.

One of the tiles tested was the Armstrong Fine Fissured Humigard Plus tile (Armstrong item no. 1732). This tile was smaller than the nominal size by at least 12.7 mm (1/2 in.) and was therefore considered to be an *undersized* tile. The other tile used in this study was the Armstrong Dune Humigard Plus tile (Armstrong item no. 1774). This tile was a *normal* sized tile. Figure 3-13 is a photograph of the Dune Humigard Plus tile.

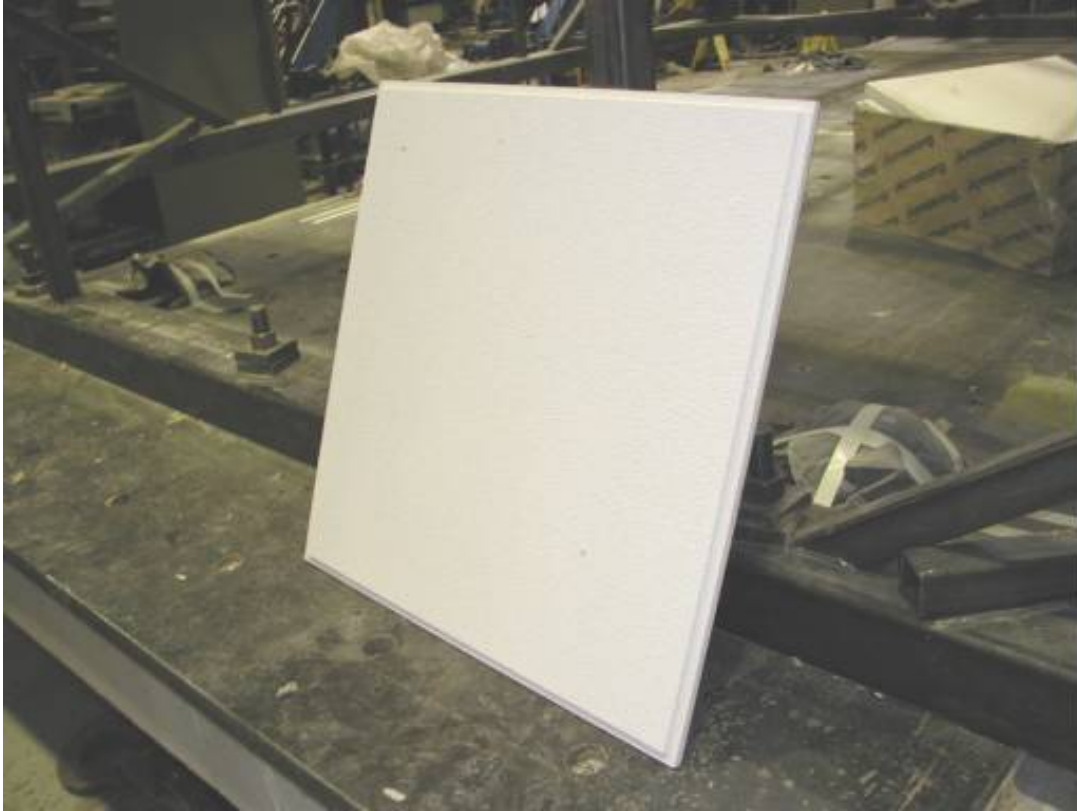


**FIGURE 3-13 Tile Dune Humigard Plus (Armstrong item no. 1774)**

Table 3-2 presents summary information on each of the two tiles used in this study. A total of 49 tiles were installed in the inner seven rows (seven tiles in each row). Cut tiles were used in the perimeter rows of the ceiling system.

**TABLE 3-2 Summary information on the ceiling tiles**

<i>Tile name</i>	<i>Description</i>	<i>Armstrong item no.</i>	<i>Panel dimensions (cm)</i> <i>[B, D, T]<sup>1</sup></i>		<i>Weight (kg/tile)</i>
			<i>Nominal size</i>	<i>Actual size</i>	
Fine Fissured	HumiGuard Plus mineral fiber tile	1732	[61 x 61 x 1.6]	[59.7 x 59.7 x 1.6]	1.3
Dune	HumiGuard Plus mineral fiber tile	1774	[61 x 61 x 1.6]	[60.3 x 60.3 x 1.6]	1.7

<sup>1</sup> B, D and T: breadth, depth and thickness, respectively

### 3.3.4 Retention Clips

Clips similar to those shown in figure 3-14 (Armstrong item no. 414) were installed to investigate possible improvements in the seismic performance of suspended ceiling systems. These clips can be attached to main beams or cross tees behind lay-in ceiling tiles and help to prevent panel dislodgement. In this study, the clips were installed on the 1.22 m (4 ft) long cross tees of the grid as shown in figure 3-15. The systems in which the clips were installed are identified in Chapter 6.

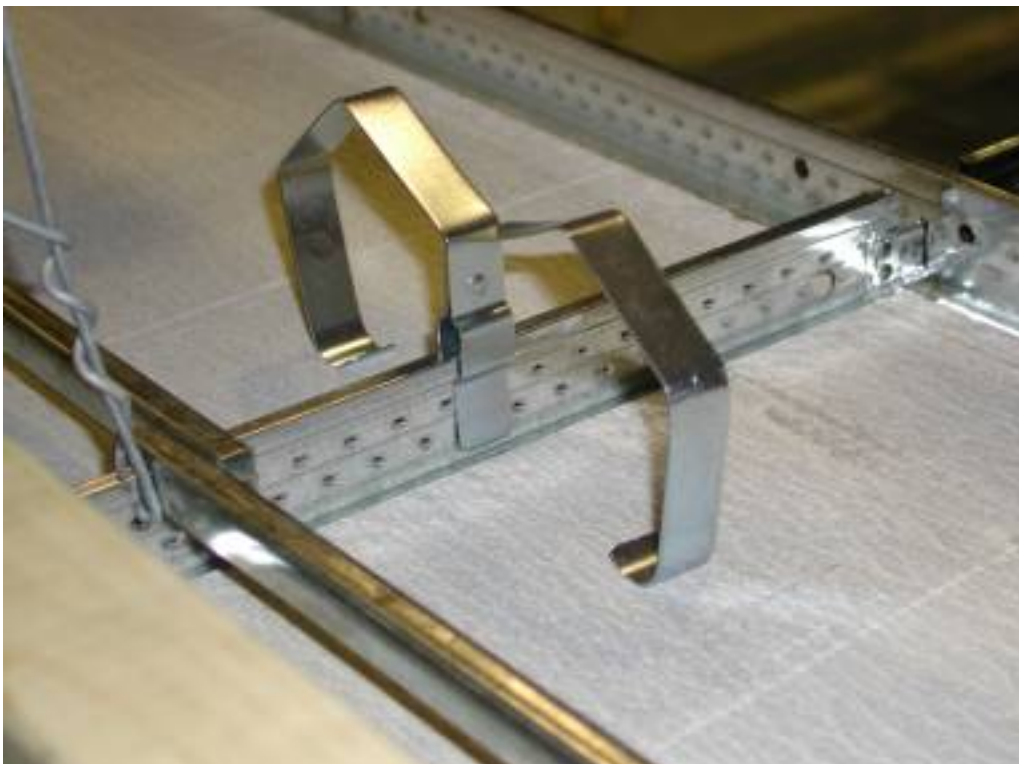


**FIGURE 3-14 Retention clips**



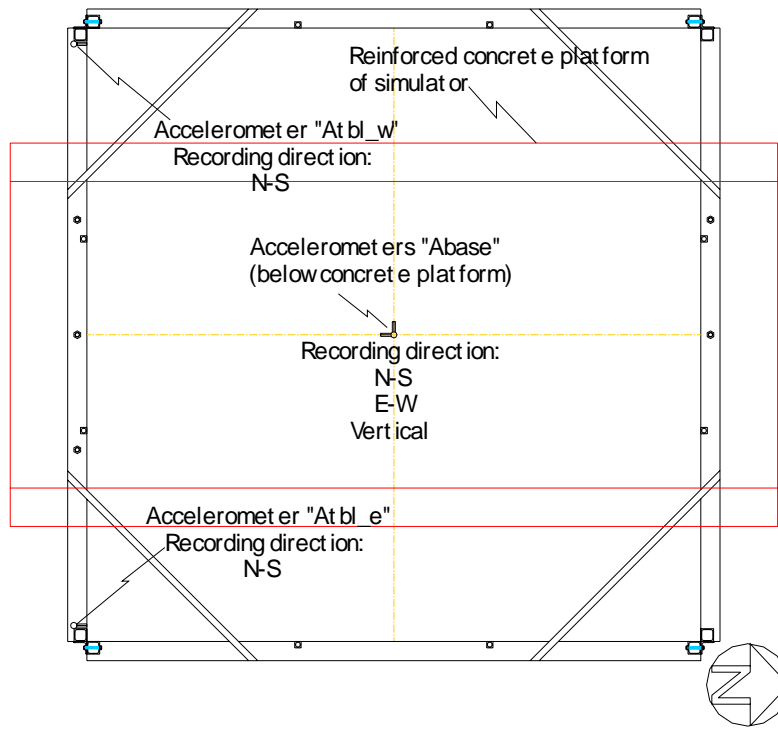
**FIGURE 3-15 Array of clips attached to the 1.22 m (4 ft) cross runners**

### **3.4 Instrumentation**

Accelerometers and displacement transducers were used to monitor the response of the simulator platform, the test frame and the ceiling support grid, in each ceiling system. Accelerometers were located in different locations of the simulator platform (see figure 3-16a), on top of the test frame (see figures 3-16b and 3-17a) and on the ceiling support grid (see figures 3-16c and 3-17b). Table 3-3 presents detailed information on the characteristics and locations of the accelerometers.

The horizontal displacements of the test frame and the earthquake simulator were measured with linear variable displacement transducers (LVDT). The actuators that drive the simulator platform are each equipped with two transducers (one LVDT and one accelerometer) installed in the actuator. The transducers used to measure the horizontal displacement of the frame were located on the South side of the frame. Three LVDTs were located on the top of the frame, one on each of the corners of the South side of the frame and one in the center of that side of the frame. A fourth LVDT was located in the middle of the bottom of the South side of the test frame. Table 3-3 lists

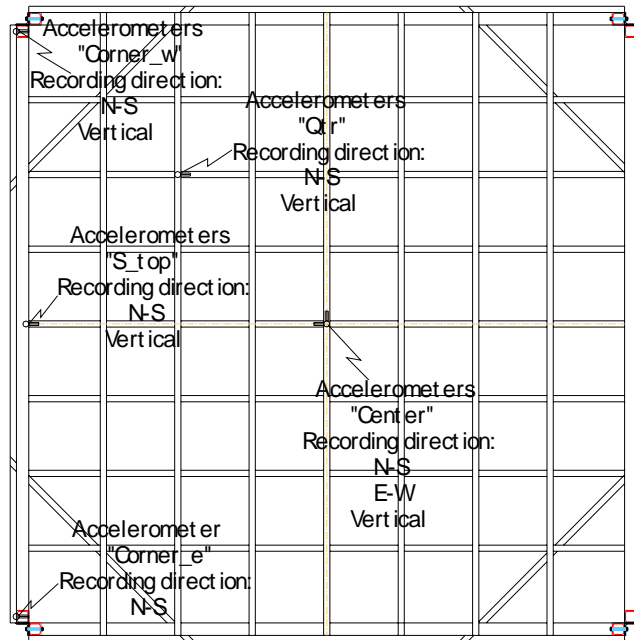
the transducers used to monitor the displacements of the simulator and the test frame. Figures 3-18 and 3-19 show the location of each transducer.



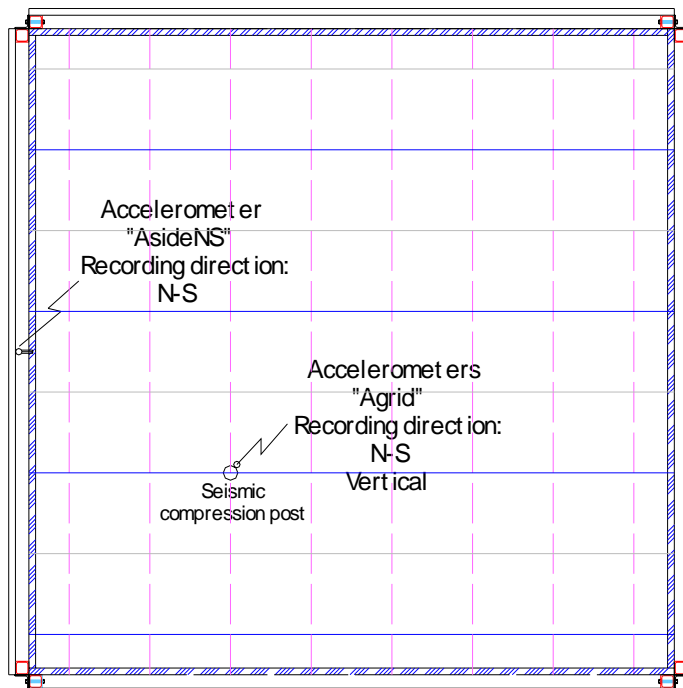
**a) accelerometers on the simulator platform**

**FIGURE 3-16 Accelerometers on the test frame**



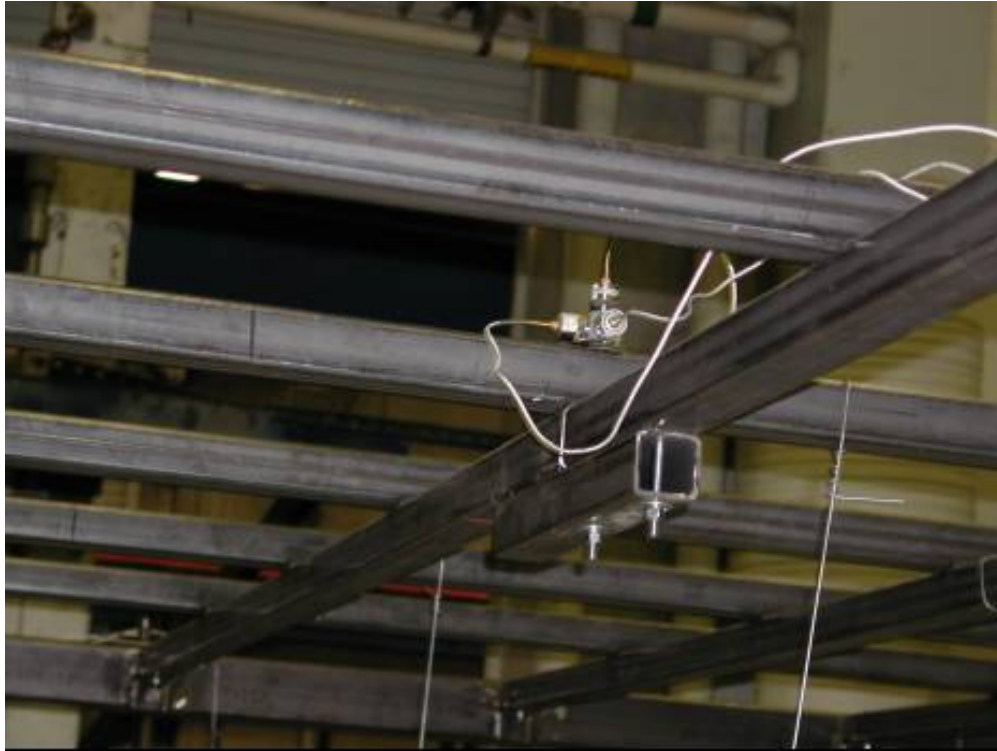


**b) accelerometers on the top of the test frame**



**c) accelerometers on the ceiling support grid**

**FIGURE 3-16 Accelerometers on the test frame (cont.)**

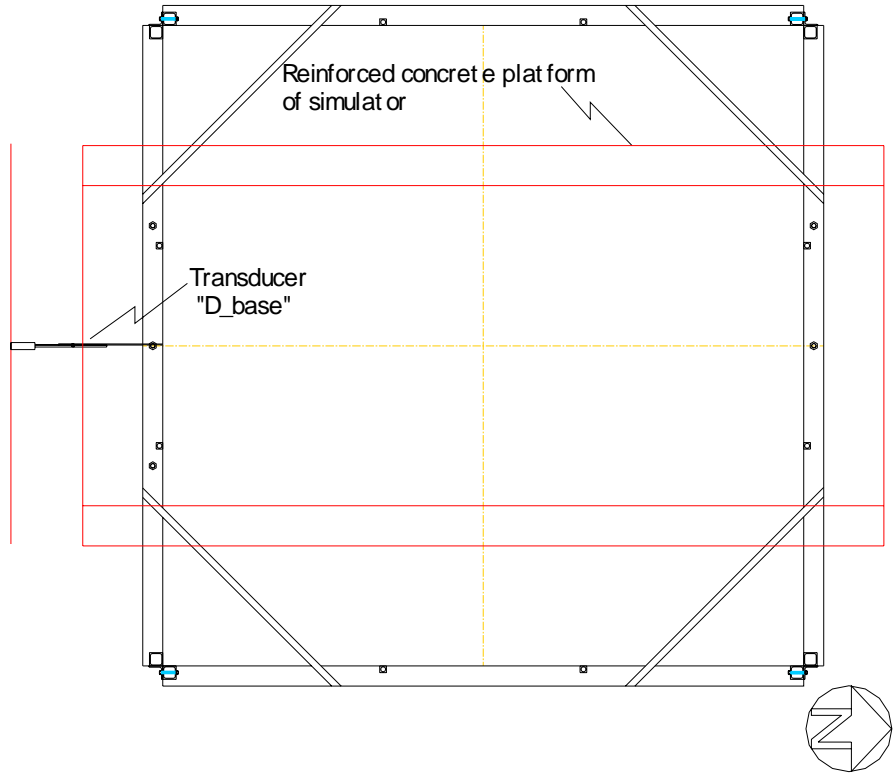


**a) accelerometers in the center at the top of the test frame**

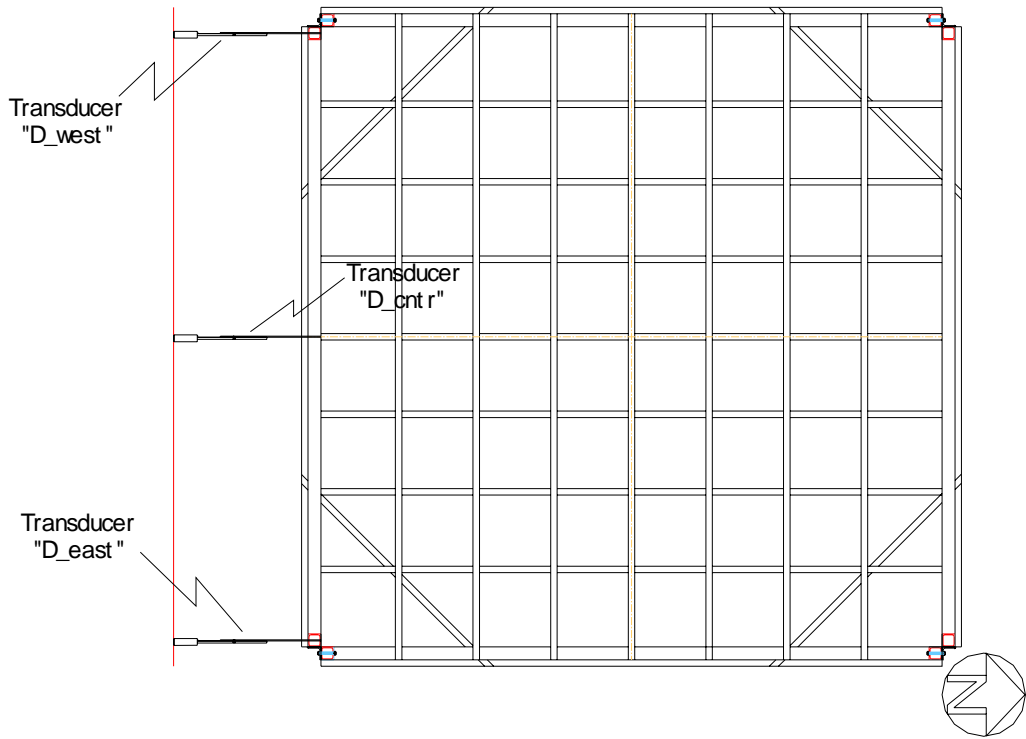


**b) accelerometers on the ceiling support grid**

**FIGURE 3-17 Accelerometers monitoring the response of the test assembly**

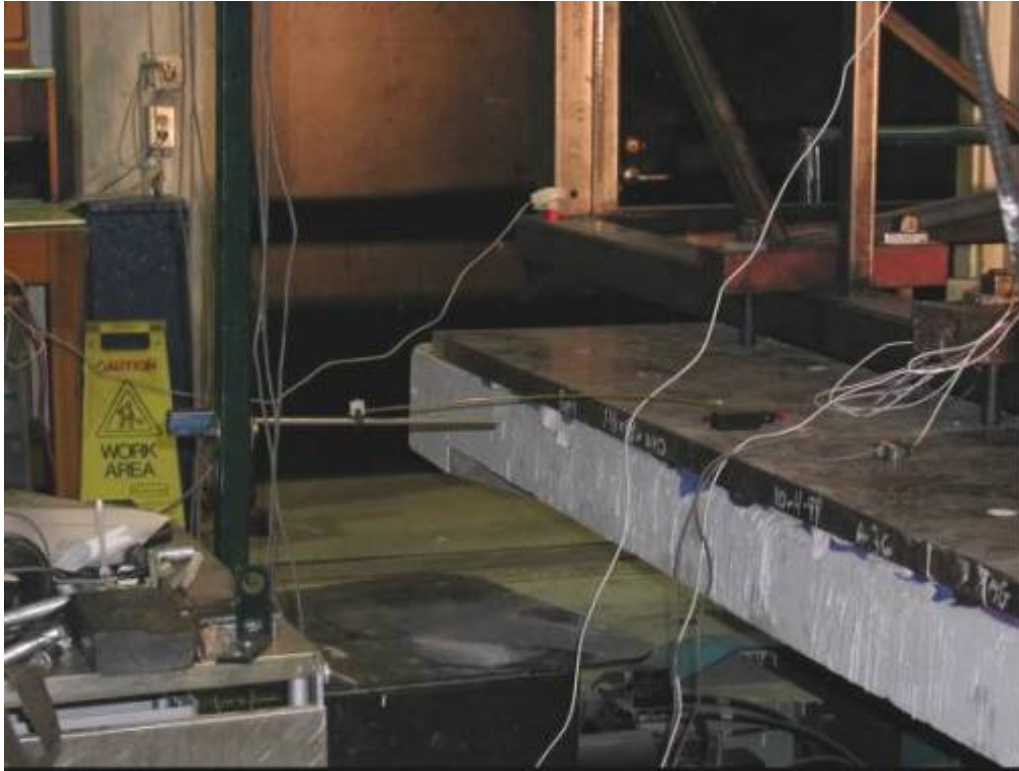


**a) transducers at the base of the frame**



**b) transducers at the top of the frame**

**FIGURE 3-18 Displacement transducers on the test frame**



**a) transducers at the base of the frame**



**b) transducers at the top of the frame**

**FIGURE 3-19 Displacement transducers mounted on the test frame**

**TABLE 3-3 Transducers used for the fragility testing program**

<i>ID</i>	<i>Type of measurement</i>	<i>Direction of recording</i>	<i>Range</i>	<i>Sensitivity</i>	<i>Location on the test frame</i>
D_west	Displacement	Horizontal N-S	+/- 20.8 cm	6.3E-4 cm	West side of top of frame
D_cntr	Displacement	Horizontal N-S	+/- 20.8 cm	6.3E-4 cm	Center of top of frame
D_east	Displacement	Horizontal N-S	+/- 20.8 cm	6.3E-4 cm	East side of top of frame
D_base	Displacement	Horizontal N-S	+/- 12.9 cm	3.8E-4 cm	Center of the North side of base of frame
Abase_NS	Acceleration	Horizontal N-S	+/- 17.7 g	0.002 g	Center of the simulator, below concrete platform
Abase_V	Acceleration	Vertical	+/- 13.1 g	4.0E-20 g	Center of the simulator, below concrete platform
Abase_EW	Acceleration	Horizontal E-W	+/- 15.2 g	4.6E-4 g	Center of the simulator, below concrete platform
Center_H	Acceleration	Horizontal N-S	+/- 18.7 g	0.001 g	Center of the roof of testing frame
Center_V	Acceleration	Vertical	+/- 11.8 g	0.01 g	Center of the roof of testing frame
Qtr_H	Acceleration	Horizontal N-S	+/- 18.46 g	5.0E-4 g	Roof of testing frame at 4 ft from the West and South sides of the frame
Qtr_V	Acceleration	Vertical	+/- 23.8 g	7.0E-4 g	Roof of testing frame at 4 ft from the West and South sides of the frame

**TABLE 3-3 Transducers used for the fragility testing program (cont'd)**

<i>ID</i>	<i>Type of measurement</i>	<i>Direction of recording</i>	<i>Range</i>	<i>Sensitivity</i>	<i>Location on the test frame</i>
Corner_w_H	Acceleration	Horizontal N-S	+/- 30.6 g	0.004 g	SW top corner of testing frame
Corner_w_V	Acceleration	Vertical	+/- 26.4 g	8.0E-4 g	SW top corner of testing frame
Corner_e_H	Acceleration	Horizontal N-S	+/- 17.7 g	5.4E-4 g	SE top corner of testing frame
Table_H	Acceleration	Horizontal N-S	+/- 2 g	6.25E-5 g	Actuator of simulator platform (horizontal control acceleration)
Table_V	Acceleration	Vertical	+/- 4 g	1.25E-4 g	Actuator of simulator platform (vertical control acceleration)
S_top_H	Acceleration	Horizontal N-S	+/- 9.3 g	2.0E-20 g	Middle of the South side of top of frame
S_top_V	Acceleration	Vertical	+/- 21.8 g	0.002 g	Middle of the South side of top of frame
Atbl_w_H	Acceleration	Horizontal N-S	+/- 16.4 g	0.013 g	SW bottom corner of testing frame
Atbl_e_H	Acceleration	Horizontal N-S	+/- 15.7 g	0.013 g	SE bottom corner of testing frame
AsideNS	Acceleration	Horizontal N-S	+/- 25.2 g	0.002E-4 g	Middle of intermediate angle of the South side of frame
Agrid_NS	Acceleration	Horizontal N-S	+/- 25.0 g	7. 6E-4 g	Bottom of the compression post in suspension system
Agrid_V	Acceleration	Vertical	+/- 23.7 g	0.002 g	Bottom of the compression post in suspension system

## **CHAPTER 4**

### **DYNAMIC CHARACTERISTICS OF THE TEST FRAME**

#### **4.1 Introduction**

The dynamic characteristics of the test frame described in Chapter 3 were evaluated along the two programmable axes of the earthquake-simulator platform, namely, the North-South and vertical directions. Several methods have been used in past studies to obtain dynamic properties of structures using earthquake simulators (Bracci et al., 1992). Three of those methods were used to identify the dynamic properties of the test frame: free vibration and two forced vibration tests. The free vibration test was performed on the test frame by means of a snap-back assembly. Forced vibration tests were conducted using resonance-search and white noise inputs. The dynamic properties of the test frame (no ceiling system installed) were obtained to compare them with the dynamic properties of the test frame with the ceiling systems installed. The three testing methods are discussed in the subsections below.

#### **4.2 Snap-Back Test**

##### **4.2.1 Horizontal Direction**

The test frame was given a small lateral displacement by loading it at the roof level via two cables attached to the upper beam on the North side of the test frame. The two cables were attached to a fast release device, forming a “Y” configuration. The fast release device was connected to a turnbuckle (which was inserted to adjust the frame displacement) and to a reaction wall. The reaction wall is located at the North side of the test frame and is anchored to the laboratory floor. A load cell was inserted between the turnbuckle and the fast release device. Figure 4-1 shows a photograph of the configuration of the set up for this test.



**FIGURE 4-1 Configuration of the snap-back test in the horizontal direction**

The earthquake simulator was first displaced in the direction of the reaction wall and the turnbuckle was adjusted to develop a significant tensile force in the two cables. The earthquake simulator was then displaced in the opposite direction to develop a significant lateral displacement at the top of the test frame. The trigger in the fast release device was activated and the free vibration of the frame was then recorded by the data acquisition system. Figure 4-2 shows the acceleration history of the free vibration of the test frame in the horizontal direction.



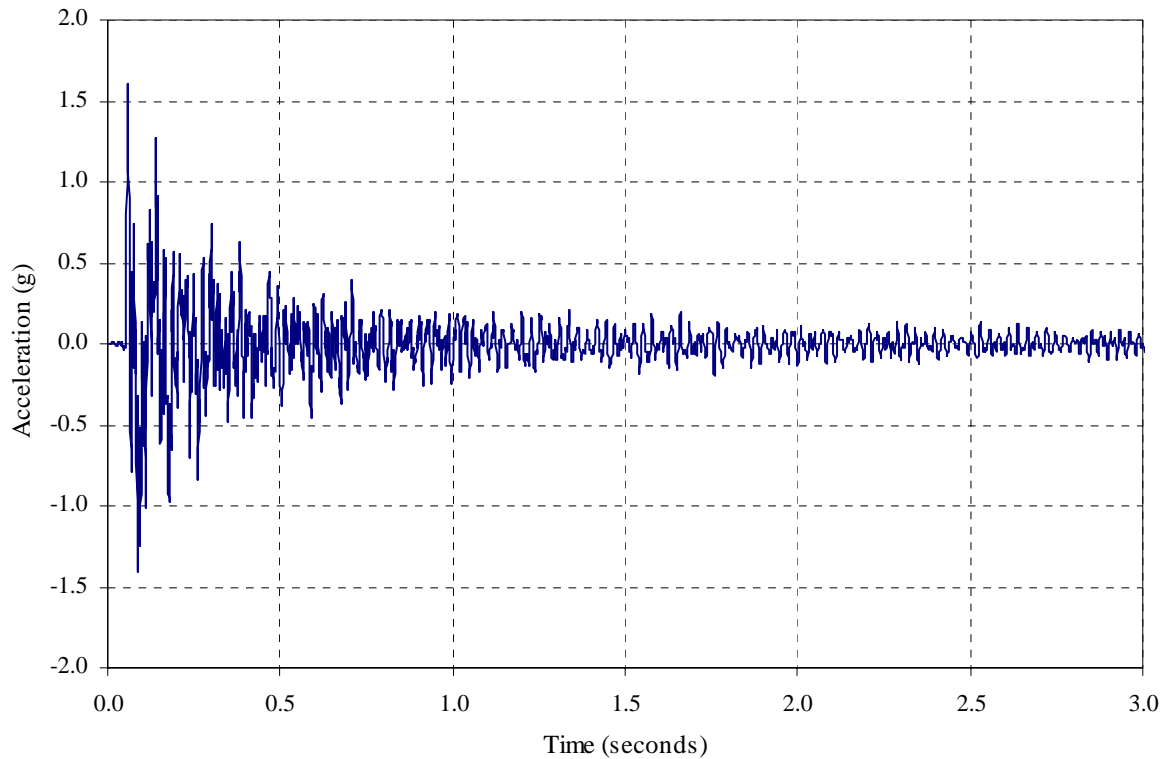


**FIGURE 4-2 Acceleration history of free vibration in the horizontal direction**

#### **4.2.2 Vertical Direction**

In the vertical direction, the frame displacement was introduced by means of a cable attached to the center of the frame grid. The cable was attached to the fast release device and to a chain attached to the laboratory crane. Figure 4-3 shows a photograph of the set up for this test.

The crane hook was then raised, providing a small vertical displacement in the frame. The trigger of the fast release device was then activated and the free vibration of the frame was recorded. Figure 4-4 shows the acceleration history of the free vibration of the test frame in the vertical direction.



**FIGURE 4-3 Configuration of the snap-back test in the vertical direction**

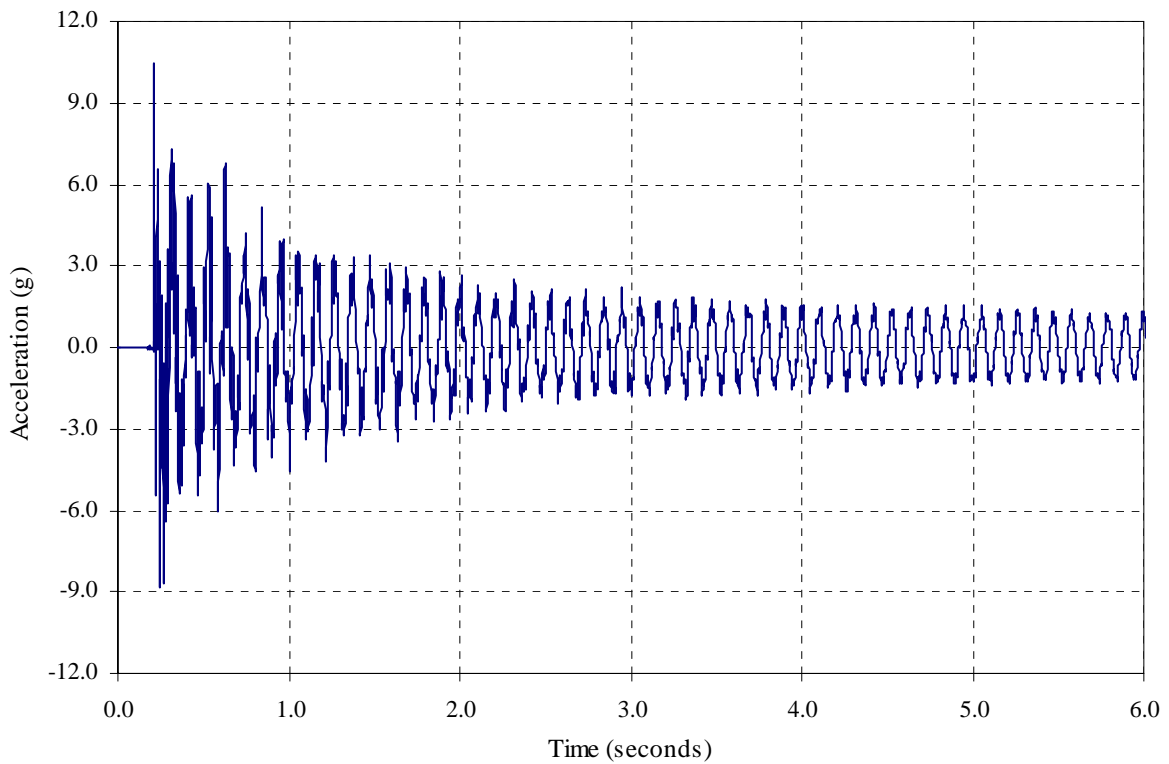


**FIGURE 4-4 Acceleration history of free vibration in the vertical direction**

### 4.2.3 Procedure to Obtain Periods and Damping Ratios

The natural periods and damping ratios in the horizontal and vertical directions were estimated using the following procedure:

1. The acceleration histories in the direction under consideration were transformed into the frequency domain using a Discrete Fast Fourier Transform (DFFT) algorithm in Matlab (Mathworks, 1999).
2. The first peak in the Fourier amplitude spectrum for each history was used to determine the natural frequency of the test frame.
3. Appropriate roll-on and roll-off frequencies were selected above and below the peaks in the Fourier amplitude spectrum and the band-passed frequency domain response was then transformed back into the time domain using an Inverse Fast Fourier Transform (IFFT) algorithm in Matlab.
4. The band-passed acceleration history was treated as the free vibration decay response of a single-degree-of-freedom system. The modal damping ratio ( $\xi$ ) was then calculated using the logarithmic decrement method (Clough and Penzien, 1993):

$$\xi = \frac{1}{2\pi j} \ln \frac{\ddot{u}_i}{\ddot{u}_{i+j}} \quad (4-1)$$

where  $\ddot{u}_i$  is the acceleration at cycle  $I$  and  $\ddot{u}_{i+j}$  is the acceleration after  $(i+j)$  cycles.

Figure 4-5 shows the Fourier amplitude spectra and figure 4-6 shows the free vibration decay in the first mode in the horizontal direction. Figures 4-7 and 4-8 show the same information in the vertical direction. From figures 4-5 and 4-7, the natural frequencies were estimated to be 12.5 Hz and 9.6 Hz for the horizontal and vertical directions, respectively. From figures 4-6 and 4-8, the fundamental mode damping ratios in the horizontal and vertical directions were estimated to be 2.6% and 0.5%, respectively.

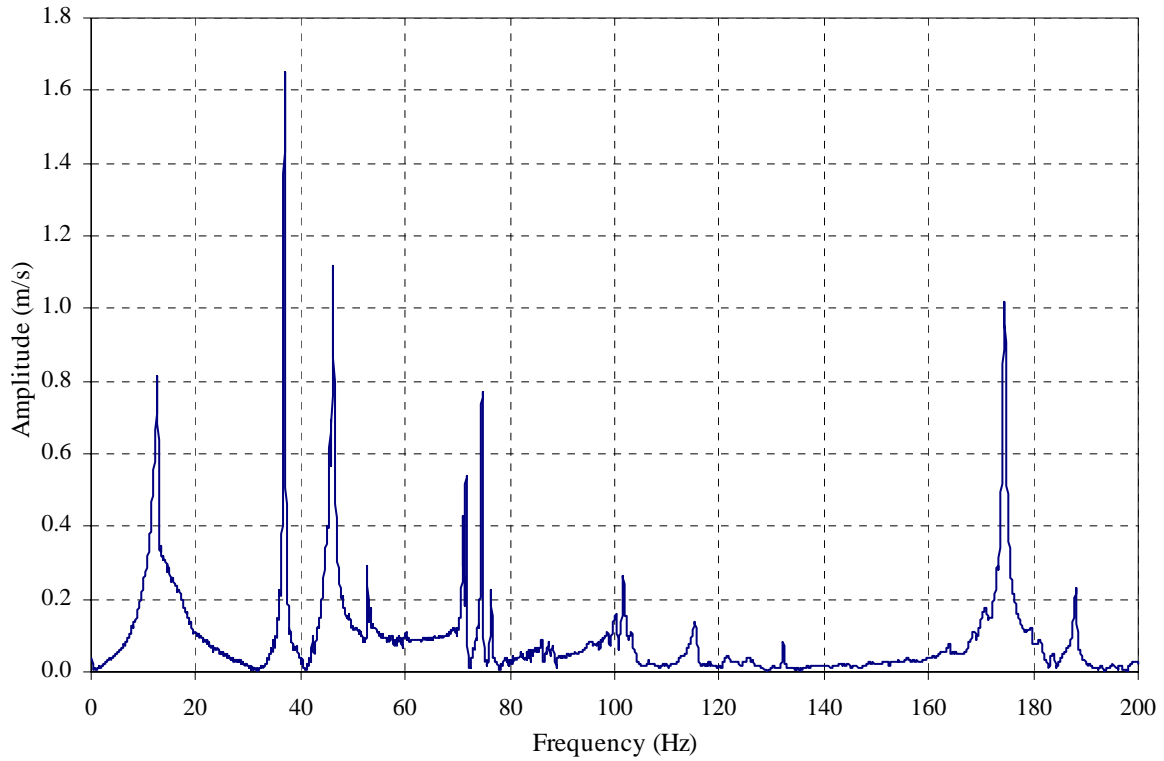


**FIGURE 4-5 Fourier amplitude spectra for the horizontal snap-back test**

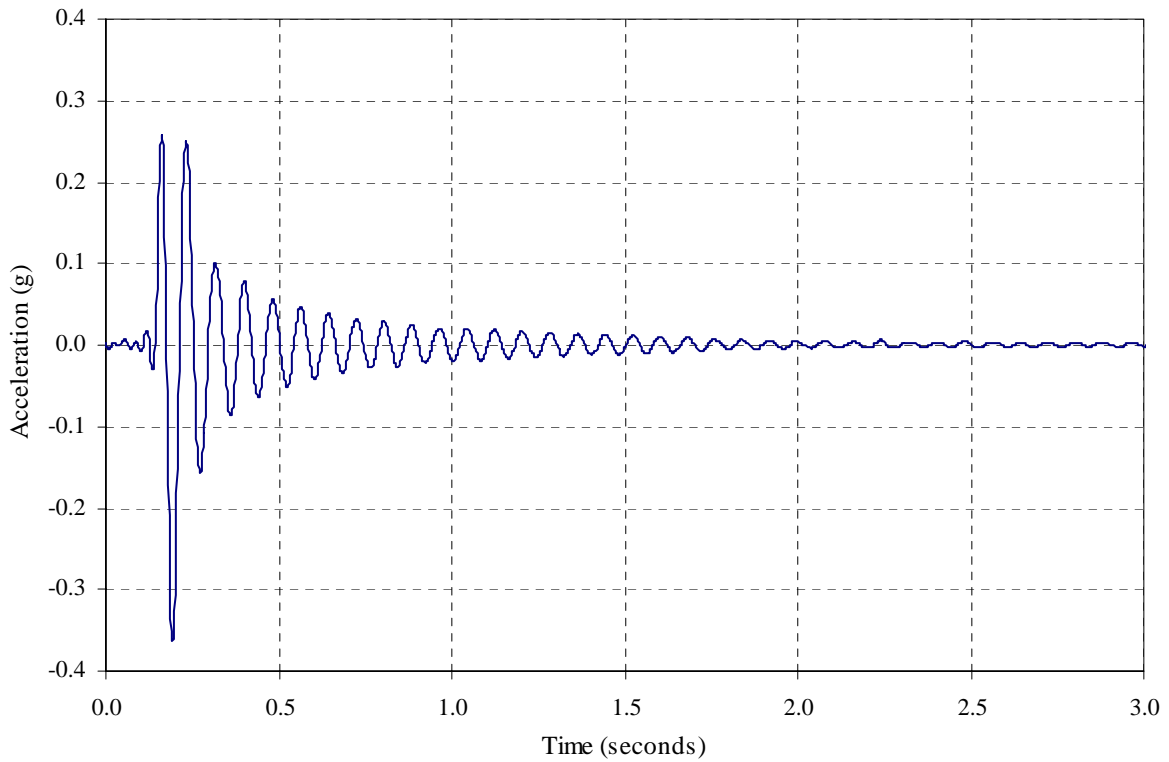


**FIGURE 4-6 First mode free vibration decay in the horizontal direction**

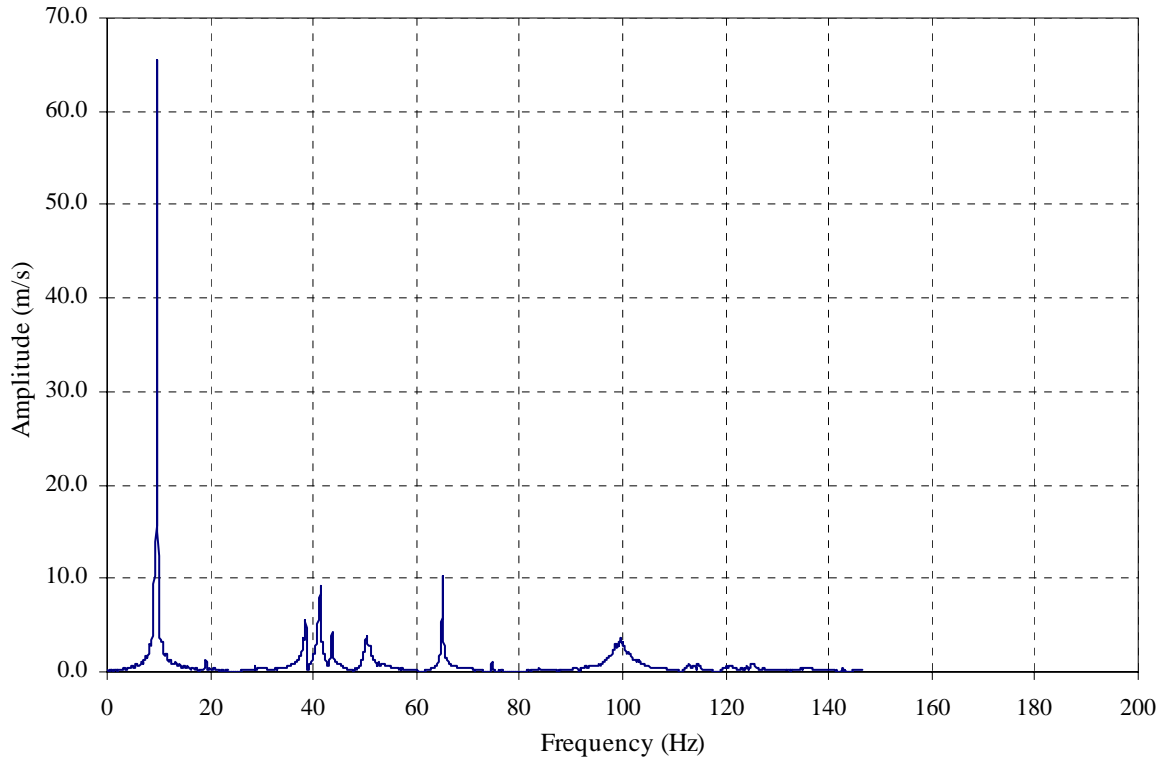


**FIGURE 4-7 Fourier amplitude spectra for the vertical snap-back test**

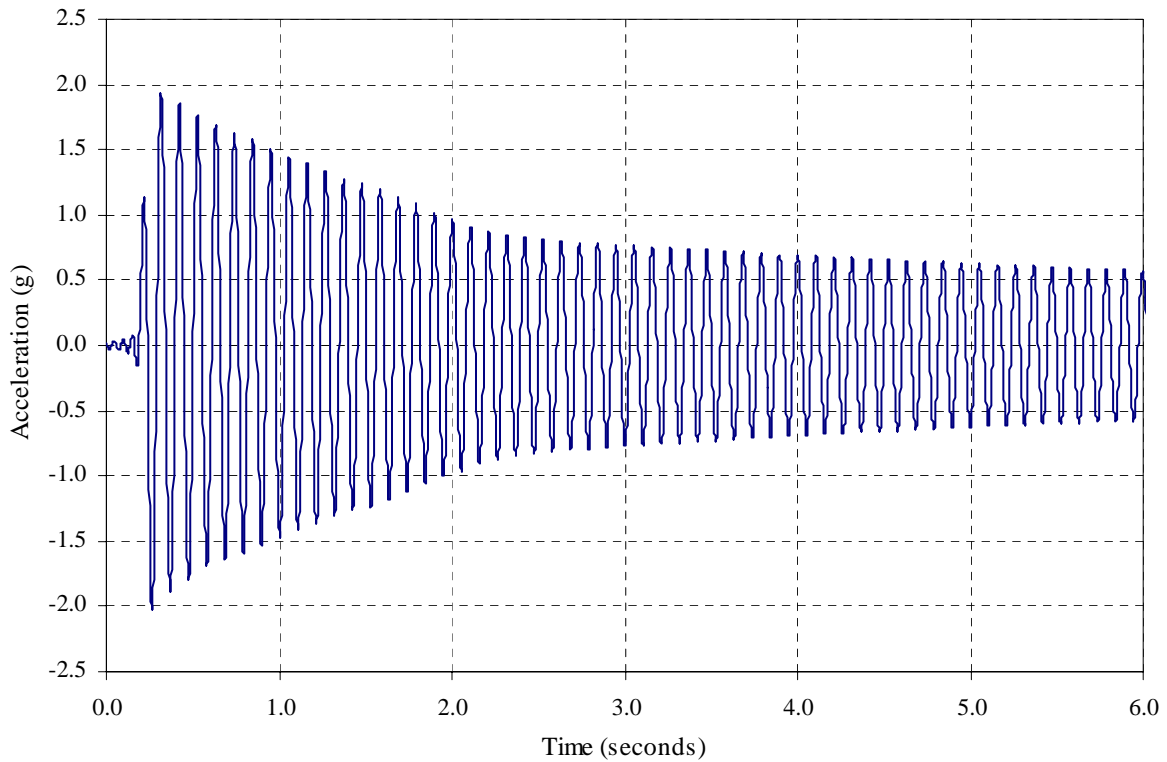


**FIGURE 4-8 First mode free vibration decay in the vertical direction**

### 4.3 Frequency Sweep

This method consists of obtaining the forced vibration response of the test frame using a varying frequency signal. The earthquake simulator provided a constant maximum acceleration in the frequency range under consideration. The acceleration was computed using 6 octaves in the frequency range from 0.5 to 32 Hz with amplitude of 0.1g. The total duration of the input record was 3 minutes (2 octaves per minute) and the sample rate was 256 Hz (0.0039 seconds). Figure 4-9 presents the first 90 seconds of the input to the earthquake simulator.

The acceleration histories of the table input and the frame response output were converted into the frequency domain using the DFFT algorithm. The records contained a considerable amount of noise. Filtering in the frequency domain was performed because the dynamic properties of the test frame could not be identified easily due to the noise.

The filtering was performed by means of a moving average filter in the frequency domain. This filter is described in section 4.3.1 below. The filtered signal of the frequency domain response of the frame was normalized by the filtered frequency domain input of the simulator to obtain a transfer function. The frequency associated with the peak response and the half power bandwidth method (Clough and Penzien, 1993) were then used to evaluate the natural frequency and damping ratio. This procedure was applied in both the horizontal and vertical directions.

The moving average filter is implemented by a convolution technique (also called finite impulse record). The moving average filter averages a number of points from the input signal (Smith, 1999) as follows:

$$y[i] = \frac{1}{M} \sum_{j=a}^b x[i + j] \quad (4-2)$$

where  $y [.]$  is the output signal,  $x [.]$  is the input signal, and  $M$  is the number of points in the calculation.

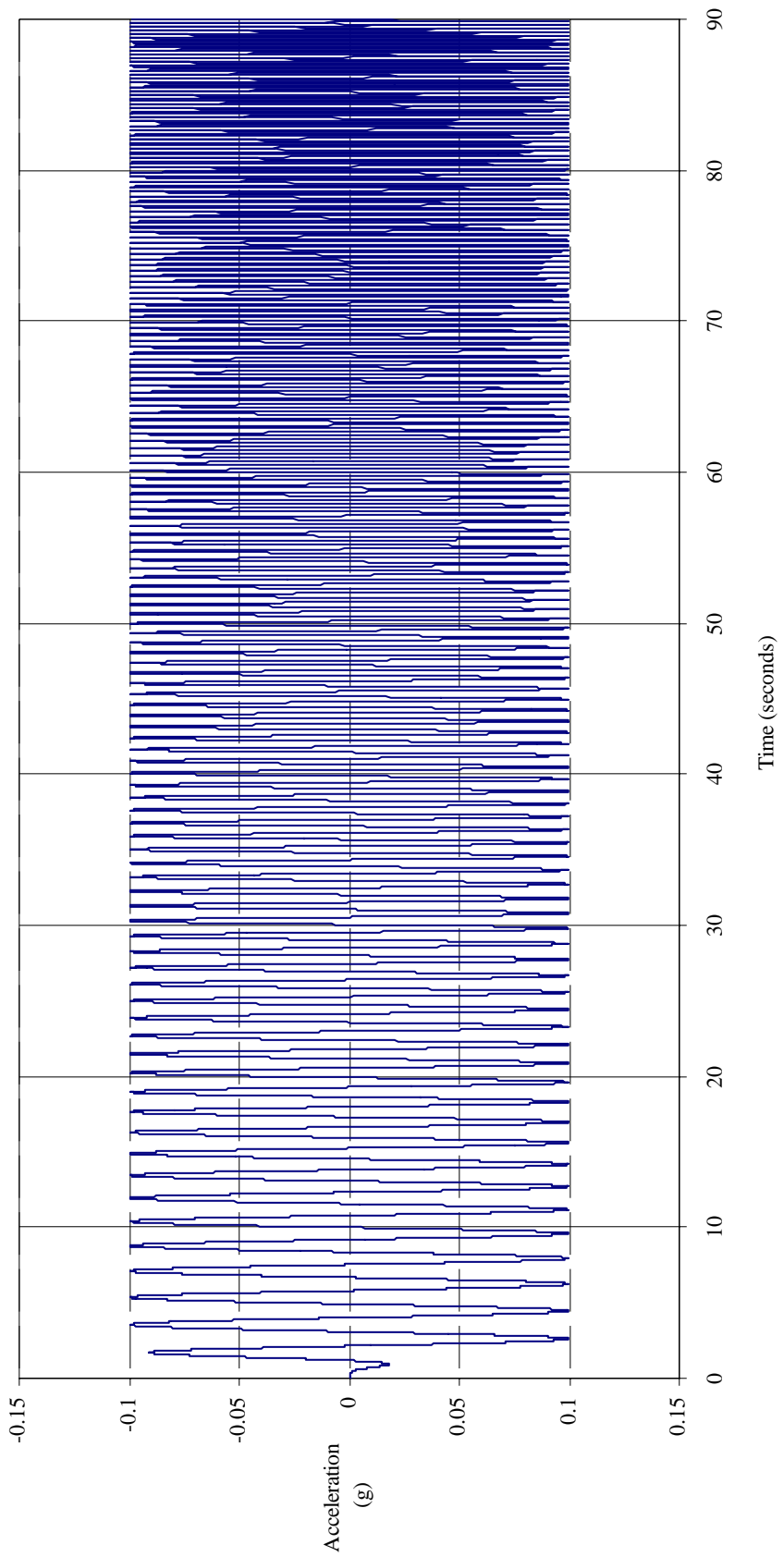
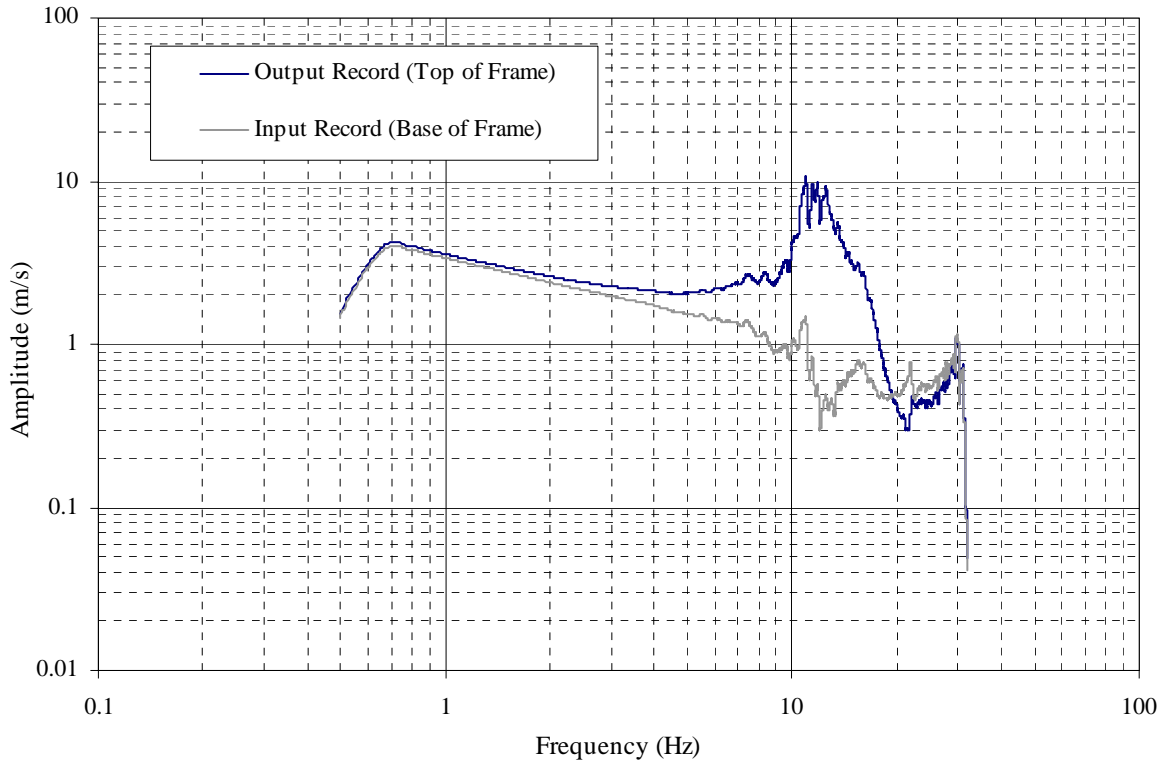


**FIGURE 4-9 Acceleration history used for the sweep of frequencies (first 90 seconds)**

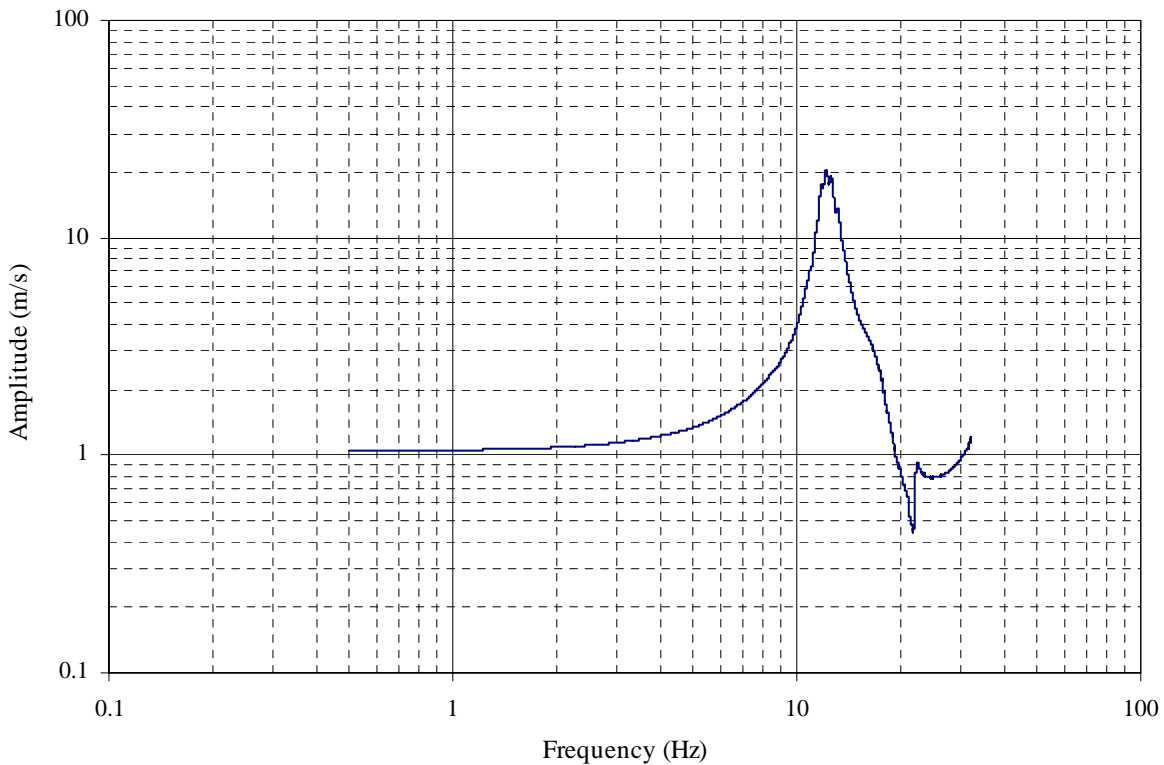
Depending on the range of the index  $j$ , two variants of the method exist to calculate the moving average filter: one side averaging or symmetrical averaging. In the one side averaging variant, the  $j$  index uses only points on one side of the output sample that are being calculated ( $a = 0$  to  $b = M-1$  in (4-2)). In the symmetrical averaging variant, the group of points from the input signal are selected symmetrically around the output point and  $j$  therefore varies from  $a = -(M-1)/2$  to  $b = (M-1)/2$ . Symmetrical averaging was used in this study.

Figure 4-10 shows the filtered frequency domain records of the table input and the frame response output using the frequency sweeps (resonance search) as excitation in the frequency range of 0.5 to 32 Hz for the horizontal direction. Figure 4-11 presents the transfer function of the horizontal direction obtained with the records previously shown on figure 4-10. Figure 4-12 and 4-13 presents the same information than figures 4-10 and 4-11, respectively, but for the case of the vertical direction. From figures 4-11 and 4-13, the natural frequencies using the frequency sweeps as excitation were estimated to be 12.1 Hz and 9.6 Hz for the horizontal and vertical directions, respectively. From the same figures, the fundamental mode damping ratios in the horizontal and vertical directions were estimated to be 5.1% and 0.4%, respectively.





**FIGURE 4-10 Filtered frequency domain records of the simulator input and the frame response output for the horizontal direction using the frequency sweep**



**FIGURE 4-11 Transfer function for the horizontal direction using the frequency sweep**

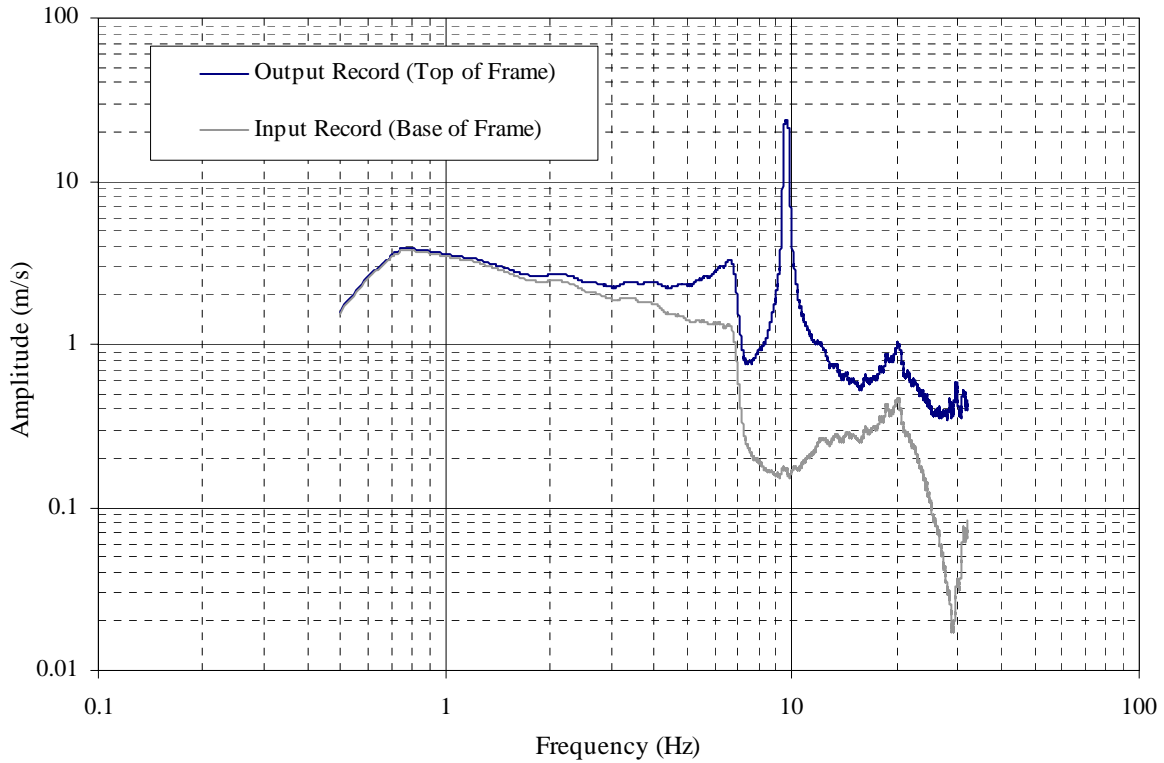


**FIGURE 4-12** Filtered frequency domain records of the simulator input and the frame response output for the vertical direction using the frequency sweep

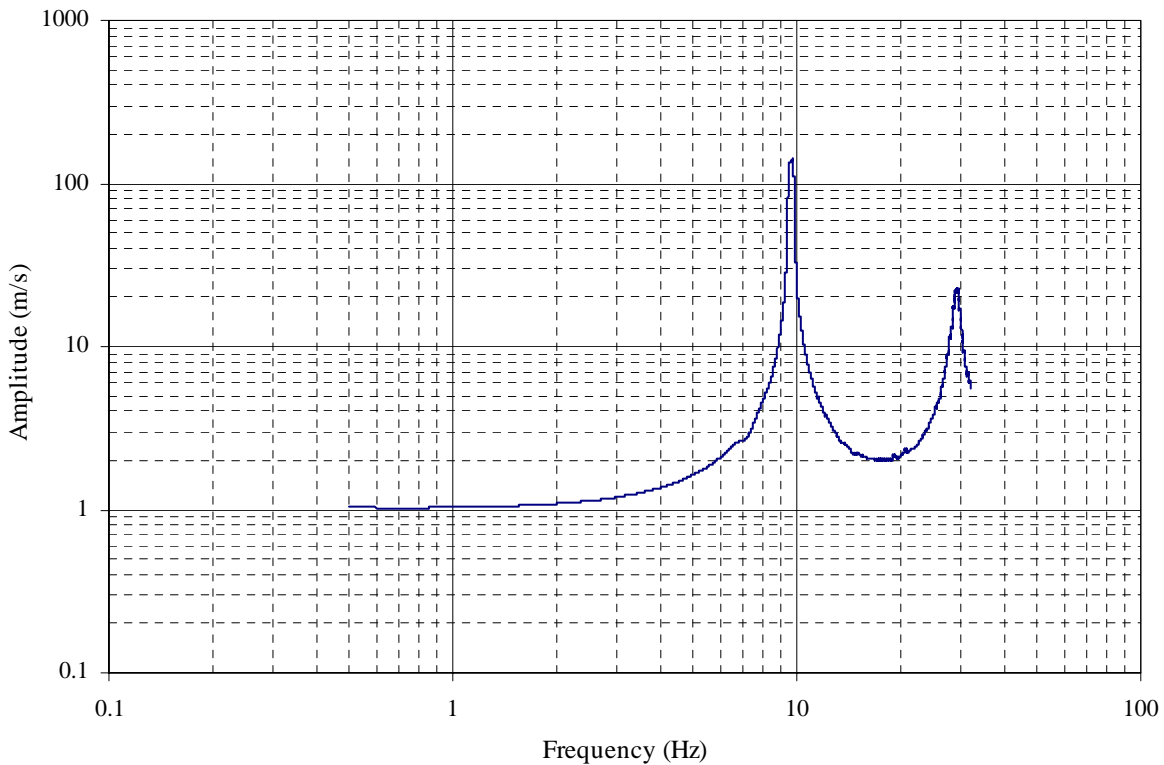


**FIGURE 4-13** Transfer function for the vertical direction using the frequency sweep

#### 4.4 White Noise

This method consists of obtaining the forced vibration response of the test frame using random noise input to the simulator that has a flat frequency spectrum. The natural frequencies for the horizontal and vertical directions were obtained by finding the peak response in the acceleration transfer function as described in the frequency sweep method. The damping ratios were obtained using the half power bandwidth. The moving average method, described in section 4.3.1, was applied to filter the frequency domain records.

Figure 4-14 shows the filtered frequency domain records of the table input and the frame response output using white noise as the excitation for the horizontal direction. Figure 4-15 presents the transfer function in the horizontal direction with the records of figure 4-14. Figures 4-16 and 4-17 present the same information than figures 4-14 and 4-15, respectively, but for the vertical direction. From figures 4-15 and 4-17, the natural frequencies were estimated to be 12.3 Hz and 9.5 Hz for the horizontal and vertical directions, respectively. From the same figures, the fundamental mode damping ratios in the horizontal and vertical directions were estimated to be 4.7% and 0.7%, respectively.

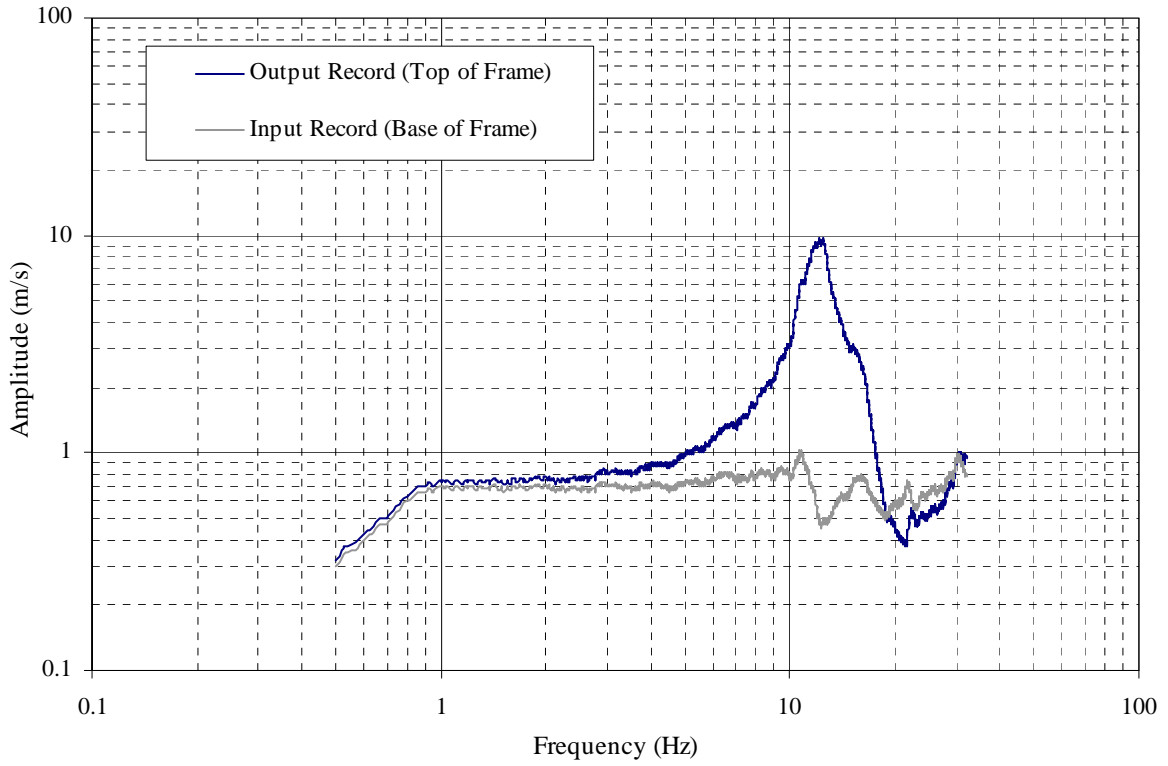


**FIGURE 4-14 Filtered frequency domain records of the simulator input and the frame response output for the horizontal direction using white noise**

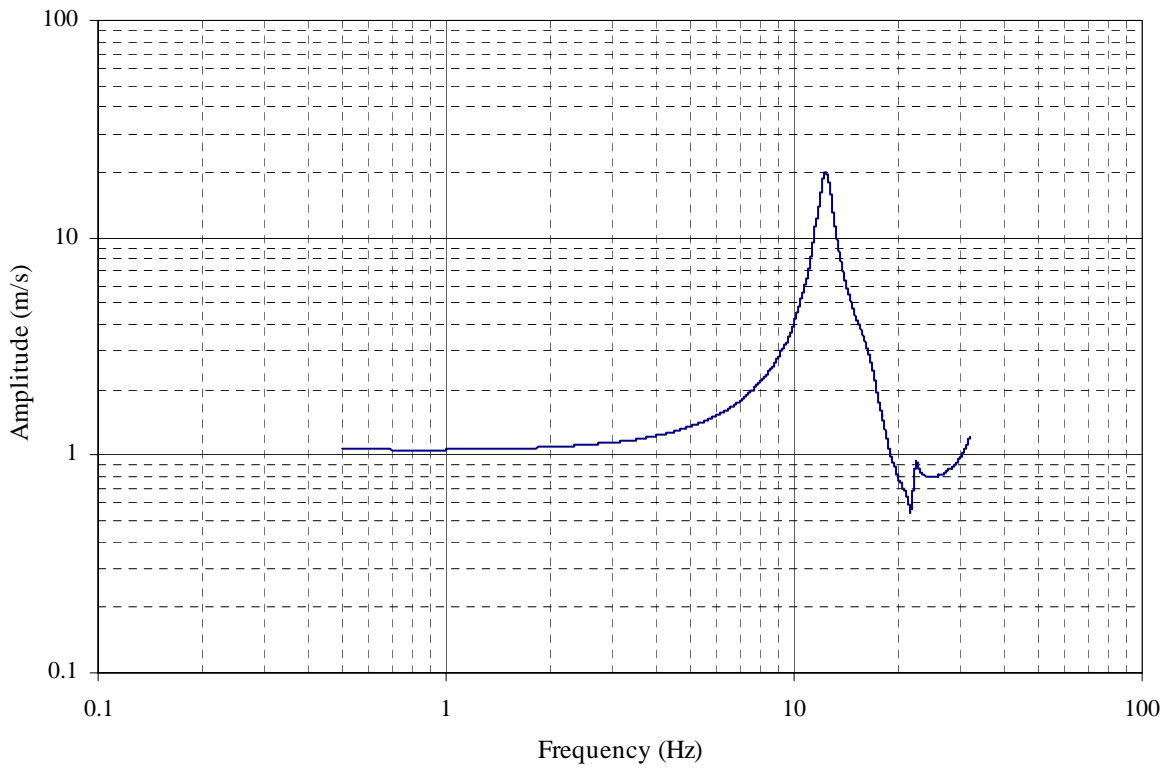


**FIGURE 4-15 Transfer function for the horizontal direction using white noise**

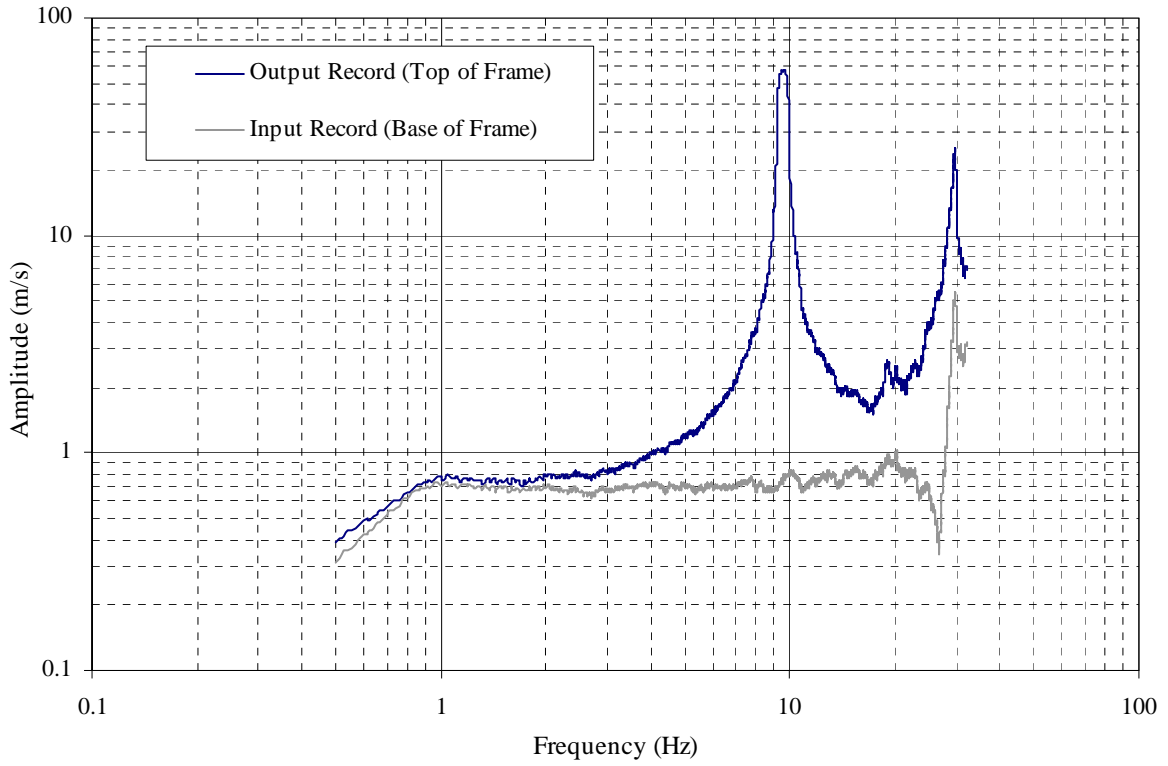


**FIGURE 4-16** Filtered frequency domain records of the simulator input and the frame response output for the vertical direction using white noise

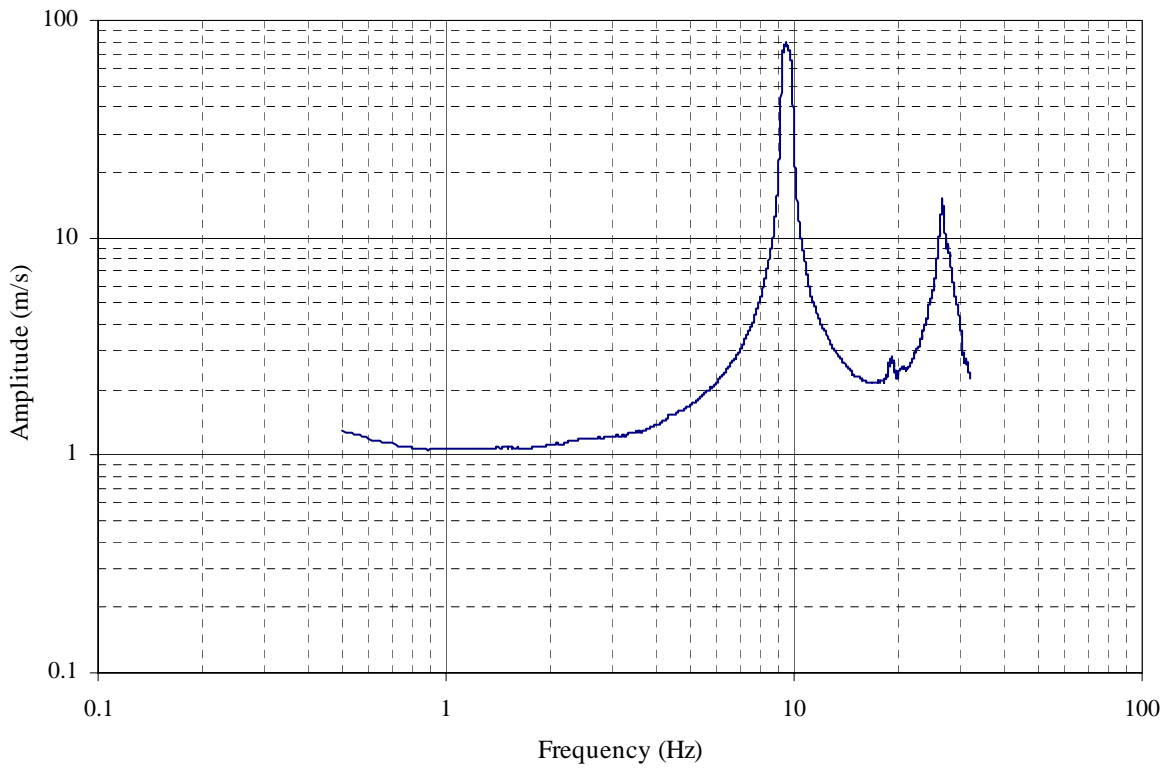


**FIGURE 4-17** Transfer function for the vertical direction using white noise

## 4.5 Summary

Tables 4-1 and 4-2 list summary information for the first mode natural frequencies and the damping ratios, respectively, for the horizontal and vertical direction, obtained using the three methods described above.

**TABLE 4-1 Frequencies obtained with the three testing methods**

	<i>Snap Back</i>	<i>Frequency Sweep</i>	<i>White Noise</i>
Horizontal	12.5 Hz	12.1 Hz	12.3 Hz
Vertical	9.6 Hz	9.6 Hz	9.5 Hz

**TABLE 4-2 Damping ratios obtained with the three testing methods**

	<i>Snap Back</i>	<i>Frequency Sweep</i>	<i>White Noise</i>
Horizontal	2.6%	5.1%	4.7%
Vertical	0.5%	0.4%	0.7%

## **CHAPTER 5**

### **SEISMIC QUALIFICATION AND FRAGILITY TESTING**

#### **5.1 Introduction**

Full-scale testing must be conducted to develop seismic fragility curves for suspended ceiling systems because ceiling systems are not amenable to structural analysis. In this research project, numerous experiments using an earthquake-shaking simulator were conducted to develop fragility curves. Each experiment involved subjecting a ceiling system to a set of horizontal and vertical (unidirectional and combined) earthquake excitations. The procedures to develop the earthquake histories generally follow the procedures set forth in the ICBO-AC156 “Acceptance Criteria for Seismic Qualification Testing of Nonstructural Components” (ICBO, 2000). The following sections in this section present summary information on seismic qualification and the generation of the earthquake histories used for the qualification and fragility testing of the suspended ceiling systems.

#### **5.2 Testing of Ceiling Systems**

##### **5.2.1 ICBO Requirements for Testing and Qualification**

Several requirements must be fulfilled for testing nonstructural components per ICBO-AC156. As part of these requirements, a general description must be provided of the system to be tested. This description must include the primary equipment product function, overall dimensions, weight and restrictions or limitations on equipment use. Seismic parameters must also be provided, such as equipment attachment elevation, structure roof elevation, seismic coefficient and equipment importance factor. The test specimen must also adequately represent the entire equipment product line. This description of the systems and equipment used for the testing discussed in this report was provided in Chapter 3.

To qualify a test system, ICBO-AC156 writes that it must be subjected to a seismic qualification-testing program. This program must include a pre-test inspection and functional compliance

verification, resonance search tests, random multifrequency seismic simulation tests, and post-test inspection and functional compliance verification.

### 5.2.2 Horizontal and Vertical Spectra for Qualification and Fragility Testing

The earthquake excitations used for the qualification and fragility testing of the ceiling systems were obtained using the spectrum-matching procedure recommended by ICBO. The first step in the process was to define a target spectrum or required response spectrum (RRS). Per ICBO, the RRS is obtained as a function of the short-period mapped spectral acceleration,  $S_S$ . The required response spectrum for horizontal shaking was developed using the normalized ICBO response spectrum shown in figure 5-1.

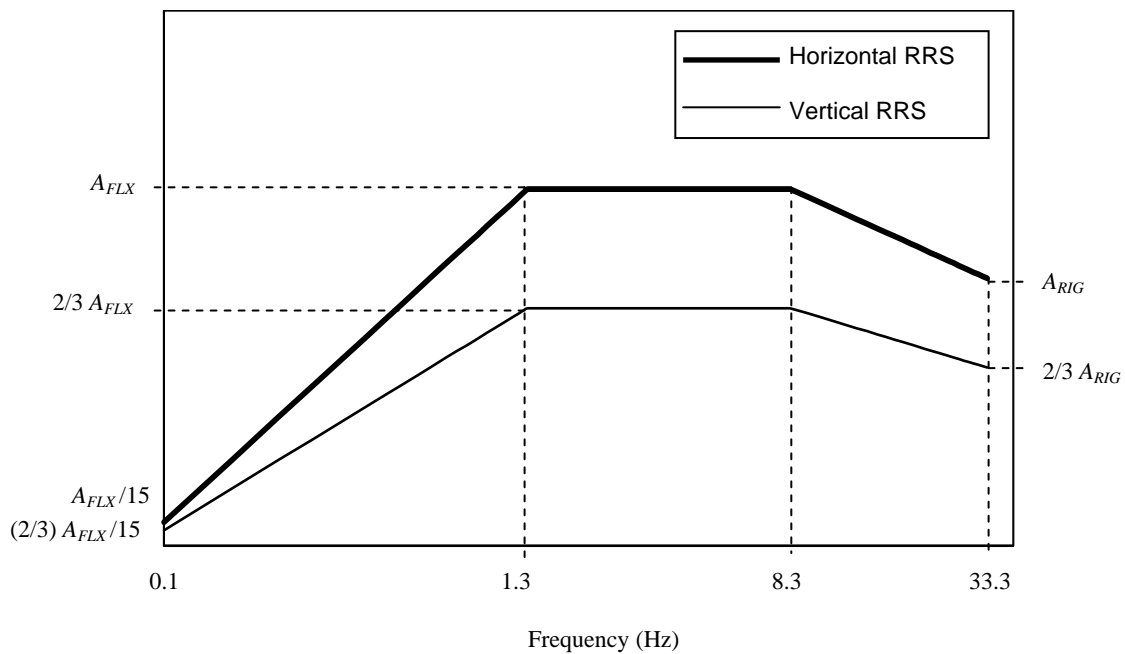


**FIGURE 5-1 ICBO Required Response Spectra for horizontal and vertical shaking**



The values of the parameters  $A_{RIG}$  and  $A_{FLX}$  that define the ordinates of the horizontal spectrum are calculated with equations presented in the following paragraphs.

For horizontal design-basis earthquake shaking, the International Building Code (IBC 2000) defines the short period design basis earthquake acceleration response as:

$$S_{DS} = \frac{2}{3} F_a S_S \quad (5-1)$$

where  $S_{DS}$  is the design spectral response acceleration at short periods,  $F_a$  is a site soil coefficient, and  $S_S$  is the mapped maximum earthquake spectral acceleration at short periods.

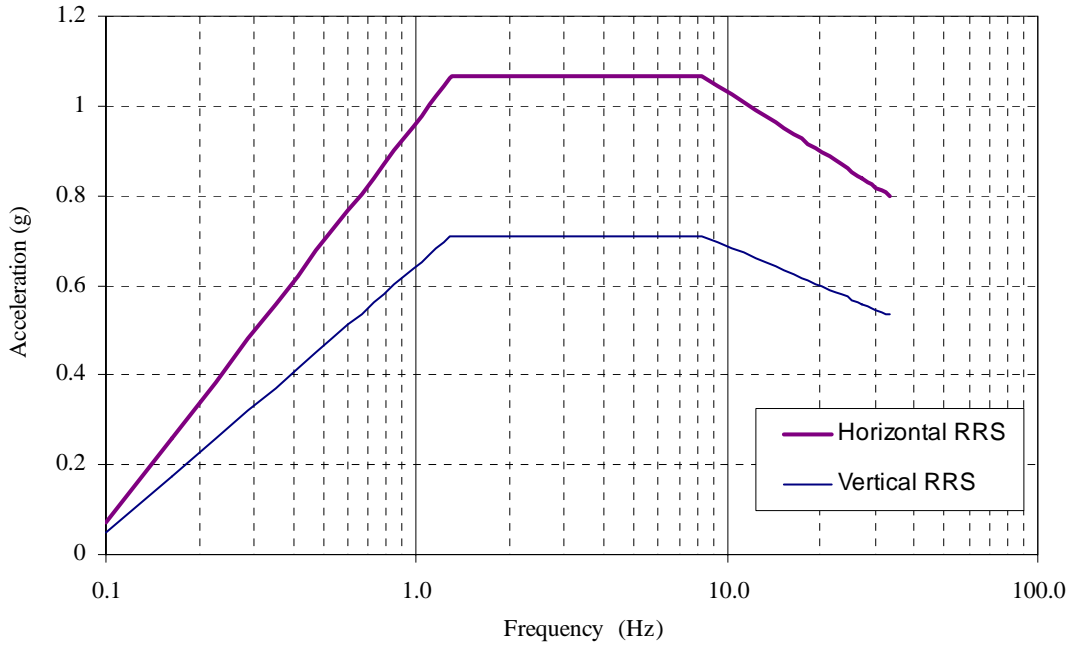
Accelerations demands for testing components attached to *floors* are obtained per ICBO-AC156 assuming that the spectral acceleration  $A_{RIG}$  of a rigid component (assumed to have a frequency  $f \geq 33$  Hz) is given by (5-2) and that of a flexible component  $A_{FLX}$  is given by (5-3).

$$A_{RIG} = 0.4 S_{DS} \left(1 + 2 \frac{z}{h}\right) \leq 1.2 S_{DS} \quad (5-2)$$

$$A_{FLX} = S_{DS} \left(1 + 2 \frac{z}{h}\right) \leq 1.6 S_{DS} \quad (5-3)$$

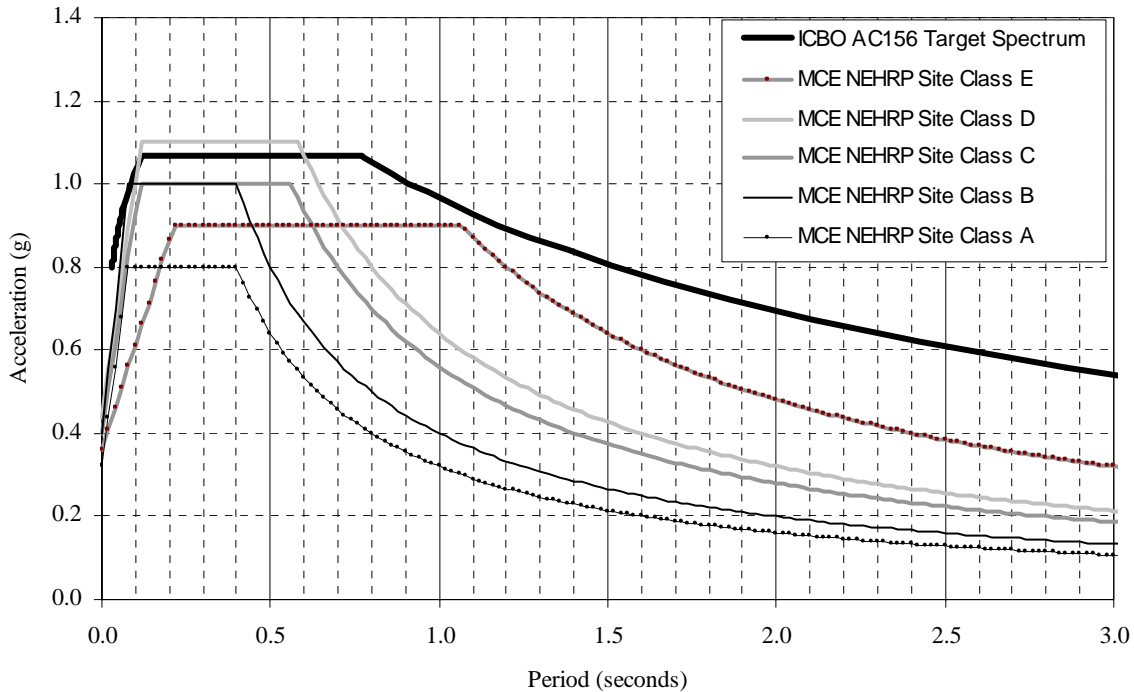
where  $z$  is the height above the building base where the equipment or component is to be installed and  $h$  is the height of the building. If the equipment or component is to be installed in the roof of the building,  $z/h = 1.0$ . If the location of the equipment or component in a building is unknown, or if it is being qualified for a general use in buildings structures, it is conservative, but appropriate, to set  $z = h$ .

Figure 5-2 shows the RRS in the horizontal and vertical directions for 5 percent damping for a mapped spectral acceleration at short period,  $S_S = 1.0g$ . The ordinates of the vertical required response spectrum (RRS) are given by ICBO as two-thirds (2/3) of those of the horizontal RRS, namely,  $A_{FLX} = 1.07g$  and  $A_{RIG} = 0.80g$  for  $S_S = 1.0g$ .



**FIGURE 5-2 RRS for horizontal and vertical shaking for  $S_S = 1.0g$**

Figure 5-3 presents 2000 NEHRP maximum considered earthquake (MCE) ground motion spectra and the ICBO-AC156 target qualification spectrum for seismic qualification for  $S_S = 1.0g$  and  $S_I = 0.4g$ . The ground motion spectra are presented for NEHRP soil types A through E. The purpose of the presentation is to relate the qualification spectral demands that are assumed to apply anywhere in a building structure to ground motion demands on a single-degree-of-freedom representation of the building. The qualification spectrum envelopes the MCE spectra (for  $S_S = 1.0g$  and  $S_I = 0.4g$ ) except in the short period range for site class D.



**FIGURE 5-3 Relationship between MCE NEHRP spectra and target qualification spectrum ( $S_S = 1.0g$ ,  $S_I = 0.4g$ )**

### 5.3 Description of the Testing Protocol for Fragility Testing

Ceiling systems were subjected to sets of horizontal and vertical earthquake excitations. Each set included unidirectional and bi-directional resonance search tests using white noise excitation along each programmable orthogonal axis of the simulation platform (North-South and vertical). The resonance search tests were undertaken to establish the natural frequencies of the ceiling-frame system. Each set of excitations also included a series of unidirectional and bi-directional earthquake motions that were established for different multiples of the target or required response spectrum (RRS). The purpose of the earthquake motions was to observe the performance of the ceiling systems under different levels of seismic excitation.

Fragility testing is intended to establish a relationship between limit states of response and a representative ground motion parameter. The range of shaking intensity was selected such that failure in the suspended ceiling systems could be identified and quantified. Table 5-1 lists the standard series of tests used for each ceiling system.

**TABLE 5-1 Test sequence (series A)**

<i>Test No.</i>	<i>Test Name</i>	<i>Test description</i> <sup>1,2</sup>
1	AWNH	White noise excitation in the horizontal direction
2	AWNV	White noise excitation in the vertical direction
3	AWNHV	Combined white noise excitation
4	A025H	Horizontal excitation corresponding to $S_S = 0.25g$
5	A025V	Vertical excitation corresponding to $S_S = 0.25g$
6	A025HV	Combined excitation corresponding to $S_S = 0.25g$
7	A050H	Horizontal excitation corresponding to $S_S = 0.50g$
8	A050V	Vertical excitation corresponding to $S_S = 0.50g$
9	A050HV	Combined excitation corresponding to $S_S = 0.50g$
10	A075H	Horizontal excitation corresponding to $S_S = 0.75g$
11	A075V	Vertical excitation corresponding to $S_S = 0.75g$
12	A075HV	Combined excitation corresponding to $S_S = 0.75g$
13	A100H	Horizontal excitation corresponding to $S_S = 1.00g$
14	A100V	Vertical excitation corresponding to $S_S = 1.00g$
15	A100HV	Combined excitation corresponding to $S_S = 1.00g$
16	A125H	Horizontal excitation corresponding to $S_S = 1.25g$
17	A125V	Vertical excitation corresponding to $S_S = 1.25g$
18	A125HV	Combined excitation corresponding to $S_S = 1.25g$
19	A150H	Horizontal excitation corresponding to $S_S = 1.50g$
20	A150V	Vertical excitation corresponding to $S_S = 1.50g$
21	A150HV	Combined excitation corresponding to $S_S = 1.50g$
22	A175H	Horizontal excitation corresponding to $S_S = 1.75g$
23	A175V	Vertical excitation corresponding to $S_S = 1.75g$
24	A175HV	Combined excitation corresponding to $S_S = 1.75g$
25	A200H	Horizontal excitation corresponding to $S_S = 2.00g$
26	A200V	Vertical excitation corresponding to $S_S = 2.00g$
27	A200HV	Combined excitation corresponding to $S_S = 2.00g$
28	A225H	Horizontal excitation corresponding to $S_S = 2.25g$
29	A225V	Vertical excitation corresponding to $S_S = 2.25g$
30	A225HV	Combined excitation corresponding to $S_S = 2.25g$
31	A250H	Horizontal excitation corresponding to $S_S = 2.50g$
32	A250V	Vertical excitation corresponding to $S_S = 2.50g$
33	A250HV	Combined excitation corresponding to $S_S = 2.50g$

<sup>1</sup> Vertical excitation is equal to 2/3 of the corresponding horizontal excitation

<sup>2</sup> Combined excitations are composed of horizontal and vertical excitations

The parameter selected to characterize the *ground motion* for input to the simulator was the mapped spectral acceleration at short periods,  $S_S$ . The target of shaking levels ranged from  $S_S = 0.25g$  through  $S_S = 2.5g$ . The earthquake histories for simulation were prepared using the procedure described in Section 5.2.2. Table 5-2 presents the parameters to obtain the corresponding RRS of Section 5.2.2.

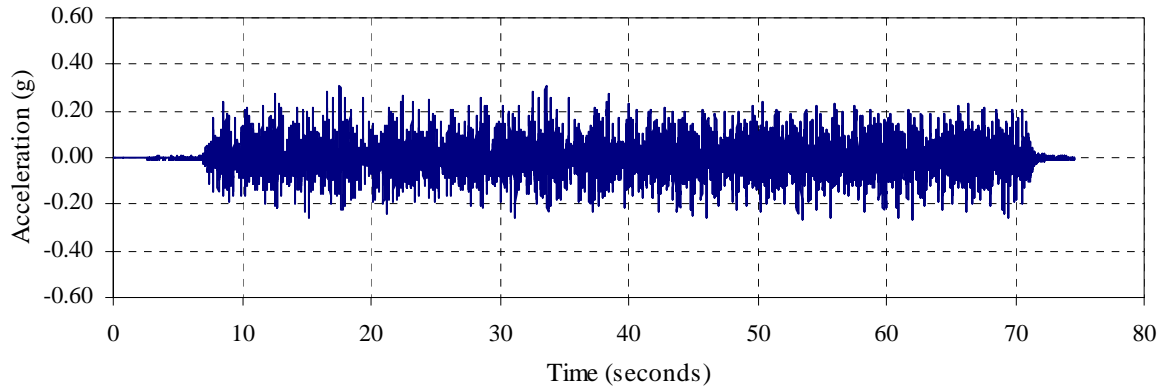
**TABLE 5-2 Parameters to calculate the horizontal RRS ( $z/h = 1.0$ )**

$S_S$ (g)	$F_a$	$S_{DS}$ (g)	$A_{FLX}$ (g)	$A_{RIG}$ (g)	$A_{FLX}/15$ (g)
0.25	1.0	0.167	0.27	0.20	0.018
0.50	1.0	0.333	0.53	0.40	0.036
0.75	1.0	0.500	0.80	0.60	0.053
1.00	1.0	0.667	1.07	0.80	0.071
1.25	1.0	0.833	1.33	1.00	0.089
1.50	1.0	1.000	1.60	1.20	0.107
1.75	1.0	1.167	1.87	1.40	0.124
2.00	1.0	1.333	2.13	1.60	0.142
2.25	1.0	1.500	2.40	1.80	0.160
2.50	1.0	1.667	2.67	2.00	0.178

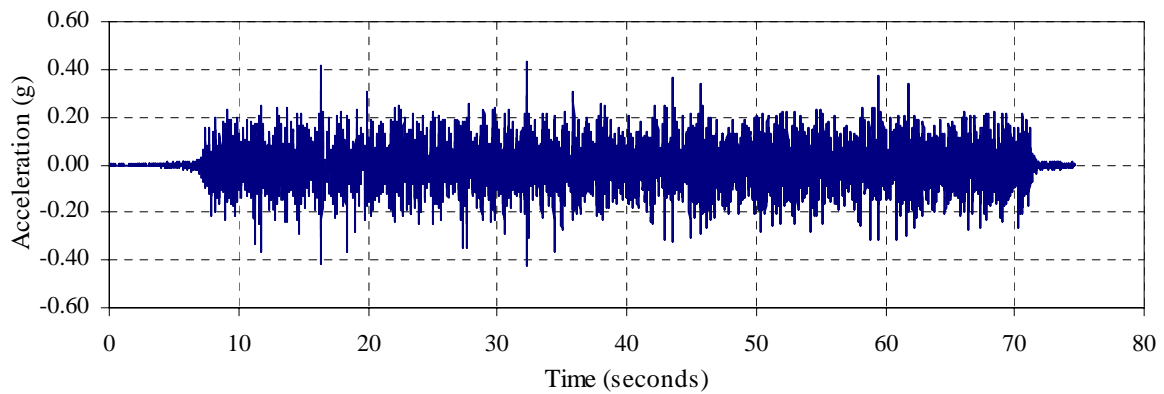
## 5.4 Dynamic Excitations

### 5.4.1 White Noise

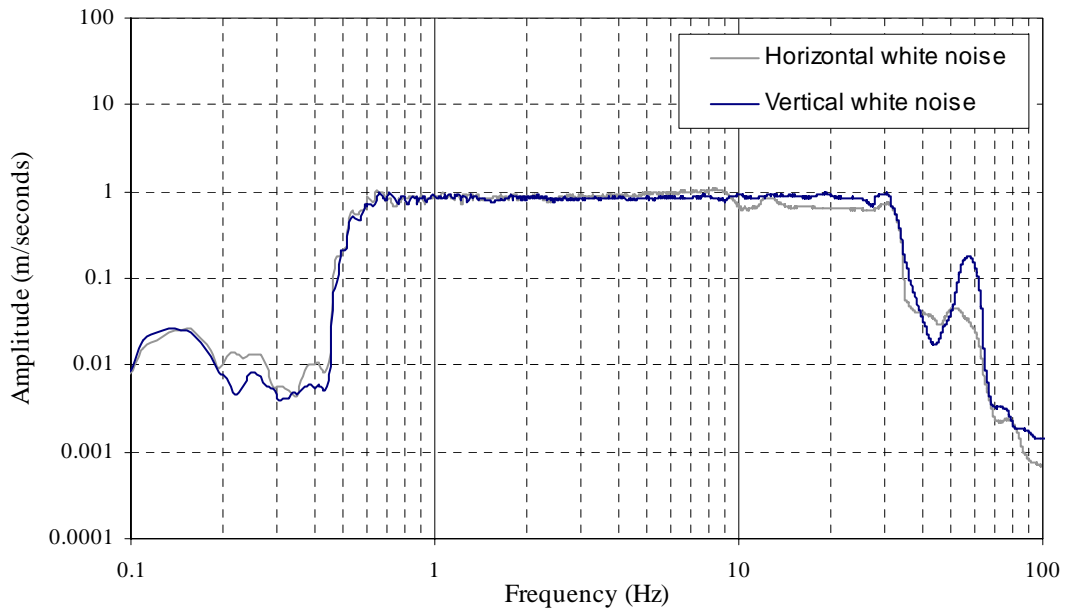
White noise testing was used to find the frequencies of the test frame and the ceiling systems. The natural frequencies for the horizontal and vertical directions of each test specimen were obtained by finding the frequency associated with the peak in the acceleration transfer function (Clough and Penzien, 1993). Figure 5-4 shows the records and the Fourier amplitude spectrum of the white noise used in this study to calculate the natural frequencies of each of the ceiling systems in the horizontal and vertical directions, respectively. The 60 Hz peak in the Fourier spectrum on figure 5-4 is associated with oil-column resonance in the vertical actuators of the simulator. This peak falls well outside the testing range of interest: 1 to 33 Hz.



**a) horizontal white noise record**



**b) vertical white noise record**



**c) Fourier amplitude spectrum of horizontal and vertical white noise**

**FIGURE 5-4 White noise records and Fourier amplitude spectra for the horizontal and vertical motions**

## 5.4.2 Earthquake Histories

The earthquake excitations used for the qualification of the ceiling system were generated using a spectrum-matching procedure from the MTS program STEX (MTS, 1991). The values of the spectral acceleration of the response spectrum obtained with the matching procedure were scaled to envelope the target spectrum (ranging from  $S_s = 0.25g$  to  $2.5g$ ) over the frequency range from 1 through 33 Hz. The low frequency content was eliminated from the scaled records for the purpose of not exceeding the displacement and velocity limits of the earthquake simulator. The subsections below present information on the procedures involved in the generation of the earthquake records used as acceleration input to the earthquake simulator for the development of fragility curves of suspended ceiling systems.

ICBO (2000) requires that the response spectra associated with the earthquake histories used for qualification must envelope the required (or target) response spectrum (RRS) using a maximum-one-third-octave bandwidth resolution over the frequency range from 1 to 33 Hz, or up to the limits of the simulator. A damping ratio of 5 percent is used to generate the response spectra for the earthquake histories. The amplitude of each matched spectrum ordinate must be independently adjusted along each of the orthogonal axes until the response spectrum envelopes the RRS. The response spectrum should not exceed the RRS by more than 30 percent. The earthquake histories used for the qualification and fragility testing of the ceiling systems were generated using the following procedure:

1. Select a baseline earthquake that defines the overall duration, the rise time, steady state, and decline time of the resultant acceleration record. The acceleration profile is interpolated to produce a time series.
2. From the baseline earthquake of 1, a new acceleration record is created using the STEX routine at 3 lines per octave for frequency resolution (as required by the qualification procedure) and the damping ratio of 5%. The process is repeated several times until the response spectrum from the generated acceleration record closely matches the RRS. The procedure is repeated to generate an independent record for the vertical motion, which is

then scaled to 2/3 of the value of the horizontal motion. Figure 5-5 shows the acceleration record and the response spectra of the earthquake excitation before (original record) and after performing the response spectrum matching procedure (RSMP) for a target spectrum corresponding to  $S_S = 1.0g$ .

3. The record obtained after applying the RSMP, is scaled to match the different levels of the target spectrum defined previously. The value of the spectral acceleration of the response spectrum of the scaled records was adjusted to envelope the target spectrum over the frequency range from 1 to 33 Hz.

For the purpose of reaching the levels of shaking considered in Section 5.3 without exceeding the limits of the earthquake simulator, the maximum accelerations, velocities and displacements for the scaled records at all the shaking levels were calculated and were compared to the simulator limits. For this payload, the earthquake simulator acceleration, velocity and displacement limits were 1.5g, 94 cm/sec (37 in/sec) and 14 cm (5.5 in.), respectively. If the values calculated from the records exceeded the earthquake simulator limits, additional low frequency content in the record was eliminated.

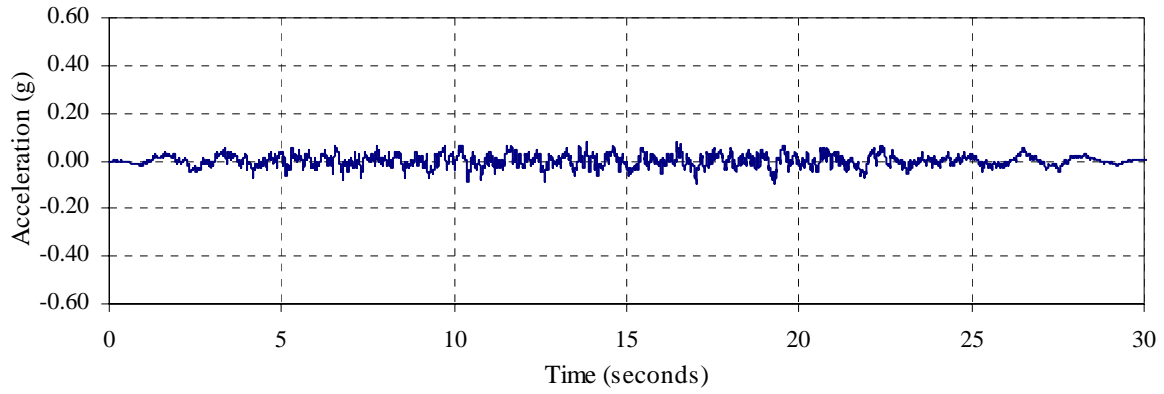
Another important factor to consider is the presence of noise in the original acceleration signal because it can produce permanent velocities and displacements at the end of the earthquake history. The intensity of the input acceleration history must be reduced when displacement and velocity residuals are larger than the earthquake simulator limits even when the maximum acceleration of the record is well below the simulator limits. Large residual displacements are not seen following earthquakes, unless in the strike parallel direction close to a major fault following a large magnitude earthquake. Residuals can be eliminated by high pass filtering the acceleration and velocity records to remove the low frequency content. The procedure used to eliminate the low frequencies in the acceleration records is described below:

1. The velocity and displacement histories were obtained by numerical integration of the corresponding scaled acceleration records for each shaking level. Figures 5-6 and 5-7

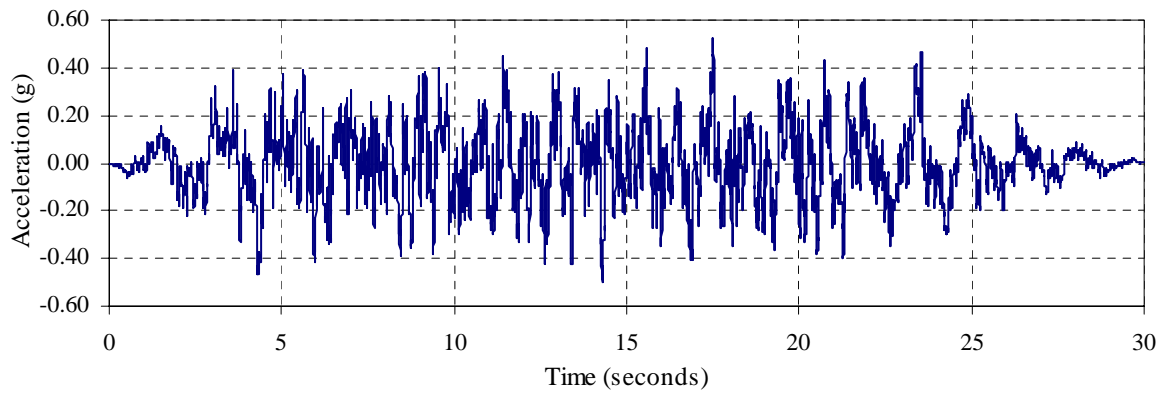


present the velocity and displacement histories calculated from the acceleration record obtained with the response spectrum matching procedure for  $S_S$ , of 1.0g (figure 5-5b).

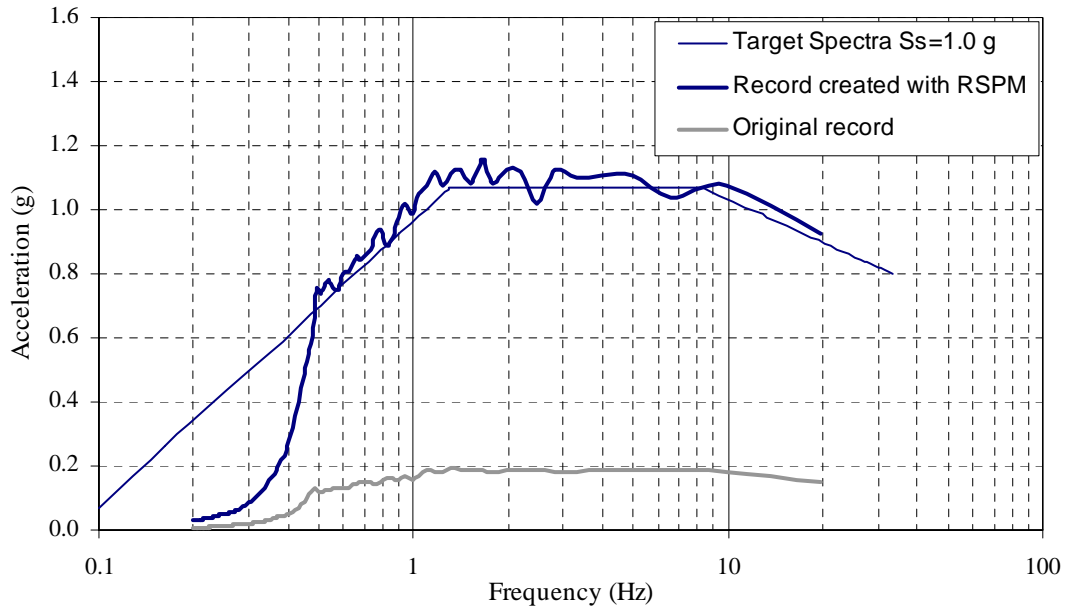
2. Since large residuals are present in the displacement record in figure 5-7, the original earthquake acceleration history was high-pass filtered by transforming it to the frequency domain using the discrete Fast Fourier Transform (FFT) function in Matlab. A rectangular modulation function identical to that of figure 5-8 was then applied to the amplitude and phase spectra to remove the low frequency content. The resulting data in the frequency domain were then transformed back into the time domain using the Inverse Fast Fourier Transform (IFFT) function in Matlab. Figure 5-9 presents the modified acceleration record for a cut-off frequency,  $f_c$ , of 0.4 Hz.
3. The velocity history record shown in figure 5-10 is calculated by numerical integration of the modified acceleration record obtained in step number 2. The velocity record was high-pass filtered using the procedure described in step 2 to remove the low frequency noise introduced by the integration. If this low frequency noise is not removed, the resulting displacement history may show a significant residual displacement such as that shown in figure 5-11, where the displacement history was obtained from the velocity record without filtering shown previously in figure 5-10. Figure 5-12 shows the modified velocity record after the high-pass filter is applied at a cut-off frequency of 0.4 Hz.
4. From the modified velocity record obtained in step number 3, new acceleration and displacement records were calculated by numerical differentiation and numerical integration, respectively. The new displacement and acceleration records are shown in figure 5-13 and 5-14, respectively. The maximum acceleration, velocity and displacement were calculated and were compared to the earthquake simulator limits. In this case, the maximum values obtained from the modified records for a level of excitation corresponding to  $S_S = 1.0g$  and a cut-off frequency of 0.4 Hz remained below the limits of the earthquake simulator.



**a) original history**

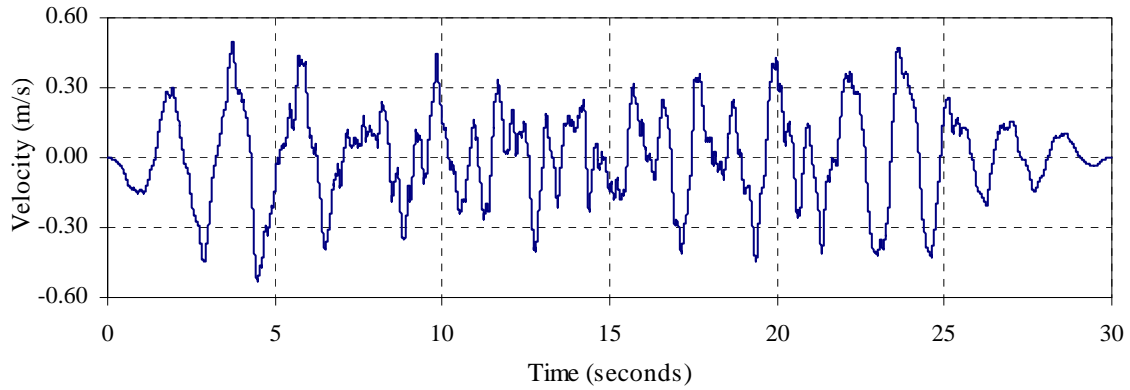


**b) spectrum-matched history created with RSMP**

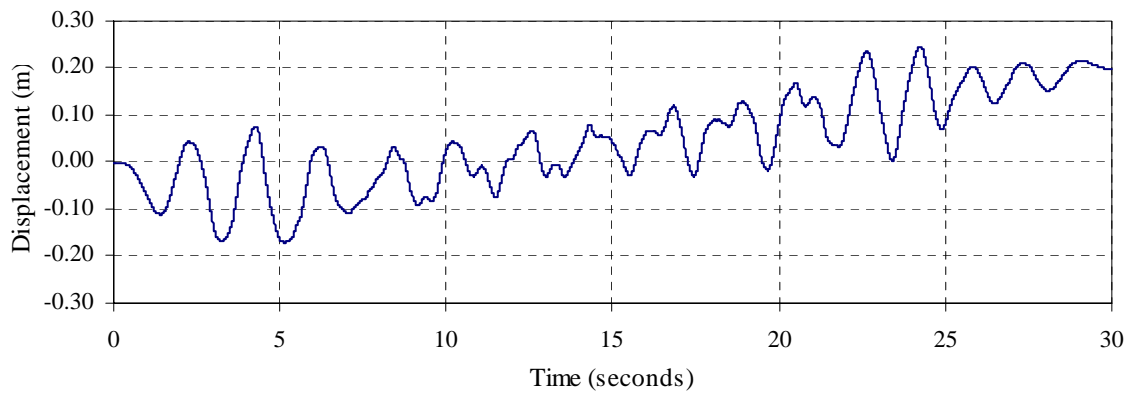


**c) response spectra of original and matched histories**

**FIGURE 5-5 Earthquake histories and response spectra before and after applying the RSMP for  $S_S = 1.0g$**



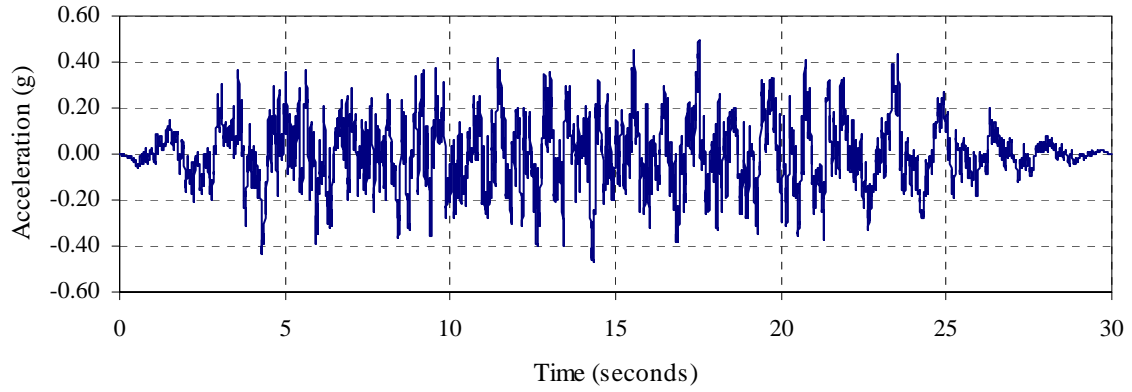
**FIGURE 5-6 Velocity history derived from the acceleration history of figure 5-5b ( $S_S = 1.0g$ )**



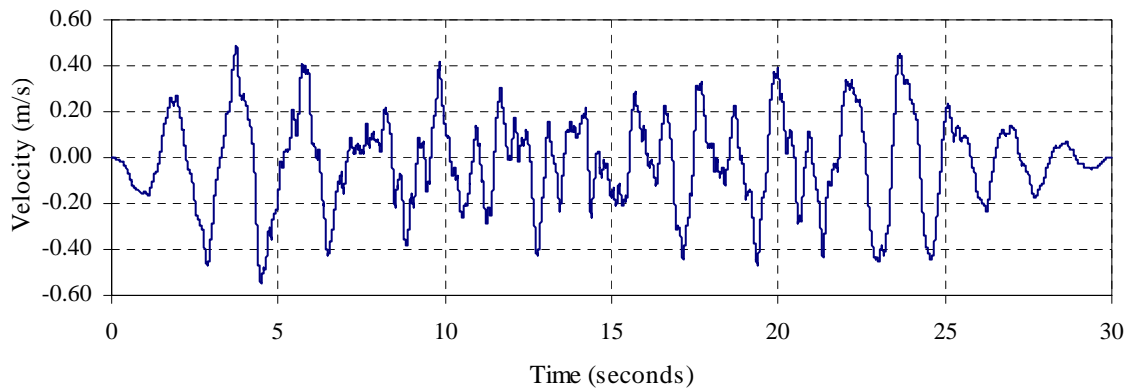
**FIGURE 5-7 Displacement record derived from the acceleration history of figure 5-5b ( $S_S = 1.0g$ )**



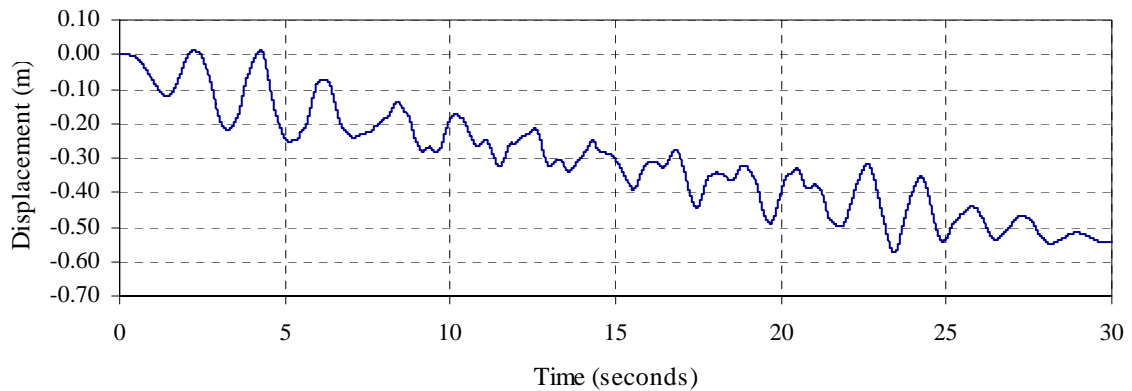
**FIGURE 5-8 Rectangular modulating function applied to remove the low frequency content in the acceleration history corresponding to  $S_S = 1.0g$  ( $f_c = 0.4$  Hz)**



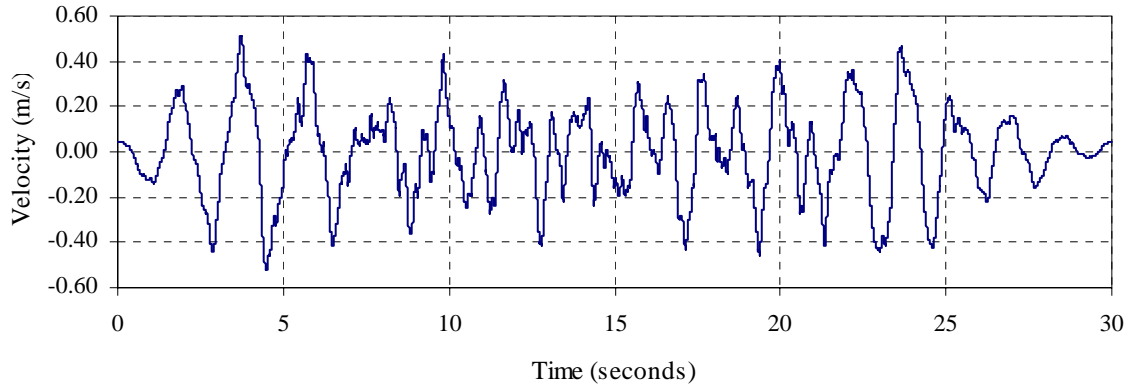
**FIGURE 5-9 Filtered acceleration history corresponding to  $S_S = 1.0g$  ( $f_c = 0.4$  Hz)**



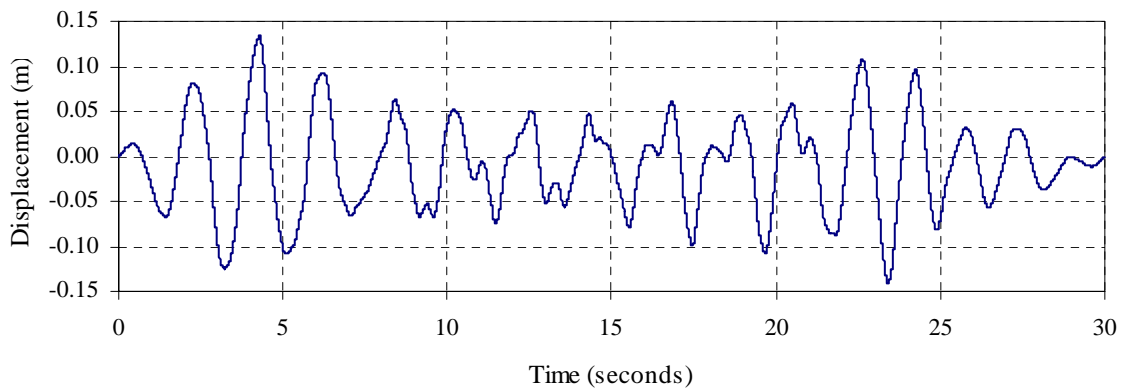
**FIGURE 5-10 Velocity history derived from the acceleration record of figure 5-9**



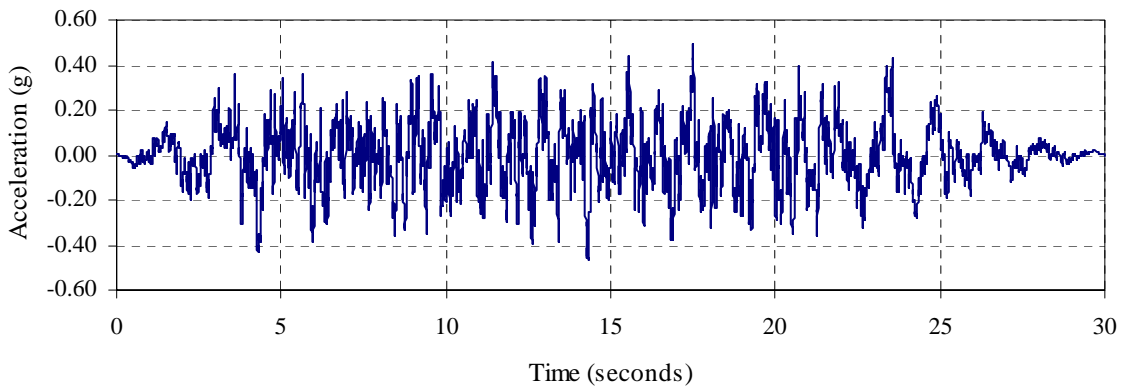
**FIGURE 5-11 Displacement history derived from the acceleration record of figure 5-9**



**FIGURE 5-12 Filtered velocity history ( $f_c = 0.4$  Hz)**

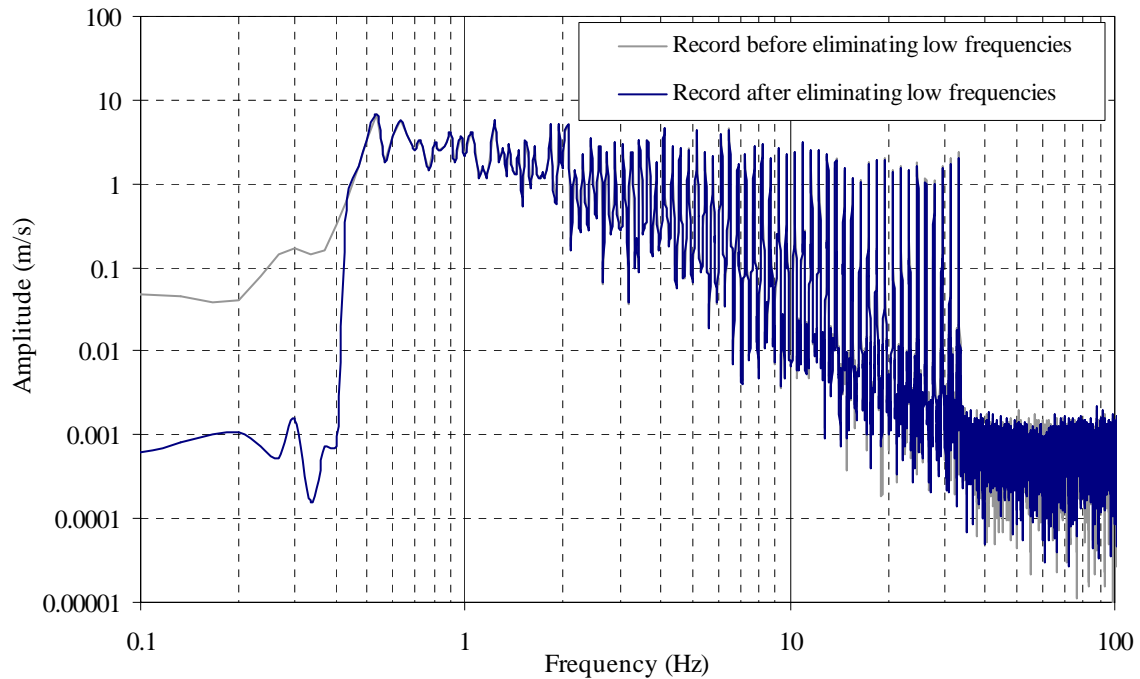


**FIGURE 5-13 Displacement history derived from the velocity history of figure 5-12**



**FIGURE 5-14 Acceleration record derived from the velocity history of figure 5-12**

Figure 5-15 presents the Fourier amplitude spectra for the acceleration record corresponding to a short period mapped spectral acceleration,  $S_S$ , of 1.0g, before and after applying the procedure described above. If the acceleration, velocity or displacement limits were exceeded for any given level of excitation, the earthquake history was high pass filtered as described in the steps 1 through 4, using a higher cut-off frequency such that the maximum displacement, velocity and acceleration of the twice filtered records were less than the limiting values. This procedure was applied to the scaled records for all levels defined in Section 5.3.



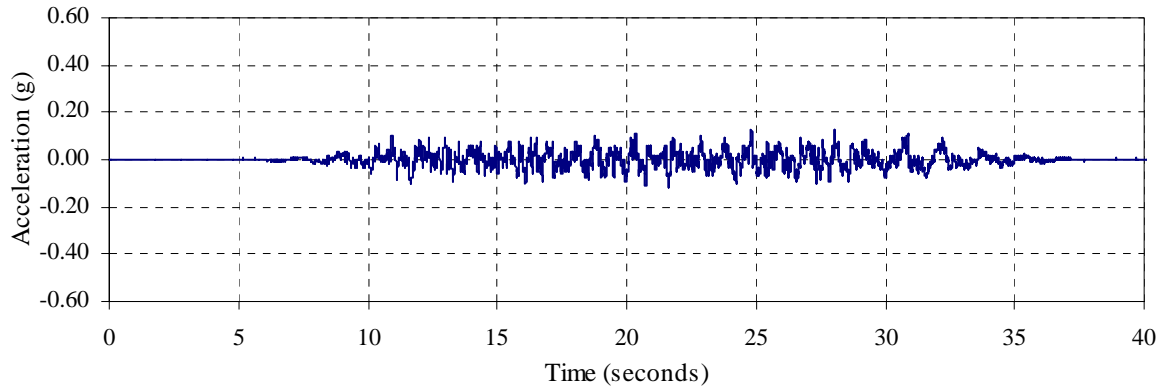
**FIGURE 5-15 Fourier amplitude spectra for the acceleration history corresponding to a short period mapped spectral acceleration,  $S_S = 1.0g$**

Table 5-3 presents the cut-off frequencies and the maximum acceleration, velocities and displacements before and after applying the procedure to eliminate the low frequency content of the scaled records for all the levels of shaking. This correction in the simulator input acceleration records does not affect the fragility testing, since the natural frequencies of the test fixtures (test frame with ceiling system included) are much larger than the frequency range eliminated, even for the highest level of excitation.

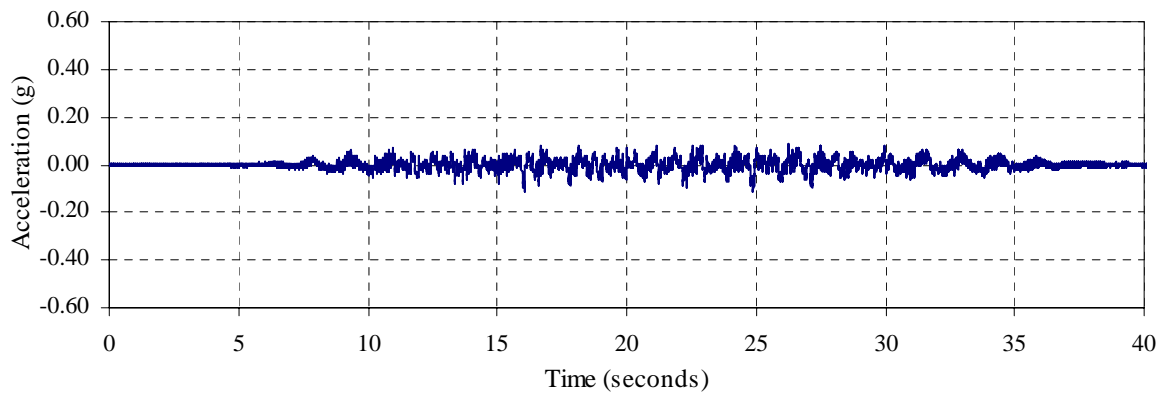
**TABLE 5-3 Cut-off frequencies and maximum acceleration, velocity and displacement before and after eliminating the low-frequency content**

$S_S$ (g)	Cut-off frequency (Hz)	Maximum values before eliminating low frequency content			Maximum values after eliminating low frequency content		
		Displ. (cm)	Vel. (cm/s)	Acc. (g)	Displ. (cm)	Vel. (cm/s)	Acc. (g)
0.25	0.2	6.1	13.3	0.12	3.6	13.3	0.12
0.50	0.2	12.3	26.6	0.25	7.2	26.6	0.24
0.75	0.4	18.4	40.0	0.37	10.6	39.4	0.37
1.00	0.4	24.6	53.3	0.49	14.0	52.5	0.49
1.25	0.8	30.7	66.6	0.62	6.7	40.0	0.57
1.50	0.8	36.9	79.9	0.74	8.1	48.0	0.68
1.75	0.8	43.1	93.3	0.86	9.4	56.0	0.80
2.00	0.8	49.2	106.6	0.99	10.8	64.0	0.91
2.25	0.8	55.3	119.9	1.11	12.1	72.0	1.03
2.50	0.8	61.5	133.2	1.24	13.5	80.0	1.14

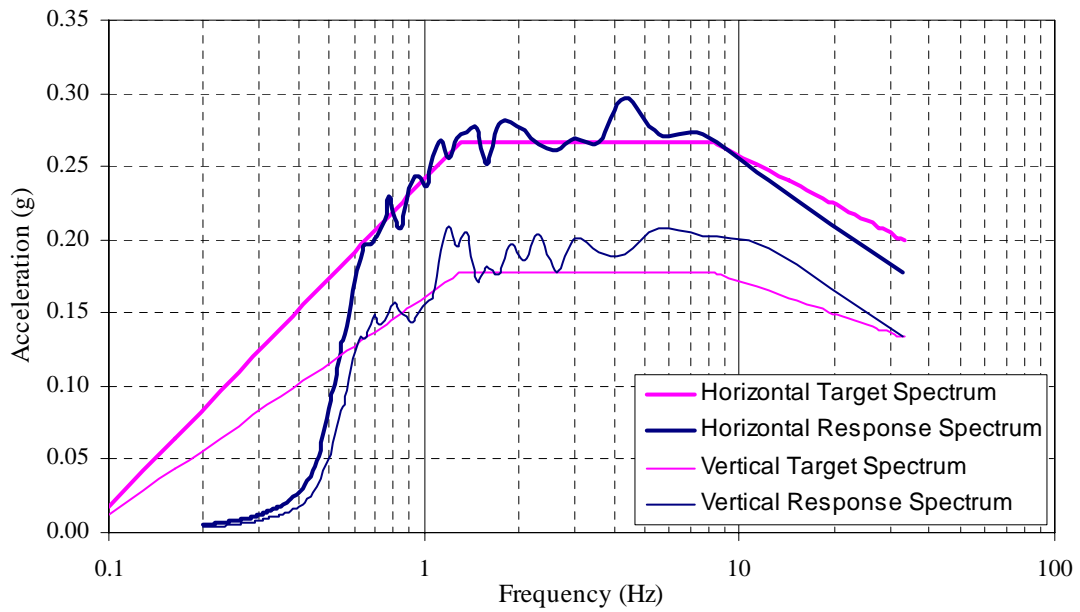
Figures 5-16 through 5-25 present the horizontal and vertical simulator input acceleration records and their corresponding response spectra after applying the procedure to eliminate the low frequency content, for all levels of shaking from  $S_S = 0.25g$  to  $2.5g$ .



**a) horizontal acceleration**



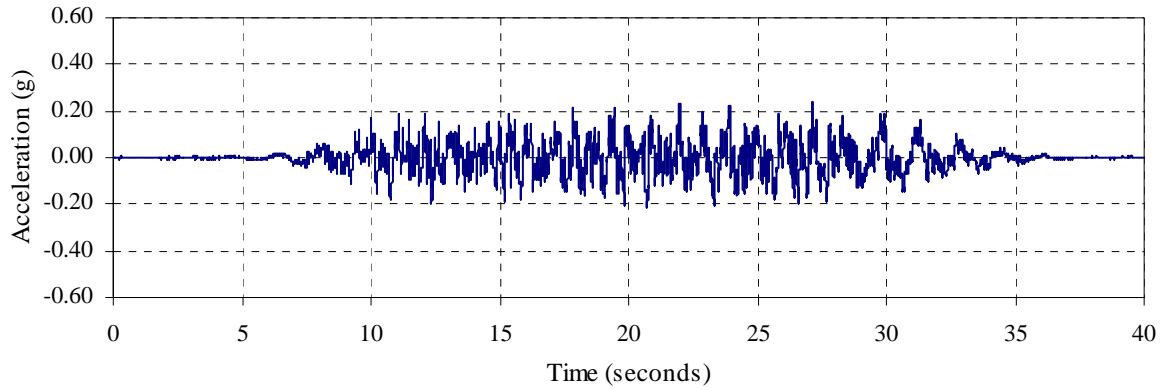
**b) vertical acceleration**



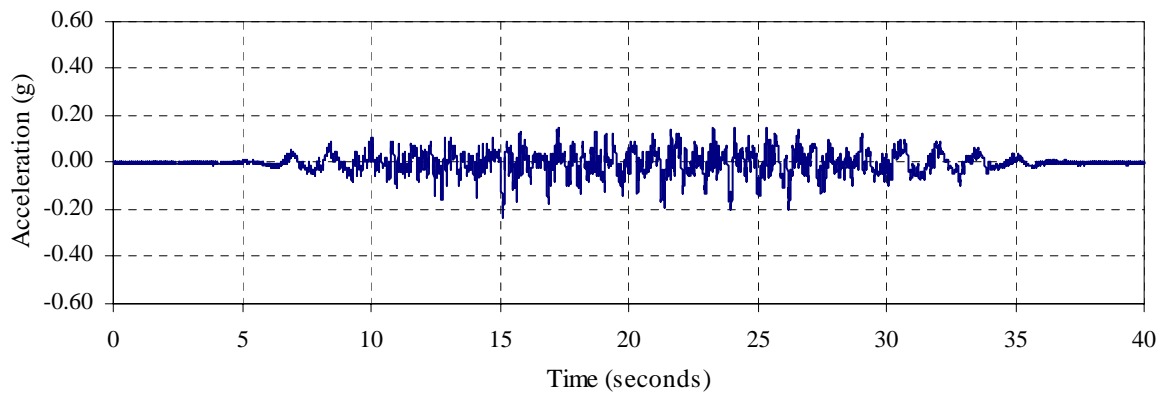
**c) horizontal and vertical response spectra (target and calculated)**

**FIGURE 5-16 Earthquake histories and spectra for test A025**

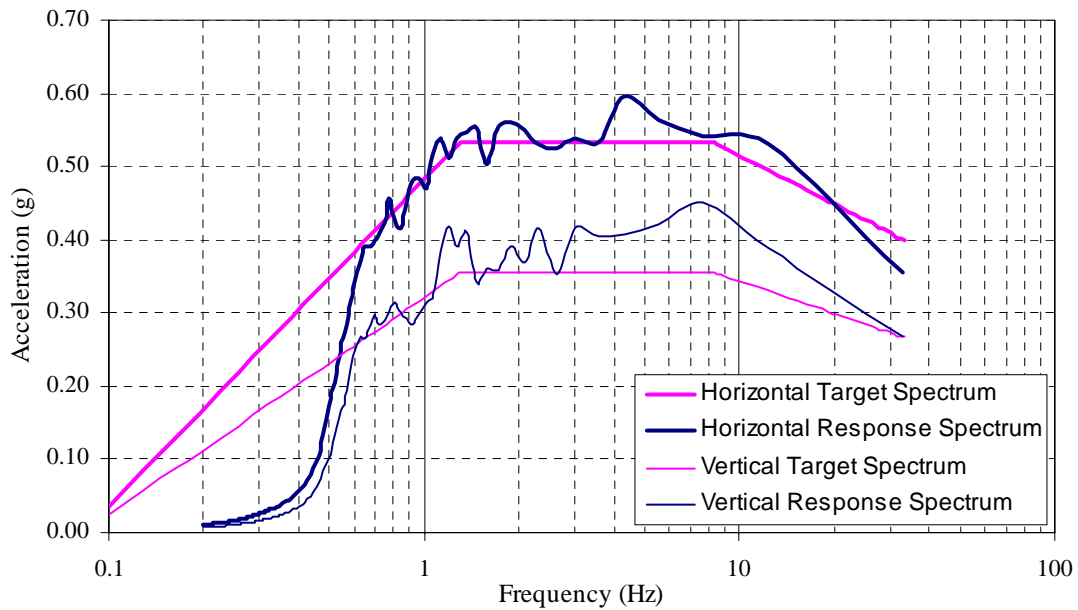




**a) horizontal acceleration**

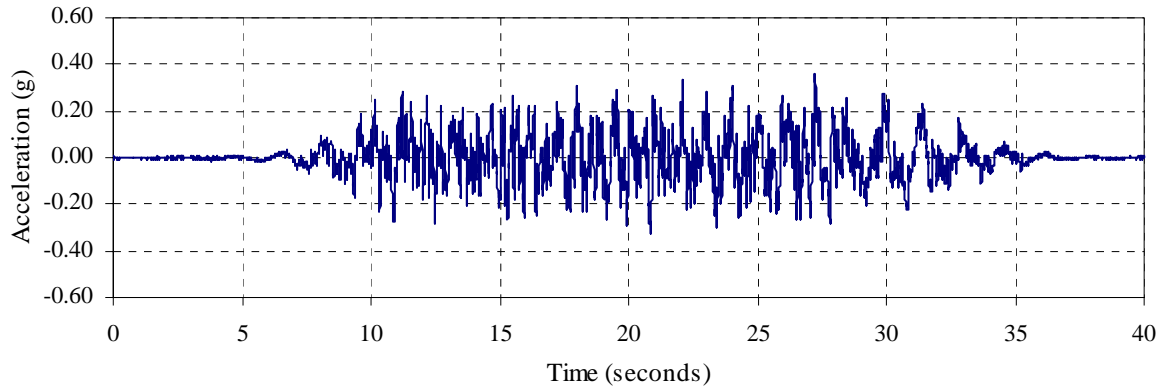


**b) vertical acceleration**

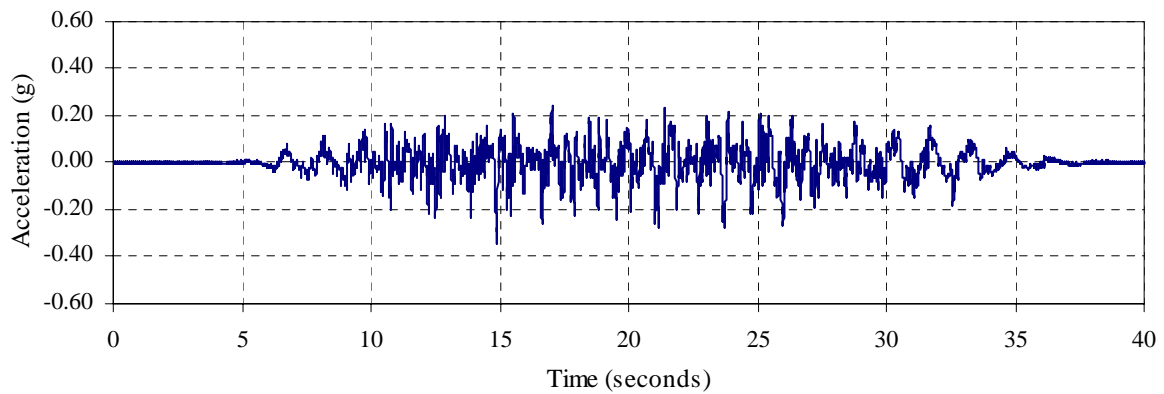


**c) horizontal and vertical response spectra (target and calculated)**

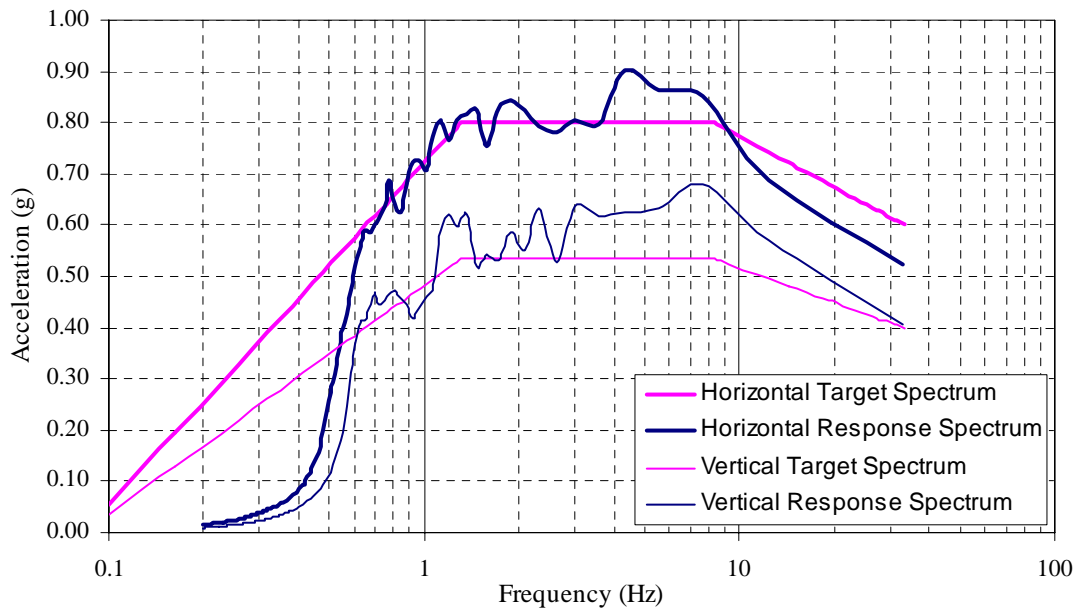
**FIGURE 5-17 Earthquake histories and spectra for test A050**



**a) horizontal acceleration**

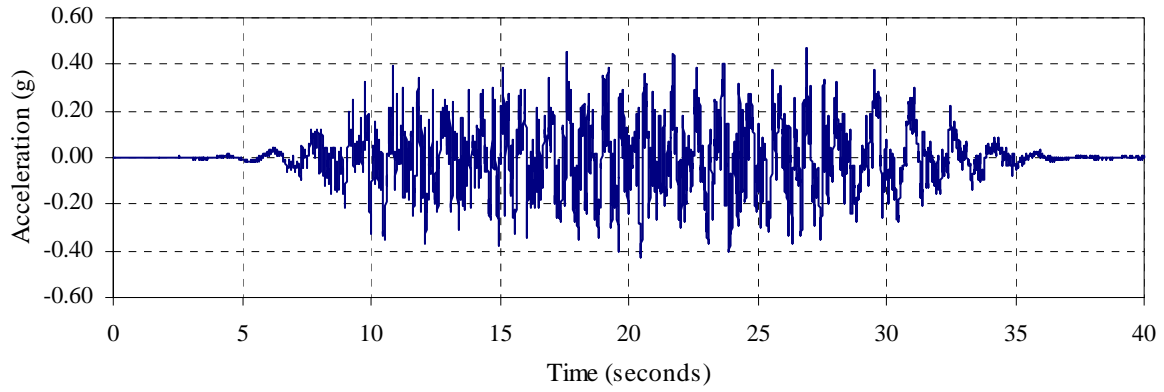


**b) vertical acceleration**

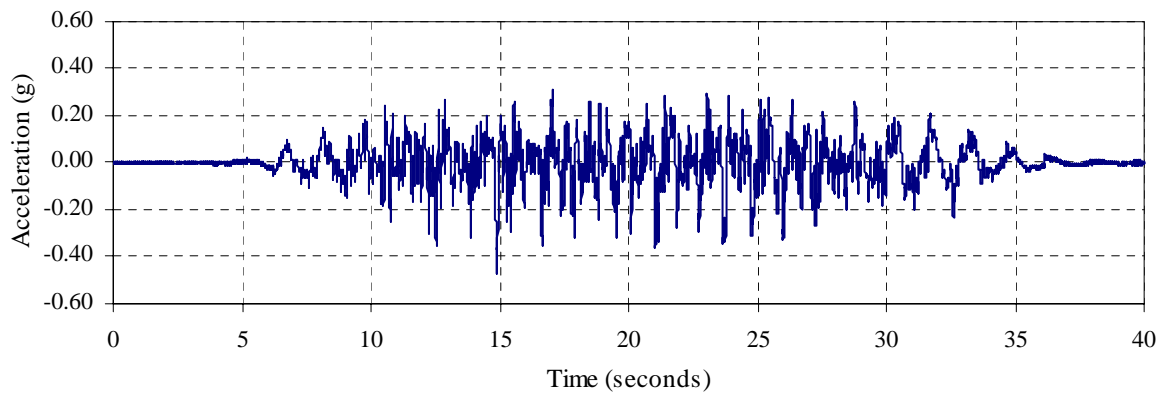


**c) horizontal and vertical response spectra (target and calculated)**

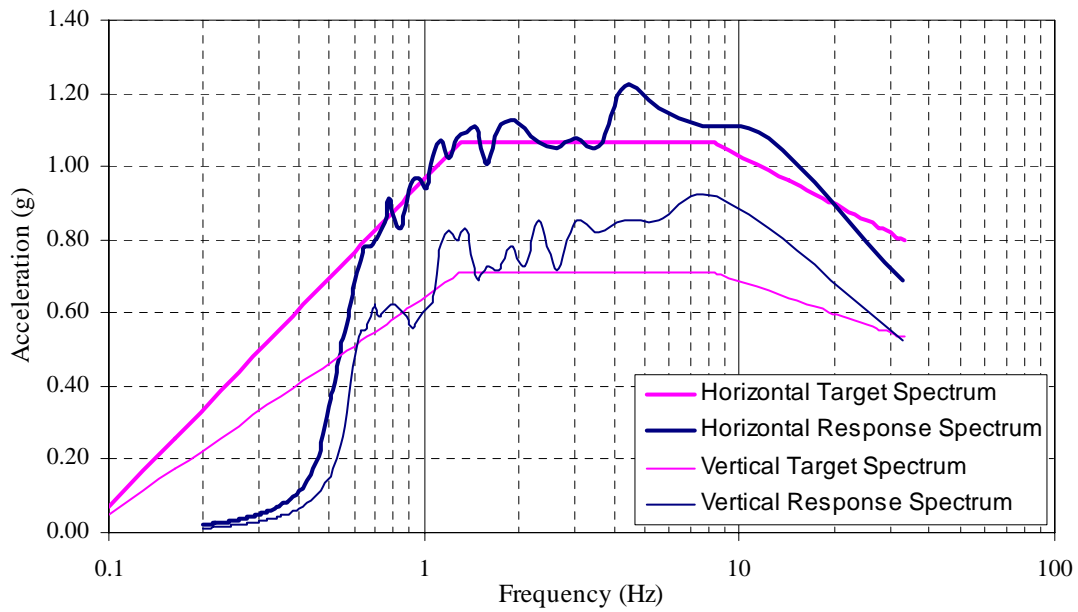
**FIGURE 5-18 Earthquake histories and spectra for test A075**



**a) horizontal acceleration**

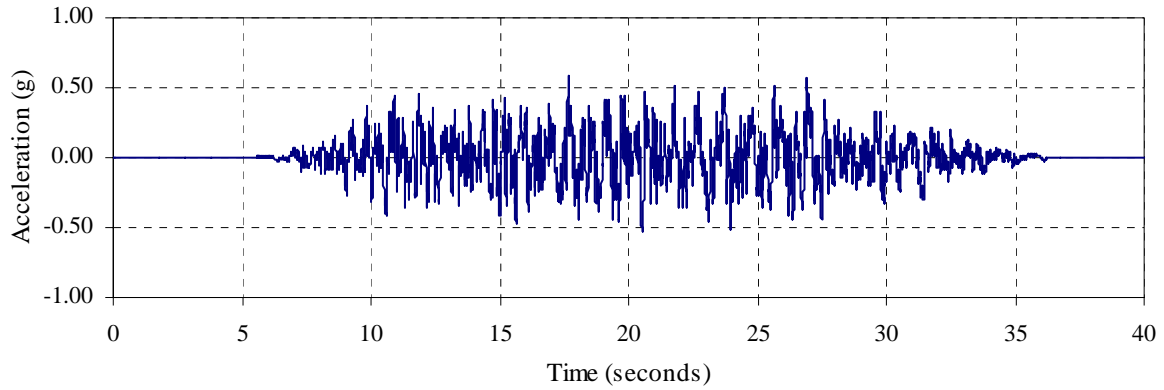


**b) vertical acceleration**

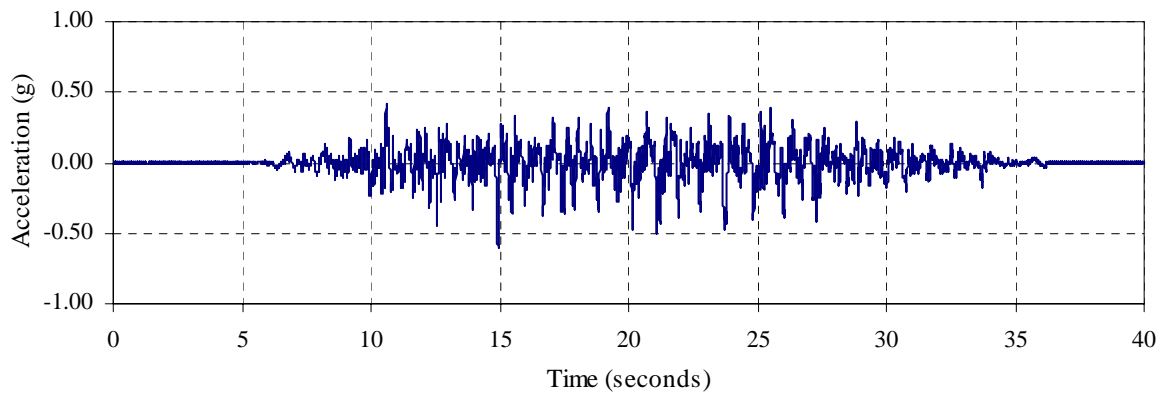


**c) horizontal and vertical response spectra (target and calculated)**

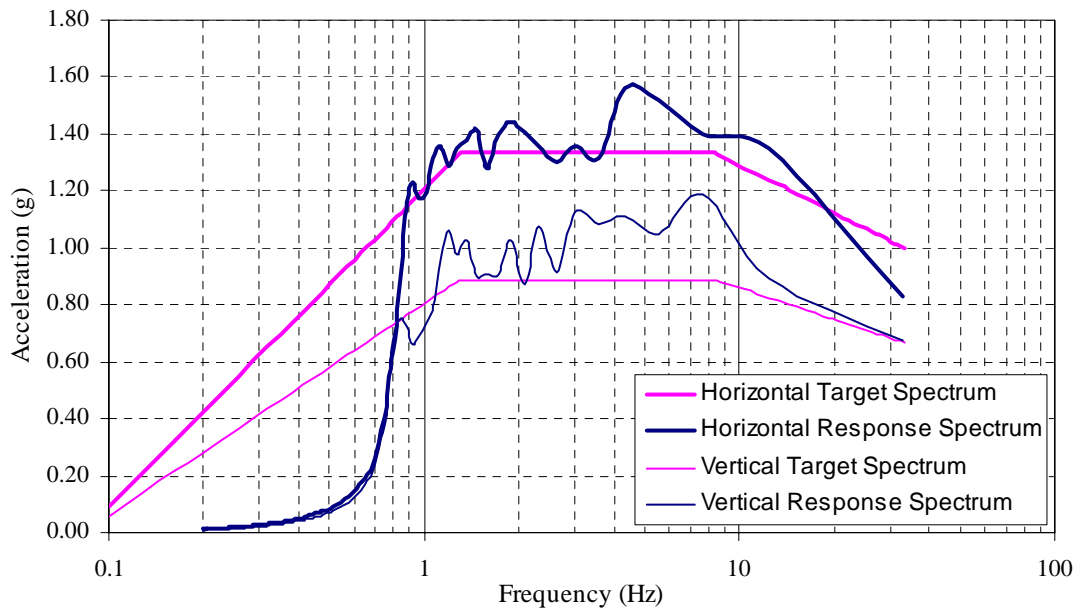
**FIGURE 5-19 Earthquake histories and spectra for test A100**



**a) horizontal acceleration**

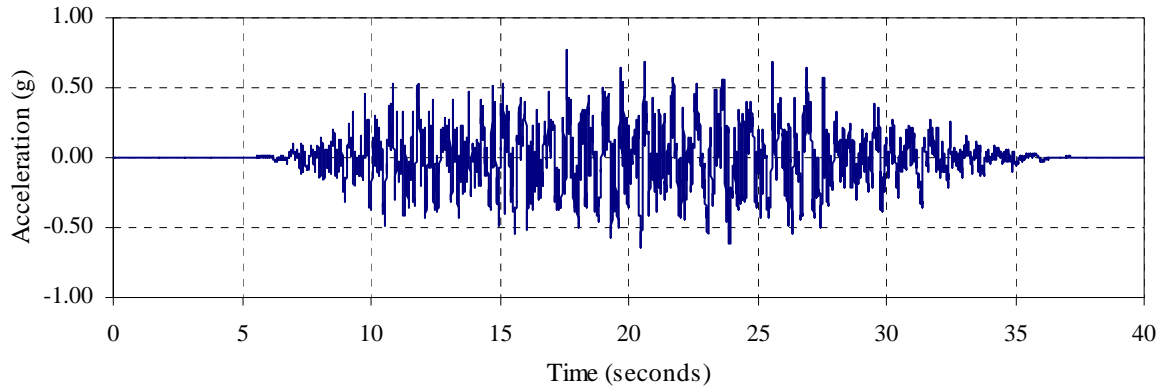


**b) vertical acceleration**

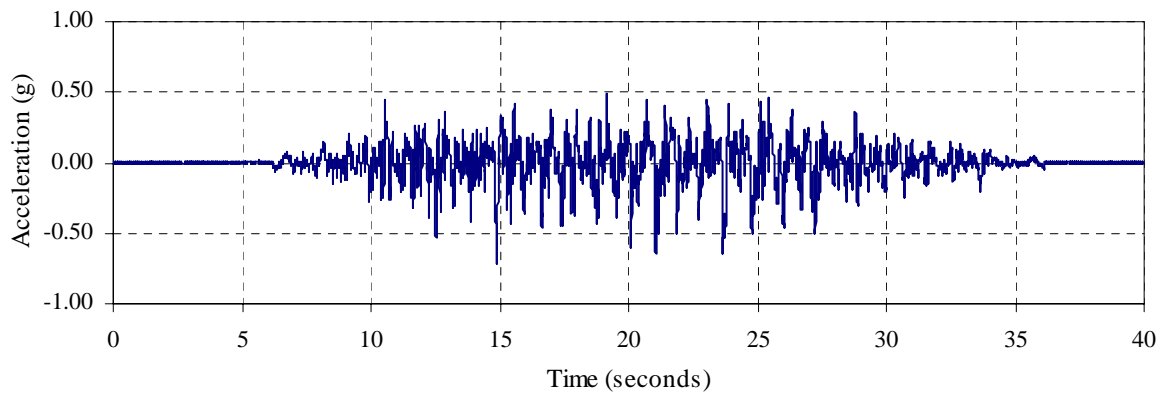


**c) horizontal and vertical response spectra (target and calculated)**

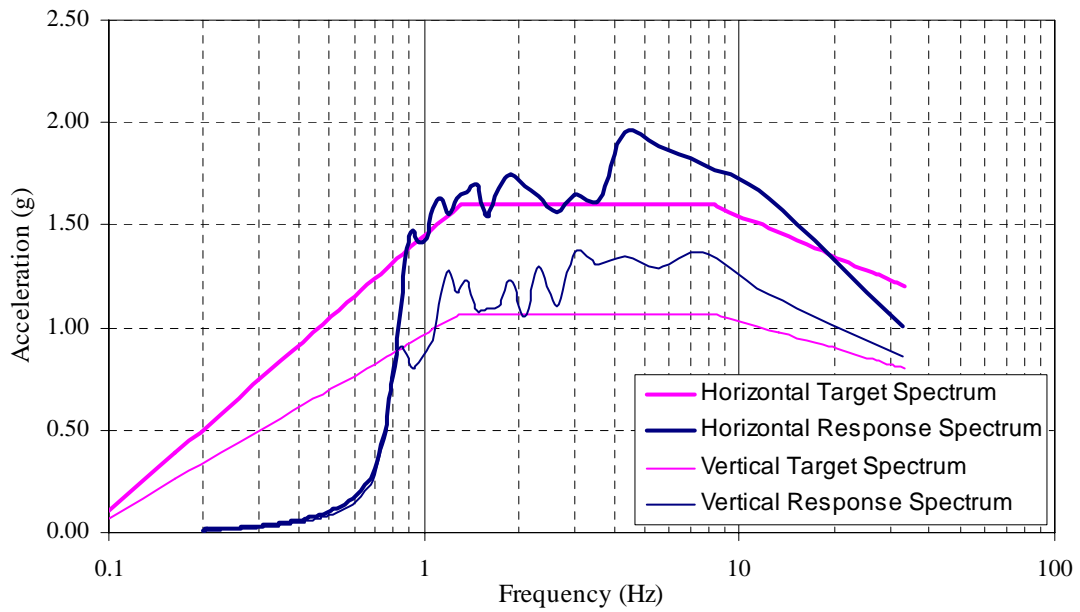
**FIGURE 5-20 Earthquake histories and spectra for test A125**



**a) horizontal acceleration**

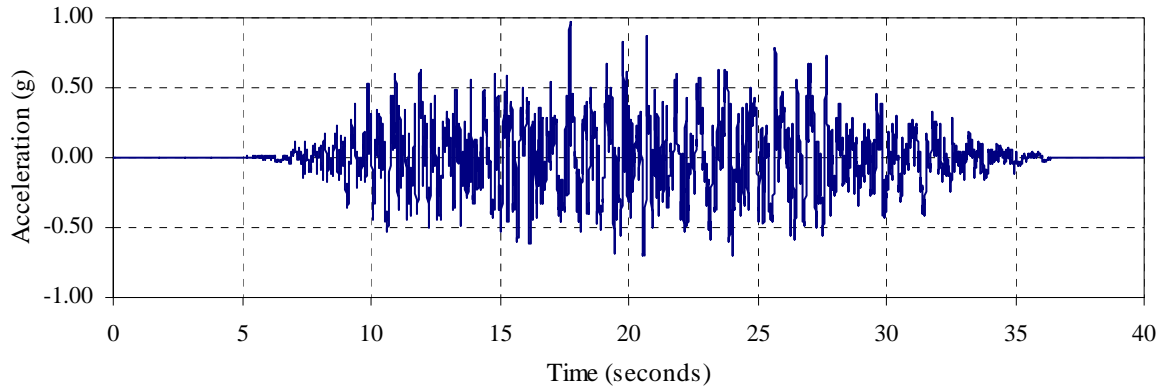


**b) vertical acceleration**

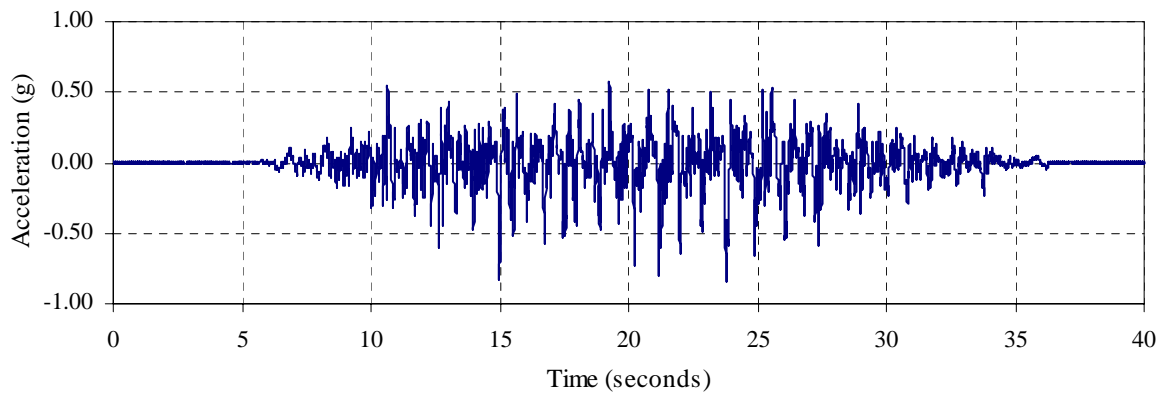


**c) horizontal and vertical response spectra (target and calculated)**

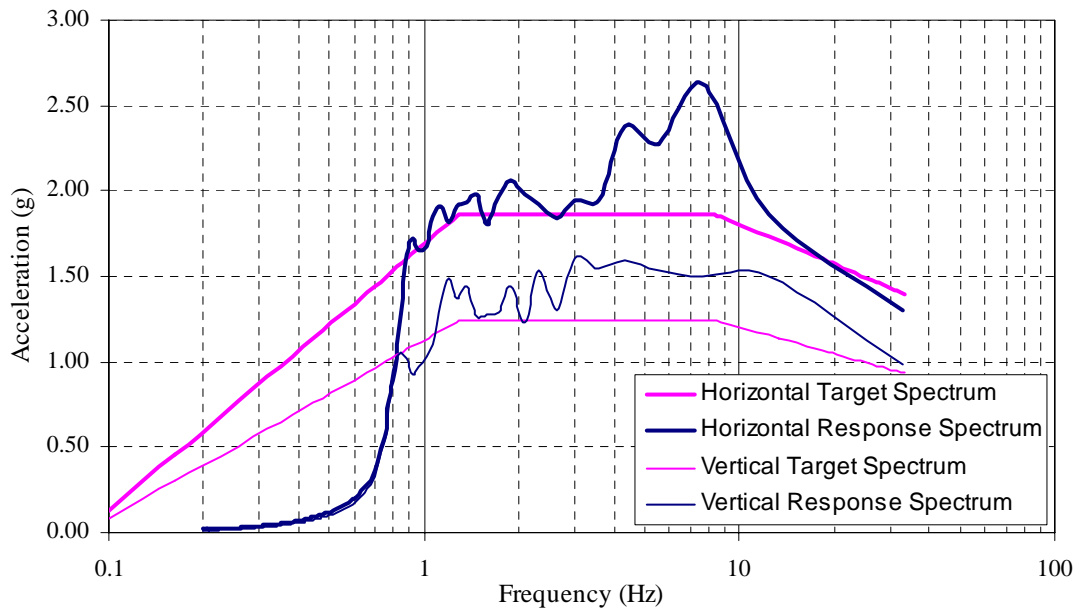
**FIGURE 5-21 Earthquake histories and spectra for test A150**



**a) horizontal acceleration**

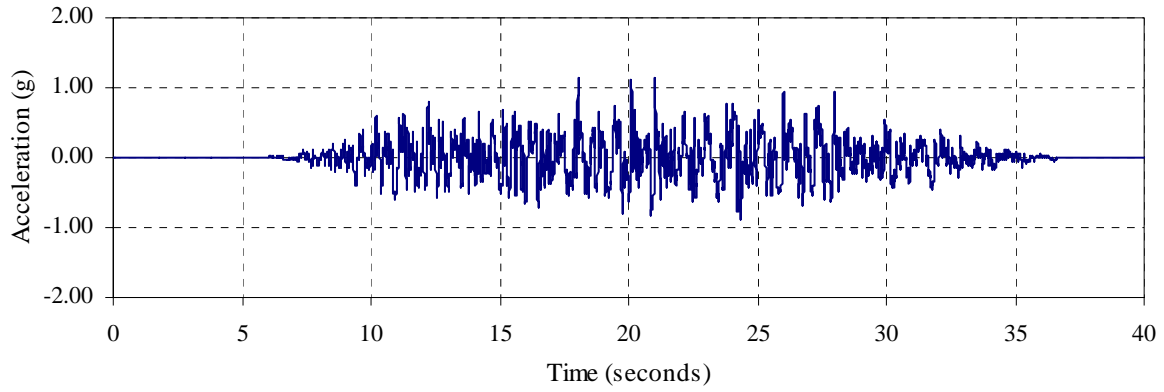


**b) vertical acceleration**

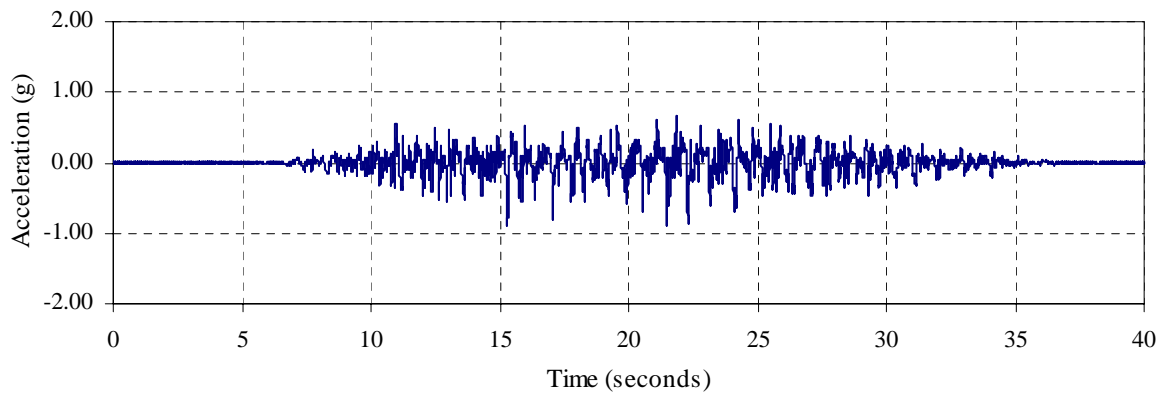


**c) horizontal and vertical response spectra (target and calculated)**

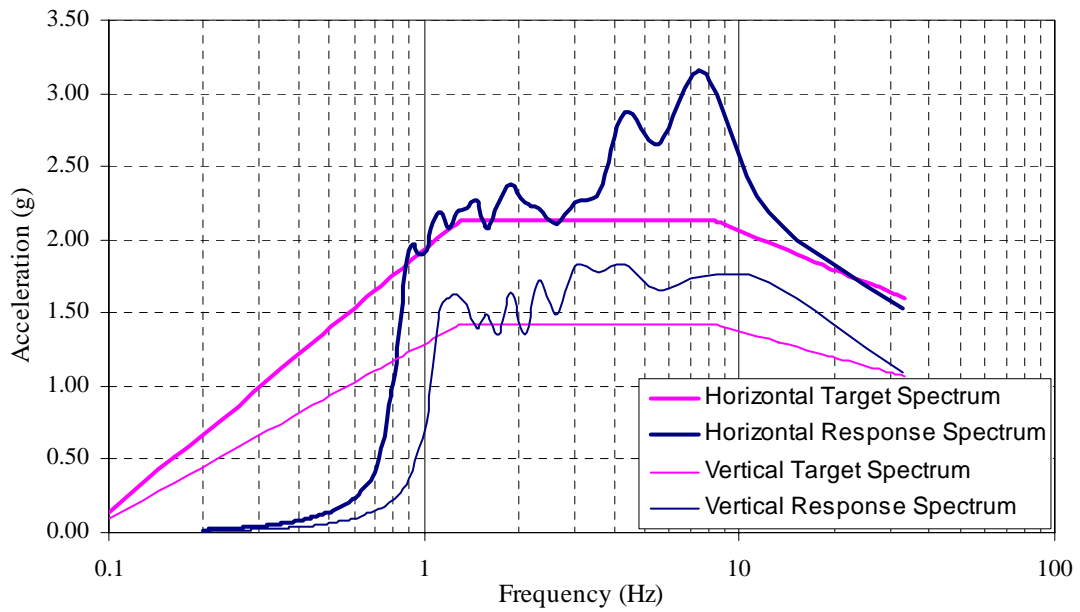
**FIGURE 5-22 Earthquake histories and spectra for test A175**



**a) horizontal acceleration**

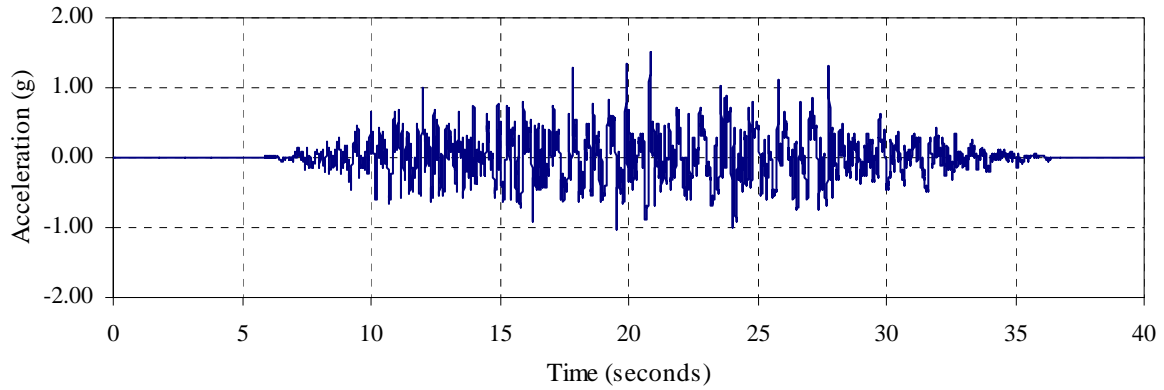


**b) vertical acceleration**

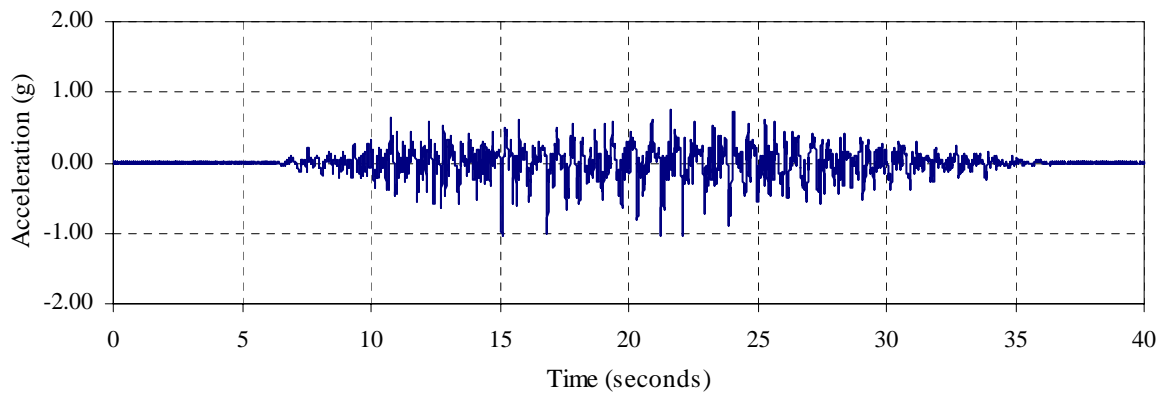


**c) horizontal and vertical response spectra (target and calculated)**

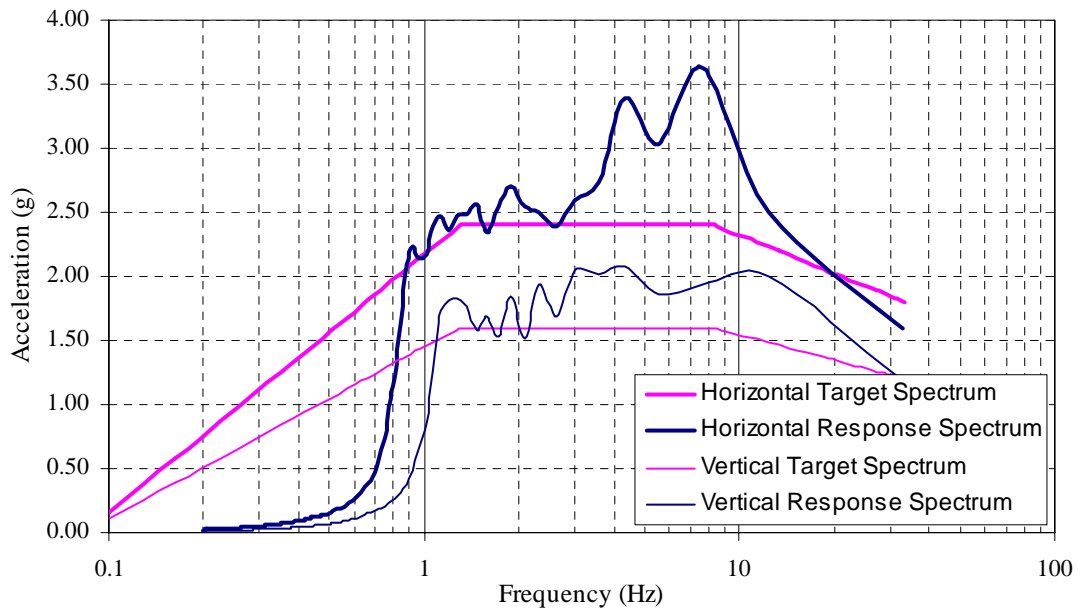
**FIGURE 5-23 Earthquake histories and spectra for test A200**



**a) horizontal acceleration**



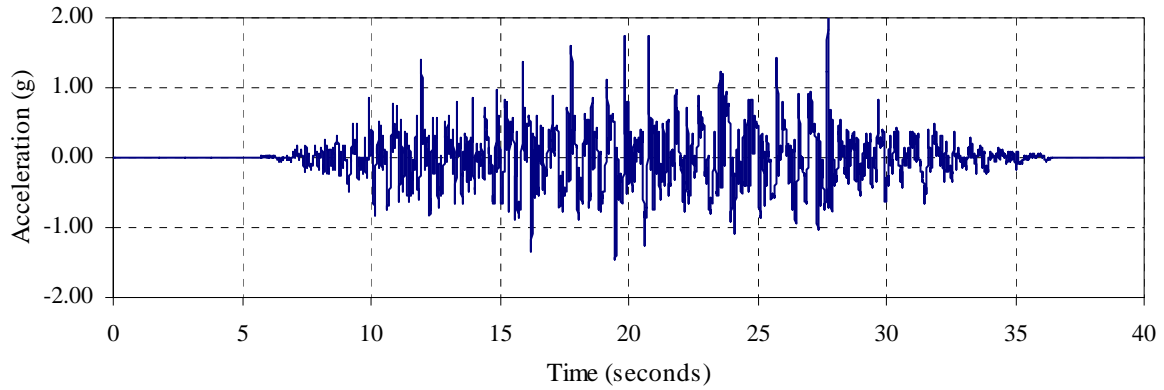
**b) vertical acceleration**



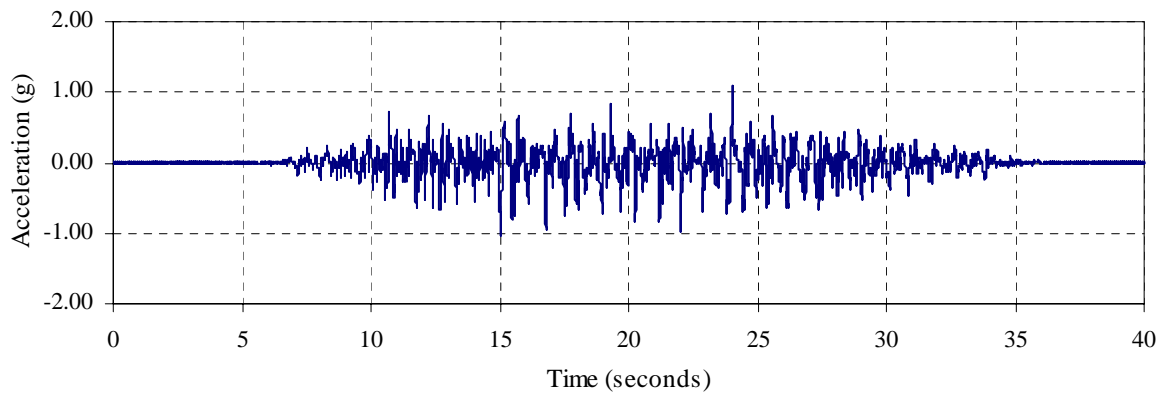
**c) horizontal and vertical response spectra (target and calculated)**

**FIGURE 5-24 Earthquake histories and spectra for test A225**

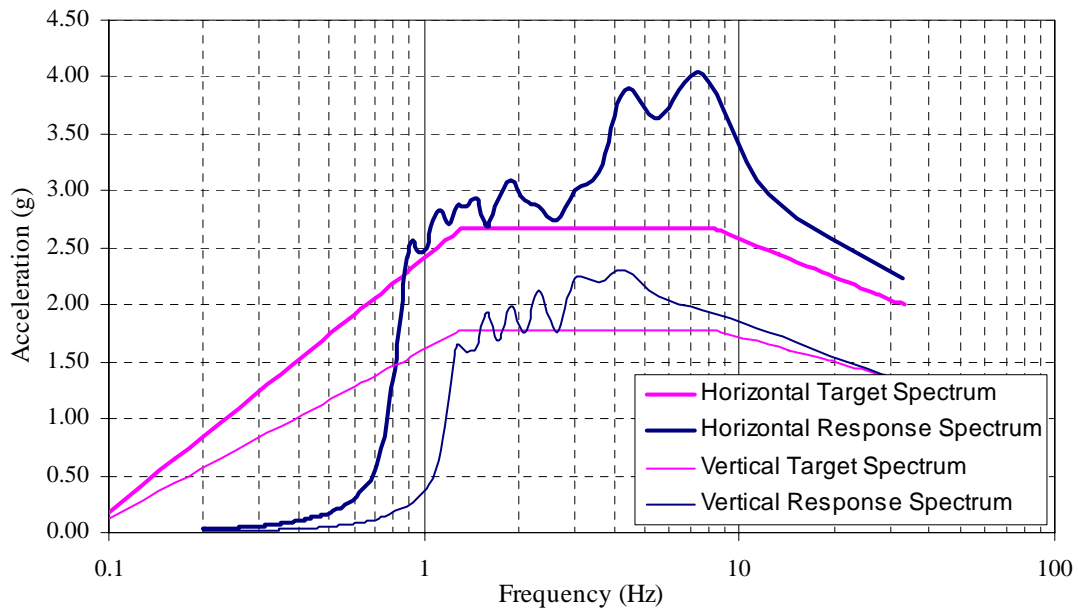




**a) horizontal acceleration**



**b) vertical acceleration**



**c) horizontal and vertical response spectra (target and calculated)**

**FIGURE 5-25 Earthquake histories and spectra for test A250**



## **CHAPTER 6**

### **SIMULATOR TESTING OF SUSPENDED CEILING SYSTEMS**

#### **6.1 Introduction**

Full-scale testing was conducted to develop fragility curves for ceiling systems because such systems are not amenable to structural analysis. Four variables that affect the seismic performance of suspended ceiling systems were investigated in this study: (1) the size and weight of tiles, (2) the use of retainer clips, (3) the use of compression posts, and (4) the physical condition of grid components. A total of six set-ups were configured using different combinations of these variables. Each set-up was tested multiple times with the protocol described in Section 5.3.

The ceiling systems were inspected visually after each test, in which all tiles, connections, anchors, hanging wires and splay wires were examined to ensure that the results obtained could be used to generate reliable fragility curves. All damaged ceiling components (e.g., broken latches of cross tees, chipped tiles) were replaced prior to the following test. After each test cycle (i.e., test no. 1 through test no. 33 in table 5-1) the entire ceiling system (tiles and grid) was disassembled and reassembled to return the ceiling system to a newly installed condition.

#### **6.2 Descriptions of Ceiling Systems**

The six test set-ups were: (1) undersized<sup>1</sup> tiles, (2) undersized tiles with retainer clips, (3) undersized tiles with recycled grid components, (4) normal sized tiles, (5) normal sized tiles with retainer clips and (6) normal sized tiles without the compression post. The following subsections describe each configuration.

---

<sup>1</sup> A tile is considered to be undersized if the plan dimensions (length and width) of the tile are smaller than the nominal dimensions by more than 1/4 in.

### **6.2.1 Configuration 1: Undersized Tiles**

The Armstrong Fine Fissured Humigard Plus tile (Armstrong item no. 1732) was used in configuration 1. The plan dimensions of this tile were 597 mm by 597 mm (23-1/2 in. by 23-1/2 in.): 12.7 mm (1/2 in.) smaller than the nominal size. The installation of the suspension system is described in Section 3.3.1. Four series of tests were performed in this configuration: series A-D. Figure 6-1 is a photograph of one of the systems of configuration 1.



**FIGURE 6-1 Configuration 1 installation, undersized tiles**

### **6.2.2 Configuration 2: Undersized Tiles with Retainer Clips**

The Armstrong Fine Fissured Humigard Plus tile (Armstrong item no. 1732) was used in configuration 2. The installation of the suspension system is described in Section 3.3.1. For this set-up, retainer clips were installed on the 1.22 m (4-ft) long cross tees in the North-South direction of the suspension grid. Three series of tests were performed in this configuration: series E-G. Figure 6-2 is a photograph of one of the systems of configuration 2.



**FIGURE 6-2 Configuration 2 installation, undersized tiles with retainer clips**

### **6.2.3 Configuration 3: Undersized Tiles with Recycled Grid Components**

The Armstrong Fine Fissured Humigard Plus tile (Armstrong item no. 1732) was used in configuration 3. The installation of the suspension system is described in Section 3.3.1. Grid components that were used in prior test set-ups and that were undamaged in those tests were used to build the suspension grid for the systems in configuration 3. Three series of tests were performed in this configuration: series H-J.

### **6.2.4 Configuration 4: Normal Sized Tiles**

The Armstrong Dune Humigard Plus tile (Armstrong item no. 1774) was used in configuration 4. The plan dimensions of this tile were 603 mm by 603 mm (23-3/4 in. by 23-3/4 in.): 6.4 mm (1/4 in.) smaller than the nominal size. The installation of the suspension system was as described in Section 3.3.1. Seven series of tests were performed in this configuration: series L-O, Q, R and BB. Figure 6-3 is a photograph of one of the systems of configuration 4.

For a point of reference, Configuration 4 would meet the requirements of the International Building Code for Seismic Design Categories D, E and F and would meet the CISCA requirements for seismic zones 3 and 4 (CISCA, 1992).



**FIGURE 6-3 Configuration 4 installation, normal sized tiles**

### **6.2.5 Configuration 5: Normal Sized Tiles with Retainer Clips**

The Armstrong Dune Humigard Plus tile (Armstrong item no. 1774) was used in configuration 5. The installation of the suspension system is described in Section 3.3.1. In this set-up, retainer clips were installed on the 1.22 m (4-ft) long cross tees in the North-South direction of the suspension grid. Four series of tests were performed in this configuration: series P-U.

### **6.2.6 Configuration 6: Normal Sized Tiles without Compression Post**

The Armstrong Dune Humigard Plus tile (Armstrong item no. 1774) was used in configuration 6. For this set-up, the compression post described in Section 3.3.1 was removed from the ceiling

system. The 45° splay cables that were installed as diagonal restraints at the compression post were left in place. Six series of tests were performed in this configuration: series V-Z and AA. Figure 6-4 is a photograph of one of the systems of configuration 6; the 45° splay cables can be seen in this photograph.



**FIGURE 6-4 Configuration 6 installation, normal sized tiles without compression post**

## **6.3 Experimental Results**

### **6.3.1 Introduction**

Each ceiling system in each configuration identified in Section 6.2 was subjected to the testing protocol described in Section 5. The testing protocol consisted of white noise tests, unidirectional shaking in the two programmable directions of the earthquake simulator (the horizontal North-South direction, and the vertical direction), and combined shaking (horizontal + vertical) for several levels of excitation. For details, see table 5-1 in Section 5. Tables 6-1 through 6-6 summarize the test results obtained for each configuration. In the summary remarks section, the

natural frequencies of each system are given for the horizontal direction,  $f_x$ , and the vertical direction,  $f_y$ , using data obtained from white noise tests.

The addition of the ceiling tiles added mass and some stiffness to the suspension grid. Only the vertical frequency of the system was altered substantially by the addition of the tiles. For example, the natural frequencies of the test frame established using white noise testing were 12.3 Hz and 9.5 Hz in the horizontal and vertical directions, respectively, whereas when the ceiling system of Series F was installed in the test frame, the frequencies were 12.0 Hz and 6.7 Hz in the horizontal and vertical directions, respectively. Similar results were obtained in the other series.

Initially, the test sequence included excitations corresponding to values of  $S_S$  between 0.25g and 2.5g. Since no failures were observed in the first few test series for the low level tests, the excitations corresponding to values of  $S_S$  between 0.25g and 0.75g in the systems with undersized tiles and between 0.25g and 1.25g in the systems with normal sized tiles, were eliminated from the test protocol. Tables 6-1 through 6-3 (systems undersized tiles) and tables 6-4 through 6-6 (systems with normal sized tiles) therefore present information only for the levels of excitation corresponding to  $S_S = 1.0g$  and above, and  $S_S = 1.5g$  and above, respectively. The following subsections present a description of the main findings obtained from observations during testing and from the information presented in tables 6-1 through 6-6.

### **6.3.2 Configuration 1: Undersized Tiles**

Of the vertical and horizontal unidirectional motions, the vertical excitations produced more damage in terms of loss of tiles. The combined motions (horizontal and vertical) produced more damage than either of the unidirectional excitations. The first loss of tiles from the grid occurred for a combined level of shaking corresponding to  $S_S = 1.5g$ . See table 6-1 for a summary of the test results. The most common mode of failure was tiles jumping up (popping up) out of the grid. If the tiles did not return to the original position on the suspension system (i.e. tiles lying on the web of the cross tees in one or more sides of the tile or tiles slightly tilted), it was very likely for the tiles to rotate and fall. Figure 6-5 shows a tile an instant before it fell to the earthquake simulator platform below. The tile is shown rotating around a diagonal axis formed between the



two corners of the tile that remain supported on the grid. Figure 6-6 shows the tile of figure 6-5 falling to the simulator platform during the combined shaking test corresponding to  $S_S = 2.5g$ , in Series C.



**FIGURE 6-5 Tile rotating before falling, configuration 1**



**Figure 6-6 Tile of figure 6-5 falling from the suspension grid**

**TABLE 6-1 Results for undersized tiles, series A-D**

<i>Test Name</i>	<i>Summary remarks</i> <sup>1, 2</sup>			
	<i>Series A</i>	<i>Series B</i>	<i>Series C</i>	<i>Series D</i>
WNH	$f_x = 11.8$ Hz	$f_x = 12.1$ Hz	$f_x = 12.2$ Hz	$f_x = 12.1$ Hz
WNV	$f_y = 11.2$ Hz	$f_y = 6.9$ Hz	$f_y = 6.9$ Hz	$f_y = 6.9$ Hz
100H	No damage	No damage	No damage	No damage
100V	No damage	No damage	No damage	No damage
100HV	No damage	No damage	No damage	No damage
125H	No damage	No damage	No damage	No damage
125V	No damage	No damage	No damage	No damage
125HV	No damage	No damage	No damage	No damage
150H	No damage	No damage	No damage	No damage
150V	No damage	No damage	No damage	No damage
150HV	1 tile fell	1 tile fell	1 tile fell	1 tile fell
175H	No damage	No damage	No damage	No damage
175V	No damage	No damage	No damage	No damage
175HV	2 tiles fell	3 tiles fell	4 tiles fell	3 tiles fell
200H	No damage	No damage	No damage	No damage
200V	No damage	No damage	No damage	1 tile fell
200HV	6 tiles fell	10 tiles fell	10 tiles fell	9 tiles fell
225H	No damage	2 tiles fell	No damage	No damage
225V	No damage	No damage	No damage	No damage
225HV	16 tiles fell	14 tiles fell	13 tiles fell	18 tiles fell
250H	No damage	No damage	No damage	1 tile fell 2 4-ft tees failed
250V	1 tile fell	3 tiles fell	1 tile fell	1 tile fell
250HV	18 tiles fell	25 tiles fell 1 2-ft tee failed	26 tiles fell	25 tiles fell 1 2-ft tee failed

<sup>1</sup> The 61 cm (2-ft) and 122 cm (4-ft) cross tees were installed in the North-South and East-West directions of the test frame, respectively. See Section 3.3.1 for details of the configuration of the suspension grid.

<sup>2</sup> The definition of failure of the cross tees included components that: (1) fell, (2) were bent, and (3) had to be replaced because they compromised the structural integrity of the entire grid if they were left in place.

### 6.3.3 Configuration 2: Undersized Tiles with Retainer Clips

Of the vertical and horizontal unidirectional motions, the vertical excitation produced more damage in configuration 2 in terms of loss of tiles and damage to the suspension system. The combined motions (horizontal and vertical) produced more damage than either of the unidirectional excitations. The first loss of tiles from the grid occurred in the vertical and combined tests for the shaking level corresponding to  $S_S = 2.25g$ . Damage in the suspension grid appeared in the vertical and combined tests for the shaking level corresponding to  $S_S = 2.0g$ . See table 6-2 for a summary of the test results.

The retainer clips substantially improved the behavior of the suspended ceiling systems in terms of loss of tiles by comparison with the systems of configuration 1 where clips were not included. For example, for the combined shaking level corresponding to  $S_S = 2.5g$  in Series B (system without clips; see table 6-1), twenty-five tiles fell. For the same level of combined shaking in Series F (system with clips; see table 6-2), only two tiles fell. The retainer clips protected the tiles from falling from the grid but led to damage to the suspension grid at lower levels of shaking:  $200V$  in configuration 2 versus  $250H$  in configuration 1. By retaining the tiles, the clips increased the inertial loads on the grid, resulting in grid damage at lower levels of shaking. Figure 6-7 shows a buckled 1.22 m (4-ft) cross tee (see table 3.1 for grid component details) following a  $250HV$  test level. Another example of damage to the grid components is presented in figure 6-8, where the latches of the cross tees are shown bent and broken. The 1.22 m (4-ft) cross tees that were damaged were replaced prior to the following test. In the systems of configuration 2, tiles were lost primarily due to failure of grid components.

**TABLE 6-2 Results for undersized tiles with retainer clips, series E-G**

<i>Test Name</i>	<i>Summary remarks</i> <sup>1, 2</sup>		
	<i>Series E</i>	<i>Series F</i>	<i>Series G</i>
WNH	$f_x = 11.8$ Hz	$f_x = 12.0$ Hz	$f_x = 11.9$ Hz
WNV	$f_y = 6.9$ Hz	$f_y = 6.7$ Hz	$f_y = 6.7$ Hz
100H	No damage	No damage	No damage
100V	No damage	No damage	No damage
100HV	No damage	No damage	No damage
125H	No damage	No damage	No damage
125V	No damage	No damage	No damage
125HV	No damage	No damage	No damage
150H	No damage	No damage	No damage
150V	No damage	No damage	No damage
150HV	No damage	No damage	No damage
175H	No damage	No damage	No damage
175V	No damage	No damage	No damage
175HV	No damage	No damage	No damage
200H	No damage	No damage	No damage
200V	1 2-ft tee failed	No damage	No damage
200HV	1 2-ft tee failed	No damage	No damage
225H	No damage	No damage	1 2-ft tee failed
225V	No damage	2 tiles fell 1 2-ft tee failed	4 4-ft tees failed
225HV	4 4-ft tees failed	2 tiles fell 2 4-ft tees failed	1 tile fell 2 4-ft tees failed
250H	No damage	No damage	No damage
250V	No damage	2 tiles fell 1 2-ft tee failed	4 4-ft tees failed
250HV	1 tile fell 2 4-ft tees failed	2 tiles fell	2 tiles fell

<sup>1</sup> The 61 cm (2-ft) and 122 cm (4-ft) cross tees were installed in the North-South and East-West directions of the test frame, respectively. See Section 3.3.1 for details of the configuration of the suspension grid.

<sup>2</sup> The definition of failure of the cross tees included components that: (1) fell, (2) were bent, and (3) had to be replaced because they compromised the structural integrity of the entire grid if they were left in place.

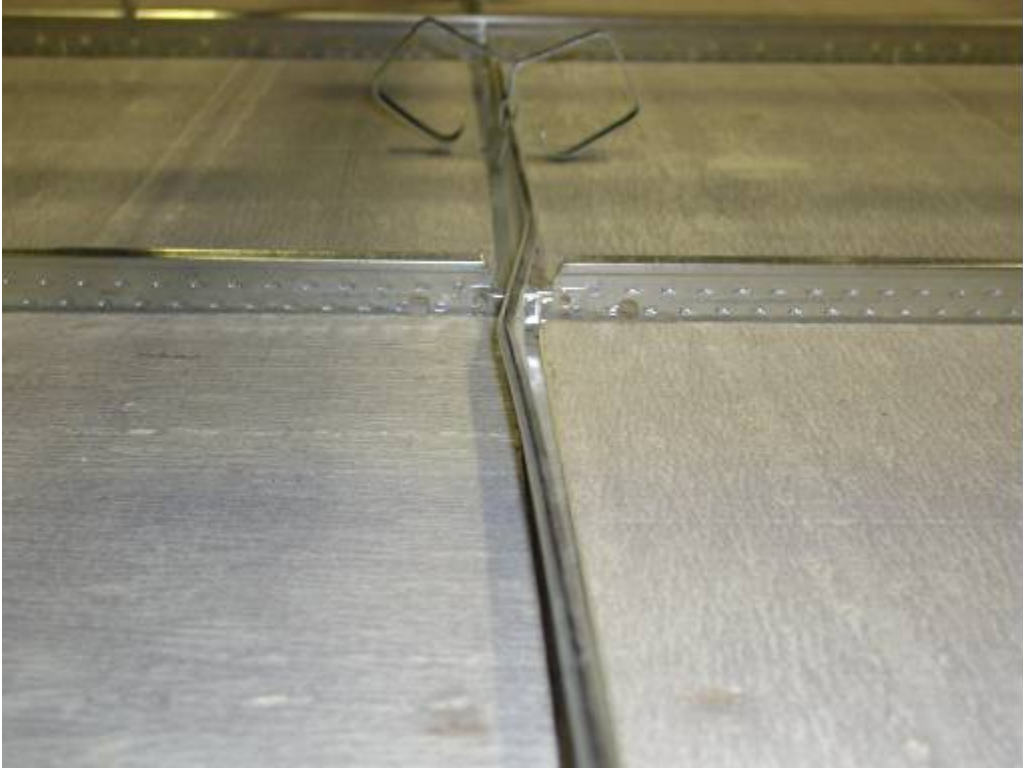


**FIGURE 6-7** Damage to the cross tees installed in the East-West direction, configuration 2

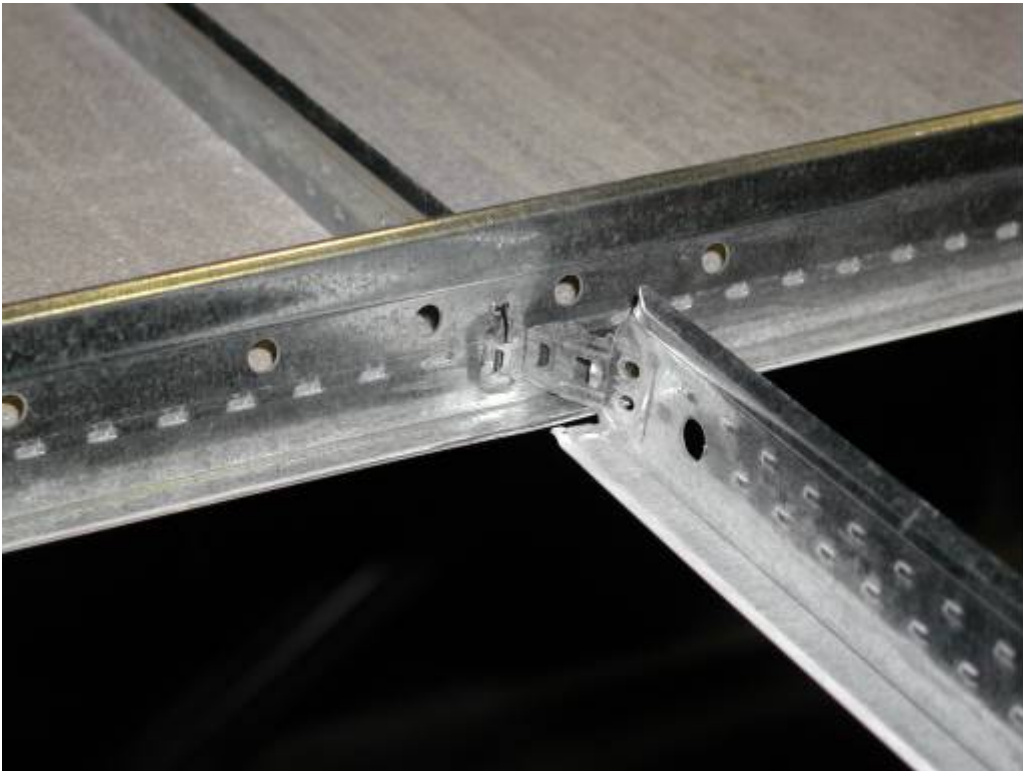


**FIGURE 6-8** Damage to the latches on the cross tees in configuration 2

### 6.3.4 Configuration 3: Undersized Tiles with Recycled Grid Components

Of the vertical and horizontal unidirectional motions, the vertical excitation produced more damage in terms of loss of tiles. The combined motions (horizontal and vertical) produced more damage than either of the unidirectional excitations. The first loss of tiles from the grid occurred for combined shaking corresponding to  $S_S = 1.0g$ . See table 6-3 for a summary of the test results.

Including recycled cross-tees in the assemblage of the suspended grid substantially increased the number of tiles that fell during the earthquake tests (unidirectional and combined motions), by comparison with the systems where only new grid components were used. For example, for the level of shaking corresponding to  $S_S = 2.5g$  in Series D (system with only new grid components), zero, one and twenty-six tiles fell for the horizontal, vertical and combined motions, respectively; whereas for the same level of shaking in Series I (system with recycled grid components), three, nine and forty-one tiles fell for the horizontal, vertical and combined motions, respectively. Although the failure pattern of the tiles was similar to that of configuration 1, the number of tiles that fell in configuration 3 was larger because the locking assembly latches that secured the connection between the cross tees did not lock completely, leaving the mechanical connection between the cross tees slightly loose. Therefore, the ability to transfer load between adjacent sections of the ceiling grid was diminished by comparison with the systems where only new grid components were used.

**TABLE 6-3 Results for undersized tiles with recycled grid components, series H-J**

<i>Test Name</i>	<i>Summary remarks</i> <sup>1, 2</sup>		
	<i>Series H</i>	<i>Series I</i>	<i>Series J</i>
WNH	$f_x = 12.0$ Hz	$f_x = 12.0$ Hz	$f_x = 12.0$ Hz
WNV	$f_y = 6.7$ Hz	$f_y = 6.7$ Hz	$f_y = 6.7$ Hz
100H	No damage	No damage	No damage
100V	No damage	No damage	No damage
100HV	No damage	No damage	No damage
125H	No damage	No damage	No damage
125V	No damage	No damage	No damage
125HV	No damage	No damage	3 tiles fell
150H	No damage	No damage	1 tile fell 1 2-ft tee failed
150V	No damage	1 tile fell	No damage
150HV	4 tiles fell	10 tiles fell	9 tiles fell
175H	No damage	No damage	No damage
175V	No damage	No damage	3 tiles fell
175HV	8 tiles fell	11 tiles fell	22 tiles fell
200H	No damage	No damage	1 tile fell
200V	1 tile fell	1 tile fell	2 tiles fell
200HV	13 tiles fell	23 tiles fell	20 tiles fell
225H	No damage	4 tiles fell 1 2-ft tee failed	5 tiles fell 1 2-ft tee failed
225V	2 tiles fell	4 tiles fell	9 tiles fell
225HV	27 tiles fell	27 tiles fell	37 tiles fell
250H	No damage	3 tiles fell 1 2-ft tee failed	6 tiles fell 1 2-ft tee failed
250V	4 tiles fell	9 tiles fell	7 tiles fell
250HV	42 tiles fell	41 tiles fell 2 2-ft tees failed	38 tiles fell

<sup>1</sup> The 61 cm (2-ft) and 122 cm (4-ft) cross tees were installed in the North-South and East-West directions of the test frame, respectively. See Section 3.3.1 for details of the configuration of the suspension grid.

<sup>2</sup> The definition of failure of the cross tees included components that: (1) fell, (2) were bent, and (3) had to be replaced because they compromised the structural integrity of the entire grid if they were left in place.

### 6.3.5 Configuration 4: Normal Sized Tiles

Of the vertical and horizontal unidirectional motions, the horizontal excitation produced more damage in terms of loss of tiles. The combined motions (horizontal and vertical) produced more damage than either of the unidirectional excitations. The first loss of tiles from the grid occurred for combined shaking corresponding to  $S_S = 1.75g$ . See table 6-4 for a summary of the test results.

The effect of a small variation in tile size on the performance of the ceiling systems was considerable in terms of loss of tiles. The number of tiles that fell during the shaking tests of ceiling systems with undersized or poorly fitting tiles was substantially larger by comparison with the systems equipped with normal sized (snug) tiles. For example, for the combined shaking level corresponding to  $S_S = 2.5g$  in Series C (system with undersized tiles, see table 6-1), twenty-six tiles fell; whereas for the same level of combined shaking in Series N (system with normal sized tiles; see table 6-4), sixteen tiles fell. However, ceiling system performance in terms of damage to grid components was better in the systems with undersized tiles. This observation is due mainly to two factors: (1) the weight of the normal sized tiles was larger (1.7 kg/tile) than the undersized tiles (1.3 kg/tile), and (2) because the number of tiles that stayed in place during shaking was larger for the systems of configuration 4 (normal sized tiles): inertial loads on the suspension grid were larger for configuration 4 than in configuration 1 (undersized tiles). Figures 6-9 and 6-10 show damage to the 1.22 m (4-ft) cross tees that were installed in the East-West direction. The buckling in the web of the 1.22 m (4-ft) cross tees was similar to the damage that the grid components experienced in configuration 2 (undersized tiles with clips) during higher levels of shaking. The tile failure pattern in configuration 4 was similar to that of configuration 1.

It is important to note that differences in boundary conditions during testing can affect substantially the seismic performance of a ceiling system. Consider the data of table 6-4 and the considerable differences between the results of Series Q and those of the other series that were part of the same set-up. The difference in response is due to damage on the wall molding, which was originally attached to the South side of the test frame, around the screws that served as the wall connectors. There was no mechanical connection between the ceiling system and the test



frame in the North-South direction for the Series Q tests. Minor changes in boundary conditions can significantly affect the response of ceiling systems and the fragility curves developed using such data. Because the series Q boundary conditions varied from those of series L, M, N, O, R and BB, the series Q data were not used to develop fragility curves.

**TABLE 6-4 Results for normal sized tiles, series L-O, Q, R and BB**

<i>Test Name</i>	<i>Summary remarks</i> <sup>1, 2</sup>			
	<i>Series L</i>	<i>Series M</i>	<i>Series N</i>	<i>Series O</i>
WNH	$f_x = 12.0$ Hz	$f_x = 12.0$ Hz	$f_x = 12.0$ Hz	$f_x = 12.2$ Hz
WNV	$f_y = 6.9$ Hz	$f_y = 6.7$ Hz	$f_y = 6.7$ Hz	$f_y = 6.8$ Hz
150H	No damage	No damage	No damage	No damage
150V	No damage	No damage	No damage	No damage
150HV	No damage	No damage	No damage	No damage
175H	No damage	No damage	No damage	No damage
175V	No damage	No damage	No damage	No damage
175HV	No damage	No damage	No damage	3 tiles fell 1 2-ft tee failed
200H	No damage	1 2-ft tee failed	No damage	1 tile fell 1 2-ft tee failed
200V	No damage	No damage	No damage	No damage
200HV	3 tiles fell	1 tile fell	4 tiles fell	5 tiles fell 1 2-ft tee failed
225H	No damage	No damage	2 tiles fell 1 2-ft tee failed	2 tiles fell 1 2-ft tee failed
225V	No damage	No damage	No damage	No damage
225HV	6 tiles fell	3 tiles fell	4 tiles fell	9 tiles fell 1 2-ft tee failed
250H	No damage	4 tiles fell 2 2-ft tees failed	4 tiles fell 1 4-ft and 1 2-ft tee failed	4 tiles fell 2 2-ft tees failed
250V	No damage	No damage	No damage	1 tile fell
250HV	13 tiles fell 2 4-ft and 4 2-ft tees failed	12 tiles fell 1 4-ft and 4 2-ft tees failed	16 tiles fell 3 4-ft and 8 2-ft tees failed	29 tiles fell 5 4-ft and 12 2-ft tees failed

**TABLE 6-4 Results for normal sized tiles, series L-O, Q, R and BB (cont'd)**

<i>Test Name</i>	<i>Summary remarks</i> <sup>1, 2</sup>		
	<i>Series Q</i> <sup>3</sup>	<i>Series R</i>	<i>Series BB</i>
WNH	$f_x = 12.2$ Hz	$f_x = 12.1$ Hz	$f_x = 12.1$ Hz
WNV	$f_y = 7.1$ Hz	$f_y = 7.1$ Hz	$f_y = 6.9$ Hz
150H	No damage	No damage	No damage
150V	No damage	No damage	No damage
150HV	1 tile fell	No damage	No damage
175H	No damage	No damage	No damage
175V	No damage	No damage	No damage
175HV	3 tiles fell	3 tiles fell	3 tiles fell
200H	No damage	No damage	No damage
200V	No damage	No damage	No damage
200HV	5 tiles fell	2 tiles fell	5 tiles fell
225H	No damage	No damage	No damage
225V	No damage	No damage	No damage
225HV	8 tiles fell 1 2-ft tee failed	8 tiles fell 1 2-ft tee failed	14 tiles fell
250H	5 tiles fell 3 2-ft tees failed	2 tiles fell 1 2-ft tee failed	1 tile fell 1 2-ft tee failed
250V	No damage	1 tile fell	2 tiles fell
250HV	44 tiles fell 14 4-ft and 17 2-ft tees failed	21 tiles fell 4 4-ft and 6 2-ft tees failed	20 tiles fell 1 4-ft and 1 2-ft tee failed

<sup>1</sup> The 61 cm (2-ft) and 122 cm (4-ft) cross tees were installed in the North-South and East-West directions of the test frame, respectively. See Section 3.3.1 for details of the configuration of the suspension grid.

<sup>2</sup> The definition of failure of the cross tees included components that: (1) fell, (2) were bent, and (3) had to be replaced because they compromised the structural integrity of the entire grid if they were left in place.

<sup>3</sup> The results of tests of system Q were not used for analysis; see explanation in Section 6.3.5.



**FIGURE 6-9** Damage to the East-West cross tees in configuration 4



**FIGURE 6-10** Damage to the East-West cross tees in configuration 4

### 6.3.6 Configuration 5: Normal Sized Tiles with Retainer Clips

In configuration 5, the combined excitations (horizontal and vertical) produced more damage than either of the unidirectional excitations. The damage produced by the horizontal and vertical unidirectional motions was minimal and was concentrated in the grid components. The first loss of tiles from the grid occurred for vertical shaking corresponding to  $S_S = 2.25g$ . Damage to the suspension grid was first observed in the combined excitation test corresponding to  $S_S = 2.0g$ . See table 6-5 for summary results.

The retainer clips substantially improved the behavior of the suspended ceiling systems in terms of loss of tiles by comparison with the systems of configuration 4, where clips were not included. For example, for the combined shaking level corresponding to  $S_S = 2.5g$ , in Series M (system without clips; see table 6-4), twelve tiles fell; whereas for the same level of combined shaking in Series U (system with clips; see table 6-5), only two tiles fell. The use of the retainer clips shifted the damage from the tiles to the suspension grid as described in Section 6.3.2. The type of damage that was observed in the East-West 1.22 m (4-ft) cross tees of configuration 2 was also observed in the systems of configuration 5. In both systems, the loss of tiles was primarily due to the failure of grid components. This damage is shown in figure 6-11 and in the data presented in table 6-5, where for the combined shaking level corresponding to  $S_S = 2.5g$  in Series T, a major failure in the suspension grid led to the loss of a considerable number of tiles, in comparison with the other systems that were part of this configuration (systems P, S and U). The photograph of figure 6-11 shows that the tiles fell together with the suspension grid, since after falling the tiles and grid were approximately in the same arrangement as that prior to shaking.

**TABLE 6-5 Results for normal sized tiles with retainer clips, series P and S-U**

<i>Test Name</i>	<i>Summary remarks</i> <sup>1, 2</sup>			
	<i>Series P</i>	<i>Series S</i>	<i>Series T</i>	<i>Series U</i>
WNH	$f_x = 11.9$ Hz	$f_x = 11.9$ Hz	$f_x = 11.9$ Hz	$f_x = 11.9$ Hz
WNV	$f_y = 7.0$ Hz	$f_y = 6.8$ Hz	$f_y = 6.8$ Hz	$f_y = 7.0$ Hz
150H	No damage	No damage	No damage	No damage
150V	No damage	No damage	No damage	No damage
150HV	No damage	No damage	No damage	No damage
175H	No damage	No damage	No damage	No damage
175V	No damage	No damage	No damage	No damage
175HV	No damage	No damage	No damage	No damage
200H	No damage	No damage	No damage	No damage
200V	No damage	No damage	No damage	No damage
200HV	2 4-ft and 1 2-ft tee failed	2 4-ft and 1 2-ft tee failed	No damage	No damage
225H	No damage	No damage	No damage	No damage
225V	No damage	1 tile fell 1 4-ft tee failed	No damage	No damage
225HV	2 tiles fell 1 4-ft and 1 2-ft tee failed	No damage	1 tile fell 1 4-ft tee failed	No damage
250H	1 2-ft tee failed	No damage	2 2-ft tees failed	1 2-ft tee failed
250V	No damage	No damage	No damage	No damage
250HV	1 tile fell 2 2-ft tees failed	6 tiles fell 1 4-ft and 2 2-ft tees failed	25 tiles fell 13 4-ft and 12 2-ft tees failed	2 tiles fell 2 2-ft tees failed

<sup>1</sup> The 61 cm (2-ft) and 122 cm (4-ft) cross tees were installed in the North-South and East-West directions of the test frame, respectively. See Section 3.3.1 for details of the configuration of the suspension grid.

<sup>2</sup> The definition of failure of the cross tees included components that: (1) fell, (2) were bent, and (3) had to be replaced because they compromised the structural integrity of the entire grid if they were left in place.



**FIGURE 6-11 Failure of grid and tiles in configuration 5**

### 6.3.7 Configuration 6: Normal Sized Tiles without Compression Post

In configuration 6, the combined excitations (horizontal and vertical) produced more damage than either of the unidirectional excitations. The damage produced by the horizontal and vertical unidirectional motions was minimal. The first loss of tiles from the grid occurred for a level of combined shaking corresponding to  $S_S = 1.5g$ . See table 6-6 for summary information and figure 6-12 for a photograph of typical damage to the ceiling system. The absence of the compression post made the suspension grid more flexible in the vertical direction than in the configurations in which the post was included.

The argument for including compression posts in suspended ceiling systems is that damage to the system will be mitigated, by reducing the vertical displacement of the tiles and grid. Compare the results obtained from tests in configurations 4 and 6. In some cases, the compression post reduced the degree of damage but in other cases did not. Consider two examples from tests in configurations 4 and 6. First, for the combined shaking corresponding to  $S_S = 2.25g$  in Series N (system with compression post, see table 6-4) four tiles fell, whereas for the same level of combined shaking in Series X (system without compression post, see table 6-6) eleven tiles fell. This result suggests that the compression post is an effective means of reducing the number of falling tiles. For the combined shaking corresponding to  $S_S = 2.5g$  in Series N, sixteen tiles fell, whereas for the same level of combined shaking in Series X, ten tiles fell, suggesting that the installation of the compression posts could lead to an increase in damage. It is not clear from these data whether including compression posts improve the seismic performance of the suspended ceiling systems.

**TABLE 6-6 Results for normal sized tiles without compression post, series V-AA**

<i>Test Name</i>	<i>Summary remarks</i> <sup>1,2</sup>		
	<i>Series V</i>	<i>Series W</i>	<i>Series X</i>
WNH	$f_x = 12.0$ Hz	$f_x = 12.0$ Hz	$f_x = 12.0$ Hz
WNV	$f_y = 6.7$ Hz	$f_y = 6.8$ Hz	$f_y = 6.7$ Hz
150H	No damage	No damage	No damage
150V	No damage	No damage	No damage
150HV	No damage	1 tile fell	No damage
175H	No damage	No damage	No damage
175V	No damage	No damage	No damage
175HV	1 tile fell	1 tile fell	1 tile fell
200H	No damage	No damage	No damage
200V	No damage	No damage	No damage
200HV	3 tiles fell	2 tiles fell 1 2-ft tee failed	5 tiles fell
225H	No damage	No damage	No damage
225V	No damage	No damage	No damage
225HV	8 tiles fell	7 tiles fell 1 2-ft tee failed	11 tiles fell
250H	3 4-ft and 2 2-ft tees failed	No damage	No damage
250V	No damage	No damage	1 tile fell
250HV	28 tiles fell 6 4-ft and 4 2-ft tees failed	15 tiles fell 1 4-ft and 1 2-ft tee failed	10 tiles fell



**TABLE 6-6 Results for normal sized tiles without compression post, series V-AA (cont'd)**

<i>Test Name</i>	<i>Summary remarks</i> <sup>1, 2</sup>		
	<i>Series Y</i>	<i>Series Z</i>	<i>Series AA</i>
WNH	$f_x = 12.0$ Hz	$f_x = 12.0$ Hz	$f_x = 12.0$ Hz
WNV	$f_y = 6.8$ Hz	$f_y = 6.9$ Hz	$f_y = 6.8$ Hz
150H	No damage	No damage	No damage
150V	No damage	No damage	No damage
150HV	No damage	No damage	No damage
175H	No damage	No damage	No damage
175V	No damage	No damage	No damage
175HV	2 tiles fell	2 tiles fell	1 tile fell
200H	No damage	No damage	No damage
200V	No damage	No damage	No damage
200HV	3 tiles fell	4 tiles fell	2 tiles fell
225H	No damage	No damage	No damage
225V	No damage	1 tile fell	No damage
225HV	15 tiles fell 2 4-ft and 2 2-ft tees failed	9 tiles fell	6 tiles fell
250H	No damage	No damage	No damage
250V	No damage	2 tiles fell	No damage
250HV	11 tiles fell	12 tiles fell	11 tiles fell

<sup>1</sup> The 61 cm (2-ft) and 122 cm (4-ft) cross tees were installed in the North-South and East-West directions of the test frame, respectively. See Section 3.3.1 for details of the configuration of the suspension grid.

<sup>2</sup> The definition of failure of the cross tees included components that: (1) fell, (2) were bent, and (3) had to be replaced because they compromised the structural integrity of the entire grid if they were left in place.



**FIGURE 6-12 Failure of tiles in configuration 6**

### 6.3.8 Observations

The following general observations were made at the conclusion of the testing program.

1. The rivets that attached the main runners and cross tees to the wall molding on the South and West sides of the test frame played a very important role in the seismic performance of the suspended ceiling systems. When a rivet came loose or was destroyed during shaking, the damage in the ceiling system in terms of loss of tiles was much larger than when all of the rivets were undamaged and the cross tees remained firmly attached to the wall molding. The arrowhead in figure 6-13 identifies the location of one of the rivets destroyed during shaking.
2. The main beams provide most of the stiffness in the suspension grid in the horizontal and vertical directions. However, the connections between the main beams were substantially more flexible than the main beams. This is clearly reflected in the performance of the ceiling systems in terms of loss of tiles because the first tiles to fall in most of the tests were the tiles located around the connections between two main beams. The circle in figure 6-14 identifies the connection between two main beams.

### 6.4 Spectral Accelerations of the Test Frame

The acceleration response at six different locations on the test frame are presented in this section. The horizontal response in the form of response spectra for each of the six accelerometers at locations the termed as *Table* (shaking table acceleration control), *Abase* (on the center of the base of the frame), *Corner\_w* (southwest corner of the roof of testing frame), *Qtr* (roof of testing frame at 4 ft. from the West and South sides of the frame) *Center* (center of the roof of testing frame) and *Agrid* (on the suspension grid, in the location of the compression post) are presented in figures 6-15 through 6-50 for each level of earthquake shaking (1.0g, 1.25g, etc.) and for each configuration. The locations of these accelerations are identified in figure 3-16.

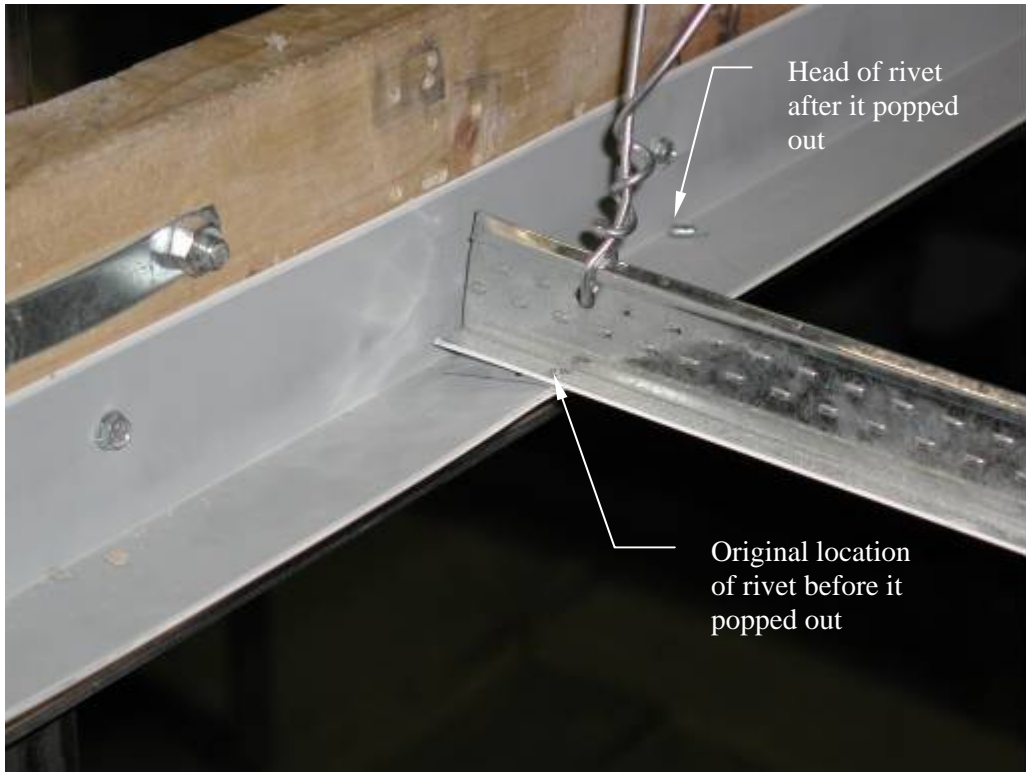


**FIGURE 6-13 Rivets on the South side wall molding destroyed during shaking**

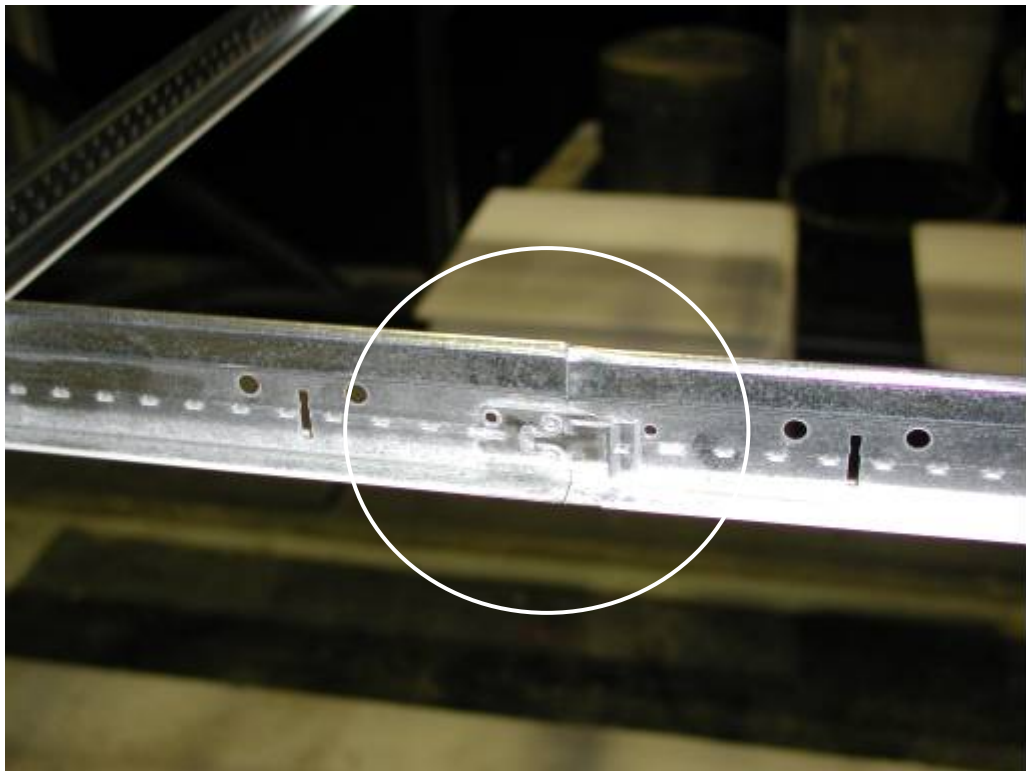


**FIGURE 6-14 Connection between two main beams**

Figure 6-51 presents the arithmetic mean spectral acceleration for each level of earthquake shaking and for each of the six locations on the test frame for configuration 1. The same information is presented in figures 6-52 through 6-56 for the other configurations. Tables 6-7 through 6-12 present the arithmetic mean spectral acceleration for selected spectral periods for the six locations on the test frame and for each configuration. Listed are the period, the level of shaking, and the horizontal spectral accelerations for the six locations.

**TABLE 6-7 Mean spectral accelerations at selected periods, undersized tiles**

<i>Period (seconds)</i>	<i>Excitation level per <math>S_s</math> (g)</i>	<i>Horizontal spectral accelerations (g)</i>					
		<i>Table</i>	<i>Abase</i>	<i>Corner_w</i>	<i>Qtr</i>	<i>Center</i>	<i>Agrid</i>
0.2	1.00	1.10	1.15	1.42	1.42	2.09	1.86
	1.25	1.42	1.53	1.79	1.80	2.58	2.38
	1.50	1.76	1.88	2.20	2.26	3.14	3.02
	1.75	2.13	2.24	2.74	2.79	4.03	3.15
	2.00	2.55	2.72	3.49	3.53	4.71	3.95
	2.25	3.06	3.23	4.18	4.25	5.05	5.18
	2.50	3.76	3.82	4.76	4.87	5.22	6.20
0.5	1.00	1.14	1.19	1.25	1.24	1.74	1.36
	1.25	1.42	1.48	1.56	1.55	2.11	1.68
	1.50	1.71	1.79	1.89	1.88	2.55	1.99
	1.75	2.02	2.09	2.20	2.20	3.07	2.26
	2.00	2.31	2.39	2.53	2.52	3.43	2.59
	2.25	2.63	2.71	2.82	2.82	3.46	2.96
	2.50	2.94	3.03	3.25	3.25	3.77	3.39
1.0	1.00	0.96	0.99	1.01	0.99	1.44	1.01
	1.25	1.15	1.21	1.22	1.20	1.69	1.22
	1.50	1.38	1.45	1.48	1.46	2.01	1.48
	1.75	1.63	1.70	1.74	1.72	2.49	1.72
	2.00	1.87	1.93	1.98	1.97	2.74	1.98
	2.25	2.11	2.18	2.24	2.23	2.85	2.22
	2.50	2.25	2.25	2.40	2.40	2.91	2.40
1.5	1.00	0.20	0.19	0.20	0.20	0.29	0.21
	1.25	0.21	0.22	0.23	0.23	0.37	0.24
	1.50	0.26	0.26	0.28	0.27	0.44	0.29
	1.75	0.30	0.31	0.34	0.33	0.55	0.33
	2.00	0.35	0.34	0.37	0.36	0.66	0.37
	2.25	0.39	0.39	0.42	0.41	0.69	0.43
	2.50	0.44	0.44	0.48	0.47	0.77	0.48
2.0	1.00	0.07	0.08	0.08	0.07	0.11	0.08
	1.25	0.09	0.10	0.10	0.09	0.16	0.11
	1.50	0.10	0.12	0.12	0.11	0.20	0.14
	1.75	0.12	0.13	0.14	0.14	0.31	0.14
	2.00	0.14	0.15	0.16	0.15	0.45	0.17
	2.25	0.16	0.17	0.18	0.17	0.53	0.19
	2.50	0.17	0.18	0.20	0.19	0.54	0.20

**TABLE 6-8 Mean spectral accelerations at selected periods, undersized tiles with clips**

<i>Period (seconds)</i>	<i>Excitation level per <math>S_s</math> (g)</i>	<i>Horizontal spectral accelerations (g)</i>					
		<i>Table</i>	<i>Abase</i>	<i>Corner_w</i>	<i>Qtr</i>	<i>Center</i>	<i>Agrid</i>
0.2	1.00	1.07	1.05	1.43	1.43	1.49	1.58
	1.25	1.44	1.45	1.82	1.82	1.94	2.17
	1.50	1.78	1.80	2.31	2.31	2.40	2.69
	1.75	2.16	2.17	2.90	2.89	2.97	3.36
	2.00	2.57	2.62	3.63	3.61	3.71	4.26
	2.25	3.03	3.11	4.36	4.35	4.50	5.18
	2.50	3.74	3.61	5.01	5.01	5.16	5.93
0.5	1.00	1.15	1.13	1.24	1.24	1.27	1.37
	1.25	1.44	1.41	1.55	1.55	1.60	1.71
	1.50	1.74	1.71	1.88	1.88	1.91	2.06
	1.75	2.04	2.01	2.20	2.20	2.26	2.41
	2.00	2.34	2.30	2.53	2.52	2.62	2.75
	2.25	2.66	2.61	2.84	2.84	2.92	3.11
	2.50	2.97	2.92	3.25	3.24	3.35	3.59
1.0	1.00	0.94	0.92	0.97	0.97	0.98	1.04
	1.25	1.17	1.16	1.22	1.22	1.22	1.32
	1.50	1.41	1.40	1.49	1.48	1.50	1.59
	1.75	1.65	1.64	1.76	1.75	1.74	1.88
	2.00	1.89	1.86	1.98	1.98	2.01	2.11
	2.25	2.14	2.10	2.25	2.25	2.27	2.42
	2.50	2.38	2.34	2.49	2.49	2.55	2.68
1.5	1.00	0.20	0.19	0.20	0.20	0.29	0.21
	1.25	0.22	0.21	0.23	0.23	0.26	0.26
	1.50	0.26	0.25	0.28	0.28	0.32	0.32
	1.75	0.30	0.30	0.33	0.33	0.33	0.38
	2.00	0.35	0.33	0.36	0.36	0.37	0.42
	2.25	0.40	0.38	0.41	0.41	0.42	0.49
	2.50	0.45	0.43	0.48	0.48	0.50	0.56
2.0	1.00	0.07	0.08	0.08	0.07	0.11	0.08
	1.25	0.09	0.09	0.09	0.09	0.13	0.13
	1.50	0.11	0.11	0.12	0.12	0.15	0.15
	1.75	0.12	0.13	0.14	0.14	0.14	0.17
	2.00	0.14	0.14	0.15	0.15	0.18	0.19
	2.25	0.16	0.16	0.17	0.17	0.18	0.23
	2.50	0.18	0.18	0.19	0.19	0.19	0.25

**TABLE 6-9 Mean spectral accelerations at selected periods, undersized tiles with recycled grid**

<i>Period (seconds)</i>	<i>Excitation level per <math>S_s</math> (g)</i>	<i>Horizontal spectral accelerations (g)</i>					
		<i>Table</i>	<i>Abase</i>	<i>Corner_w</i>	<i>Qtr</i>	<i>Center</i>	<i>Agrid</i>
0.2	1.00	1.06	1.04	1.41	1.42	1.47	1.45
	1.25	1.43	1.45	1.81	1.82	1.90	2.04
	1.50	1.77	1.79	2.29	2.30	2.38	2.56
	1.75	2.14	2.16	2.84	2.86	2.94	3.10
	2.00	2.55	2.61	3.58	3.61	3.64	3.89
	2.25	3.01	3.09	4.30	4.33	4.36	4.69
	2.50	3.72	3.59	4.98	5.00	5.06	5.40
0.5	1.00	1.14	1.13	1.23	1.24	1.27	1.34
	1.25	1.43	1.41	1.54	1.54	1.55	1.68
	1.50	1.73	1.70	1.87	1.87	1.89	2.03
	1.75	2.03	2.00	2.19	2.19	2.27	2.37
	2.00	2.33	2.29	2.50	2.51	2.57	2.70
	2.25	2.64	2.59	2.81	2.82	2.86	3.05
	2.50	2.95	2.91	3.22	3.22	3.27	3.49
1.0	1.00	0.93	0.91	0.97	0.97	0.92	1.03
	1.25	1.17	1.15	1.21	1.21	1.19	1.31
	1.50	1.40	1.39	1.47	1.47	1.44	1.58
	1.75	1.64	1.63	1.74	1.74	1.71	1.86
	2.00	1.88	1.85	1.96	1.96	1.98	2.10
	2.25	2.12	2.09	2.23	2.24	2.24	2.39
	2.50	2.37	2.33	2.47	2.48	2.51	2.66
1.5	1.00	0.20	0.19	0.20	0.20	0.29	0.21
	1.25	0.22	0.21	0.23	0.23	0.25	0.26
	1.50	0.26	0.25	0.28	0.28	0.28	0.31
	1.75	0.30	0.29	0.33	0.33	0.34	0.37
	2.00	0.35	0.33	0.36	0.36	0.38	0.40
	2.25	0.40	0.38	0.41	0.41	0.43	0.47
	2.50	0.44	0.43	0.47	0.47	0.48	0.54
2.0	1.00	0.07	0.08	0.08	0.07	0.11	0.08
	1.25	0.09	0.09	0.09	0.09	0.11	0.12
	1.50	0.11	0.11	0.11	0.11	0.13	0.14
	1.75	0.12	0.13	0.14	0.13	0.15	0.17
	2.00	0.14	0.14	0.15	0.15	0.17	0.18
	2.25	0.16	0.16	0.17	0.17	0.18	0.21
	2.50	0.18	0.18	0.19	0.19	0.20	0.24



**TABLE 6-10 Mean spectral accelerations at selected periods, normal sized tiles**

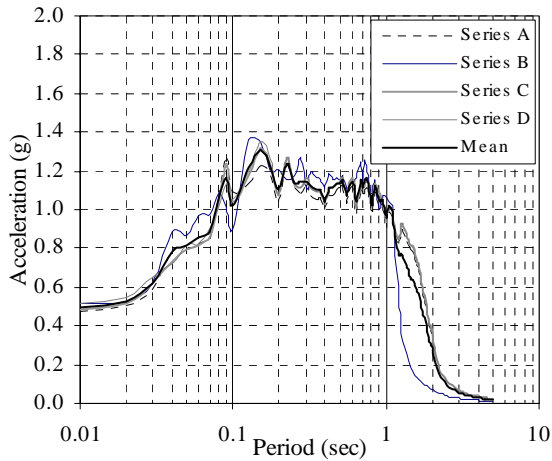
<i>Period (seconds)</i>	<i>Excitation level per <math>S_s</math> (g)</i>	<i>Horizontal spectral accelerations (g)</i>					
		<i>Table</i>	<i>Abase</i>	<i>Corner_w</i>	<i>Qtr</i>	<i>Center</i>	<i>Agrid</i>
0.2	1.50	1.75	1.75	2.32	2.33	2.40	2.43
	1.75	2.14	2.12	2.87	2.90	2.94	2.97
	2.00	2.55	2.56	3.60	3.63	3.73	3.70
	2.25	3.18	3.13	4.34	4.42	4.60	4.55
	2.50	3.69	3.53	5.00	5.04	5.18	5.20
0.5	1.50	1.72	1.68	1.89	1.90	1.95	1.96
	1.75	2.02	1.97	2.21	2.23	2.28	2.24
	2.00	2.32	2.26	2.53	2.55	2.64	2.50
	2.25	2.64	2.57	2.92	2.94	3.00	2.88
	2.50	2.95	2.88	3.27	3.29	3.35	3.22
1.0	1.50	1.40	1.37	1.49	1.50	1.50	1.53
	1.75	1.64	1.61	1.76	1.77	1.78	1.72
	2.00	1.88	1.83	2.00	2.02	2.04	1.95
	2.25	2.13	2.08	2.29	2.30	2.33	2.22
	2.50	2.36	2.31	2.52	2.53	2.55	2.48
1.5	1.50	0.26	0.25	0.28	0.28	0.32	0.30
	1.75	0.30	0.30	0.33	0.33	0.39	0.34
	2.00	0.35	0.33	0.37	0.37	0.49	0.37
	2.25	0.40	0.38	0.42	0.42	0.55	0.44
	2.50	0.45	0.43	0.48	0.48	0.49	0.52
2.0	1.50	0.11	0.11	0.12	0.12	0.16	0.13
	1.75	0.12	0.12	0.14	0.14	0.19	0.16
	2.00	0.14	0.14	0.16	0.16	0.27	0.17
	2.25	0.16	0.16	0.18	0.18	0.32	0.22
	2.50	0.18	0.17	0.19	0.19	0.20	0.26

**TABLE 6-11 Mean spectral accelerations at selected periods, normal sized tiles with clips**

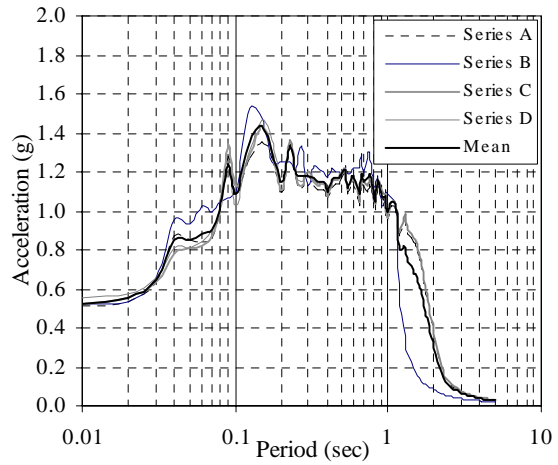
<i>Period (seconds)</i>	<i>Excitation level per <math>S_s</math> (g)</i>	<i>Horizontal spectral accelerations (g)</i>					
		<i>Table</i>	<i>Abase</i>	<i>Corner_w</i>	<i>Qtr</i>	<i>Center</i>	<i>Agrid</i>
0.2	1.50	1.68	1.64	2.22	2.27	2.34	2.24
	1.75	2.08	1.99	2.74	2.81	2.91	2.79
	2.00	2.48	2.42	3.45	3.53	3.65	3.55
	2.25	3.29	3.10	4.17	4.31	4.55	4.43
	2.50	4.14	3.79	5.03	5.10	5.31	5.20
0.5	1.50	1.67	1.59	1.84	1.88	1.91	1.85
	1.75	1.96	1.87	2.15	2.20	2.25	2.16
	2.00	2.26	2.15	2.48	2.52	2.59	2.48
	2.25	2.56	2.45	2.96	3.01	3.12	2.92
	2.50	2.84	2.75	3.20	3.27	3.34	3.22
1.0	1.50	1.36	1.31	1.46	1.47	1.51	1.46
	1.75	1.60	1.54	1.72	1.74	1.79	1.72
	2.00	1.84	1.75	1.97	2.01	2.04	1.98
	2.25	2.08	2.00	2.27	2.31	2.35	2.27
	2.50	2.30	2.23	2.55	2.60	2.64	2.52
1.5	1.50	0.25	0.24	0.28	0.27	0.28	0.27
	1.75	0.30	0.29	0.33	0.33	0.34	0.32
	2.00	0.34	0.32	0.36	0.36	0.37	0.36
	2.25	0.39	0.37	0.42	0.42	0.43	0.45
	2.50	0.45	0.44	0.54	0.55	0.56	0.53
2.0	1.50	0.10	0.10	0.11	0.11	0.12	0.11
	1.75	0.12	0.12	0.14	0.13	0.14	0.14
	2.00	0.14	0.13	0.15	0.15	0.16	0.16
	2.25	0.15	0.15	0.17	0.17	0.18	0.20
	2.50	0.18	0.17	0.21	0.21	0.22	0.22

**TABLE 6-12 Mean spectral accelerations at selected periods, normal sized tiles without post**

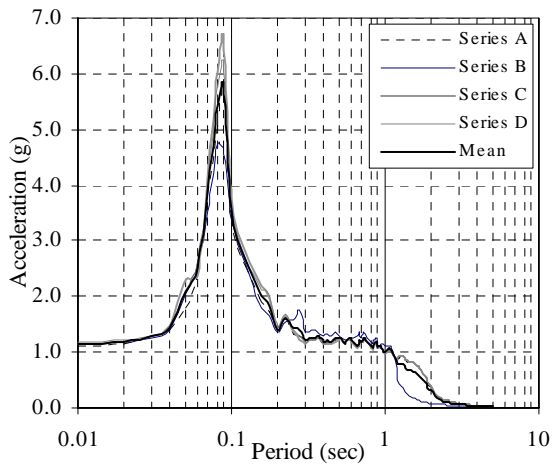
<i>Period (seconds)</i>	<i>Excitation level per <math>S_S</math> (g)</i>	<i>Horizontal spectral accelerations (g)</i>					
		<i>Table</i>	<i>Abase</i>	<i>Corner_w</i>	<i>Qtr</i>	<i>Center</i>	<i>Agrid</i>
0.2	1.50	1.66	1.58	2.20	2.18	2.30	2.52
	1.75	2.05	1.92	2.69	2.69	2.86	2.74
	2.00	2.46	2.32	3.36	3.37	3.55	3.65
	2.25	2.86	2.75	4.09	4.11	4.33	4.32
	2.50	3.39	3.17	4.77	4.79	5.03	4.97
0.5	1.50	1.66	1.56	1.84	1.83	1.90	1.56
	1.75	1.95	1.82	2.15	2.14	2.23	1.77
	2.00	2.25	2.10	2.47	2.47	2.56	2.05
	2.25	2.55	2.38	2.79	2.79	2.88	2.34
	2.50	2.86	2.67	3.18	3.18	3.30	2.65
1.0	1.50	1.36	1.28	1.46	1.43	1.51	1.19
	1.75	1.59	1.50	1.72	1.69	1.78	1.38
	2.00	1.83	1.71	1.95	1.94	2.00	1.58
	2.25	2.06	1.93	2.22	2.21	2.28	1.80
	2.50	2.30	2.15	2.46	2.44	2.52	2.04
1.5	1.50	0.25	0.24	0.28	0.27	0.28	0.23
	1.75	0.29	0.28	0.33	0.32	0.34	0.30
	2.00	0.34	0.31	0.36	0.35	0.37	0.31
	2.25	0.38	0.36	0.41	0.40	0.41	0.36
	2.50	0.43	0.40	0.47	0.46	0.47	0.63
2.0	1.50	0.10	0.10	0.12	0.11	0.12	0.13
	1.75	0.12	0.11	0.14	0.13	0.14	0.21
	2.00	0.14	0.13	0.15	0.15	0.15	0.19
	2.25	0.15	0.15	0.17	0.17	0.17	0.19
	2.50	0.17	0.16	0.19	0.18	0.19	0.44



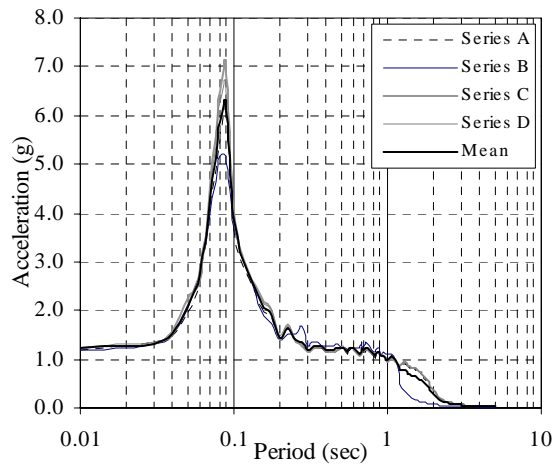
**a) Table**



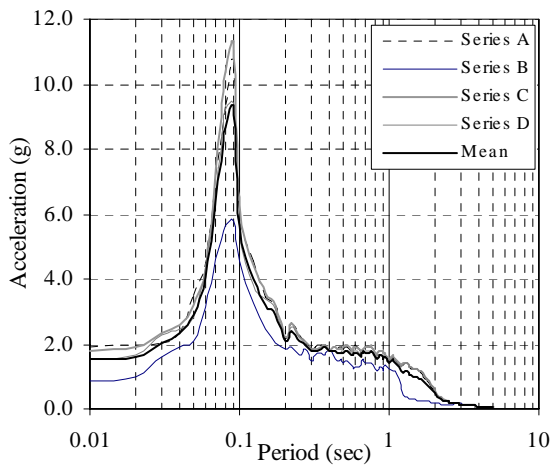
**b) Abase**



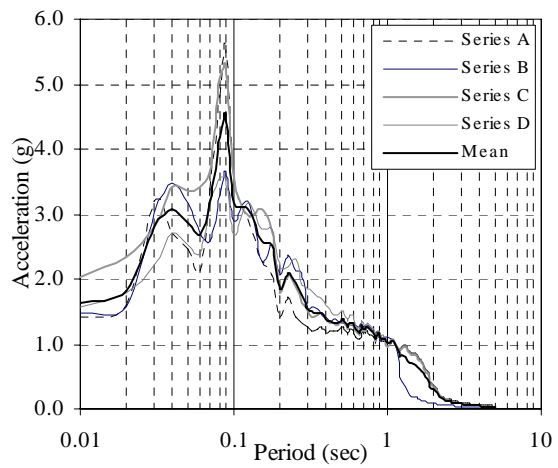
**c) Corner\_w**



**d) Qtr**

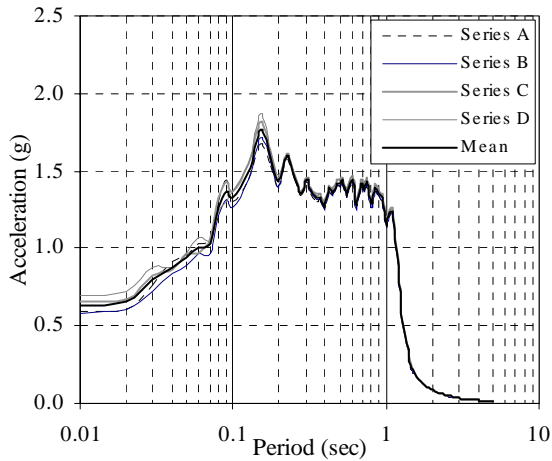


**e) Center**

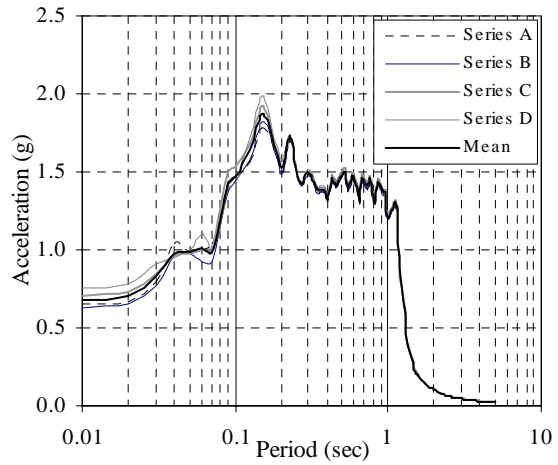


**f) Agrid**

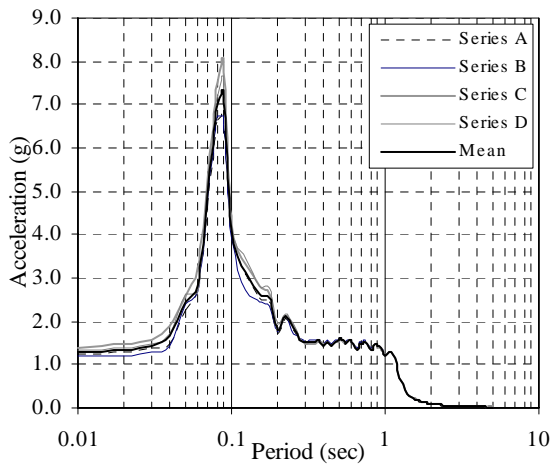
**FIGURE 6-15 Response spectra corresponding to  $S_S = 1.0g$ , undersized tiles**



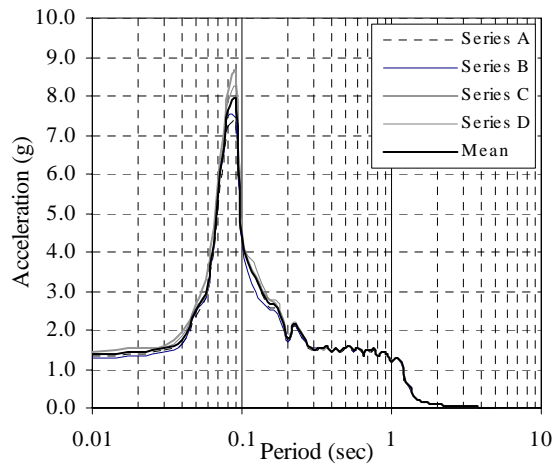
**a) Table**



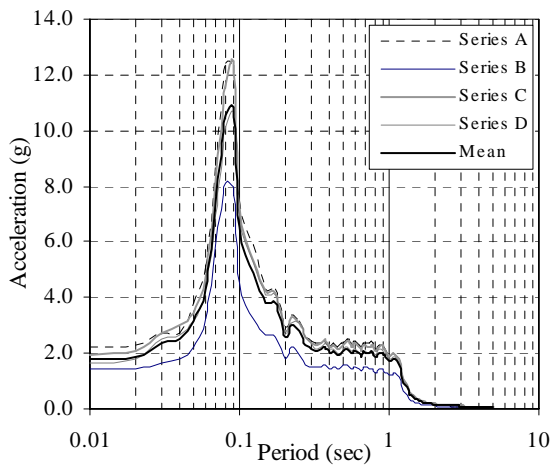
**b) Abase**



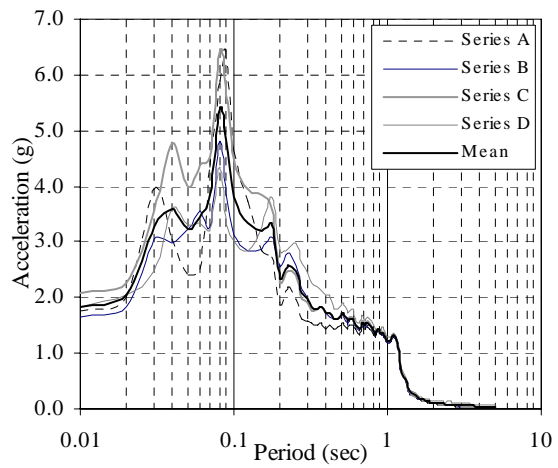
**c) Corner\_w**



**d) Qtr**

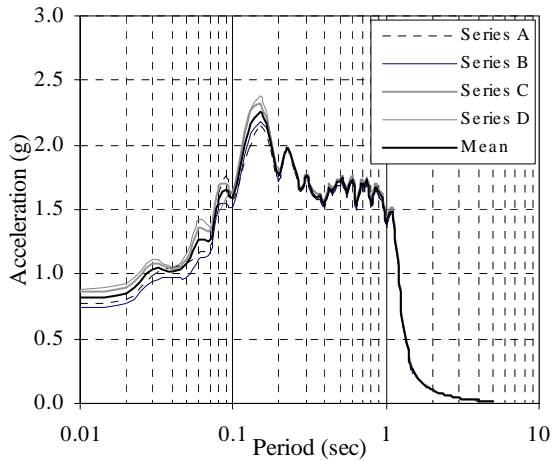


**e) Center**

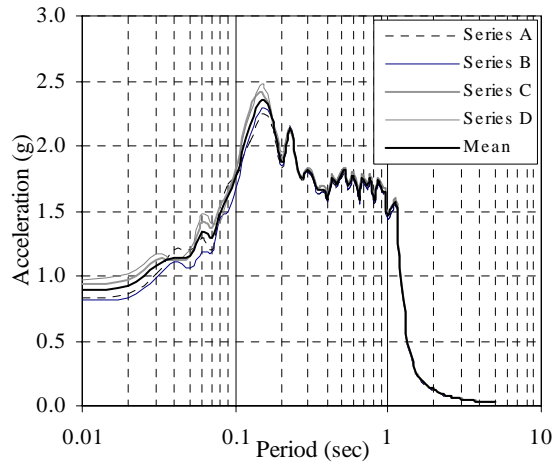


**f) Agrid**

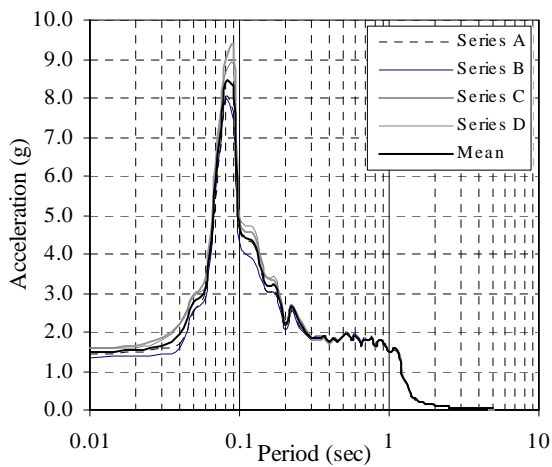
**FIGURE 6-16** Response spectra corresponding to  $S_S = 1.25g$ , undersized tiles



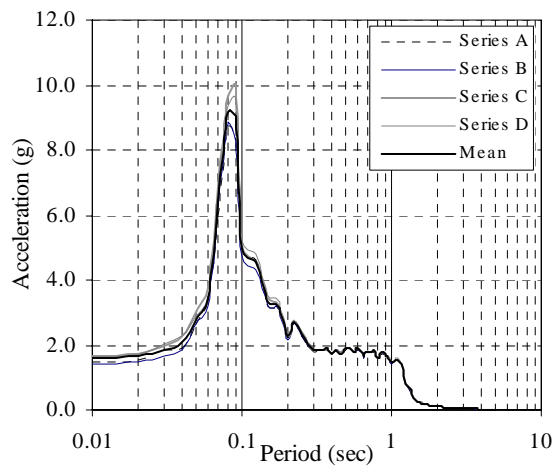
**a) Table**



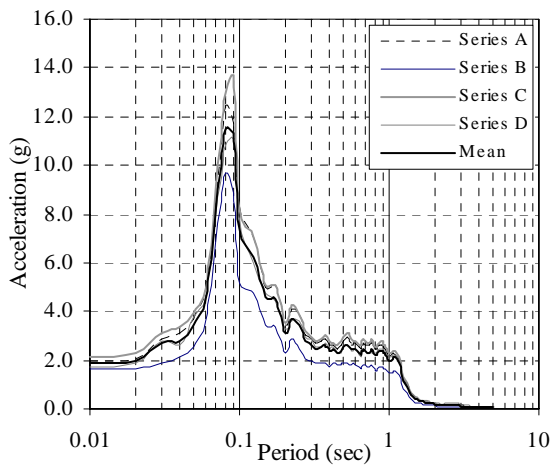
**b) Abase**



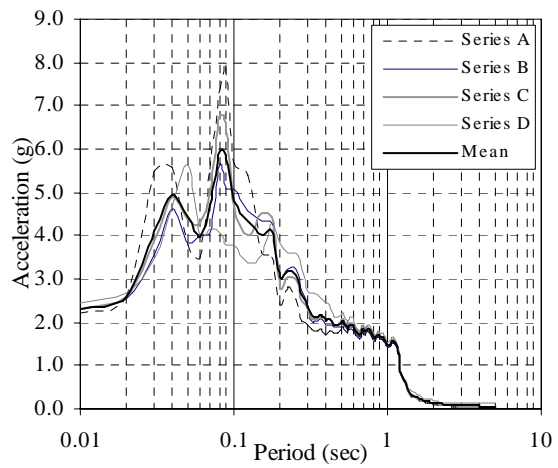
**c) Corner\_w**



**d) Qtr**

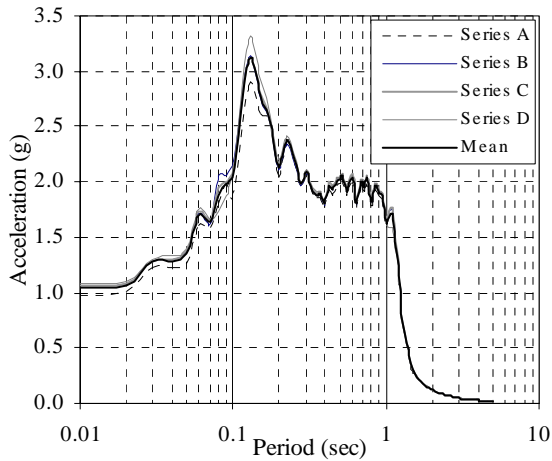


**e) Center**

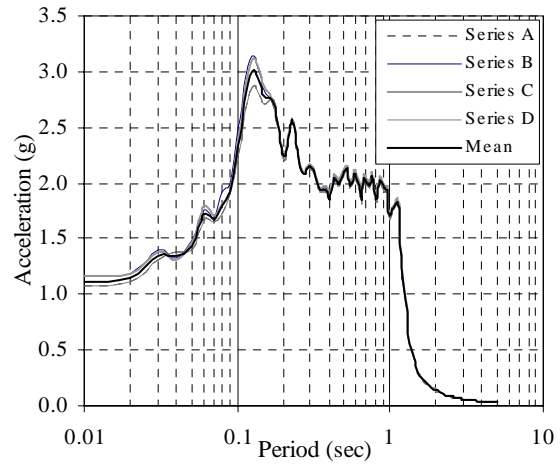


**f) Agrid**

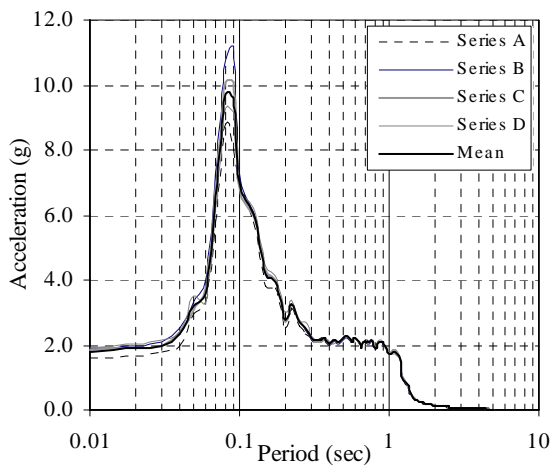
**FIGURE 6-17 Response spectra corresponding to  $S_S = 1.5g$ , undersized tiles**



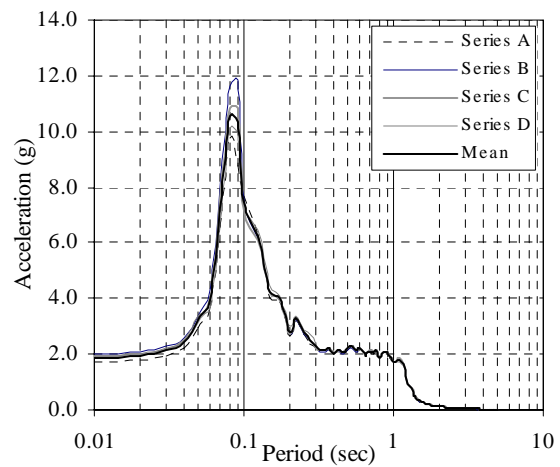
**a) Table**



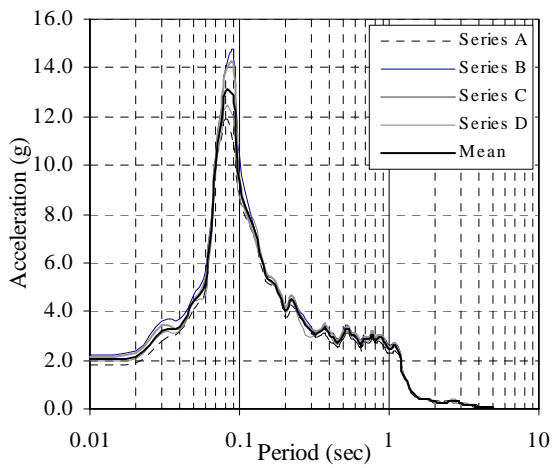
**b) Abase**



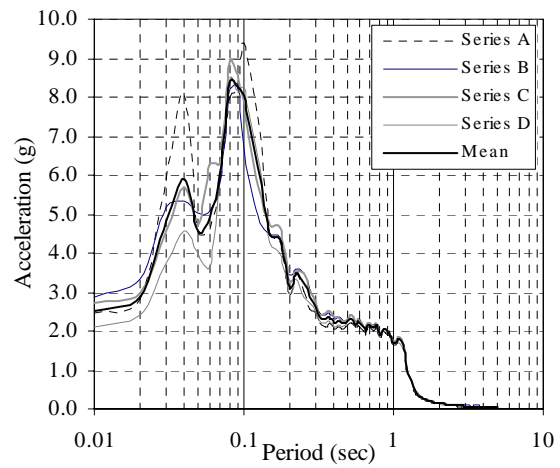
**c) Corner\_w**



**d) Qtr**

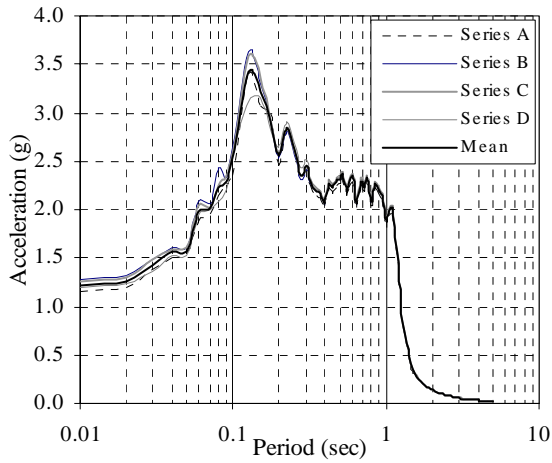


**e) Center**

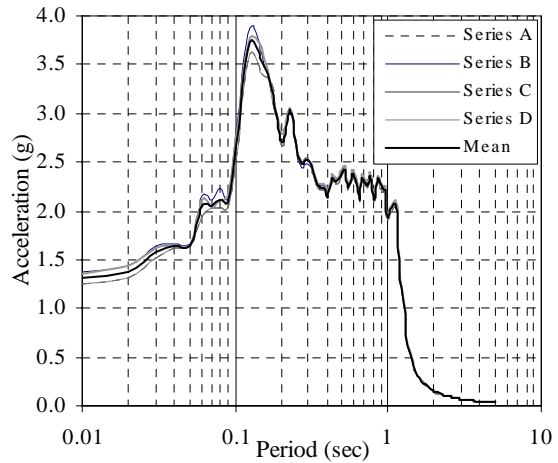


**f) Agrid**

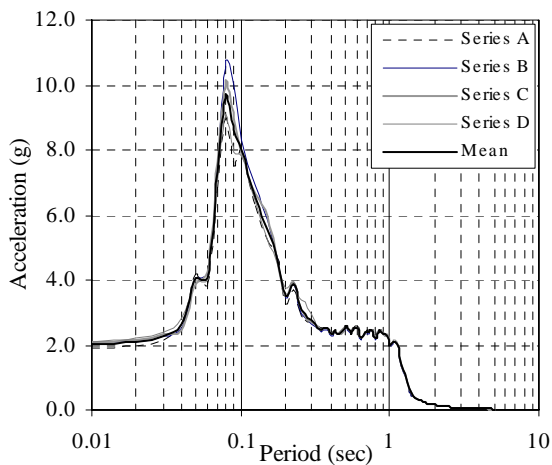
**FIGURE 6-18** Response spectra corresponding to  $S_S = 1.75g$ , undersized tiles



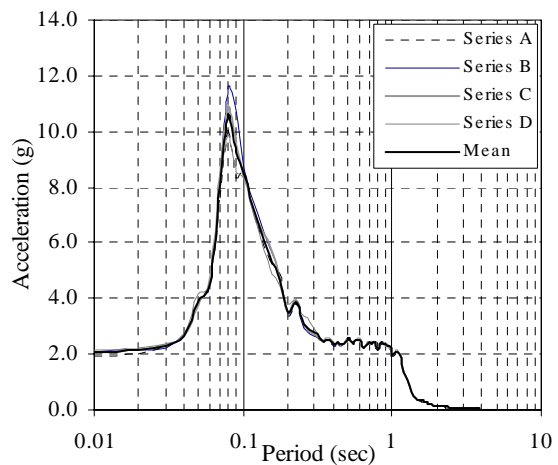
**a) Table**



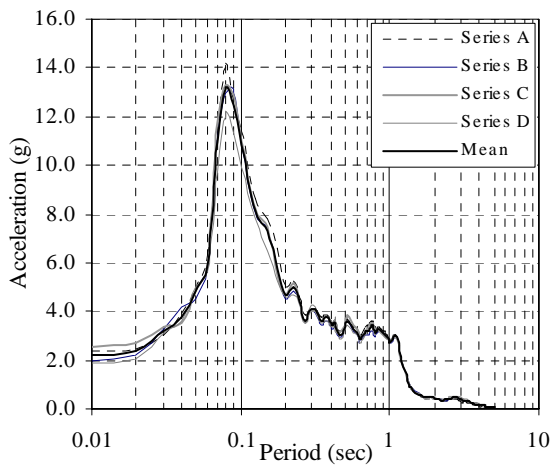
**b) Abase**



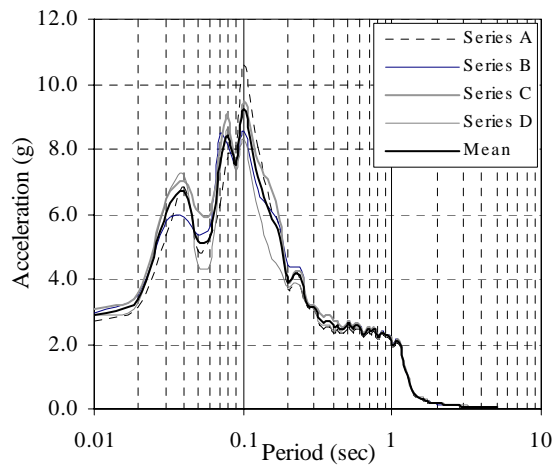
**c) Corner\_w**



**d) Qtr**



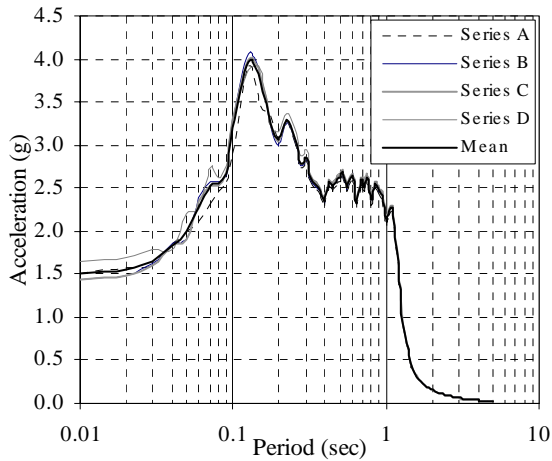
**e) Center**



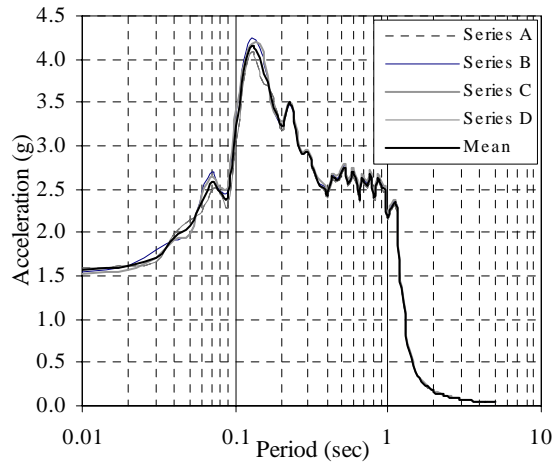
**f) Agrid**

**FIGURE 6-19 Response spectra corresponding to  $S_S = 2.0g$ , undersized tiles**

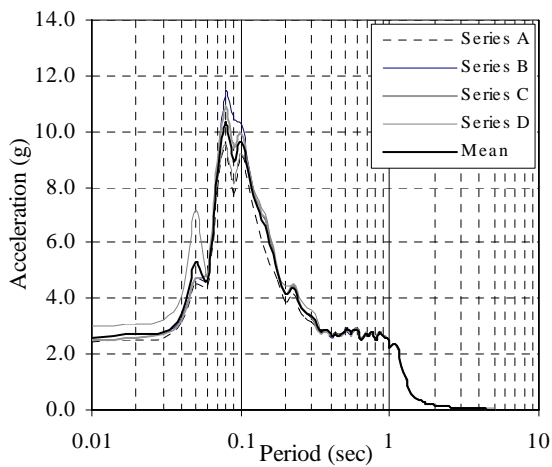




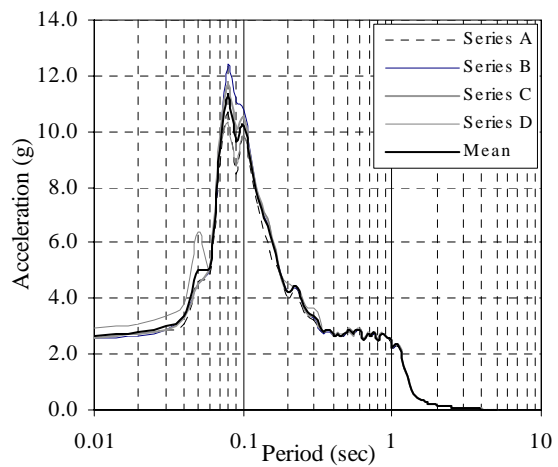
**a) Table**



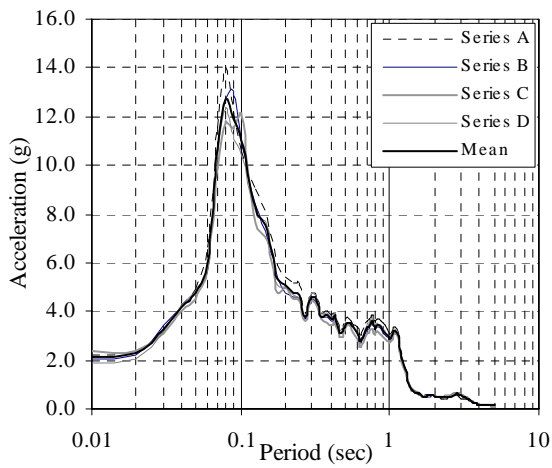
**b) Abase**



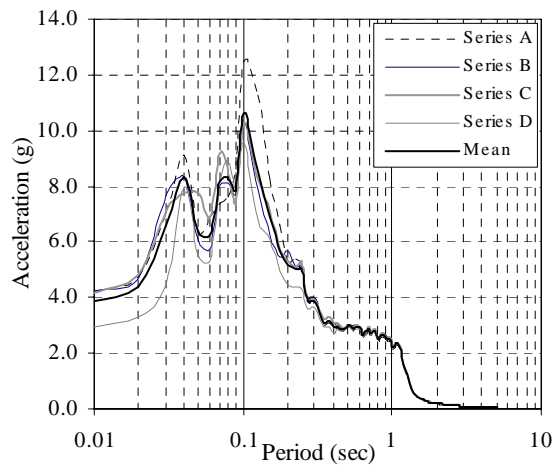
**c) Corner\_w**



**d) Qtr**

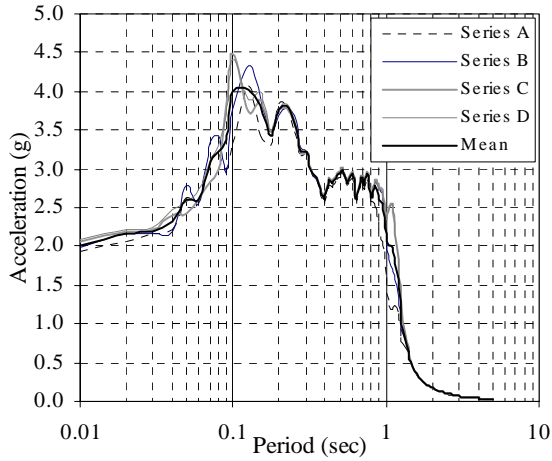


**e) Center**

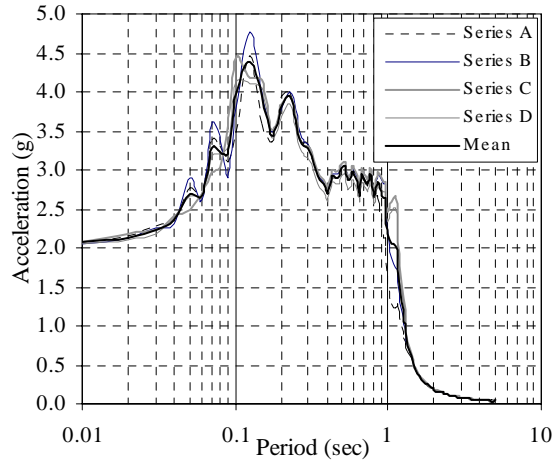


**f) Agrid**

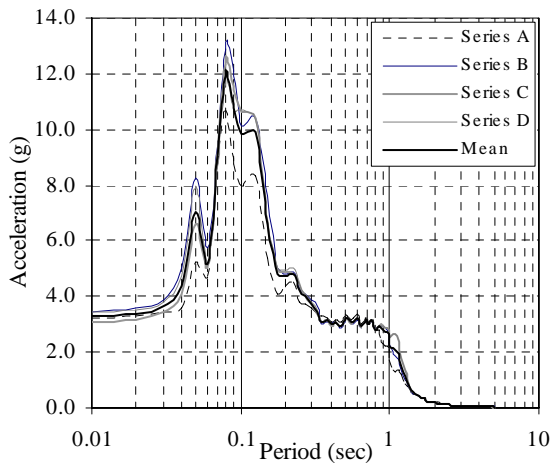
**FIGURE 6-20** Response spectra corresponding to  $S_S = 2.25g$ , undersized tiles



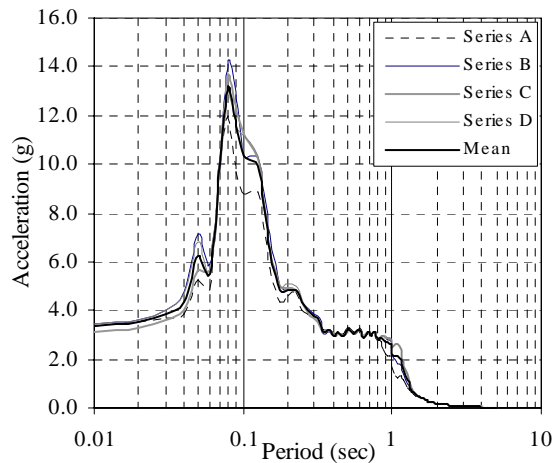
**a) Table**



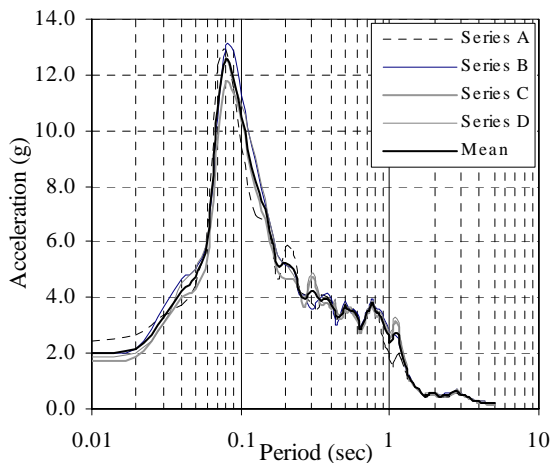
**b) Abase**



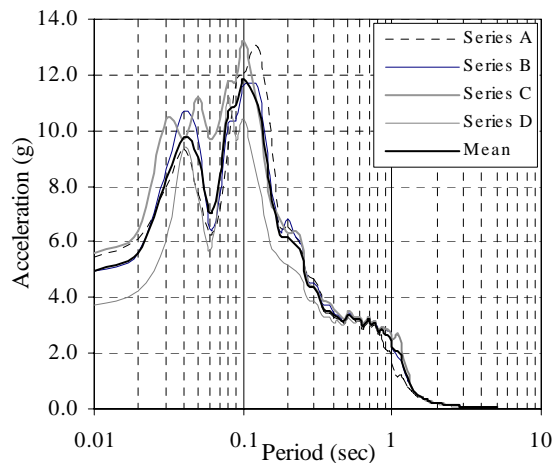
**c) Corner\_w**



**d) Qtr**

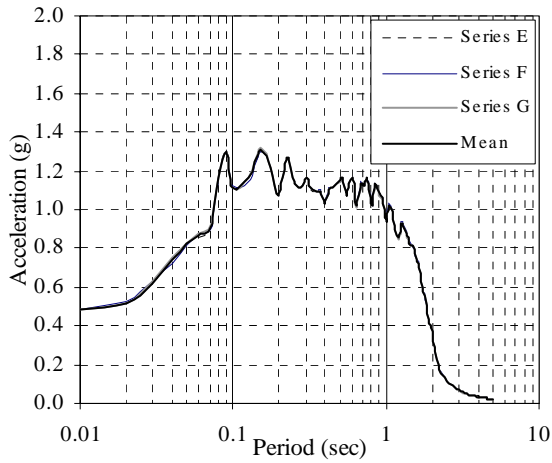


**e) Center**

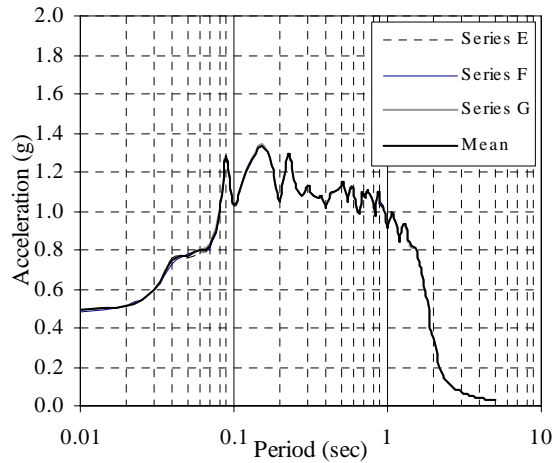


**f) Agrid**

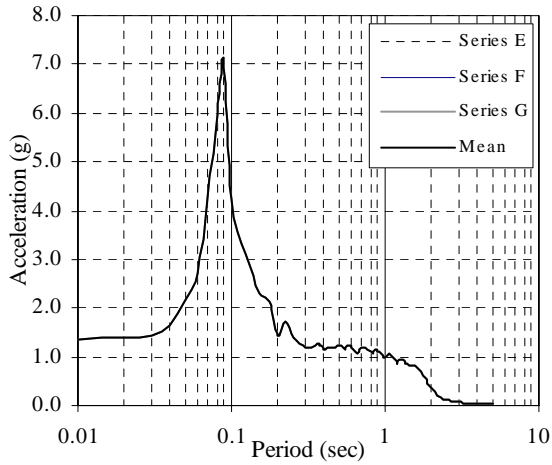
**FIGURE 6-21 Response spectra corresponding to  $S_S = 2.5g$ , undersized tiles**



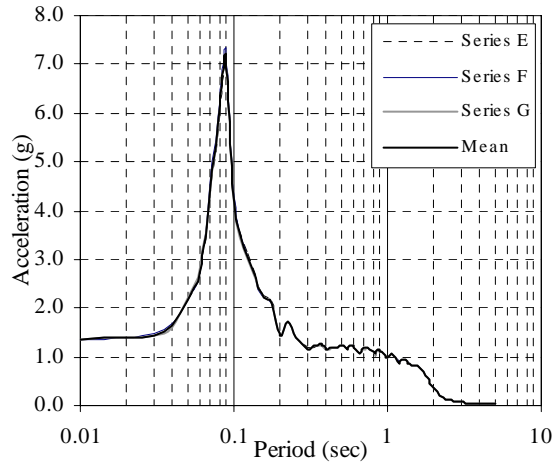
**a) Table**



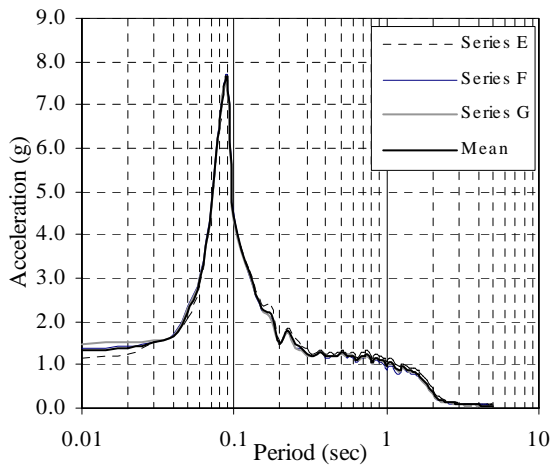
**b) Abase**



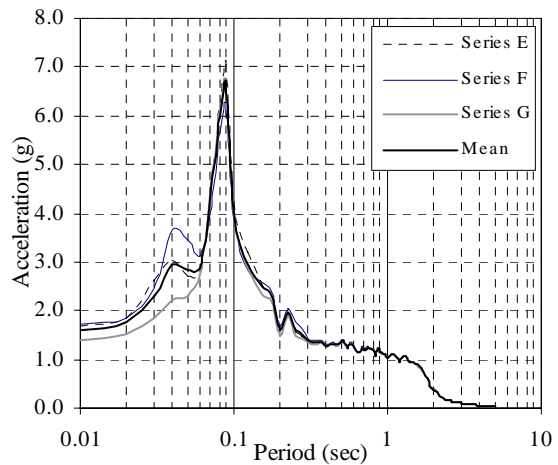
**c) Corner\_w**



**d) Qtr**

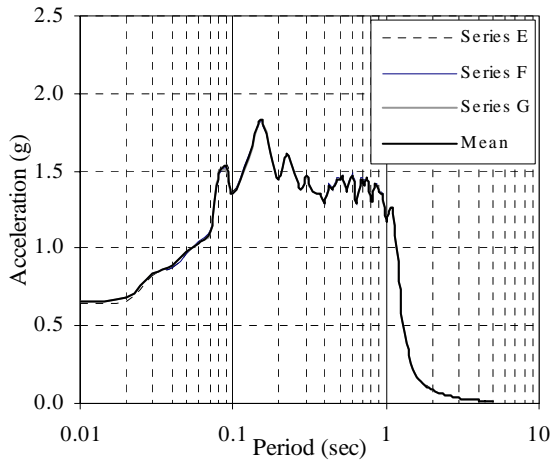


**e) Center**

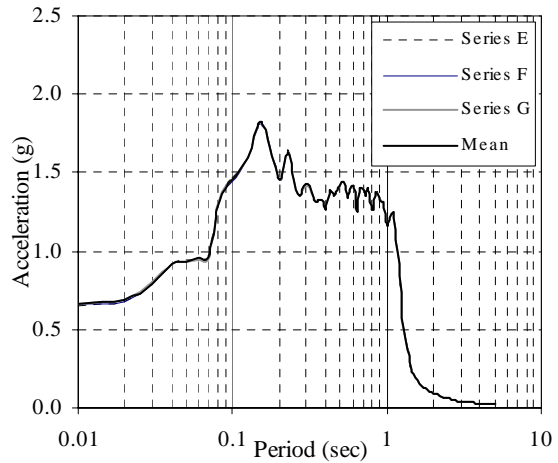


**f) Agrid**

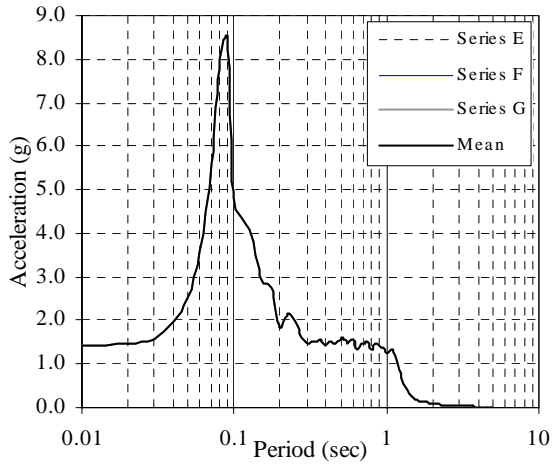
**FIGURE 6-22** Response spectra corresponding to  $S_S = 1.0g$ , undersized tiles with clips



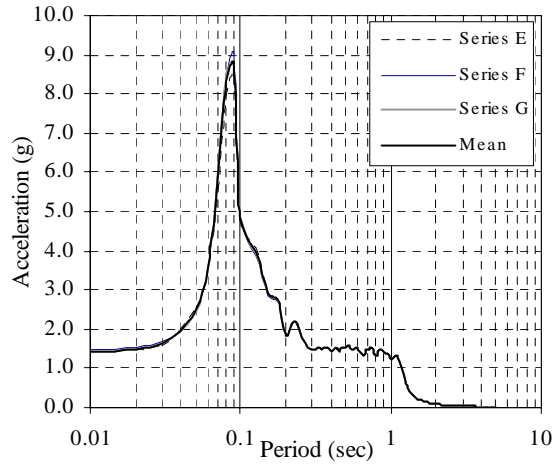
**a) Table**



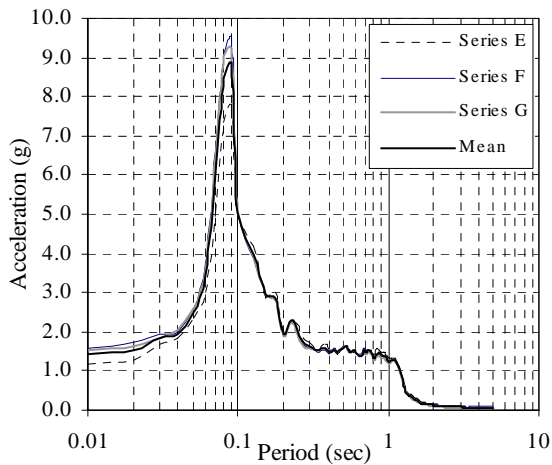
**b) Abase**



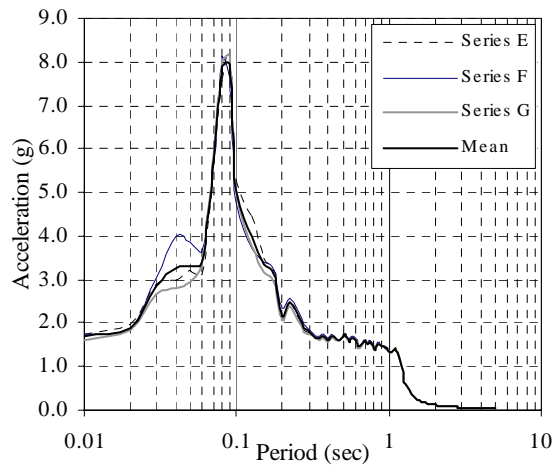
**c) Corner\_w**



**d) Qtr**

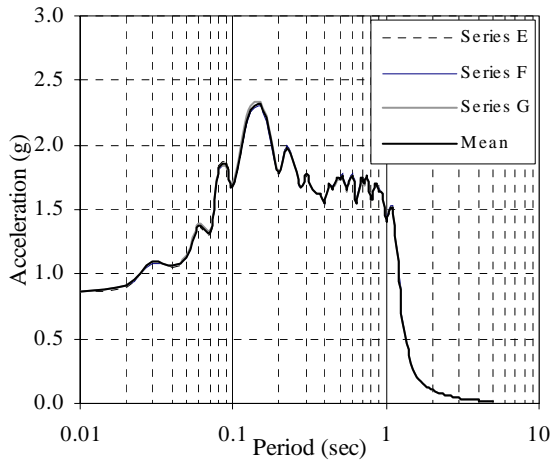


**e) Center**

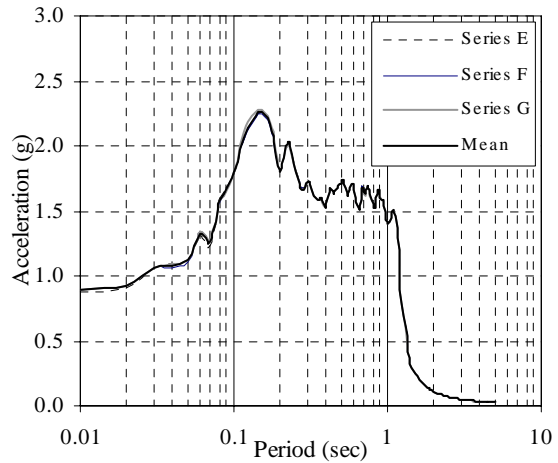


**f) Agrid**

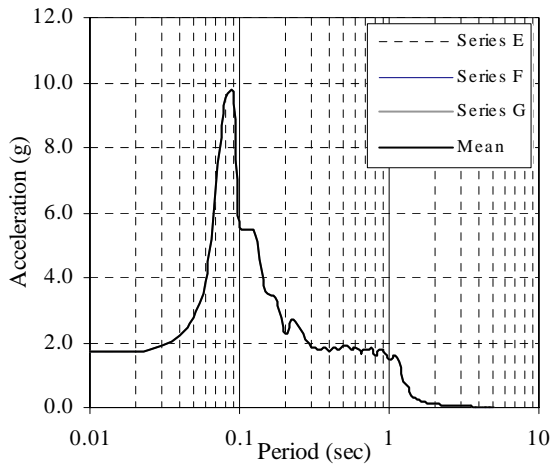
**FIGURE 6-23** Response spectra corresponding to  $S_S = 1.25g$ , undersized tiles with clips



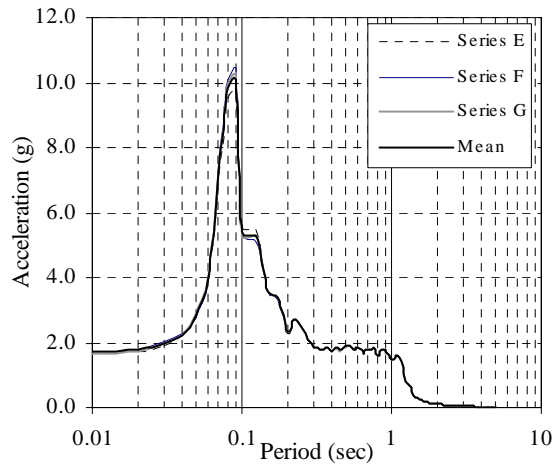
**a) Table**



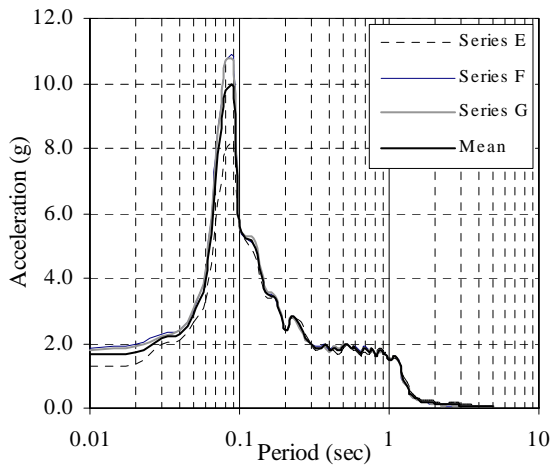
**b) Abase**



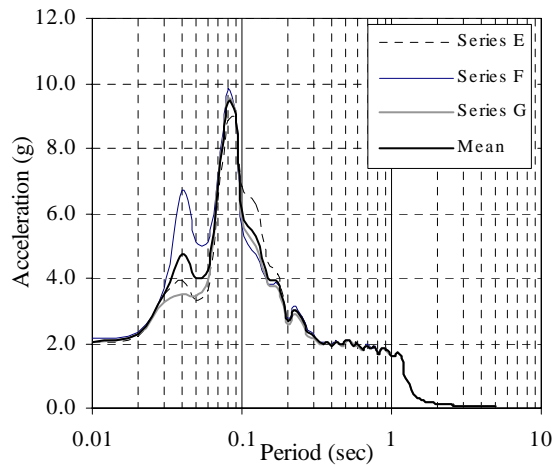
**c) Corner\_w**



**d) Qtr**

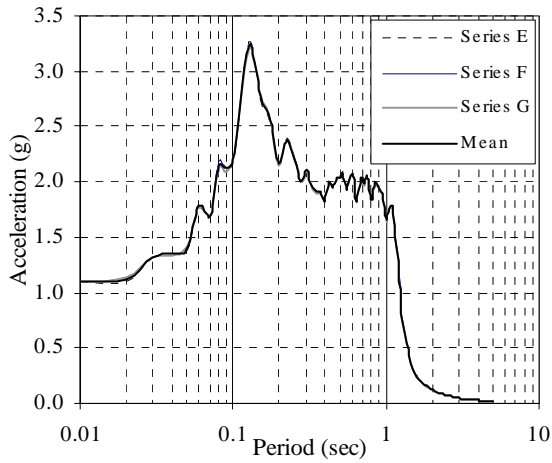


**e) Center**

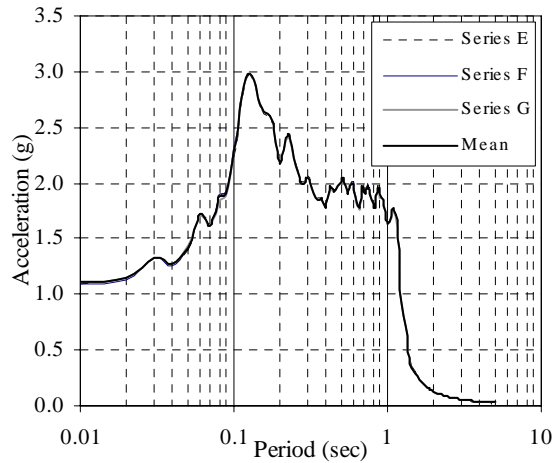


**f) Agrid**

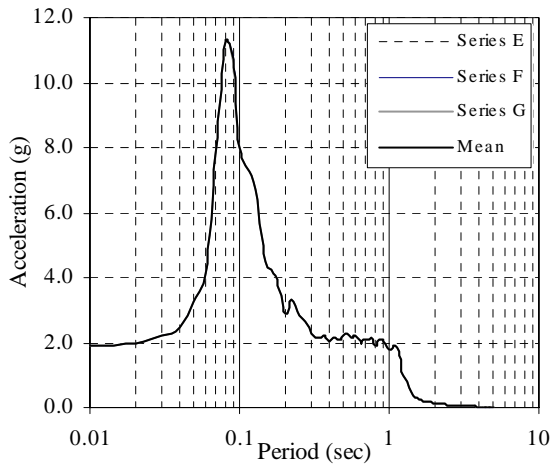
**FIGURE 6-24** Response spectra corresponding to  $S_S = 1.5g$ , undersized tiles with clips



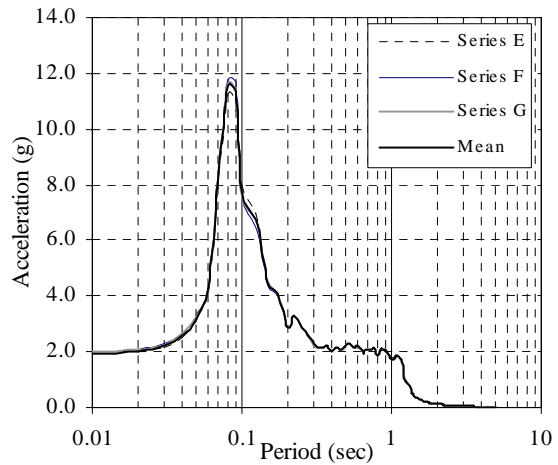
**a) Table**



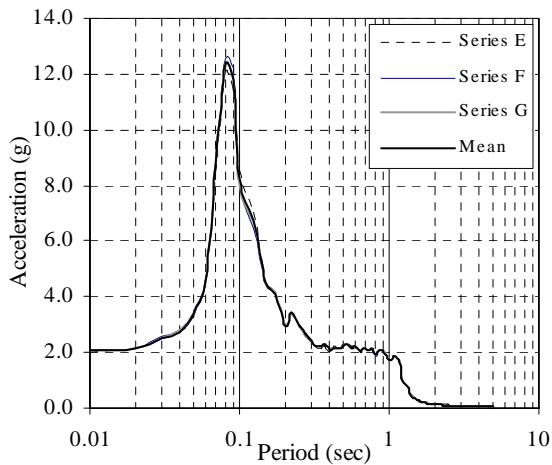
**b) Abase**



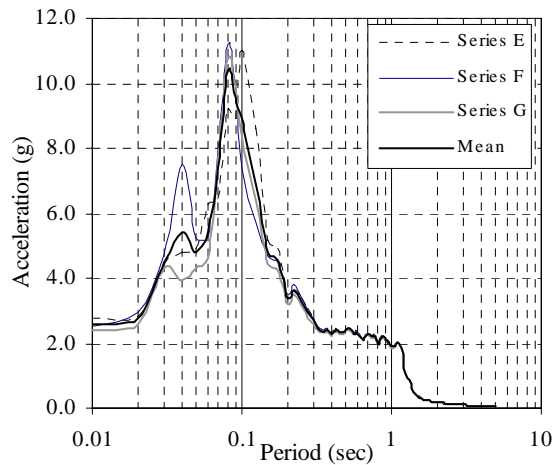
**c) Corner\_w**



**d) Qtr**

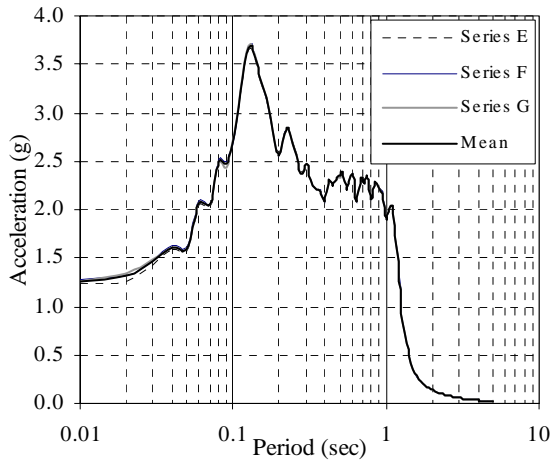


**e) Center**

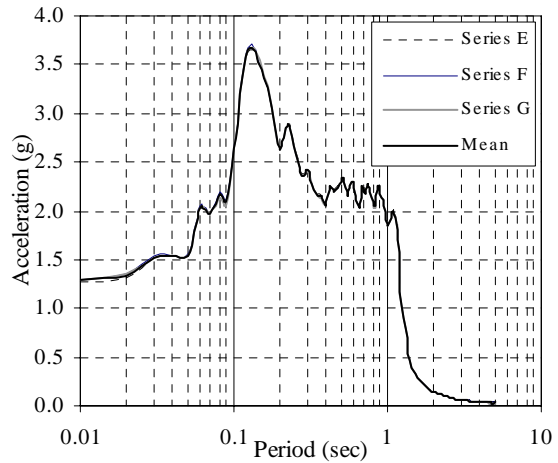


**f) Agrid**

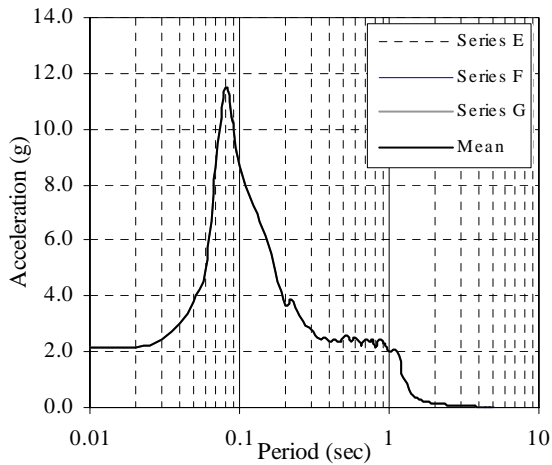
**FIGURE 6-25** Response spectra corresponding to  $S_S = 1.75g$ , undersized tiles with clips



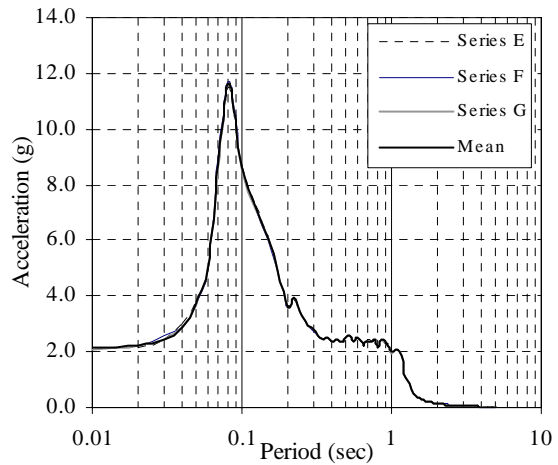
**a) Table**



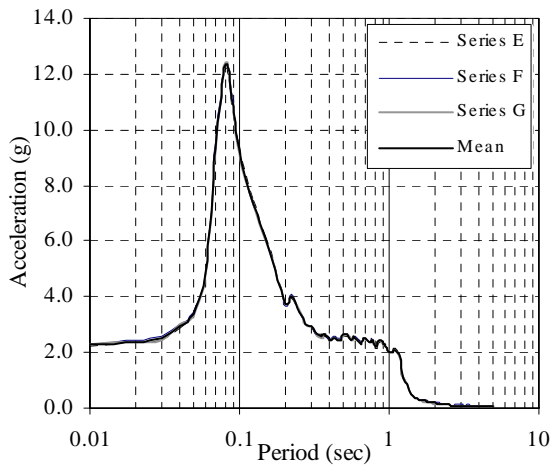
**b) Abase**



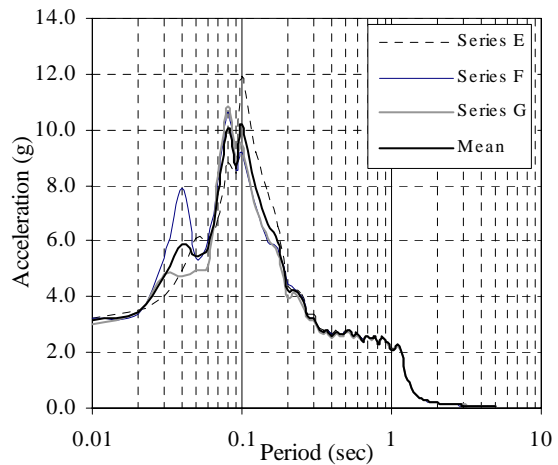
**c) Corner\_w**



**d) Qtr**

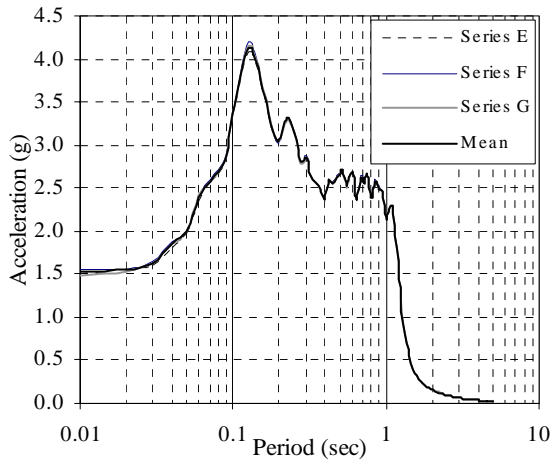


**e) Center**

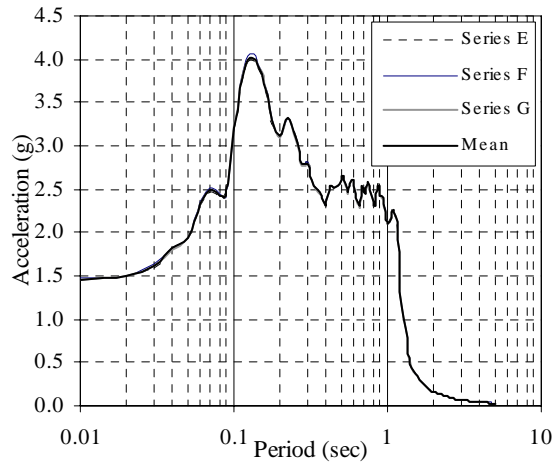


**f) Agrid**

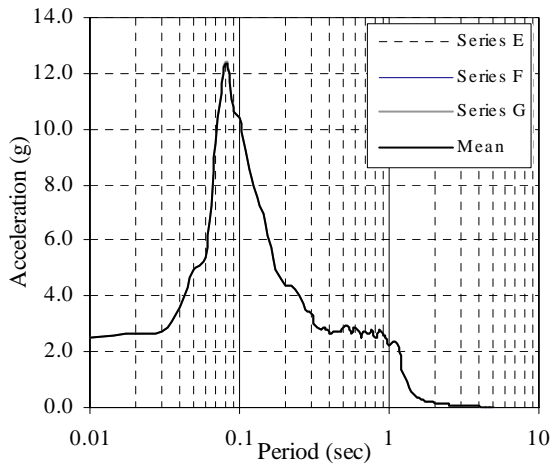
**FIGURE 6-26** Response spectra corresponding to  $S_S = 2.0g$ , undersized tiles with clips



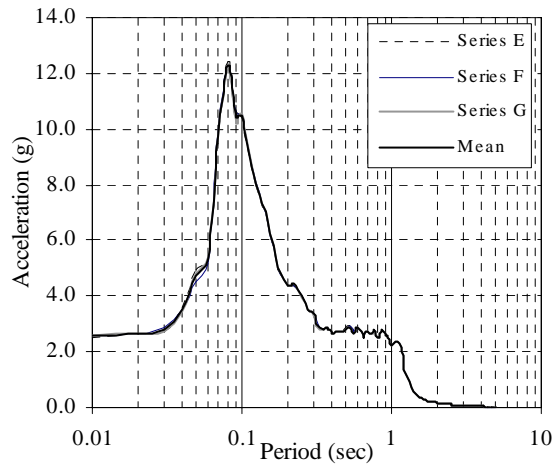
**a) Table**



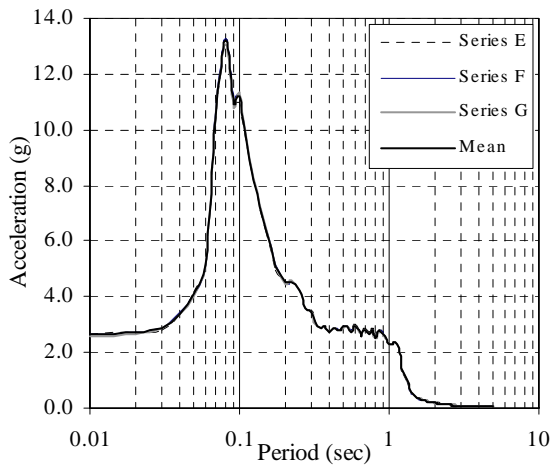
**b) Abase**



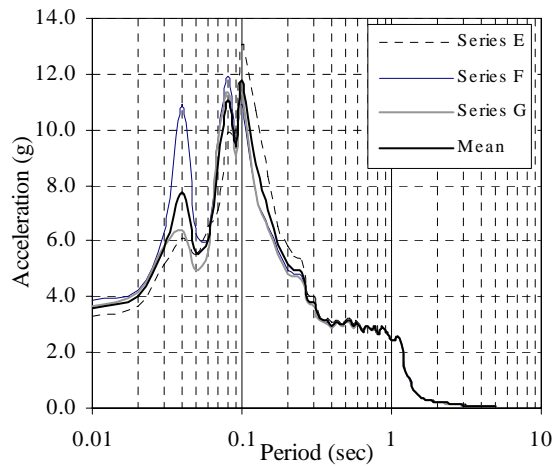
**c) Corner\_w**



**d) Qtr**



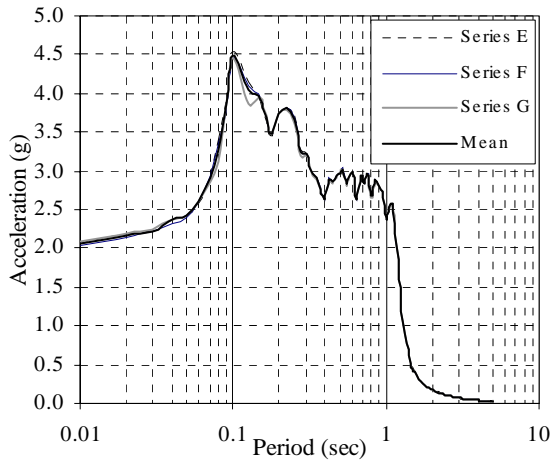
**e) Center**



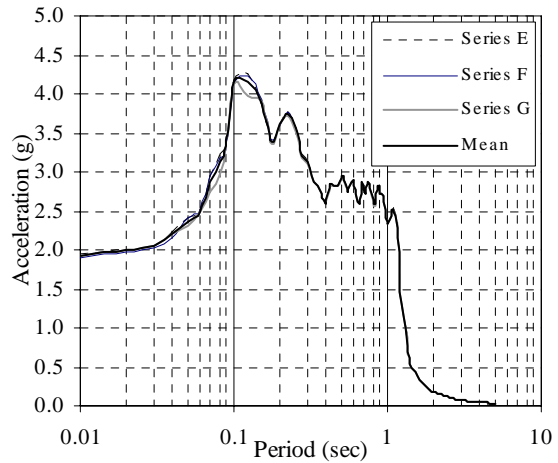
**f) Agrid**

**FIGURE 6-27** Response spectra corresponding to  $S_S = 2.25g$ , undersized tiles with clips

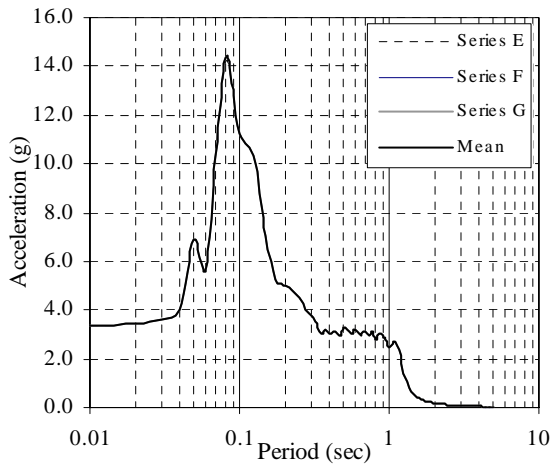




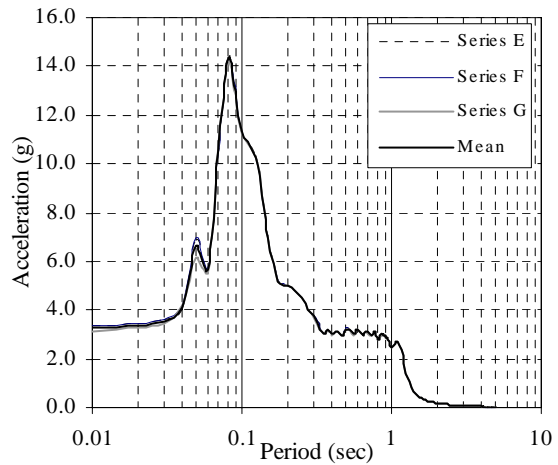
**a) Table**



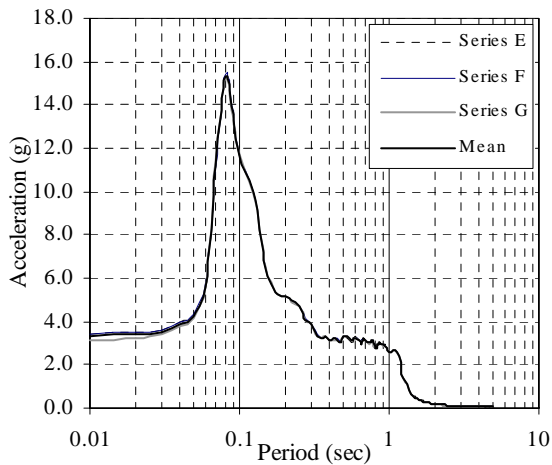
**b) Abase**



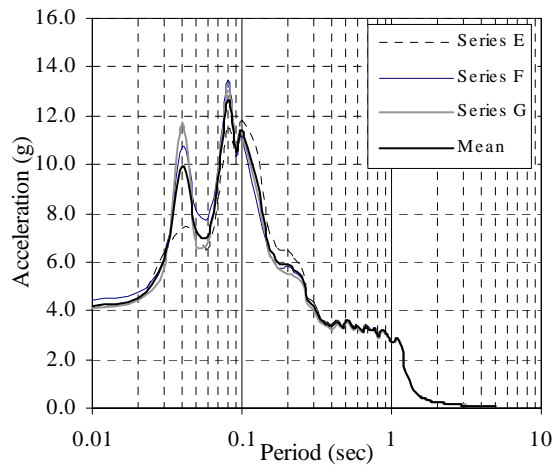
**c) Corner\_w**



**d) Qtr**

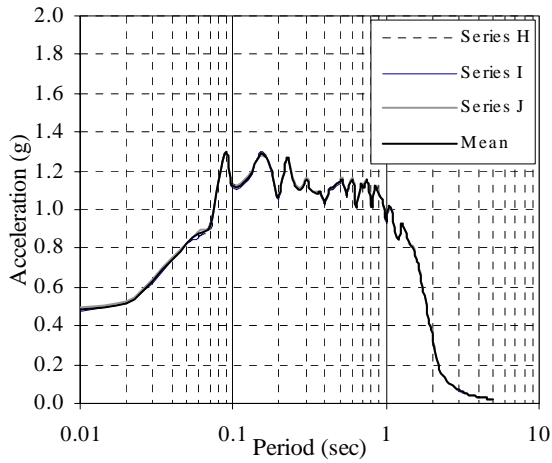


**e) Center**

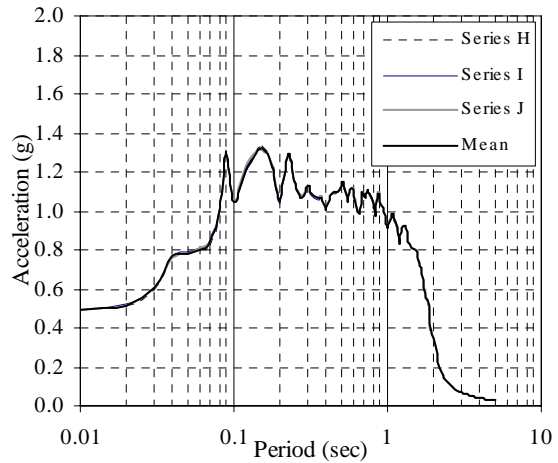


**f) Agrid**

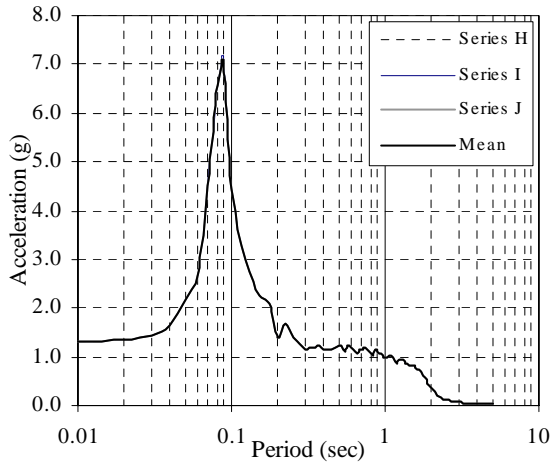
**FIGURE 6-28** Response spectra corresponding to  $S_S = 2.5g$ , undersized tiles with clips



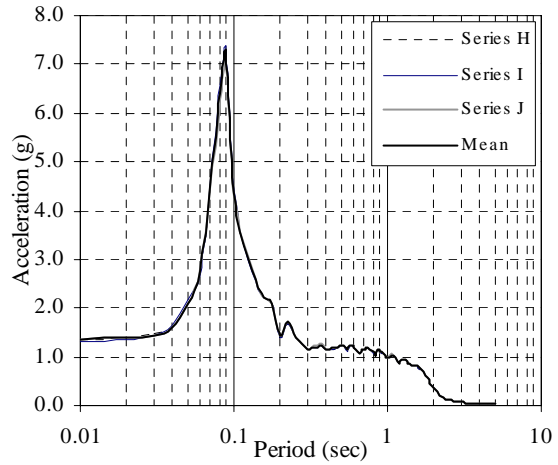
**a) Table**



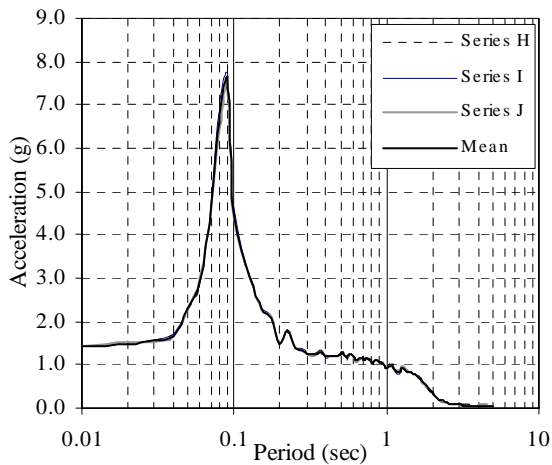
**b) Abase**



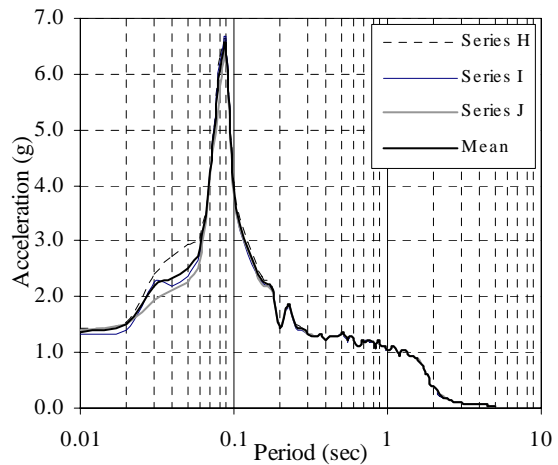
**c) Corner\_w**



**d) Qtr**

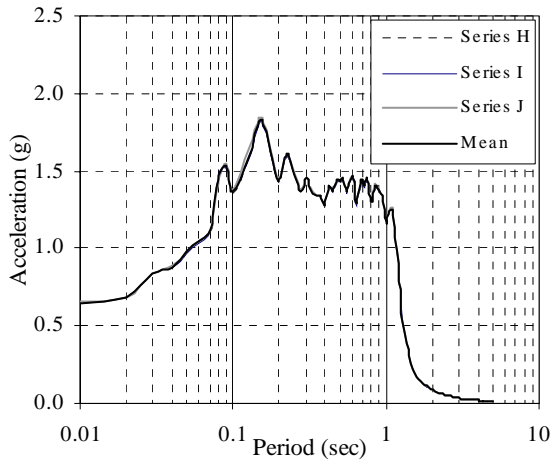


**e) Center**

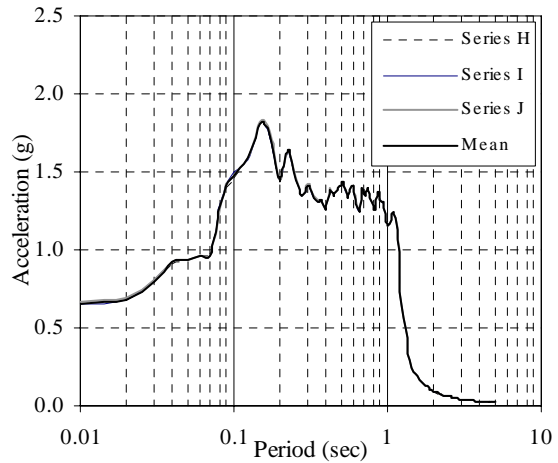


**f) Agrid**

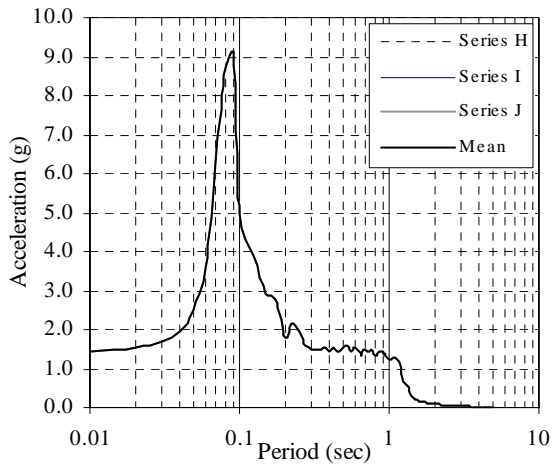
**FIGURE 6-29** Response spectra corresponding to  $S_S = 1.0g$ , undersized tiles with recycled grid



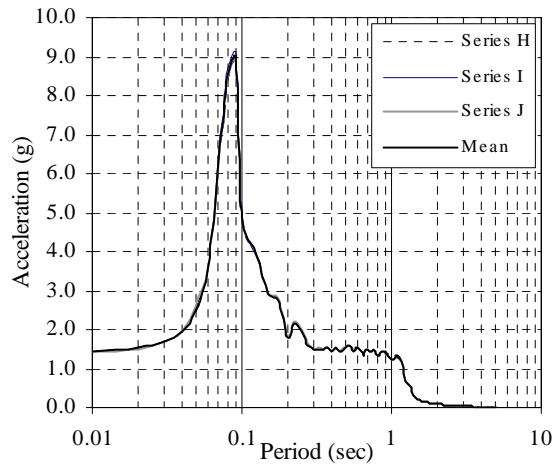
**a) Table**



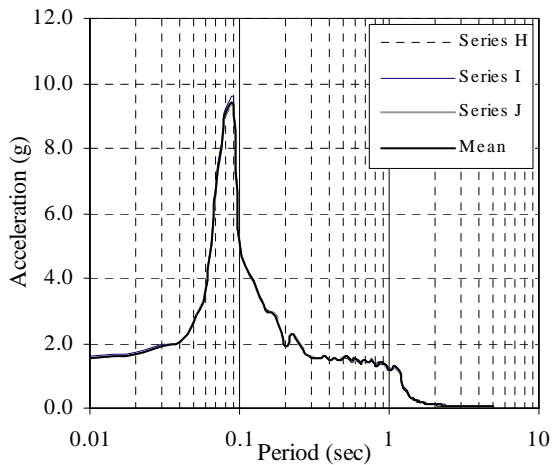
**b) Abase**



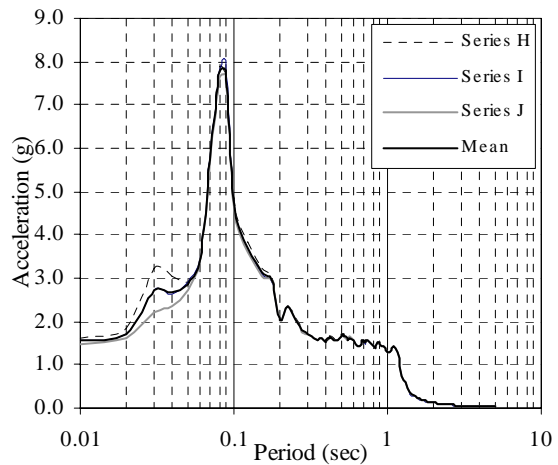
**c) Corner\_w**



**d) Qtr**

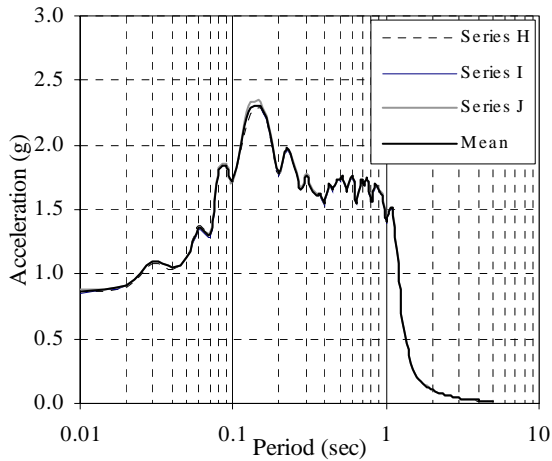


**e) Center**

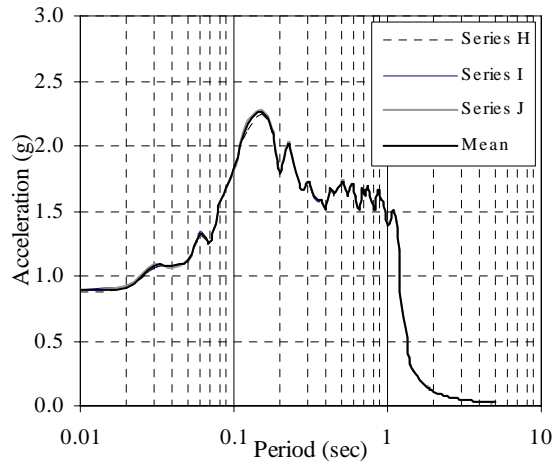


**f) Agrid**

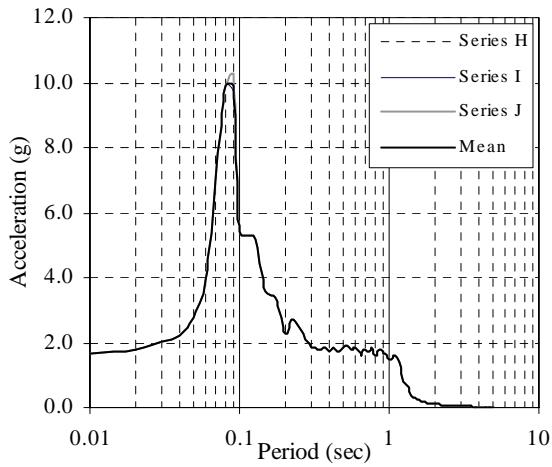
**FIGURE 6-30** Response spectra corresponding to  $S_S = 1.25g$ , undersized tiles with recycled grid



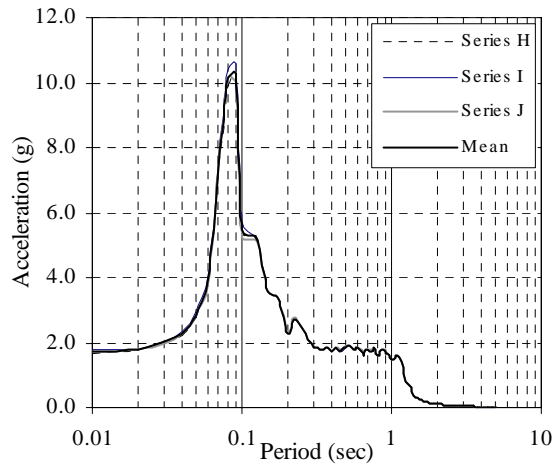
**a) Table**



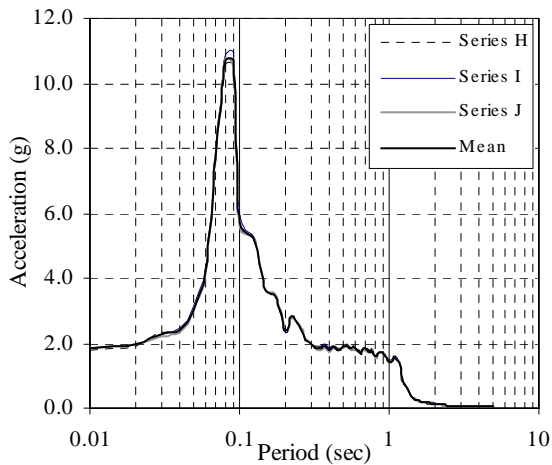
**b) Abase**



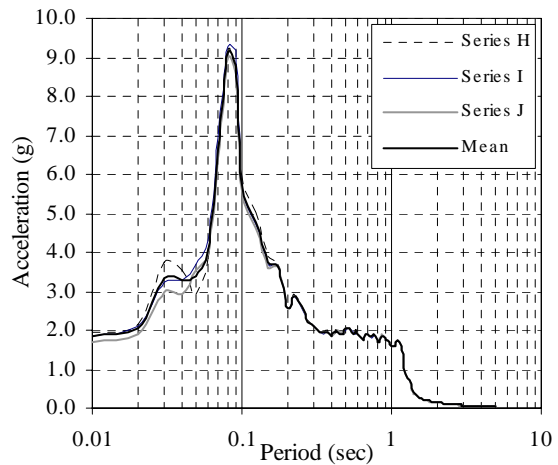
**c) Corner\_w**



**d) Qtr**

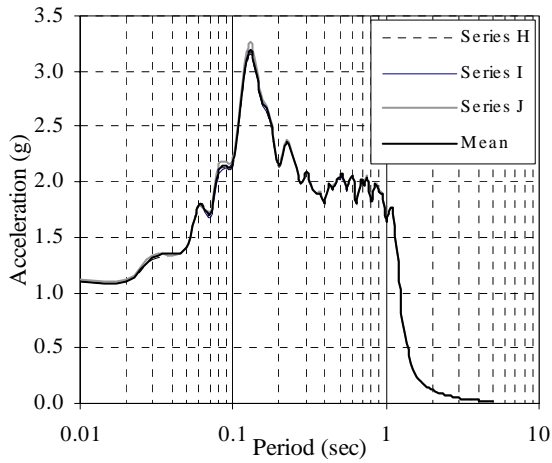


**e) Center**

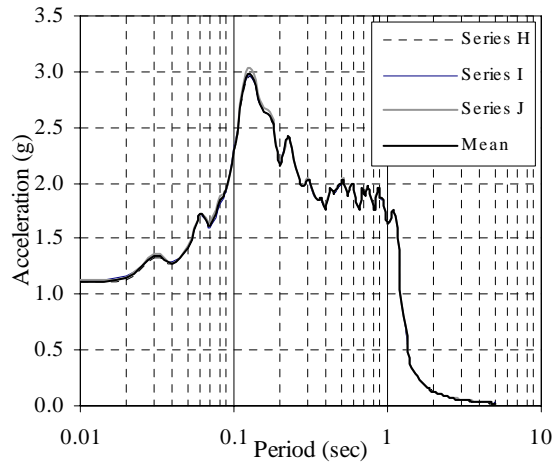


**f) Agrid**

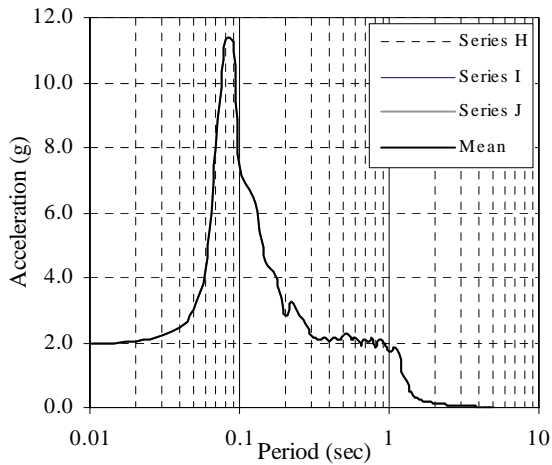
**FIGURE 6-31 Response spectra corresponding to  $S_S = 1.5g$ , undersized tiles with recycled grid**



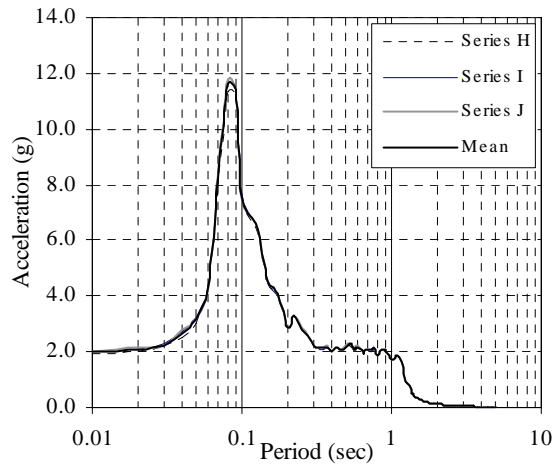
**a) Table**



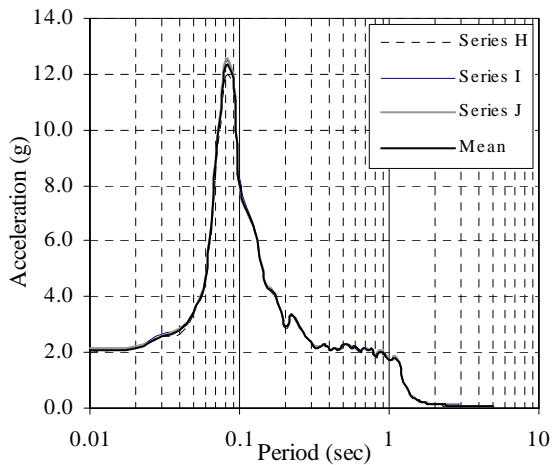
**b) Abase**



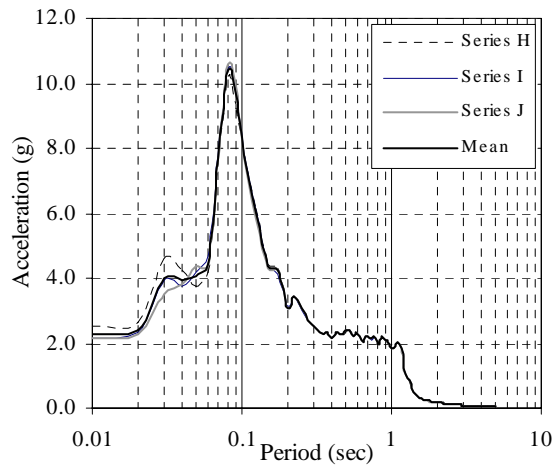
**c) Corner\_w**



**d) Qtr**

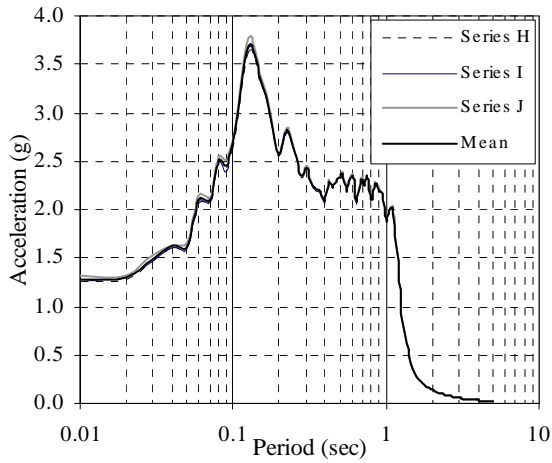


**e) Center**

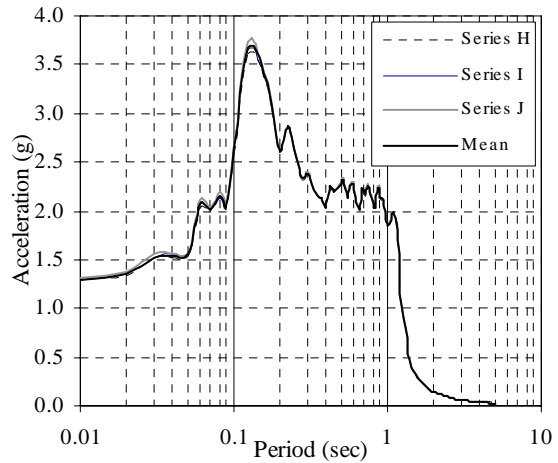


**f) Agrid**

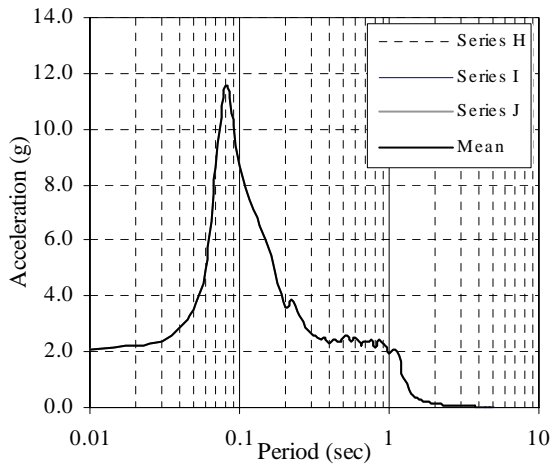
**FIGURE 6-32 Response spectra corresponding to  $S_S = 1.75g$ , undersized tiles with recycled grid**



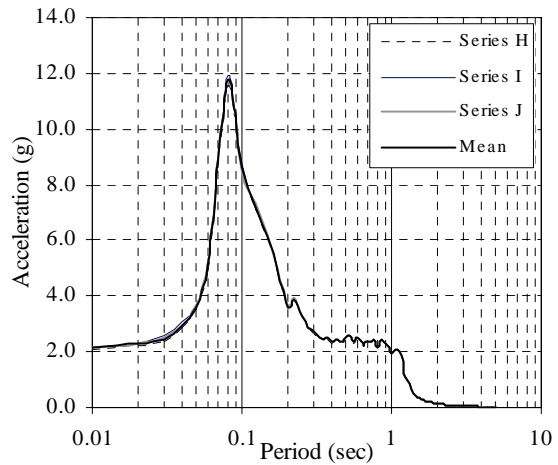
**a) Table**



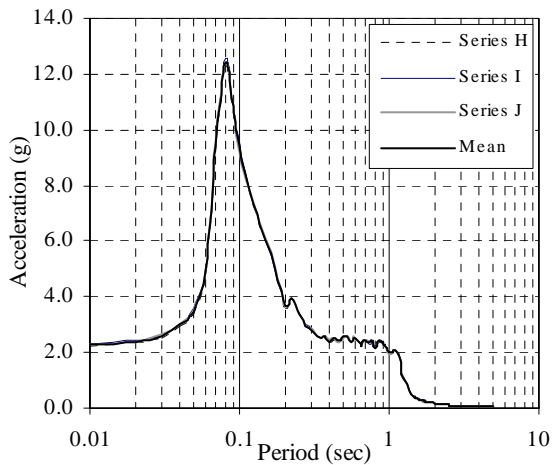
**b) Abase**



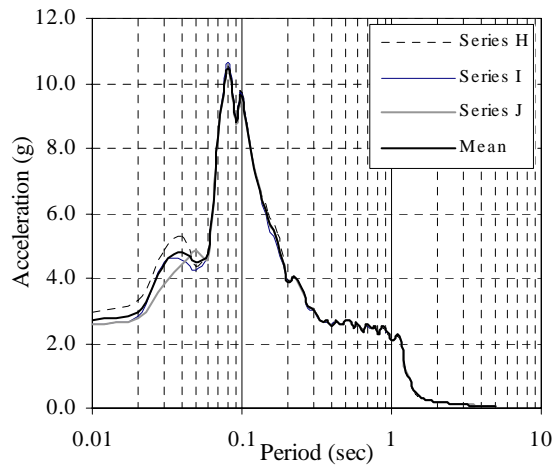
**c) Corner\_w**



**d) Qtr**

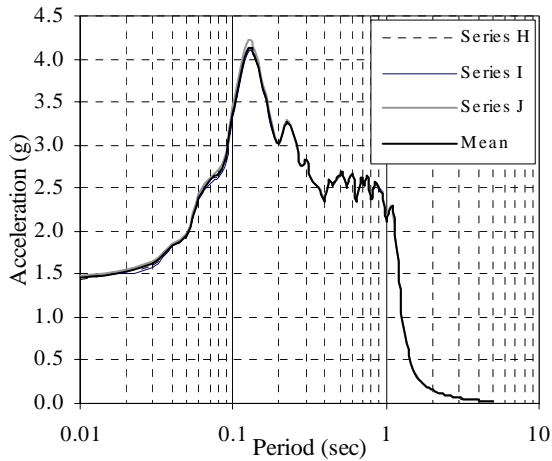


**e) Center**

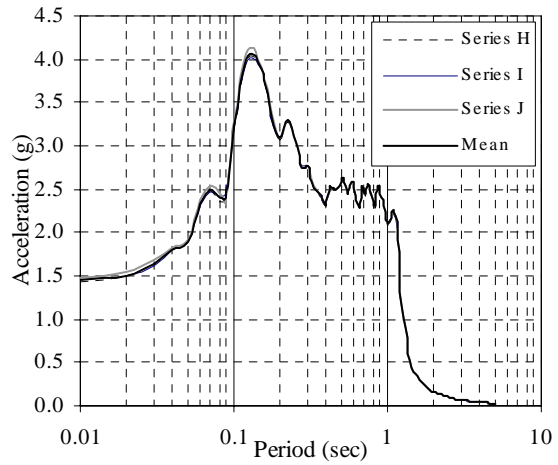


**f) Agrid**

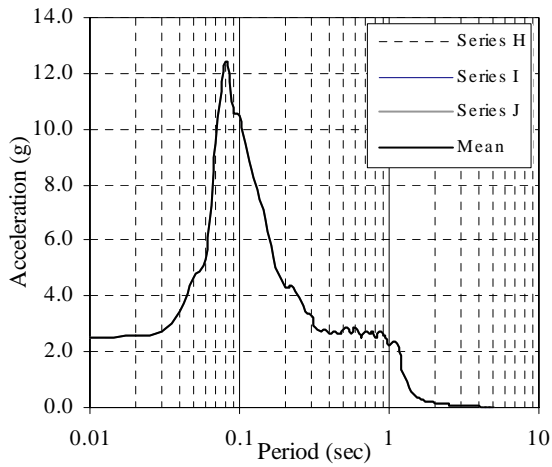
**FIGURE 6-33** Response spectra corresponding to  $S_S = 2.0g$ , undersized tiles with recycled grid



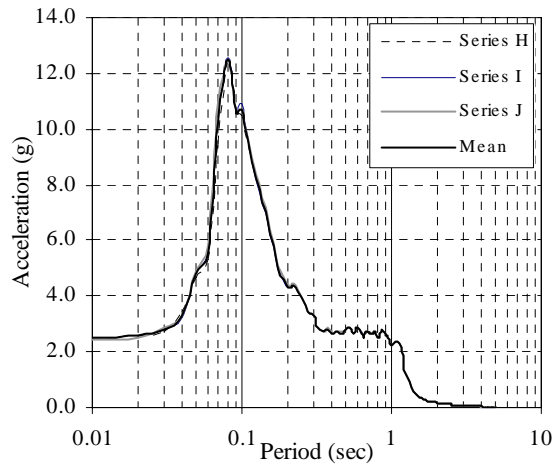
**a) Table**



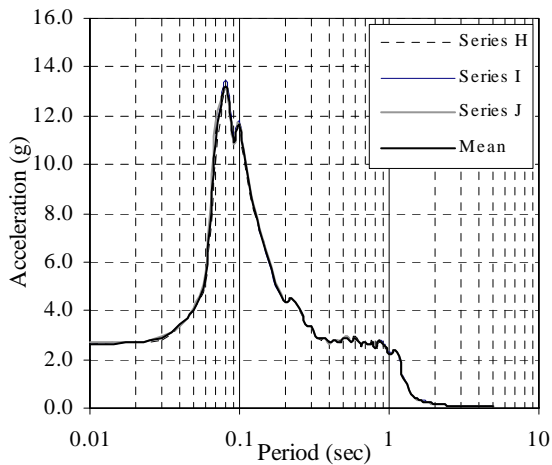
**b) Abase**



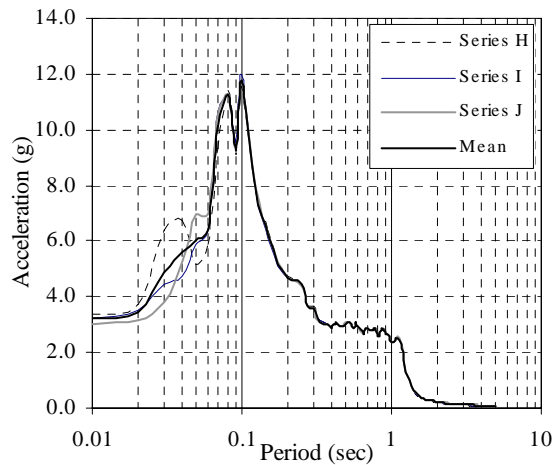
**c) Corner\_w**



**d) Qtr**

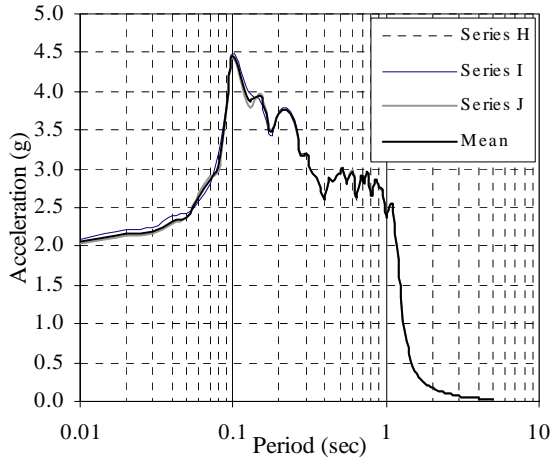


**e) Center**

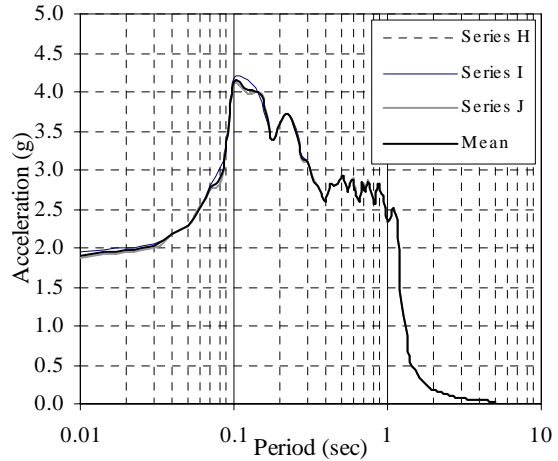


**f) Agrid**

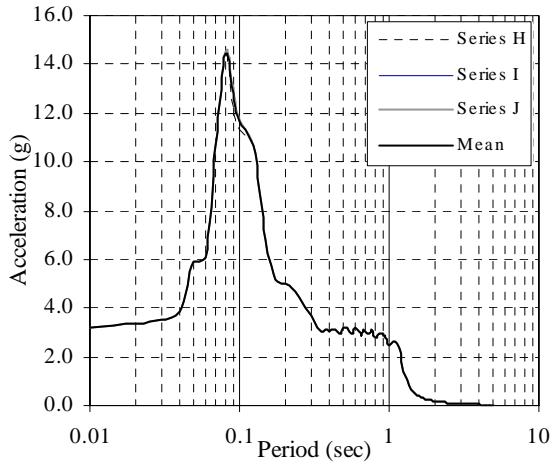
**FIGURE 6-34 Response spectra corresponding to  $S_S = 2.25g$ , undersized tiles with recycled grid**



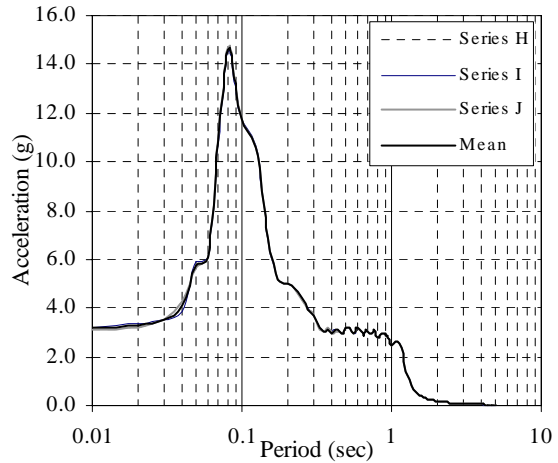
**a) Table**



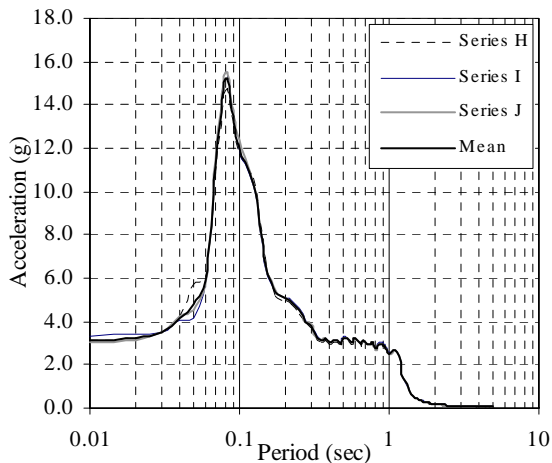
**b) Abase**



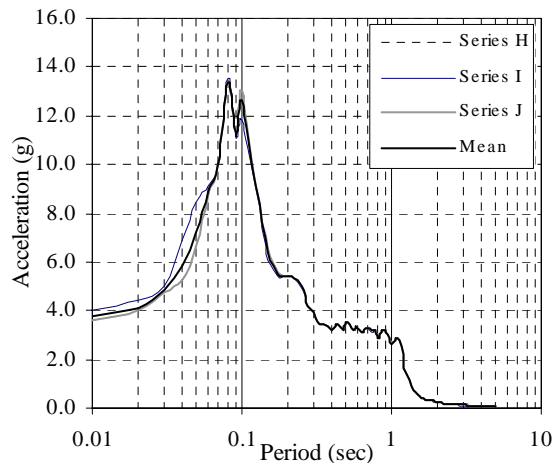
**c) Corner\_w**



**d) Qtr**



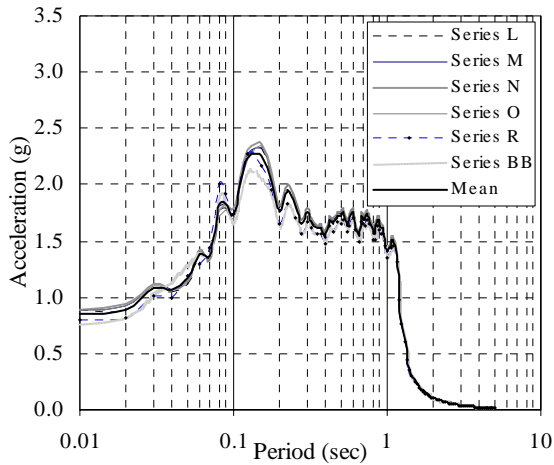
**e) Center**



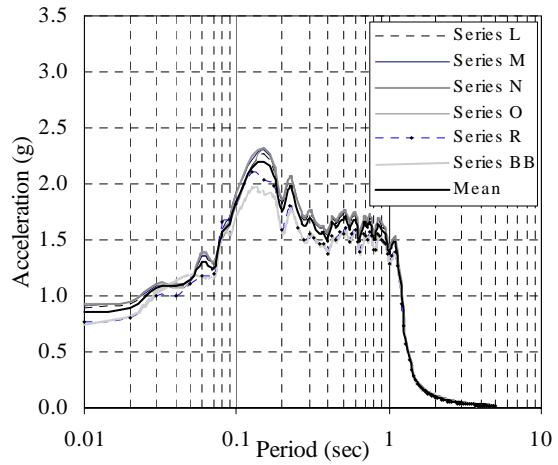
**f) Agrid**

**FIGURE 6-35 Response spectra corresponding to  $S_S = 2.5g$ , undersized tiles with recycled grid**

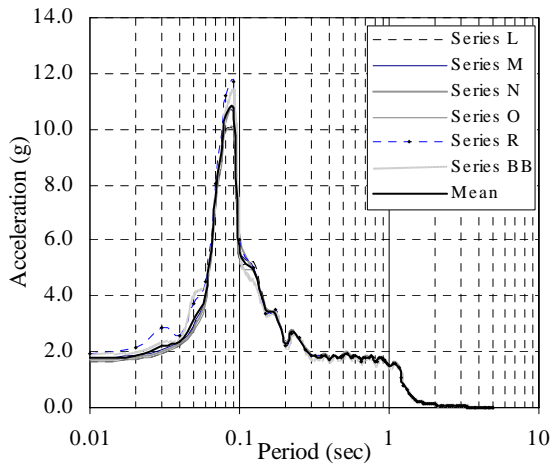




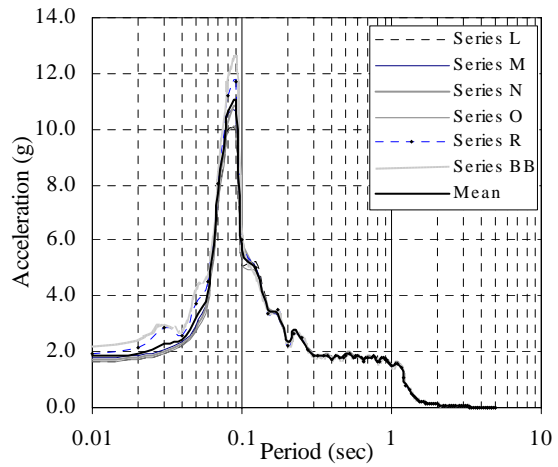
**a) Table**



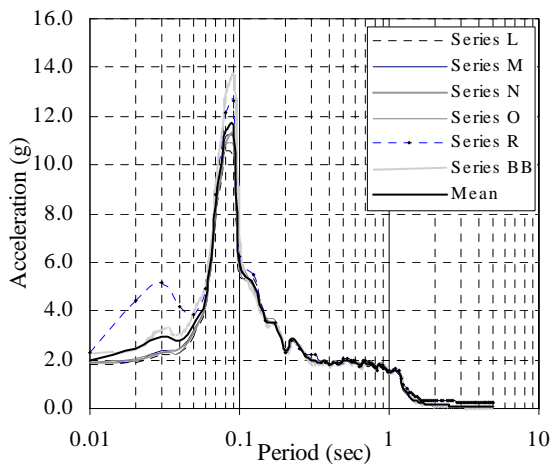
**b) Abase**



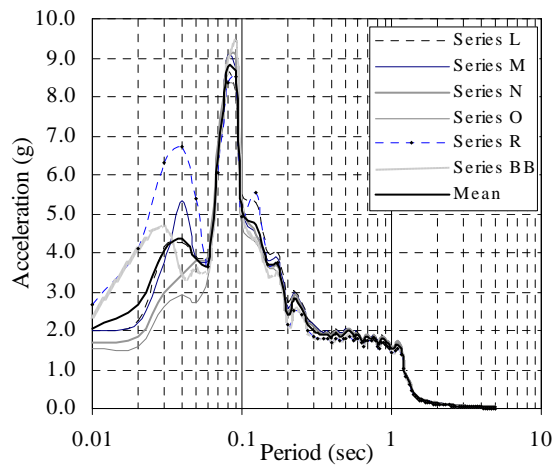
**c) Corner\_w**



**d) Qtr**

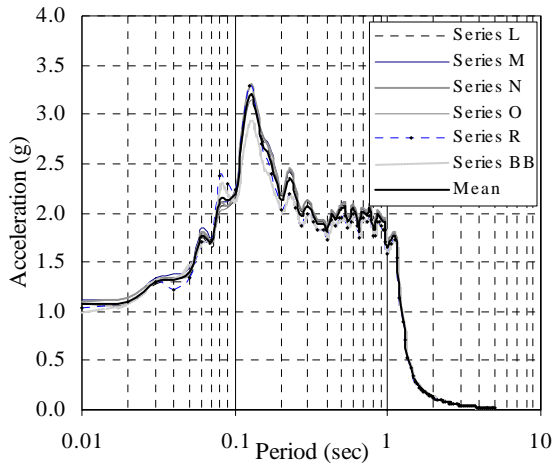


**e) Center**

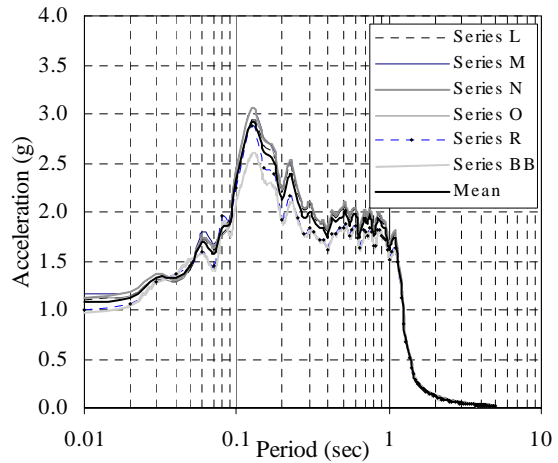


**f) Agrid**

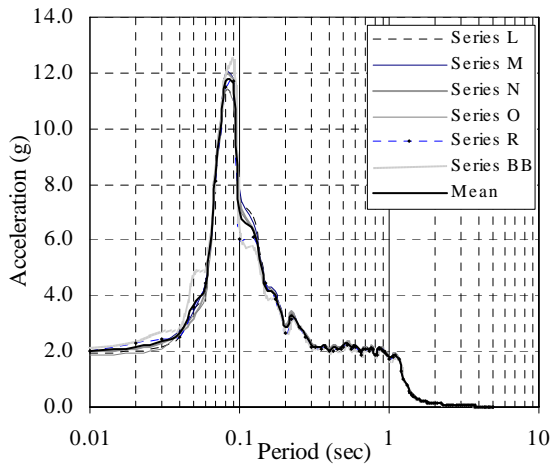
**FIGURE 6-36 Response spectra corresponding to  $S_S = 1.5g$ , normal sized tiles**



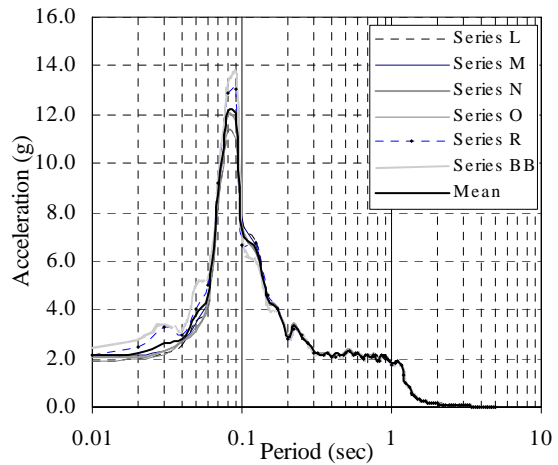
**a) Table**



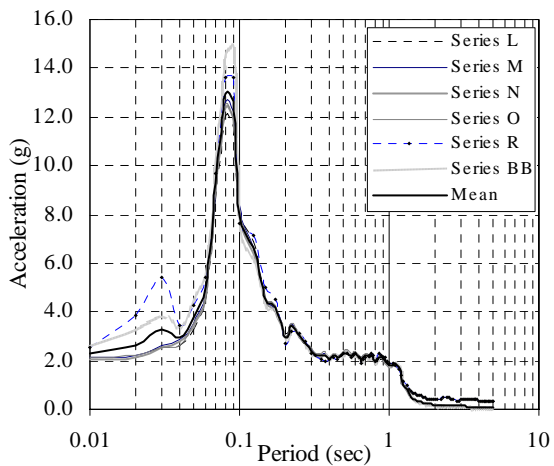
**b) Abase**



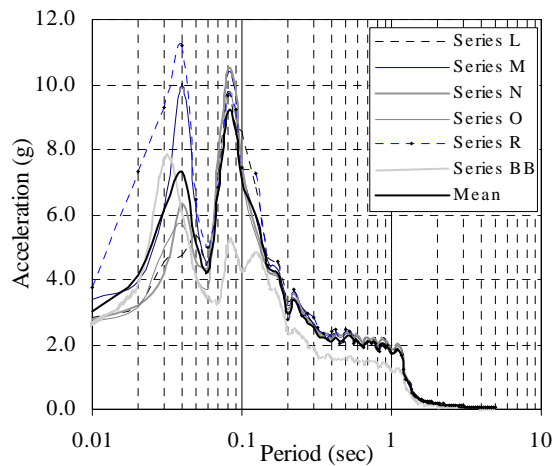
**c) Corner\_w**



**d) Qtr**

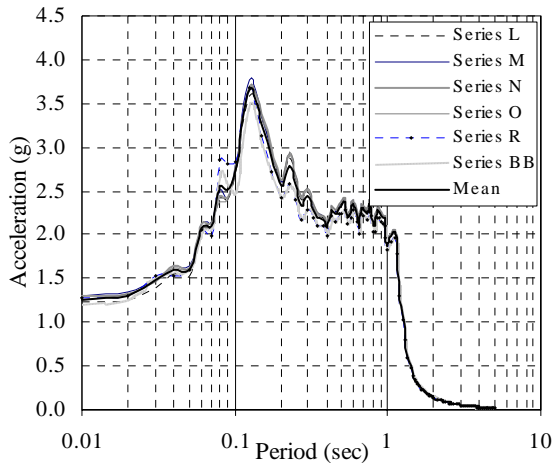


**e) Center**

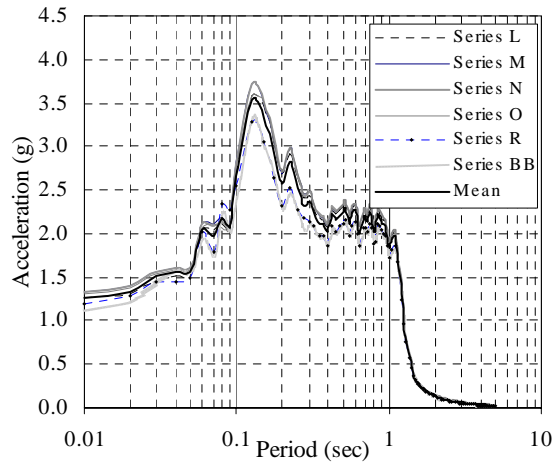


**f) Agrid**

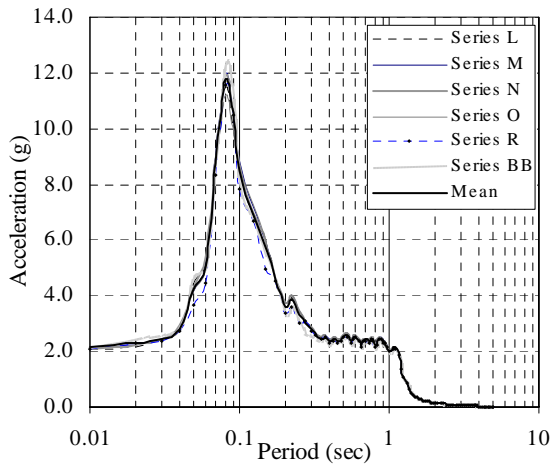
**FIGURE 6-37** Response spectra corresponding to  $S_S = 1.75g$ , normal sized tiles



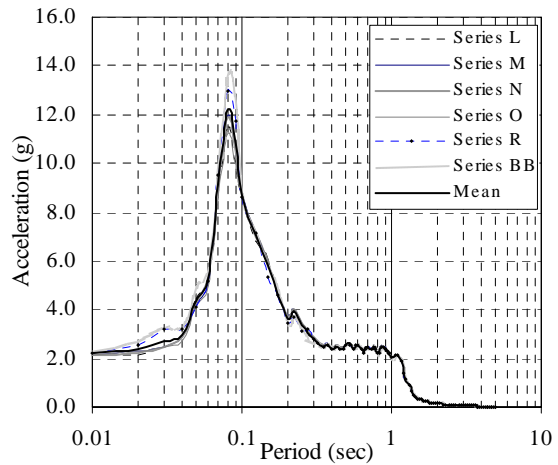
**a) Table**



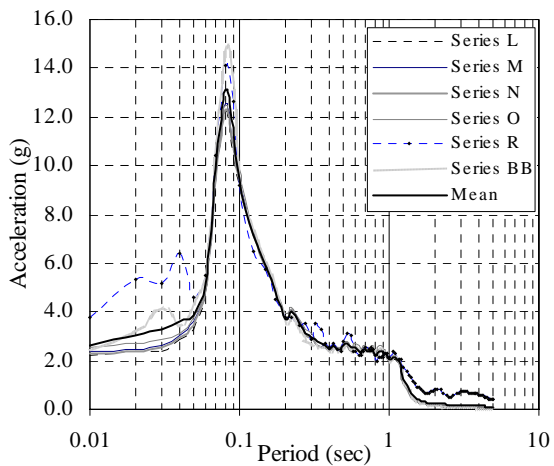
**b) Abase**



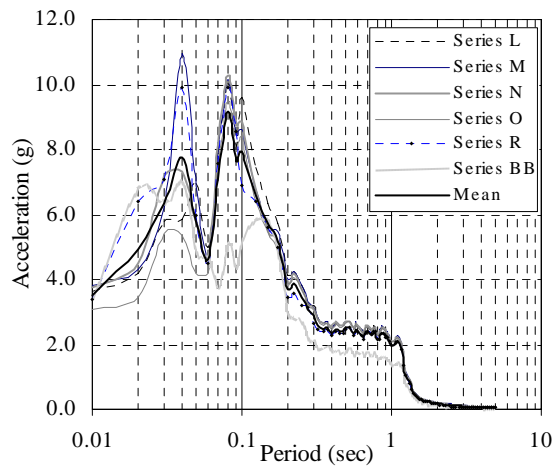
**c) Corner\_w**



**d) Qtr**

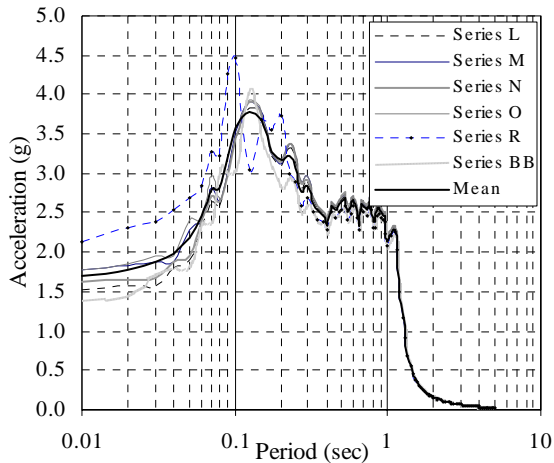


**e) Center**

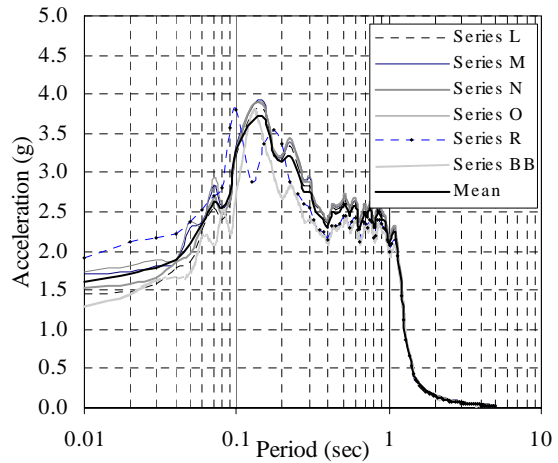


**f) Agrid**

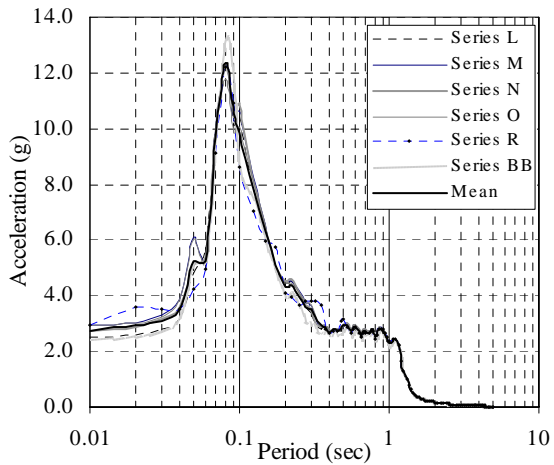
**FIGURE 6-38 Response spectra corresponding to  $S_S = 2.0g$ , normal sized tiles**



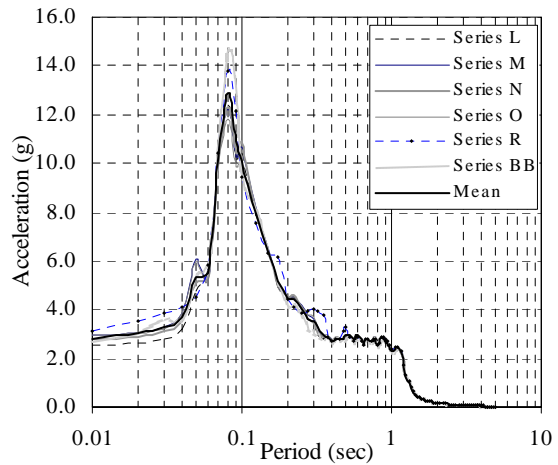
**a) Table**



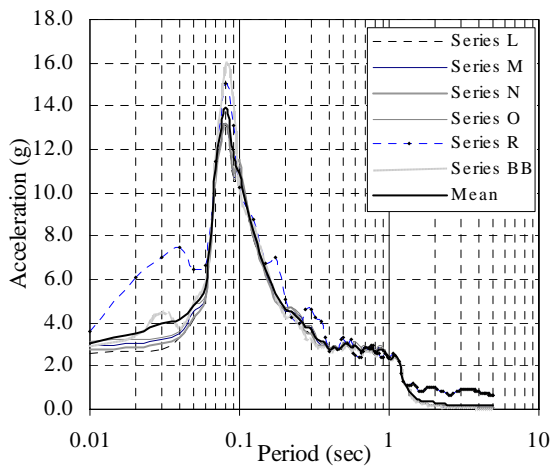
**b) Abase**



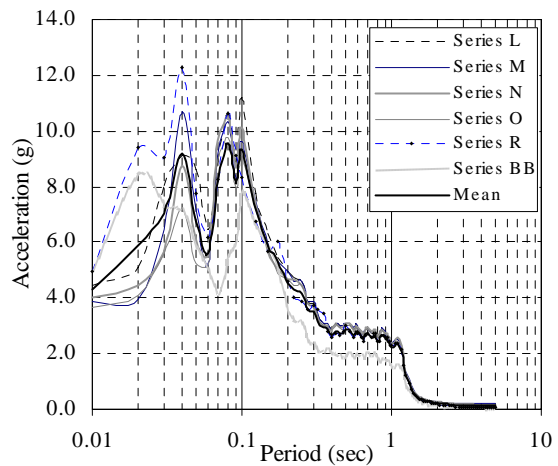
**c) Corner\_w**



**d) Qtr**

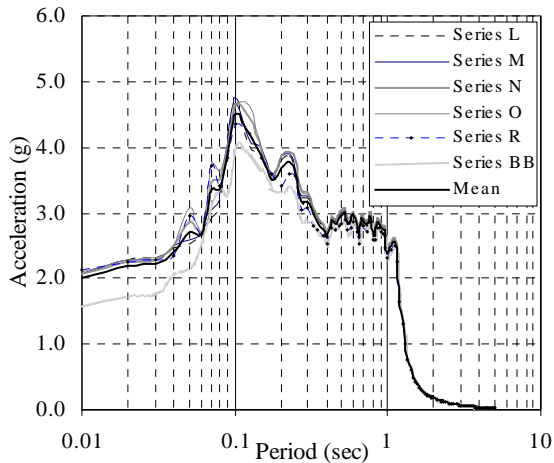


**e) Center**

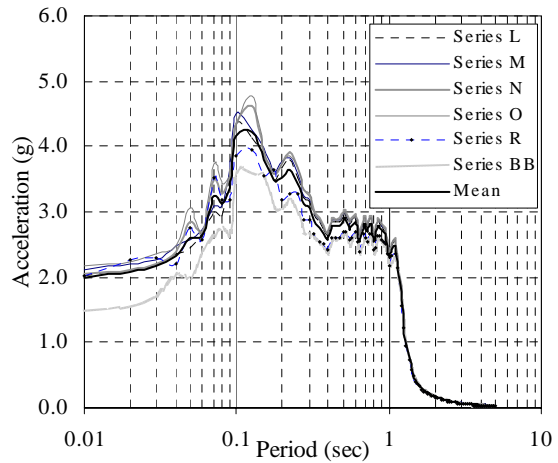


**f) Agrid**

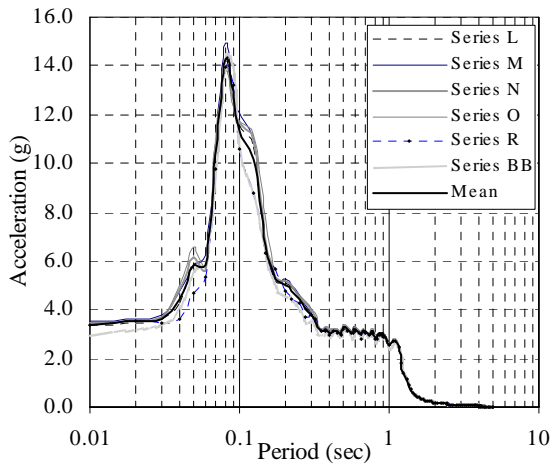
**FIGURE 6-39** Response spectra corresponding to  $S_S = 2.25g$ , normal sized tiles



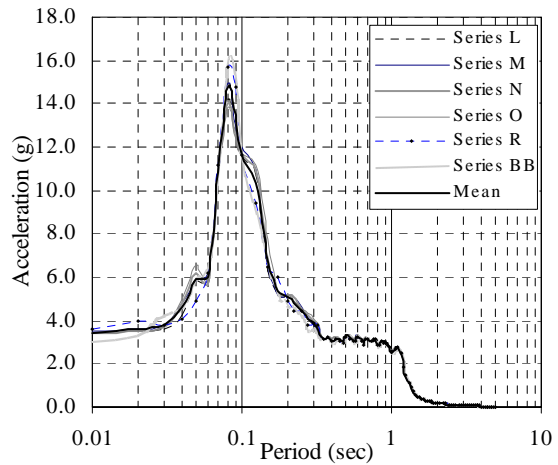
**a) Table**



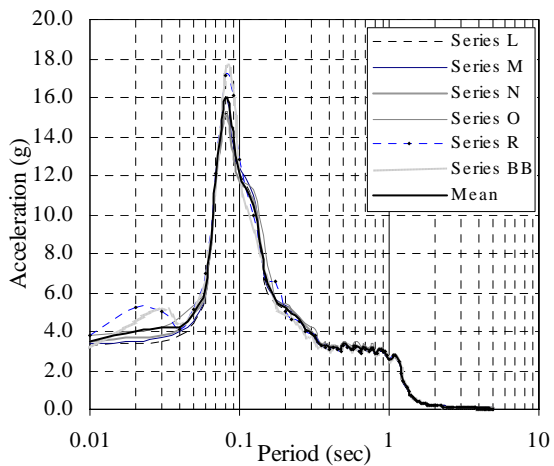
**b) Abase**



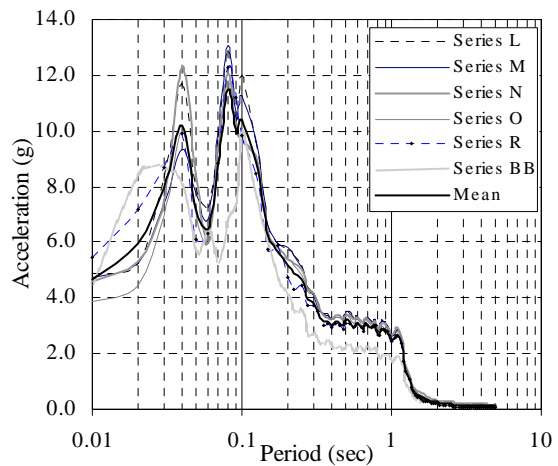
**c) Corner\_w**



**d) Qtr**

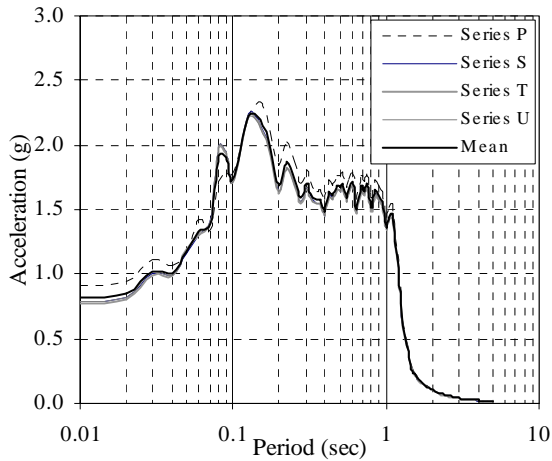


**e) Center**

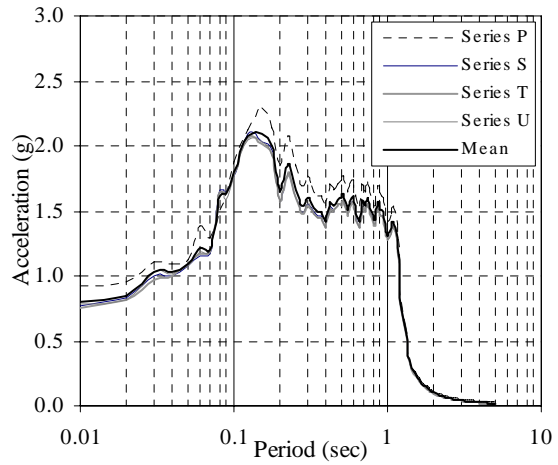


**f) Agrid**

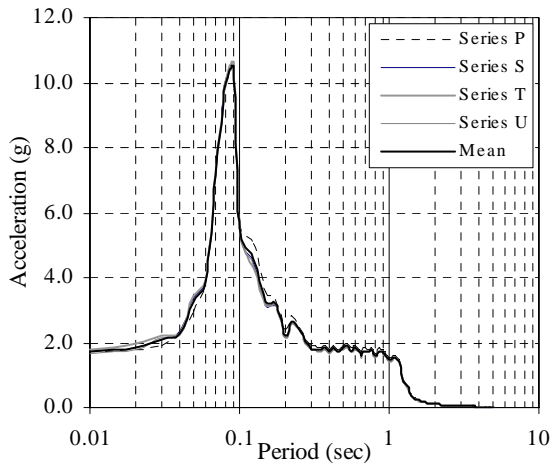
**FIGURE 6-40 Response spectra corresponding to  $S_S = 2.5g$ , normal sized tiles**



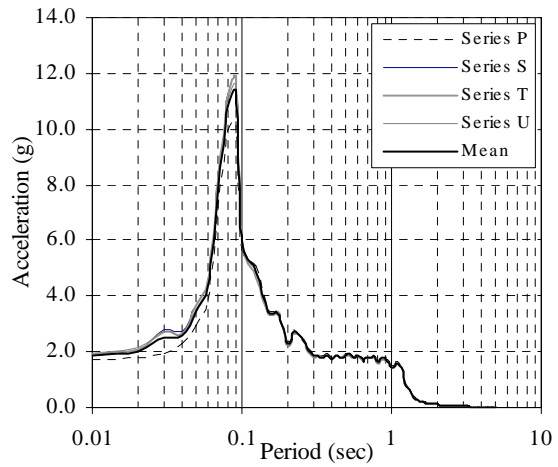
**a) Table**



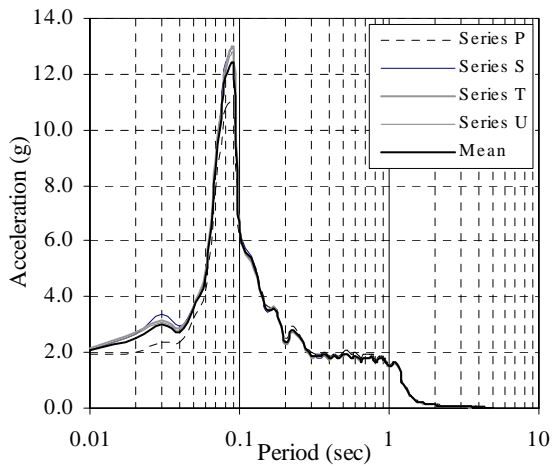
**b) Abase**



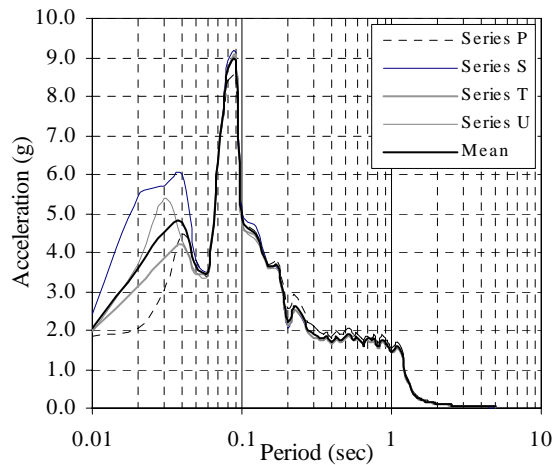
**c) Corner\_w**



**d) Qtr**

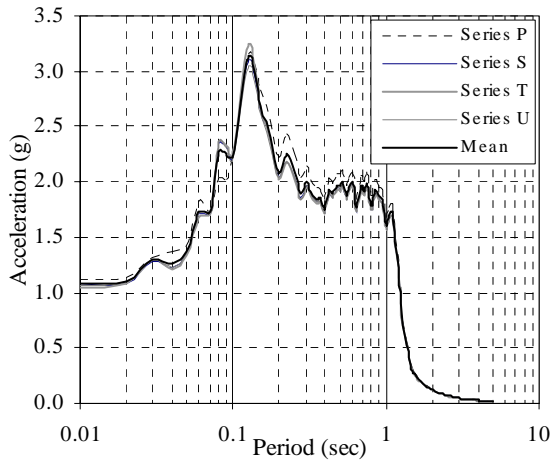


**e) Center**

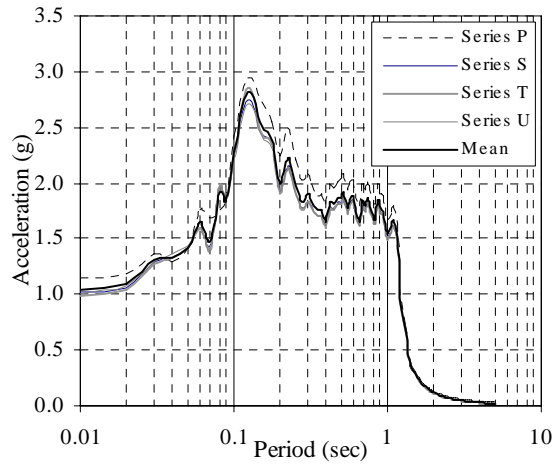


**f) Agrid**

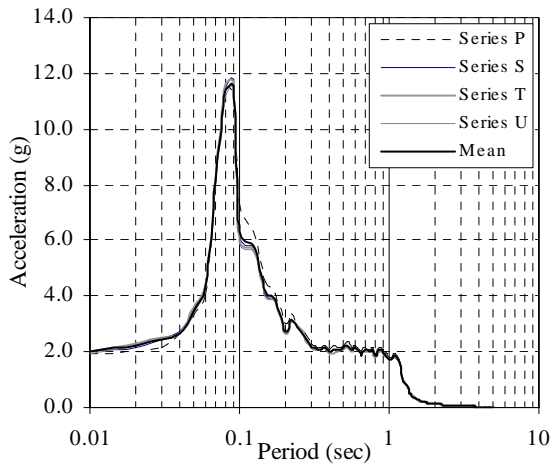
**FIGURE 6-41 Response spectra corresponding to  $S_S = 1.5g$ , normal sized tiles with clips**



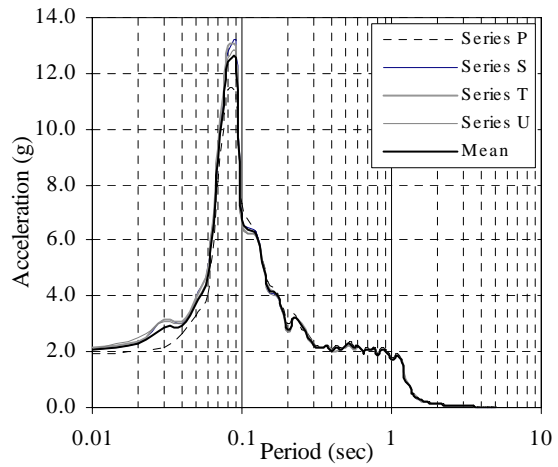
**a) Table**



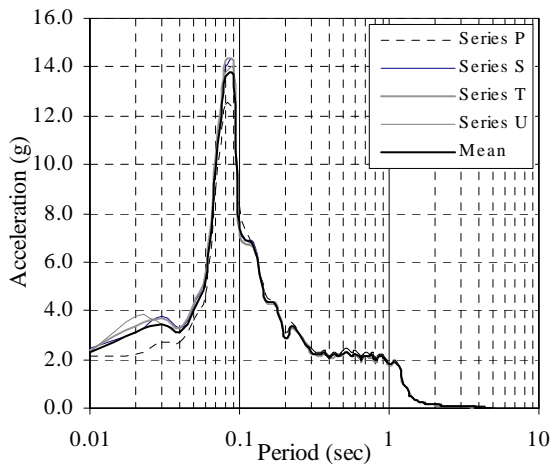
**b) Abase**



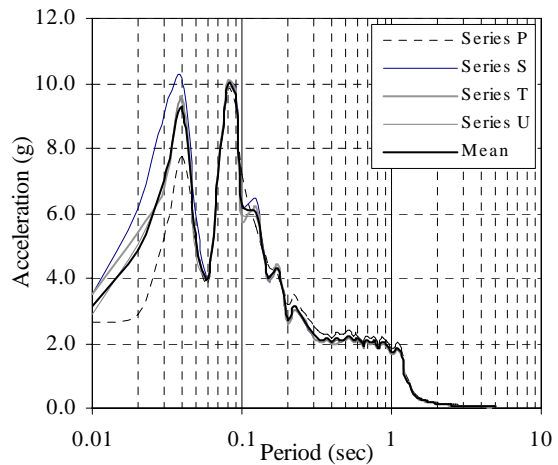
**c) Corner\_w**



**d) Qtr**

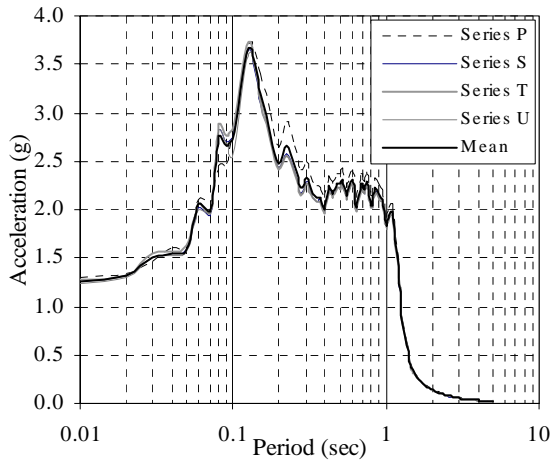


**e) Center**

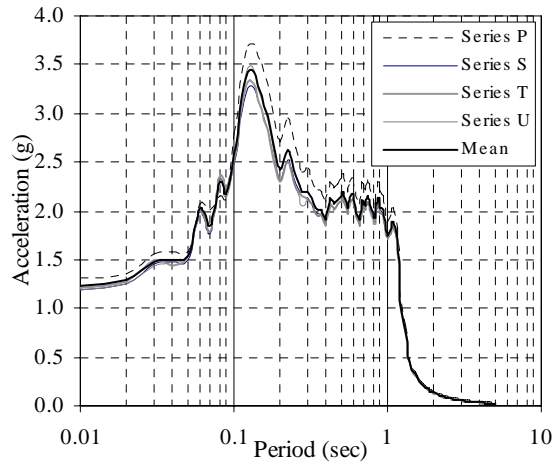


**f) Agrid**

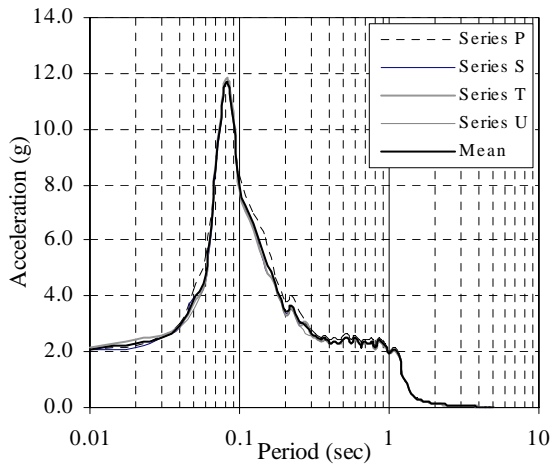
**FIGURE 6-42** Response spectra corresponding to  $S_S = 1.75g$ , normal sized tiles with clips



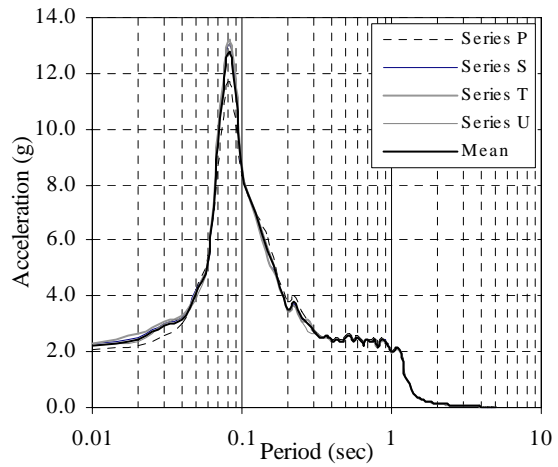
**a) Table**



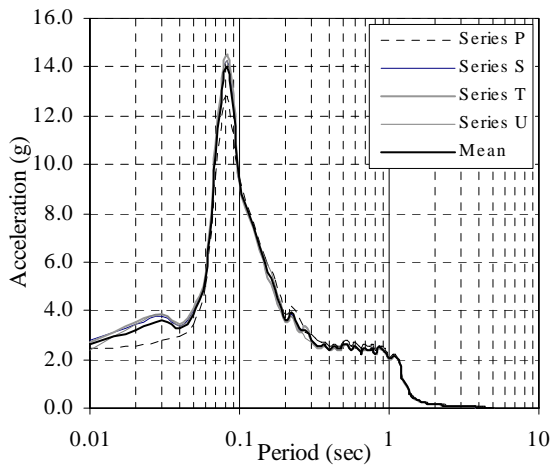
**b) Abase**



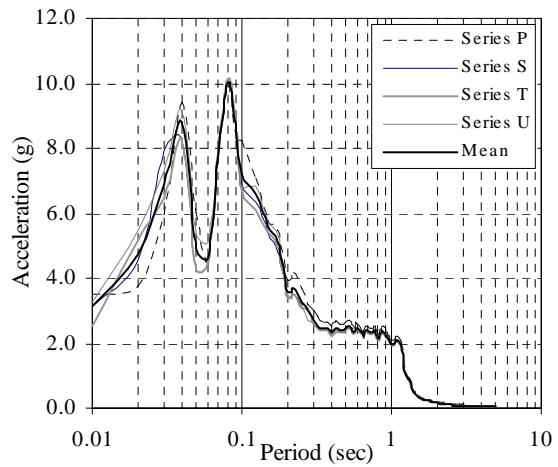
**c) Corner\_w**



**d) Qtr**



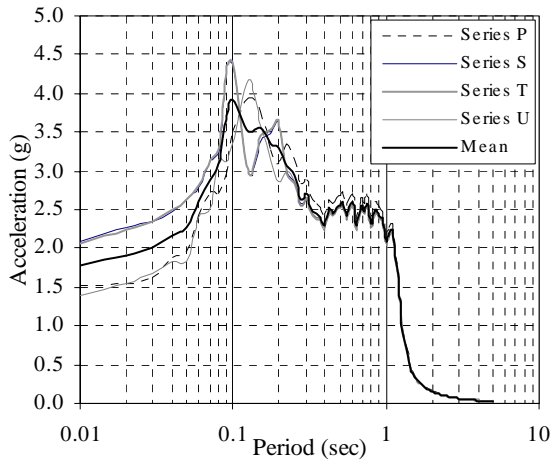
**e) Center**



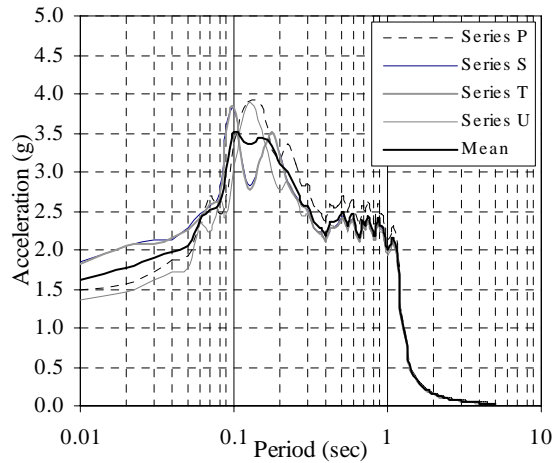
**f) Agrid**

**FIGURE 6-43** Response spectra corresponding to  $S_S = 2.0g$ , normal sized tiles with clips

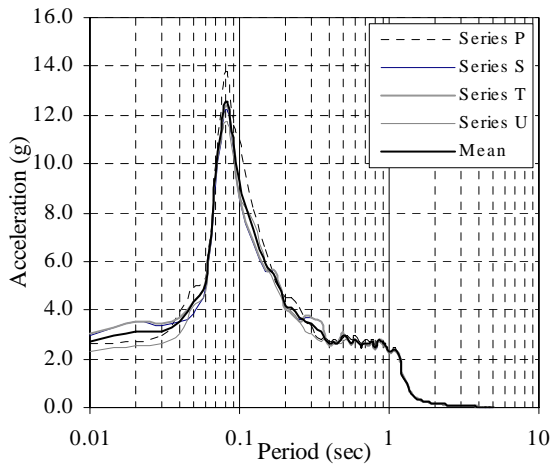




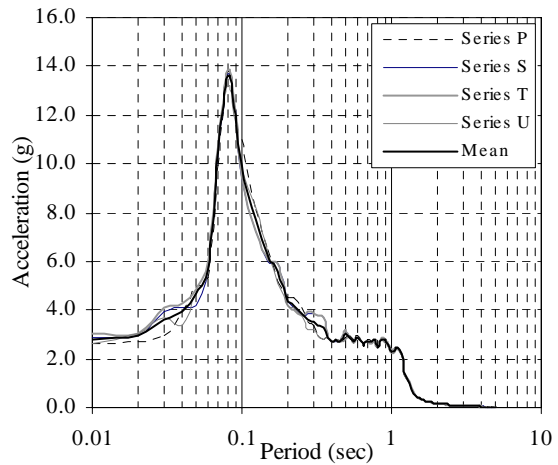
**a) Table**



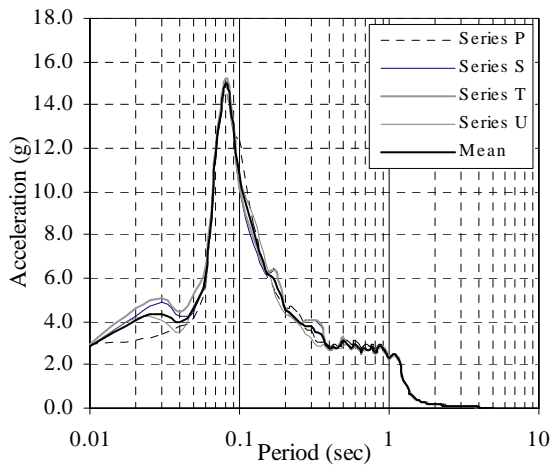
**b) Abase**



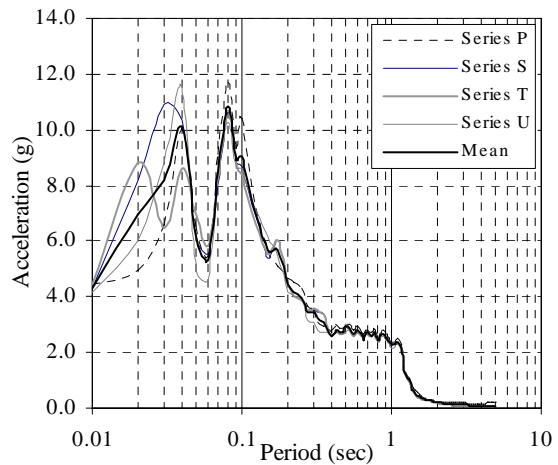
**c) Corner\_w**



**d) Qtr**

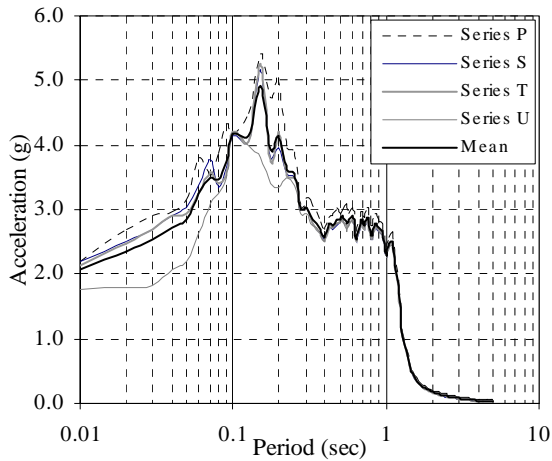


**e) Center**

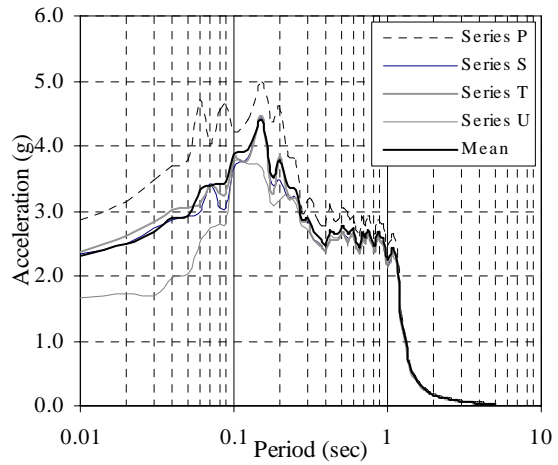


**f) Agrid**

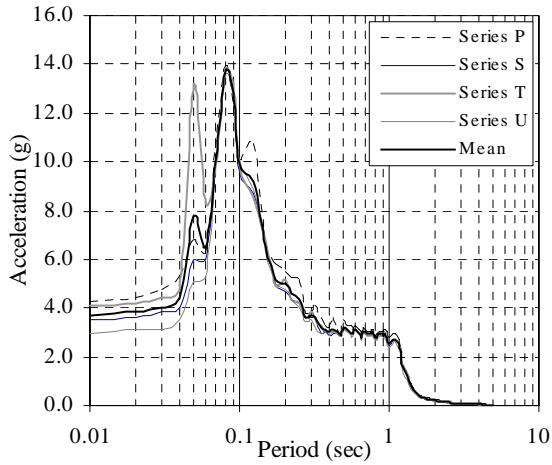
**FIGURE 6-44** Response spectra corresponding to  $S_S = 2.25g$ , normal sized tiles with clips



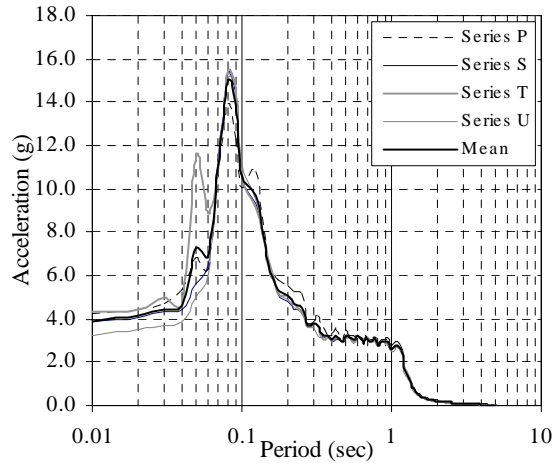
**a) Table**



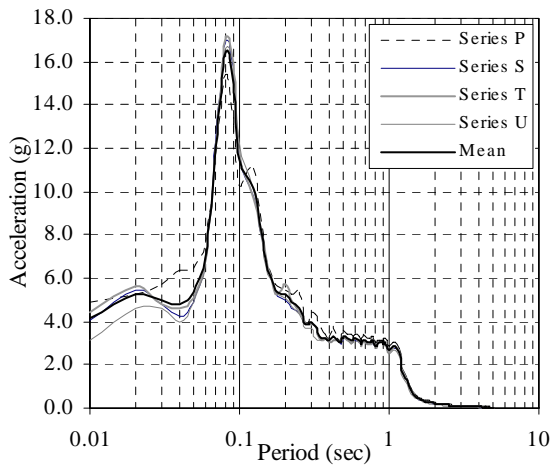
**b) Abase**



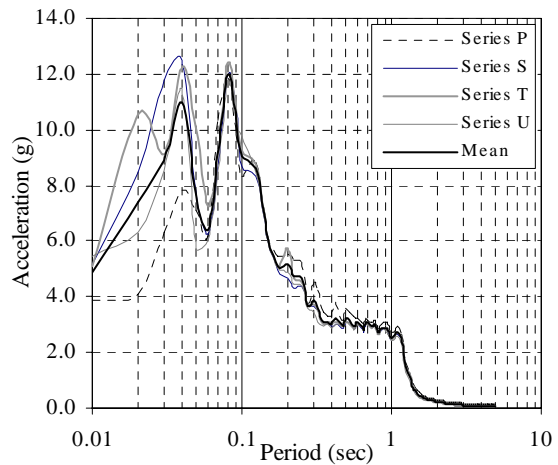
**c) Corner\_w**



**d) Qtr**

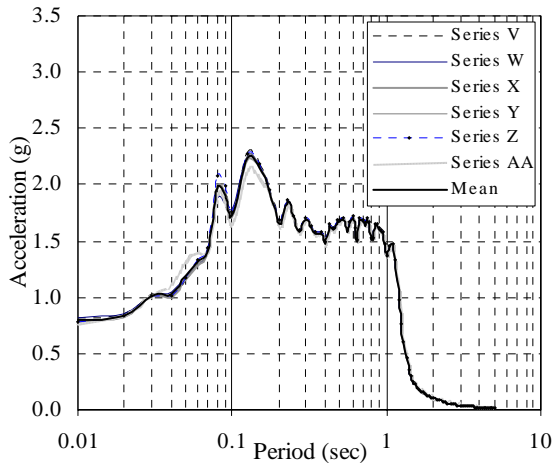


**e) Center**

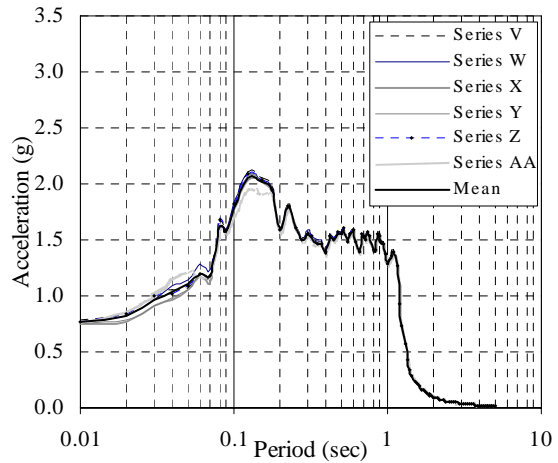


**f) Agrid**

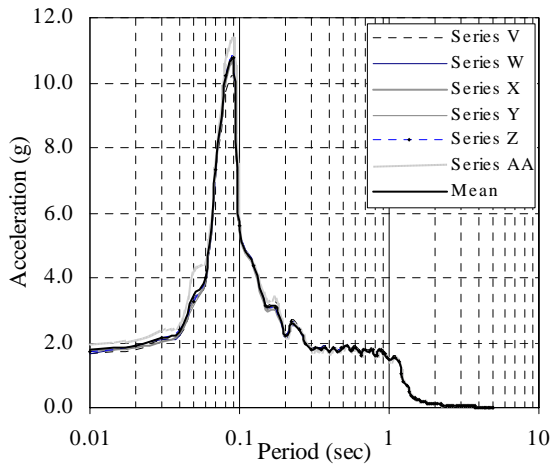
**FIGURE 6-45** Response spectra corresponding to  $S_S = 2.5g$ , normal sized tiles with clips



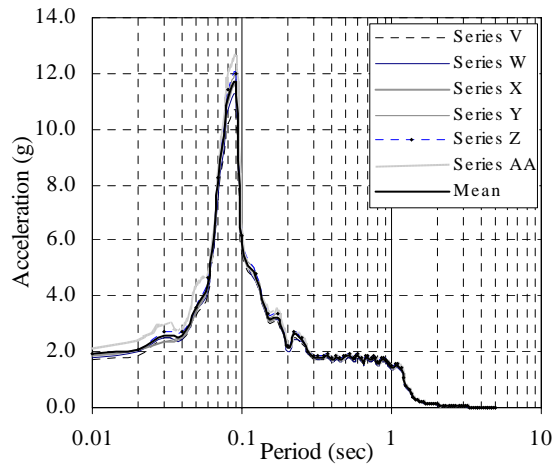
**a) Table**



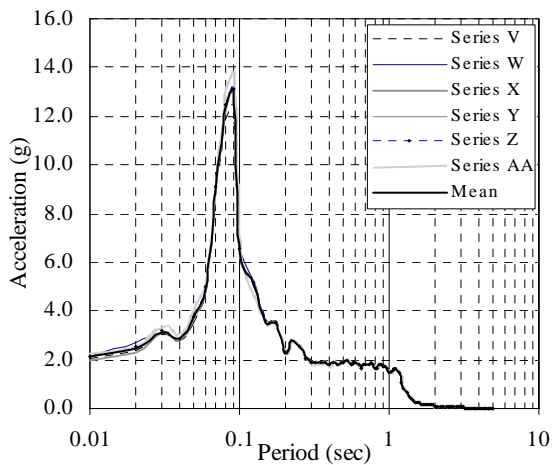
**b) Abase**



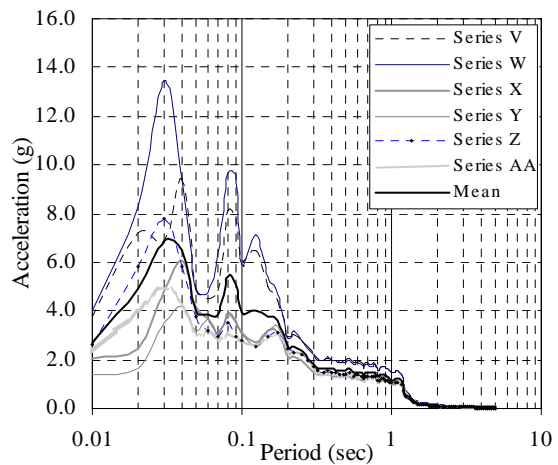
**c) Corner\_w**



**d) Qtr**

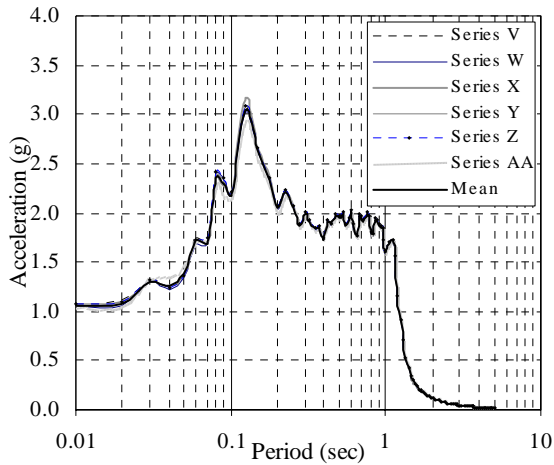


**e) Center**

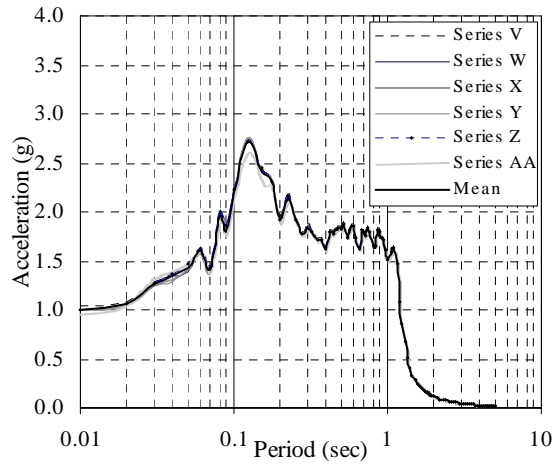


**f) Agrid**

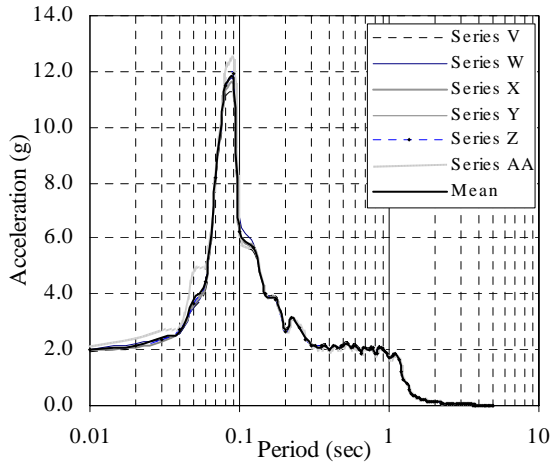
**FIGURE 6-46** Response spectra corresponding to  $S_S = 1.5g$ , normal sized tiles without post



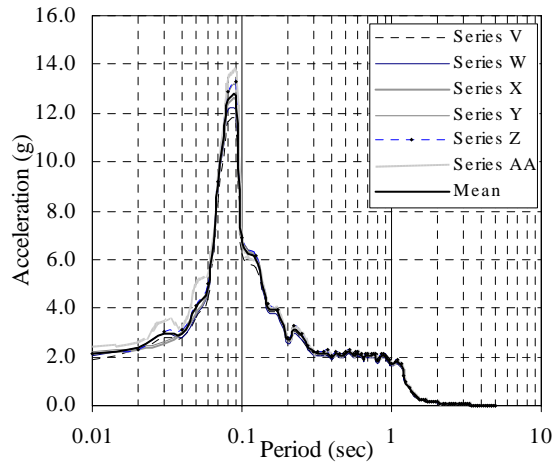
a) Table



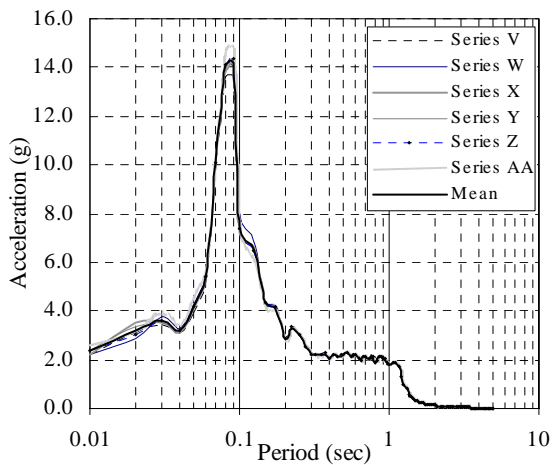
b) Abase



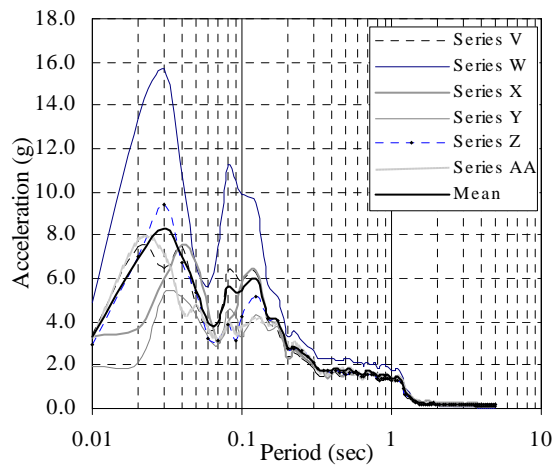
c) Corner\_w



d) Qtr

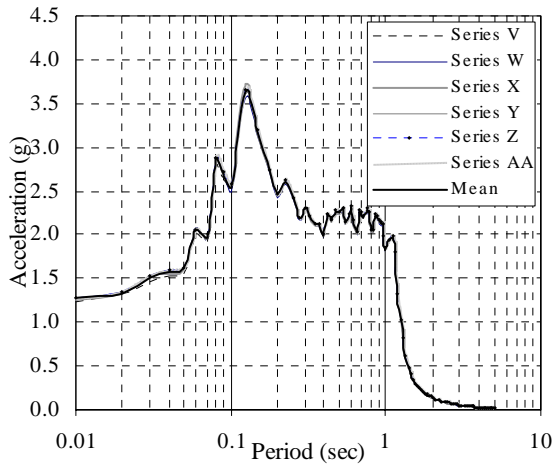


e) Center

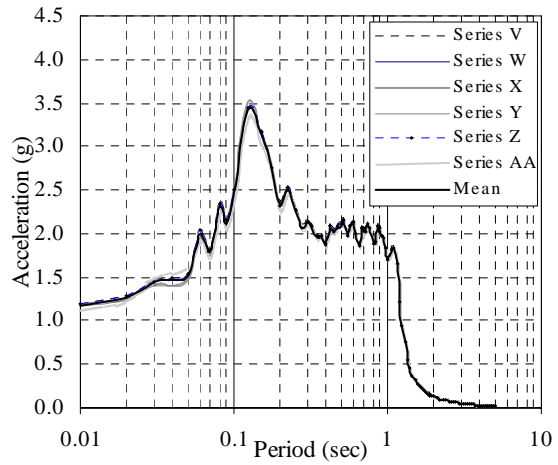


f) Agrid

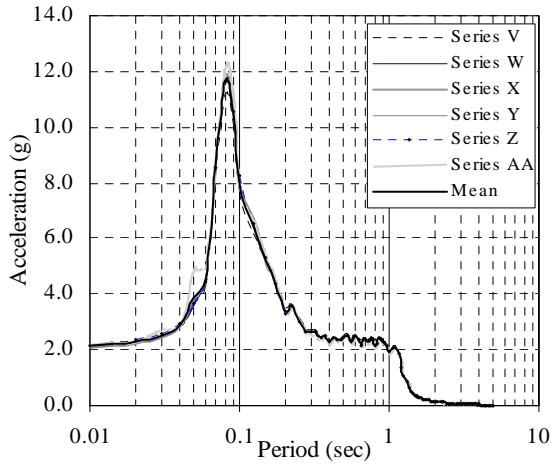
**FIGURE 6-47 Response spectra corresponding to  $S_S = 1.75g$ , normal sized tiles without post**



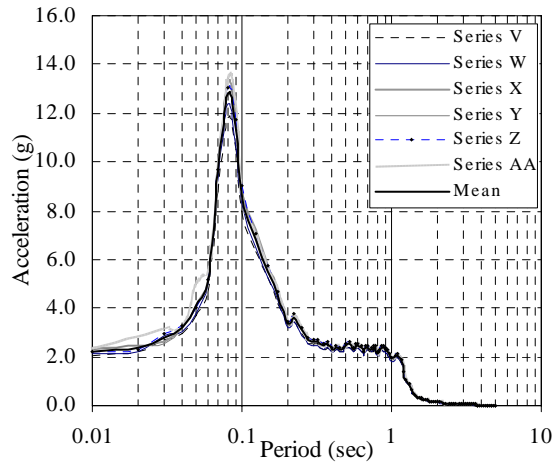
**a) Table**



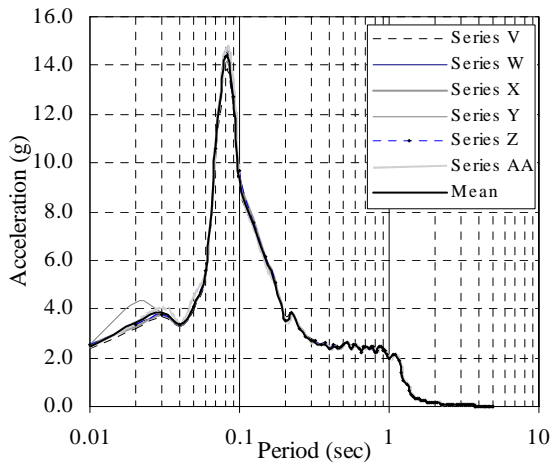
**b) Abase**



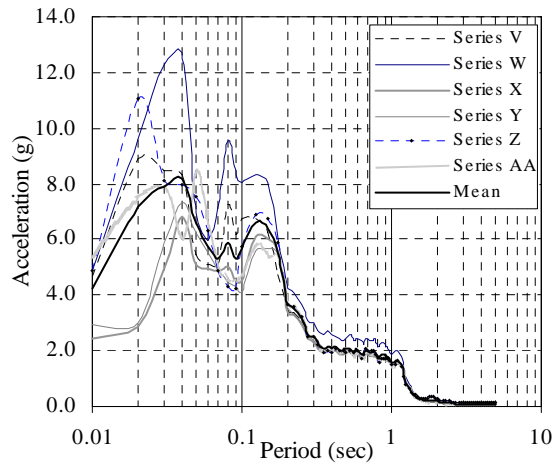
**c) Corner\_w**



**d) Qtr**

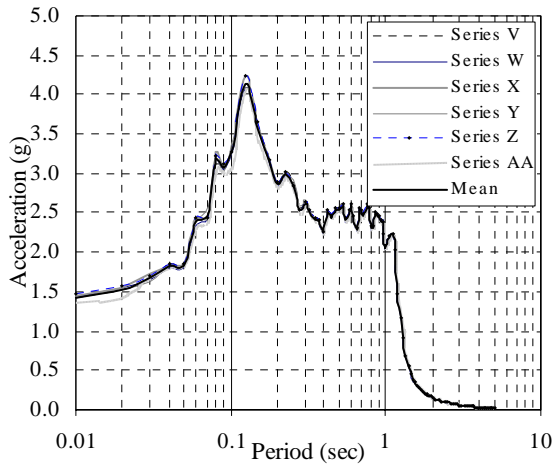


**e) Center**

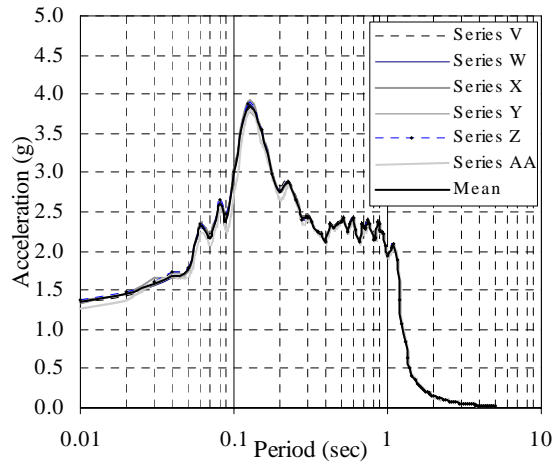


**f) Agrid**

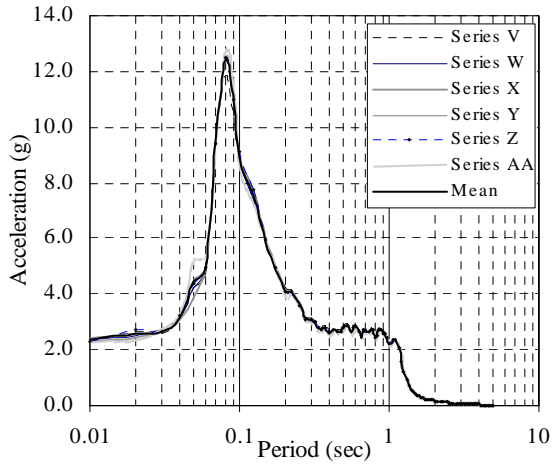
**FIGURE 6-48** Response spectra corresponding to  $S_S = 2.0g$ , normal sized tiles without post



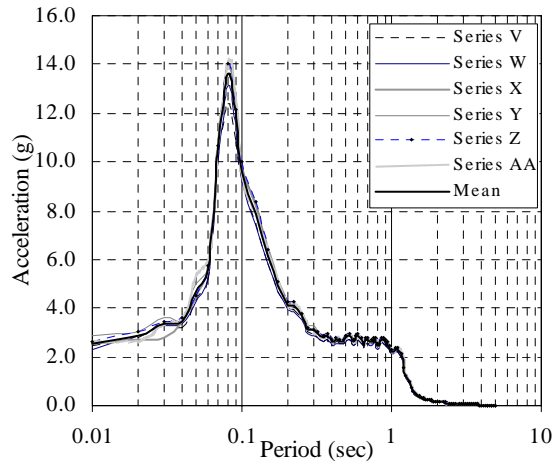
**a) Table**



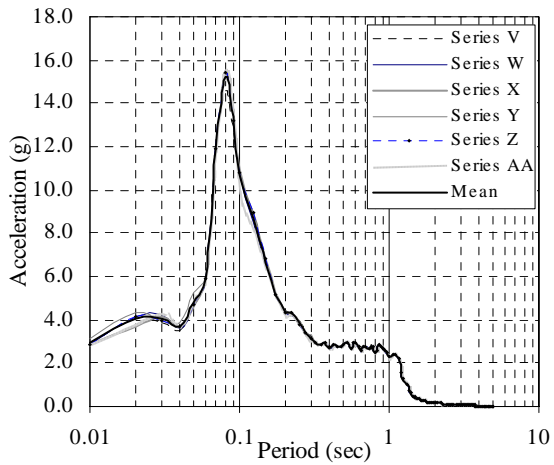
**b) Abase**



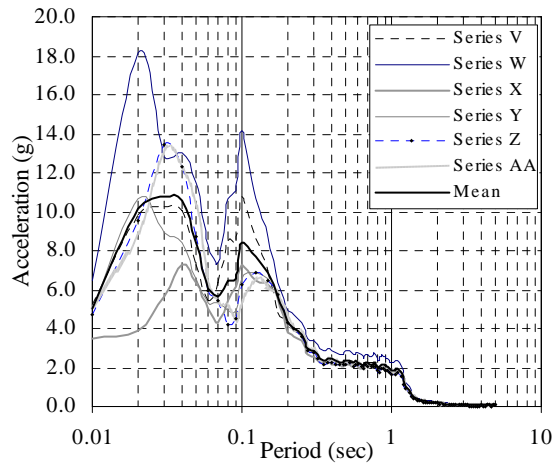
**c) Corner\_w**



**d) Qtr**

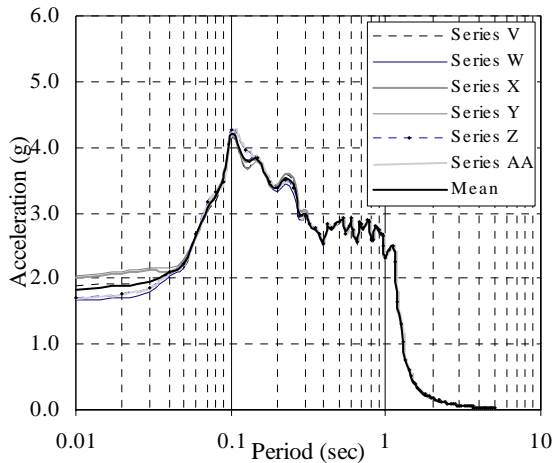


**e) Center**

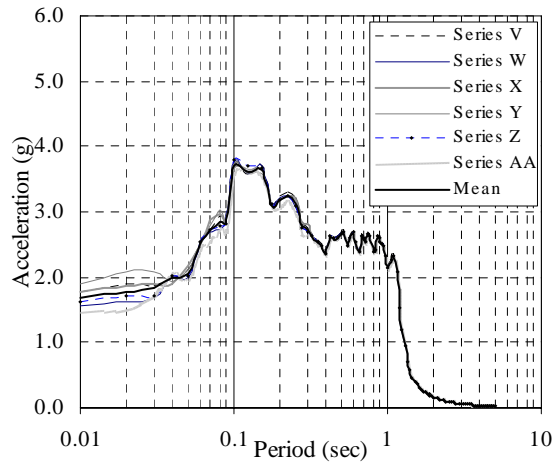


**f) Agrid**

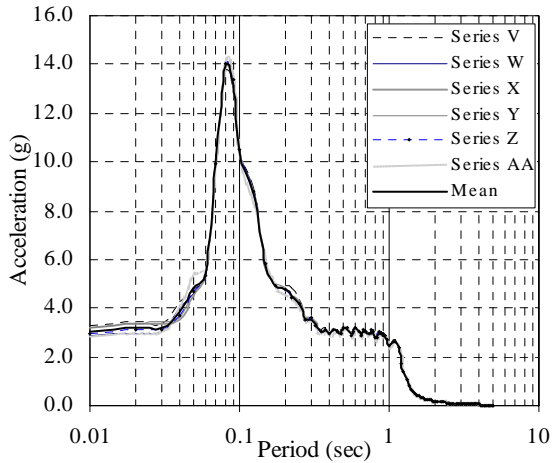
**FIGURE 6-49** Response spectra corresponding to  $S_S = 2.25g$ , normal sized tiles without post



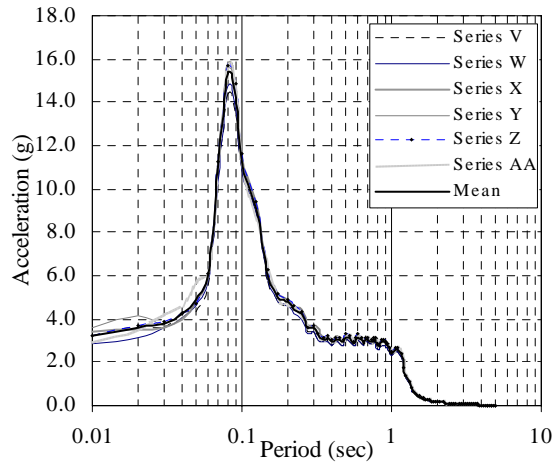
**a) Table**



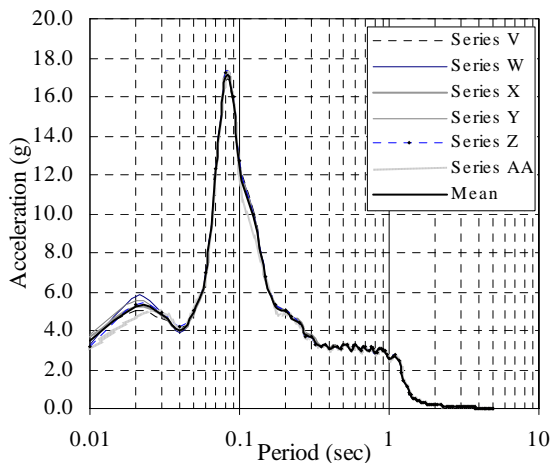
**b) Abase**



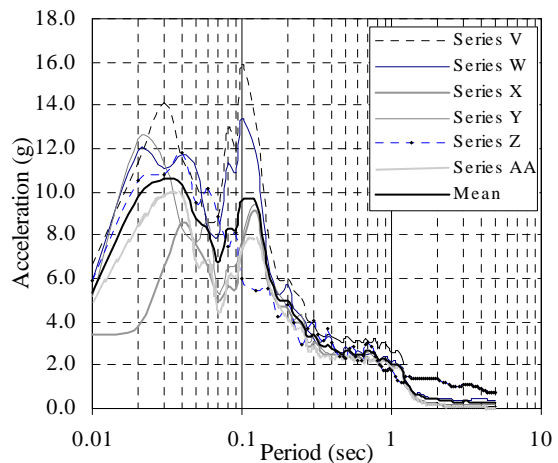
**c) Corner\_w**



**d) Qtr**

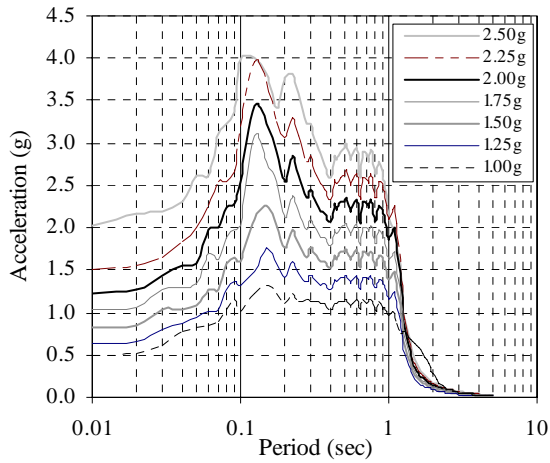


**e) Center**

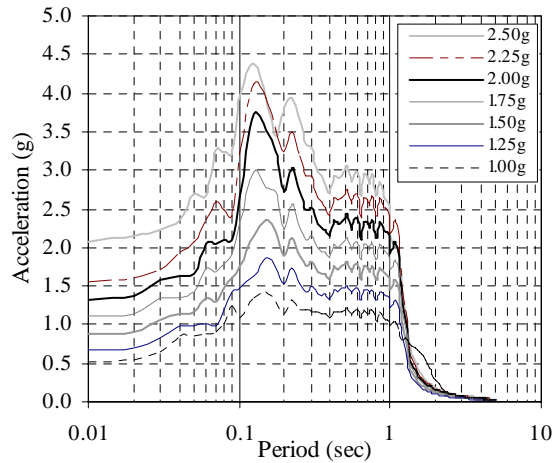


**f) Agrid**

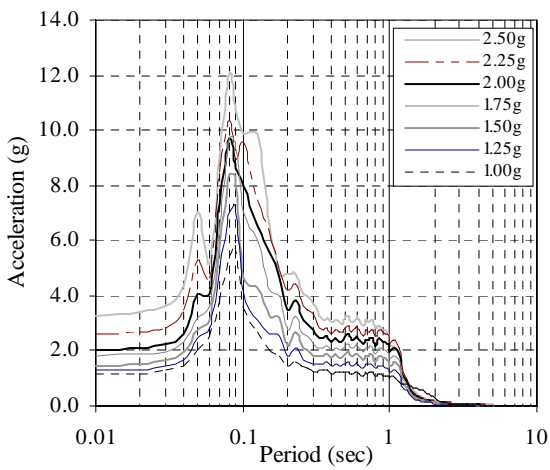
**FIGURE 6-50** Response spectra corresponding to  $S_S = 2.5g$ , normal sized tiles without post



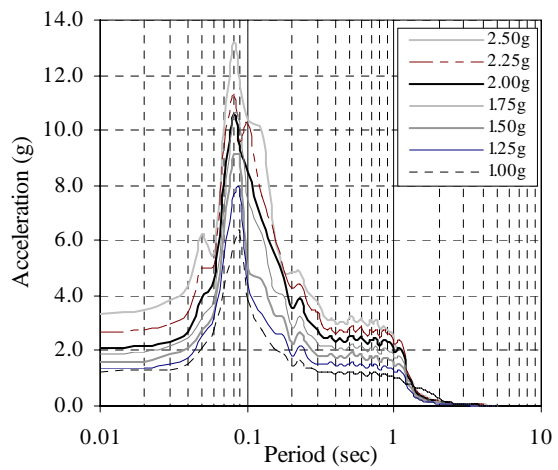
**a) Table**



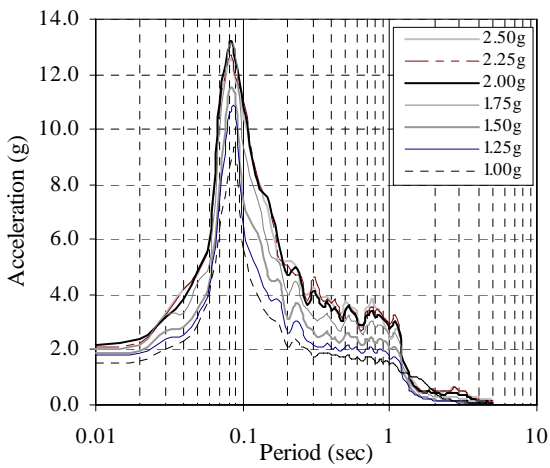
**b) Abase**



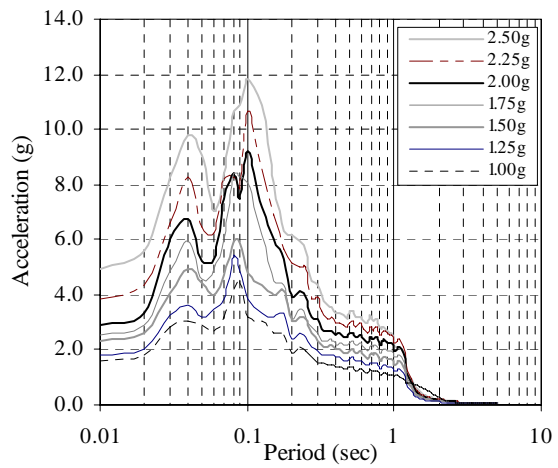
**c) Corner\_w**



**d) Qtr**



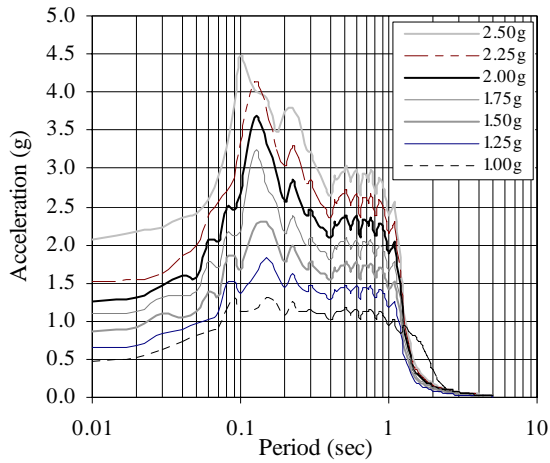
**e) Center**



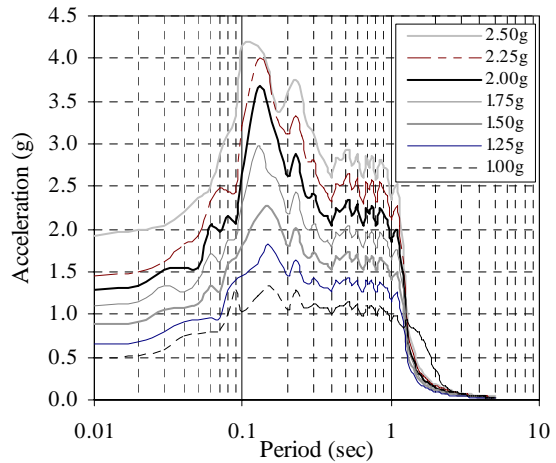
**f) Agrid**

**FIGURE 6-51 Mean response spectra at selected locations, undersized tiles**

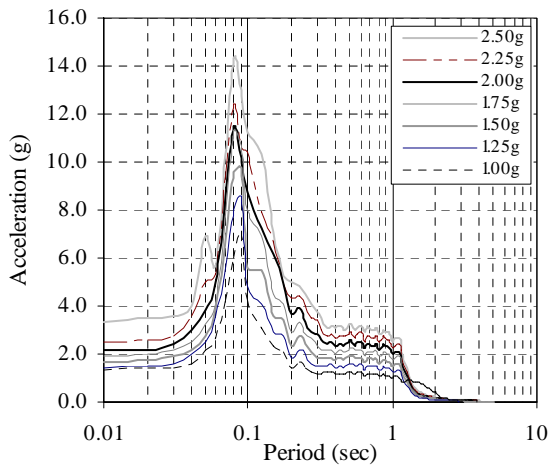




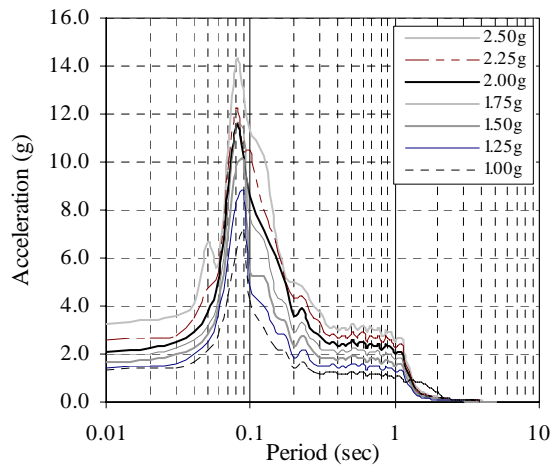
**a) Table**



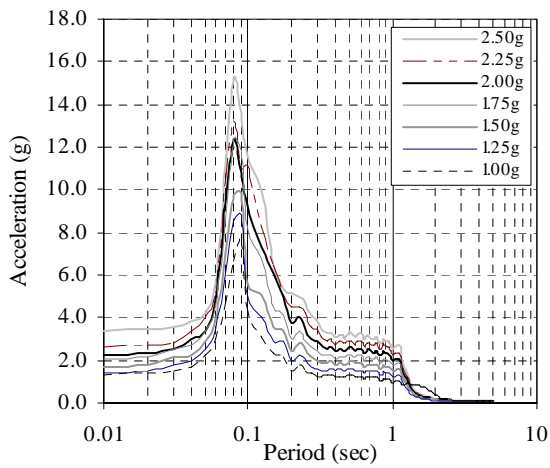
**b) Abase**



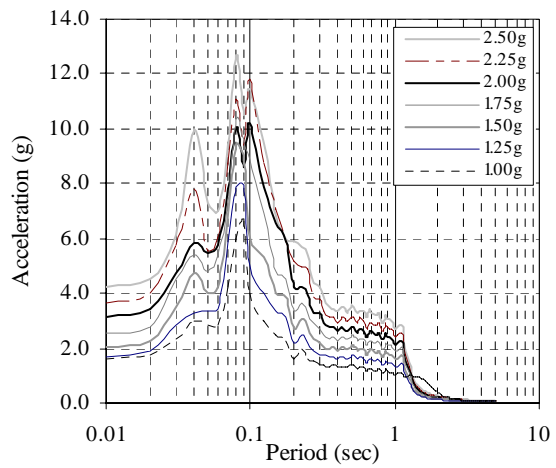
**c) Corner\_w**



**d) Qtr**

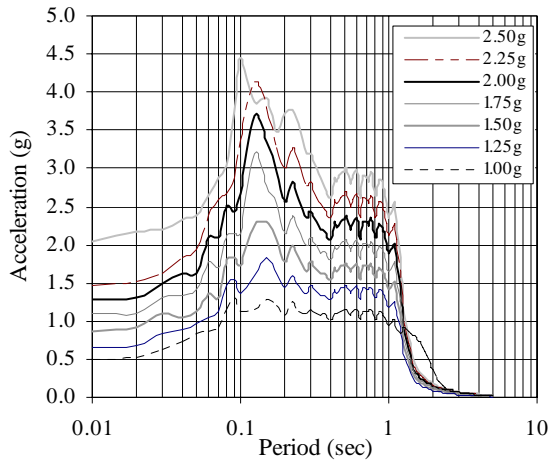


**e) Center**

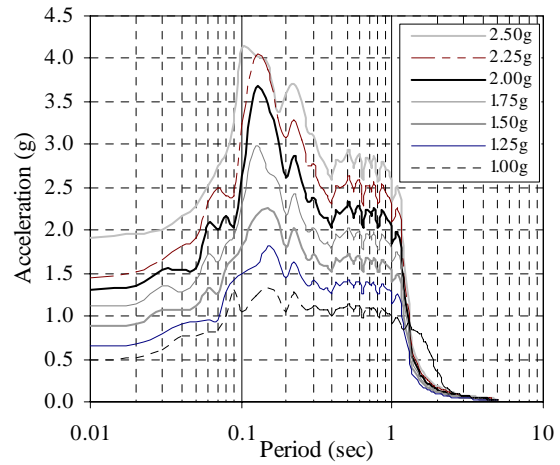


**f) Agrid**

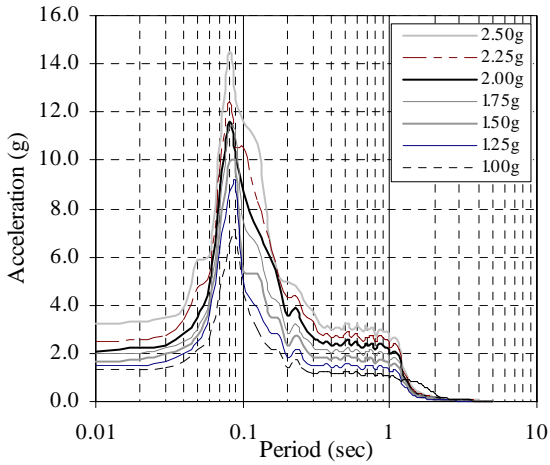
**FIGURE 6-52 Mean response spectra at selected locations, undersized tiles with clips**



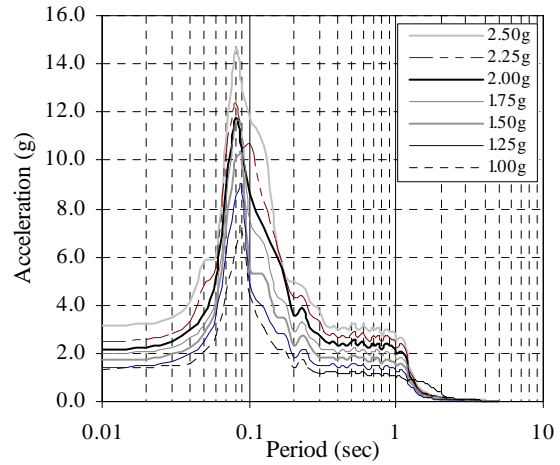
**a) Table**



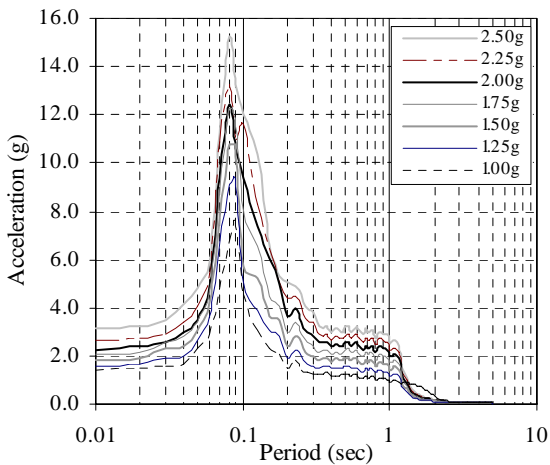
**b) Abase**



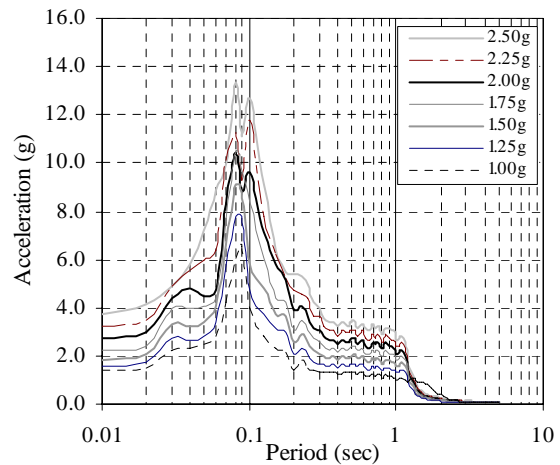
**c) Corner\_w**



**d) Qtr**

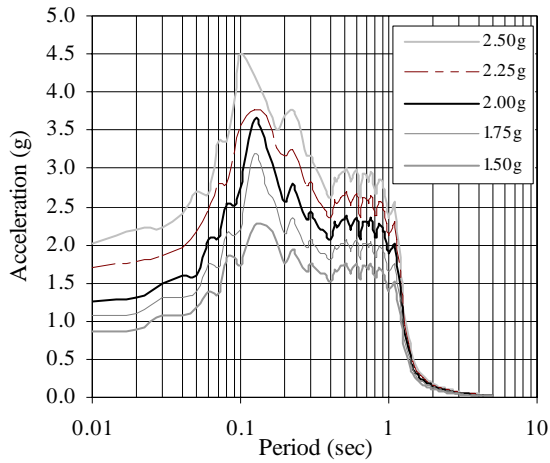


**e) Center**

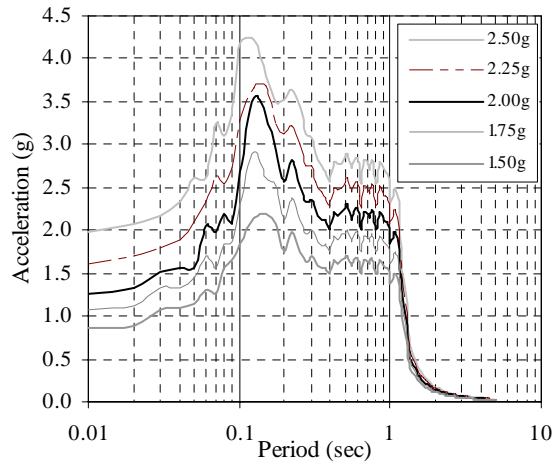


**f) Agrid**

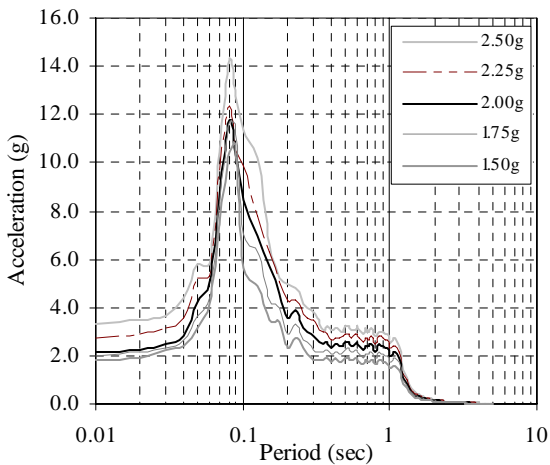
**FIGURE 6-53 Mean response spectra at selected locations, undersized tiles with recycled grid**



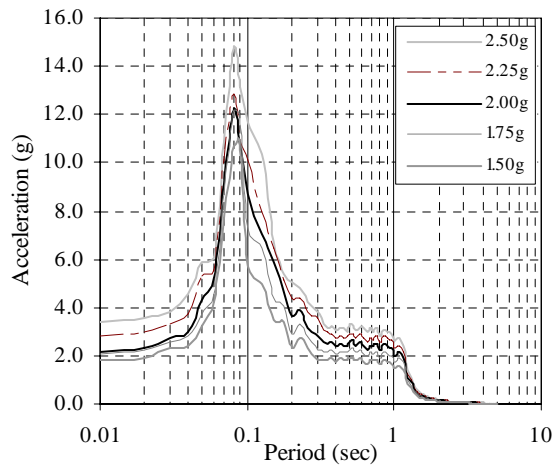
**a) Table**



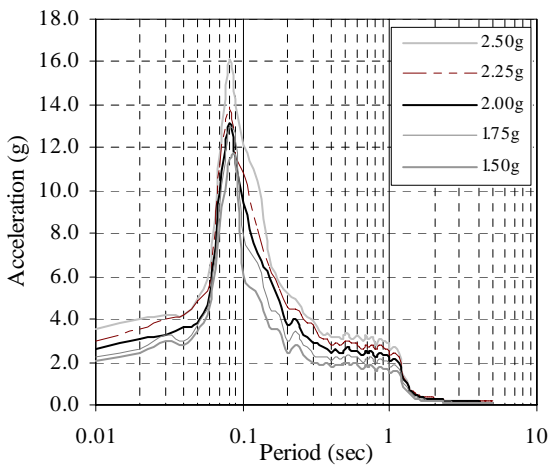
**b) Abase**



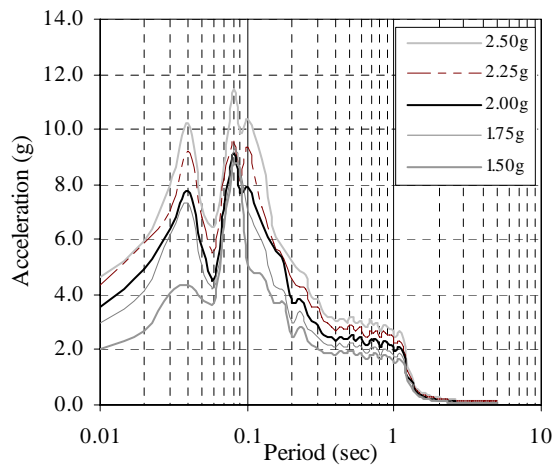
**c) Corner\_w**



**d) Qtr**

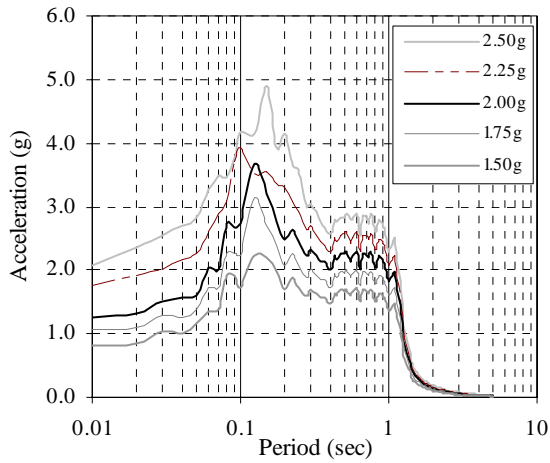


**e) Center**

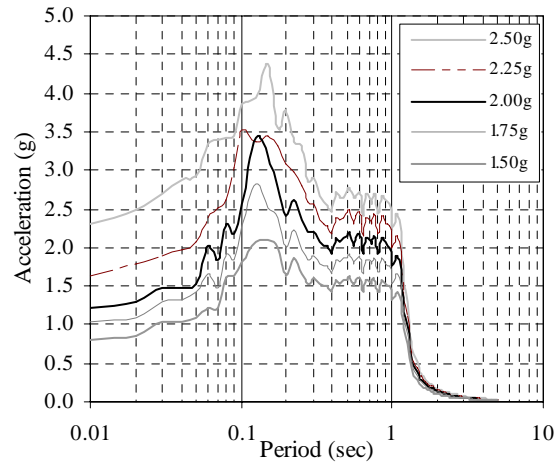


**f) Agrid**

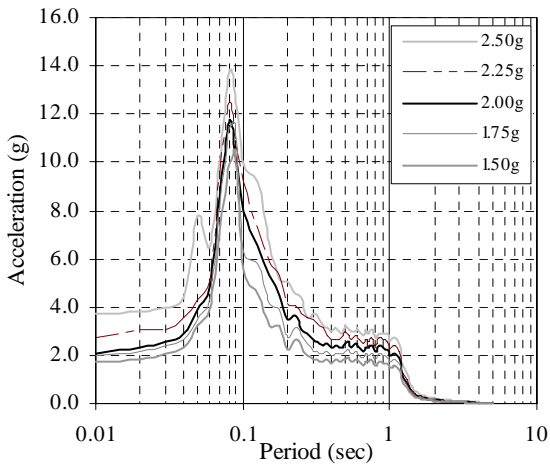
**FIGURE 6-54 Mean response spectra at selected locations, normal sized tiles**



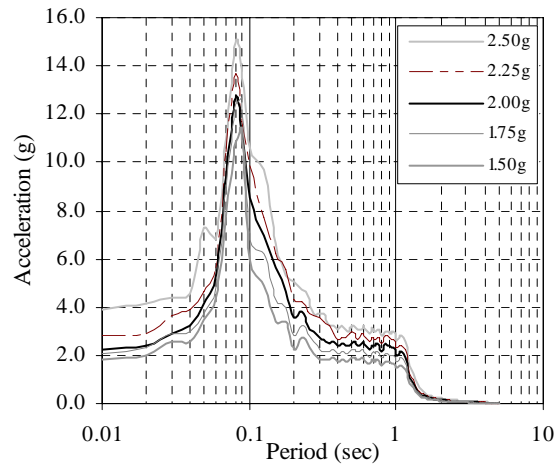
**a) Table**



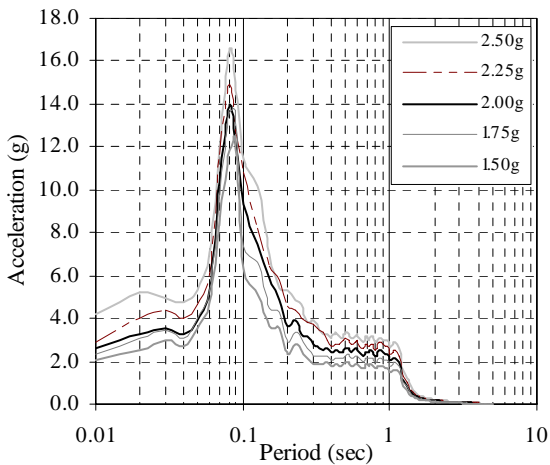
**b) Abase**



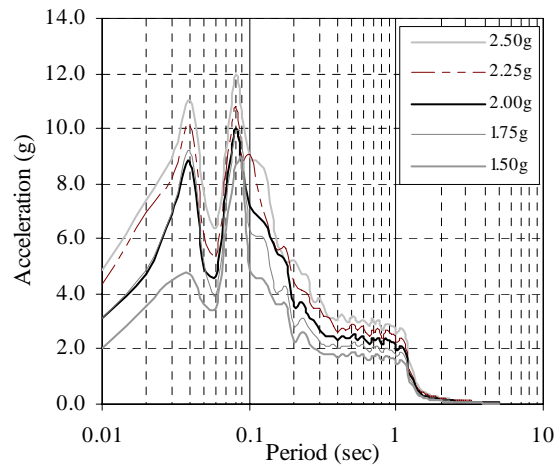
**c) Corner\_w**



**d) Qtr**

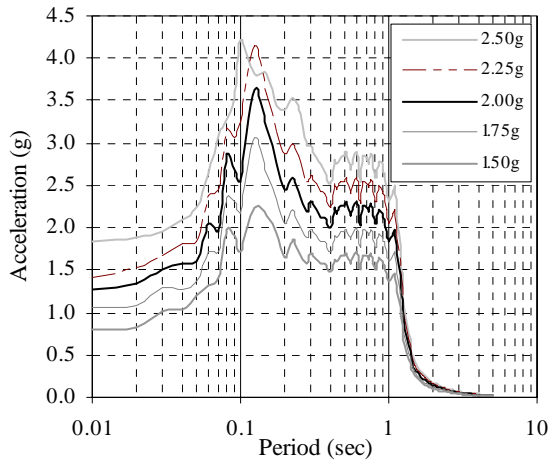


**e) Center**

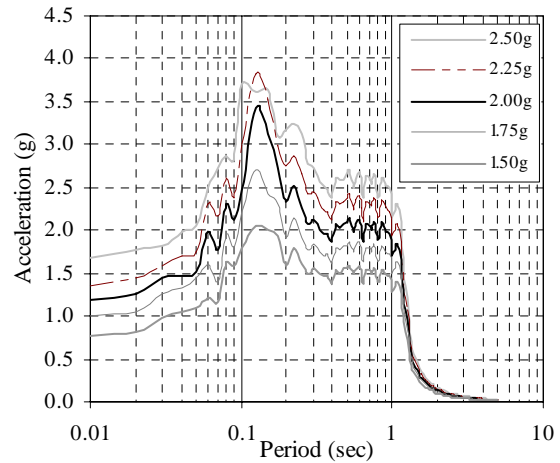


**f) Agrid**

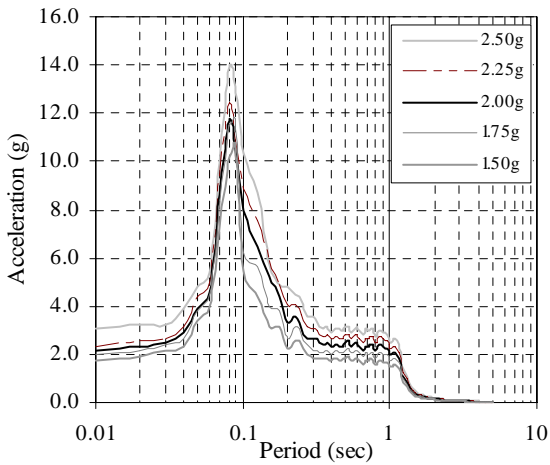
**FIGURE 6-55 Mean response spectra at selected locations, normal sized tiles with clips**



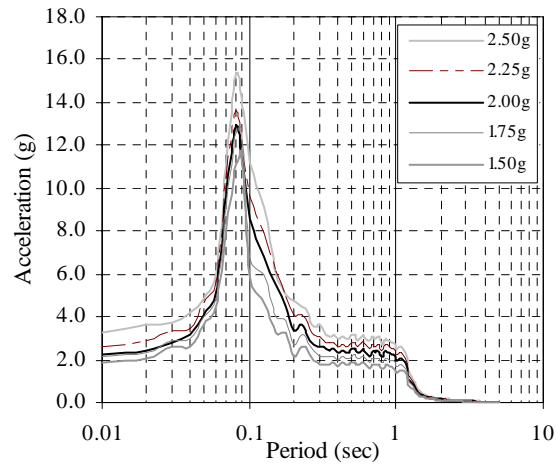
**a) Table**



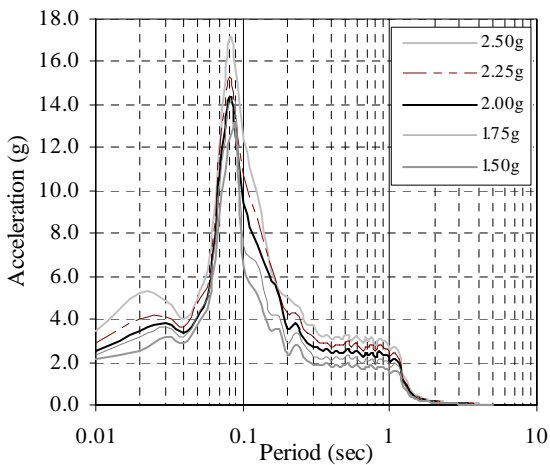
**b) Abase**



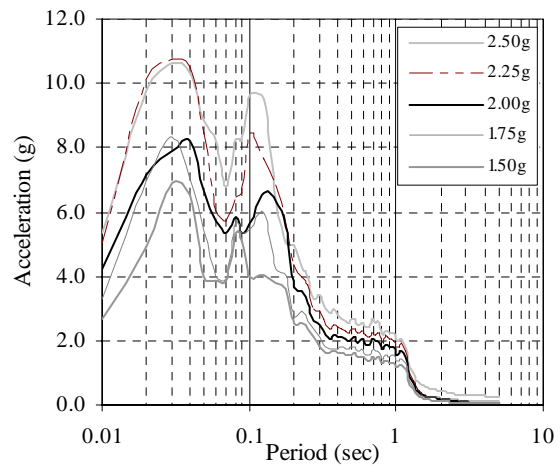
**c) Corner\_w**



**d) Qtr**



**e) Center**



**f) Agrid**

**FIGURE 6-56 Mean response spectra at selected locations, normal sized tiles without post**



## CHAPTER 7

### FRAGILITY ANALYSIS AND DATA EVALUATION

#### 7.1 Introduction

Assessment of the seismic vulnerability of structural and non-structural components is a key step in performance-based design and loss assessment. Fragility-based techniques can be used to identify such components and several methodologies have been proposed (e.g., Reed and Kennedy, 1994; Singhal and Kiremidjian, 1996; Reinhorn et al., 2002; Moehle, 2003; Hamburger et al., 2004). Implementation of these methodologies is contingent on the development of a family of fragility curves for structural and nonstructural components.

A fragility curve describes the probability of reaching or exceeding a damage (or limit) state as a function of the level of excitation or demand. The conditional probability of damage  $D$  reaching or exceeding a damage state  $ds_i$  is given by (7-1):

$$P_{ik} = P[D \geq ds_i | Y = y_k] \quad (7-1)$$

where  $P_{ik}$  is the probability of reaching or exceeding a damage state  $ds_i$  given that the demand is  $y_k$ ,  $D$  is a damage random variable, and  $Y$  is a demand random variable (e.g., peak floor acceleration, story drift). Numerous references provide information on fragility curves including Reed and Kennedy (1994), Sasani and Der Kiureghian (2001), Shinozuka et al. (2002a, 2002b), and Cimellaro et al. (2006).

Fragility curves for suspended ceiling systems are developed and presented in the following sections of this chapter. Four damage (limit) states are defined in Section 7.2. The fragility curves of Section 7.5 were derived using these limit states, the experimental data of Chapter 6, the demand parameters of Section 7.3, and the curve-fitting technique described in Section 7.4.

## **7.2 Limit States**

A limit (damage) state describes the seismic performance of a component or system by characterizing its post-earthquake condition. Limit states express levels of damage using either qualitative (e.g., physical condition of components, failure in specific areas of the structure) or quantitative (e.g., internal forces, number of elements that fail in a system, damage indices of the overall structure) measures. Four limit states were used in this study to characterize the seismic response of suspended ceiling systems. Limit states 1 through 3 account for the number (or percentage) of tiles that fall from the suspension grid. The fourth limit state is associated with structural damage to the suspension grid. The qualitative descriptions of the four limit states are (1) minor damage, (2) moderate damage, (3) major damage, and (4) grid failure. Specific definitions of damage, in terms of percentages of falling tiles and damage to grid components are given in the following subsections.

### **7.2.1 Limit State 1: Minor Damage**

Limit state 1 is the loss of 1% of tiles from the suspension grid. The intent of state 1 is to define minor damage that should not impact the post-earthquake function of a building. Limit state 1 might represent acceptable damage in a ceiling system installed in an essential or special facility (e.g., hospitals, computer and communication centers with fragile equipment, facilities with hazardous materials), where modest levels of tile failure could lead to evacuation or closure of the building.

### **7.2.2 Limit State 2: Moderate Damage**

Limit state 2 is the loss of 10% of tiles from the suspension grid. The intent of state 2 is to limit the expected damage so that the facility is somewhat functional after the earthquake, that is, basic ingress/egress and life safety systems remain operational. Damage in terms of percent loss of tiles is moderate and some repair/replacement of dislodged and fallen tiles might be required. Limit state 2 could represent the permissible level of damage in ceiling systems installed in high occupancy, non-essential facilities.



### **7.2.3 Limit State 3: Major Damage**

Limit state 3 is the loss of 33% of tiles from the suspension grid. State 3 could be associated with the traditional building performance level of life safety. Damage in terms of percent loss of tiles is large and extensive repair/replacement might be required in the tiles and grid components. Limit state 3 could define permissible damage to a ceiling system installed in a low occupancy, non-essential facility.

### **7.2.4 Limit State 4: Grid Failure**

Limit state 4 is a damage state associated with failure of part or the entire suspension grid. The definition of grid failure includes cross tees that fall, cross tees that are bent, and cross tees that have to be replaced after testing. Two types of grid failures have been observed in past testing, namely, isolated component failures and assembly failures involving multiple cross tees. In the case of isolated component failures, minor or moderate damage in terms of percent loss of tiles can occur because of localized grid failure. The repair effort can be significant when several isolated grid components are damaged since disassembly of the ceiling system is generally required. However, the likelihood of life-threatening damage is low. For grid-assembly failures, the damage can be extensive and the falling debris might pose a life-safety hazard.

## **7.3 Demand Parameters**

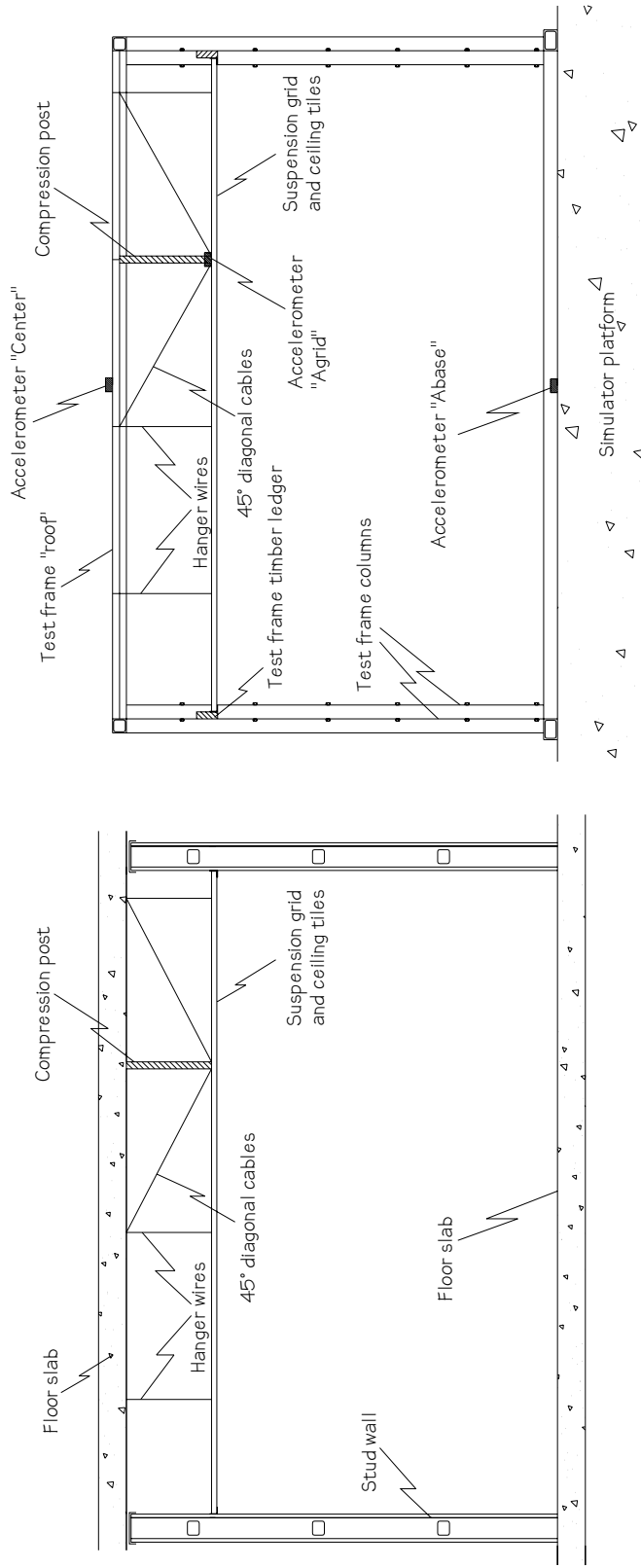
Several demand (intensity) parameters have been used in previous studies to create fragility curves, including peak ground acceleration, peak ground velocity, story drift, spectral acceleration at specific periods, and spectral acceleration over a frequency range (e.g., Reed and Kennedy, 1994; Cornell et al., 2002; Whittaker et al., 2003). In this study, two demand parameters were used to construct fragility curves, namely, peak ground acceleration (0-second period) and average horizontal spectral accelerations at periods of 0.2, 0.5, 1.0, 1.5 and 2.0 seconds. The period range of 0.0 to 2.0 seconds brackets the first and second mode periods of most buildings.

## 7.4 Generation of Fragility Curves

The four limit (damage) states used to characterize the seismic performance of suspended ceiling systems were selected with the intent of covering most of the performance levels described in current seismic codes and guidelines for the performance of nonstructural components. However, different levels could be specified if desired by individual owners, constructors, and manufacturers. Sufficient information is provided in the figures and in Chapter 6 to enable the construction of fragility curves for alternate damage states.

Figure 7-1a is a schematic part section through a typical building, which shows two adjacent floor slabs, a suspended ceiling system, and two stud partition walls. The ceiling system is supported by the stud wall via a molding attached to the wall and by wires attached to the roof slab. Figure 7-1b is a schematic cross-section through the test fixture, and shows the simulator platform, two of the four corner test frame columns, the braced roof of the test frame (see figure 3-2), two of the test frame timber ledgers (see figure 3-3), and a suspended ceiling system. The location of the accelerometers, *Abase*, *Agrid*, and *Center*, are indicated in the figure.

In the part section of figure 7-1a, the ceiling system is excited primarily in the vertical direction by motion of upper floor and secondarily by vertical motion of the stud walls, and excited primarily in the horizontal direction by motion of the stud walls and secondarily by the motion of the upper floor. In the multi-story building frame depicted in part in figure 7-1a, the motions of the lower and upper floor slabs are a function of the base excitation and the dynamic properties of the building frame. In the test fixture of figure 7-1b, the motion of the test frame roof is dependent on the simulator-platform excitation and the dynamic properties of the test frame. Although the ceiling system of figure 7-1b is loaded in a similar manner (ledgers/stud wall and test-frame roof/upper floor) to that of figure 7-1a, differences in the *loading* system and the dynamic properties of the test frame/building frame, will ensure that the excitation experienced by the test ceiling system differs from that in a building. Accordingly, response data collected from a testing program similar to that described in the previous chapters of this report must be interpreted with care.



**a) building frame**

**b) test fixture**

**FIGURE 7-1 Schematic representation of a story of typical building and the test fixture**

Figure 7-2 illustrates steps in the development of the fragility curves. The experimental data points were established using results from tests involving simultaneous horizontal and vertical shaking as follows: (1) compute the mean horizontal acceleration response spectrum for each shaking level with the accelerometer  $A_{base}$  (e.g., see the heavy solid line in figure 7-2a), (2) compute the spectral acceleration at selected periods (0.0, 0.2, 0.5, 1.0, 1.5 and 2.0 seconds) from the mean horizontal acceleration response spectrum (see the arrows in figure 7-2a for the 1-second calculation,  $S_{1.0} = 2.36g$ ), (3) count the number of tiles that fell from the grid for each system (6 systems in this example) at each shaking level as a percentage of the total number of tiles in the ceiling system, (4) compare the percent tile failure with each limit state for each system, and (5) calculate the probability  $P_f$  of reaching or exceeding the limit state as:

$$P_f = \frac{N_f}{N} \quad (7-2)$$

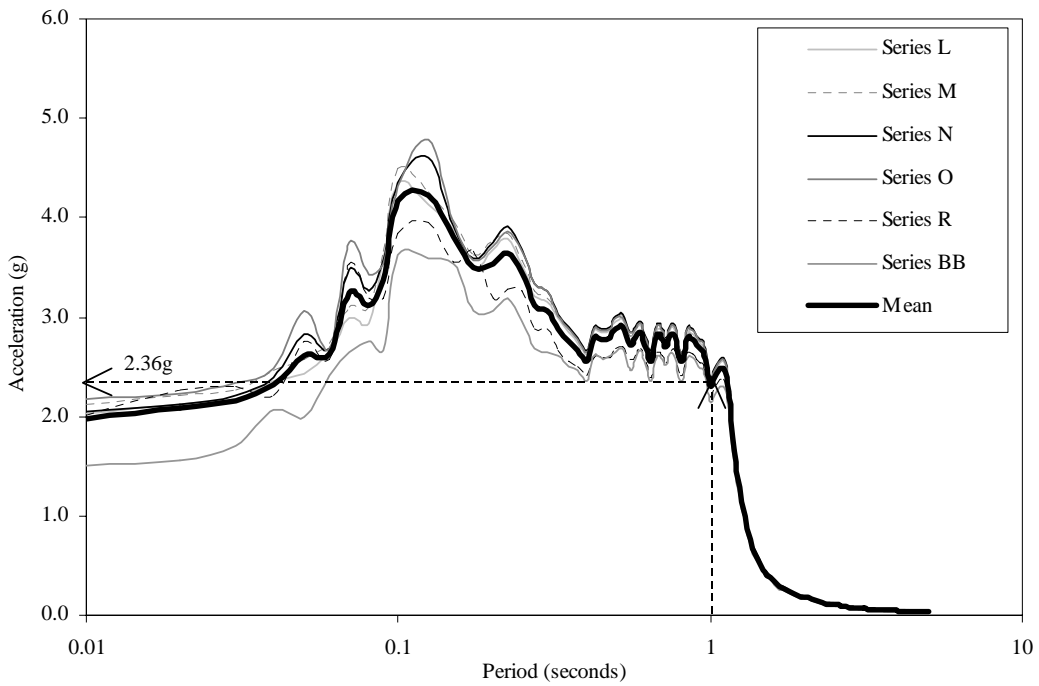
where  $N_f$  is the number of systems (trials) where the limit state was reached or exceeded, and  $N$  is the total number of systems (trials) in the ceiling system configuration (= 4, 3, 3, 6, 4, 6 for configurations 1 through 6, respectively)<sup>1</sup>. As  $N$  approaches infinity,  $P_f$  approaches the true probability of reaching or exceeding a limit state.

The fragility curves were prepared for each ceiling-system configuration by plotting the probability of reaching or exceeding a limit state versus the corresponding mean horizontal spectral acceleration<sup>2</sup>. Figure 7-2b presents a sample fragility curve and the experimental data used to derive the curve; the demand parameter is peak floor acceleration. Experimental data points are shown with solid triangles. The experimental data points were transformed into a fragility curve assuming that the response of the ceiling system was lognormally distributed with the cumulative lognormal distribution function of (7-3):

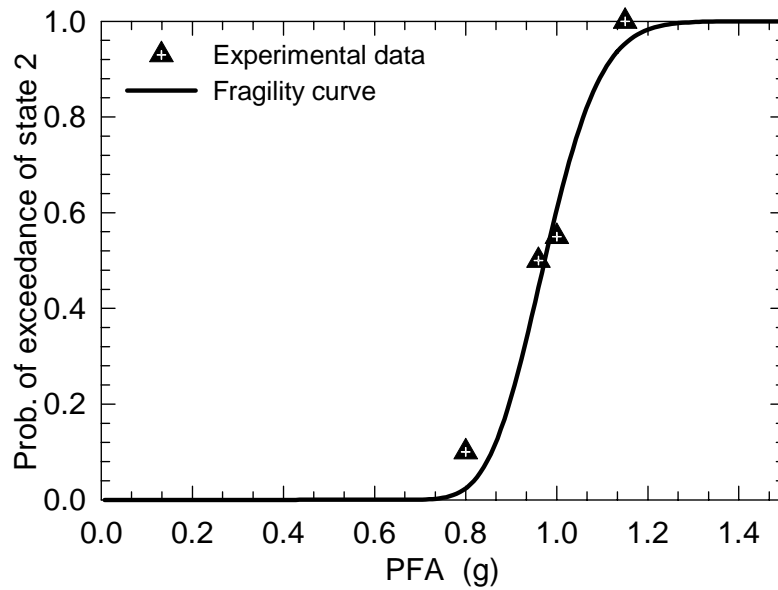
---

<sup>1</sup> Seven systems (L, M, N, O, P, Q, R and BB) of configuration 4 were tested but the data from tests of system Q were set aside for the reasons given in Section 6.3.5.

<sup>2</sup> The ceiling systems were subjected to simultaneous horizontal and vertical shaking but herein, demand is characterized using the effects of horizontal shaking only.



a) mean spectral acceleration at 1.0 second for shaking level corresponding to  $S_S = 2.5g$



b) fragility curve for limit state 2

FIGURE 7-2 Illustration of part of the procedure to develop fragility curves

$$F_Y(y) = P(Y \leq y) = \int_{-\infty}^y f_Y(y) dy = \int_{-\infty}^y \frac{1}{y \cdot \beta \cdot \sqrt{2\pi}} \cdot e^{\left[ -\frac{1}{2\beta^2} \cdot \ln^2\left(\frac{y}{\theta_y}\right) \right]} dy \quad y \geq 0 \quad (7-3)$$

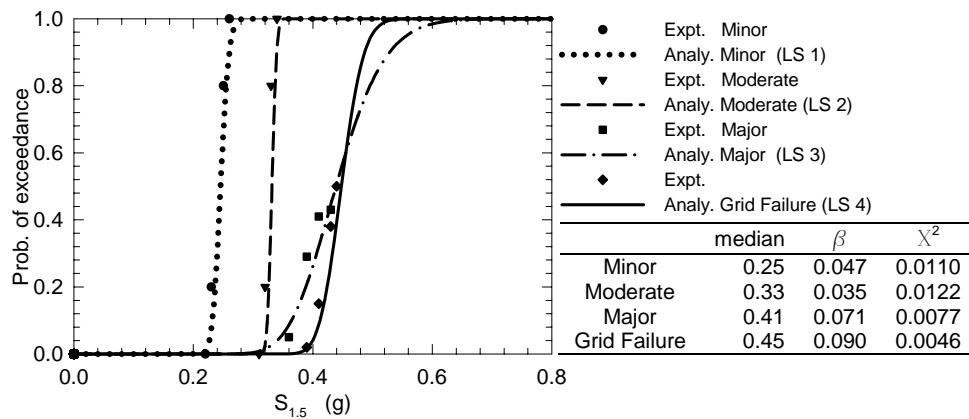
or in its more compact form

$$F_Y(y) = \Phi \left[ \frac{1}{\beta} \ln(y/\theta_y) \right] \quad y \geq 0 \quad (7-4)$$

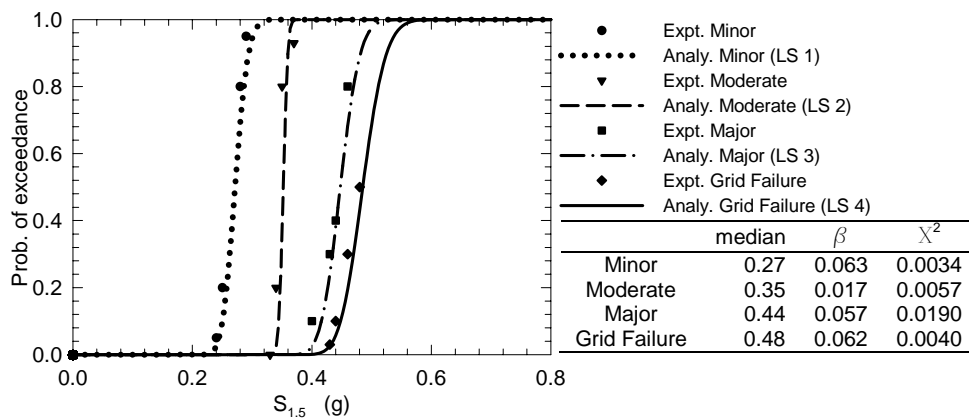
where  $\Phi$  is the standardized cumulative normal distribution function,  $\theta_y$  is the median of  $y$ , and  $\beta$  is the standard deviation of the natural logarithm of  $y$  (Soong, 2004). A chi-squared ( $\chi^2$ ) goodness-of-fit test was used to select the optimal values of the parameters of the lognormal distribution ( $\theta_y$  and  $\beta$ ). If fewer than 4 experimental data points were available for curve fitting, additional *data* points were generated by linear interpolation.

Figures 7-3 and 7-4 were prepared for the purpose of illustrating the importance of selecting the acceleration history that best reflects the excitation of the suspended ceiling system. Figure 7-3 presents fragility curves for ceiling system configuration 1: undersized tiles, for spectral accelerations at 1.5 seconds calculated from accelerometer-histories located at three different locations on the test frame: *Abase*, an accelerometer mounted on the simulator platform; *Center*, an accelerometer mounted on the top and at the center of the test frame; and *Agrid*, an accelerometer mounted on the suspension grid. Figure 3-16 shows the location of these accelerometers. Figure 7-4 presents the same information but for the four limit states defined in Section 7.2.

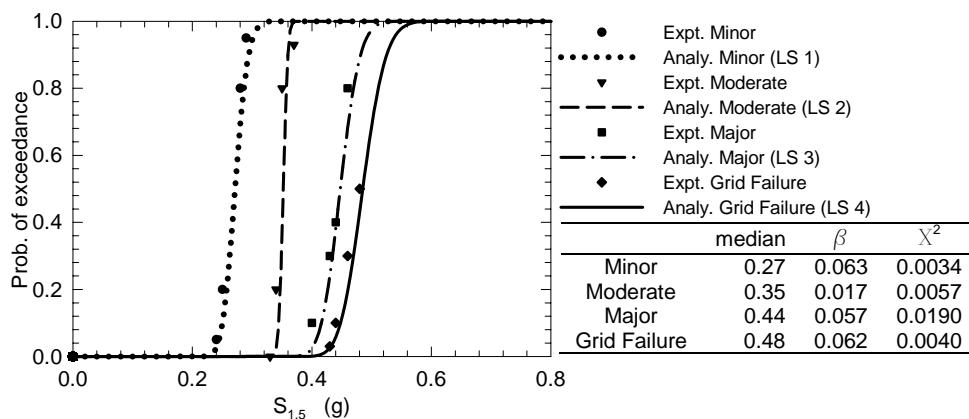
It is not clear from figure 7-1b which accelerometer should be used to characterize the excitation because the ceiling system is excited at both the level of the ceiling system (ledger/stud wall) and the supporting frame (test frame roof/upper floor). The most and least conservative characterizations of ceiling-system vulnerability are given by the *Abase* and *Center* excitations, respectively. The accelerations recorded with the accelerometer denoted as *Center* (figure 7-3b) likely best characterize the horizontal excitation experienced by the suspended ceiling system,



a) *Abase* accelerometer history

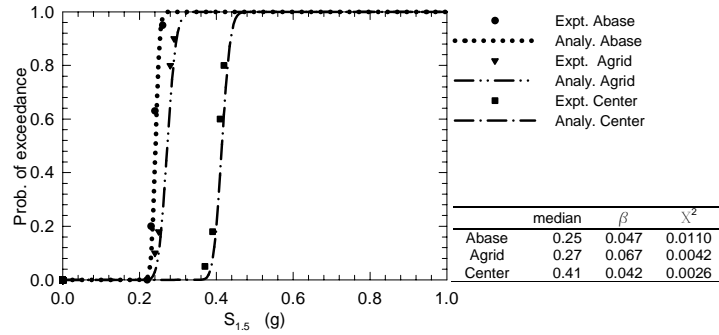


b) *Center* accelerometer history

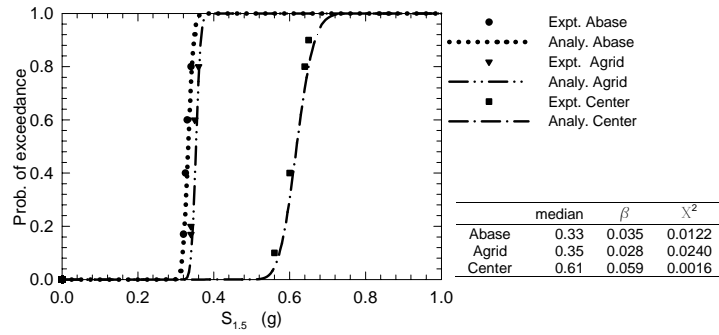


c) *Agrid* accelerometer history

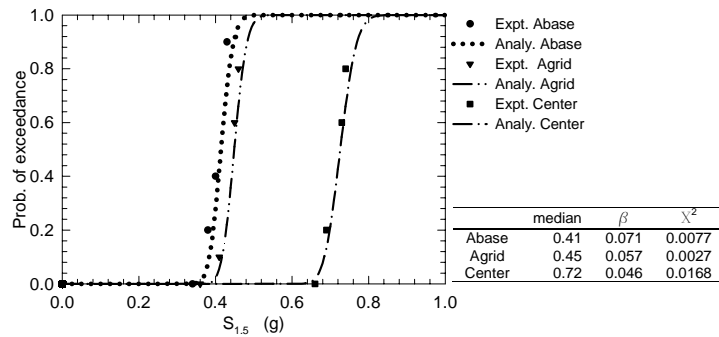
**FIGURE 7-3 Fragility curves for 1.5-second spectral acceleration based on different accelerometer histories, configuration 1: undersized tiles**



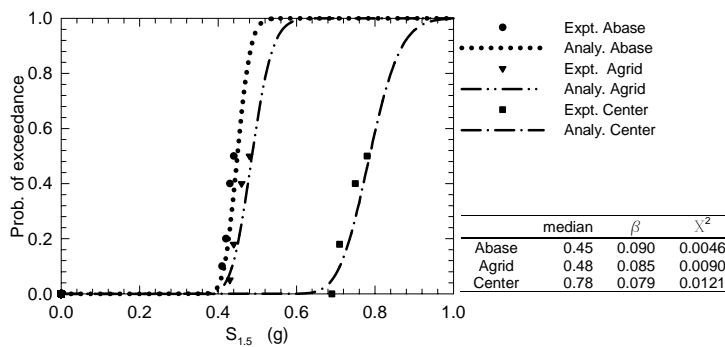
**a) Minor damage: 1% tiles lost**



**b) Moderate damage: 10% tiles lost**



**c) Major damage: 33% tiles lost**



**d) Grid failure**

**FIGURE 7-4 Fragility curves for 1.5-second spectral acceleration for different limit states, configuration 1: undersized tiles**



but not the vertical excitation because the vertical shaking was amplified by the out-of-plane flexibility of the *roof* of the test frame. Despite the fact that the fragility curves derived from the accelerometer denoted *Abase* (figure 7-3a) are likely conservative (i.e., overestimate the vulnerability of the ceiling system), the fragility curves developed in this study were created using excitation histories from *Abase*.

## 7.5 Ceiling System Fragility Data and Interpretation

Fragility curves for the six ceiling-system configurations are presented in Figures 7-5 through 7-40. Curves are presented for the four limit states (denoted LS in the figures) that were defined in Section 7.2 and spectral demands at periods of 0.0, 0.2, 0.5, 1.0, 1.5 and 2.0 seconds; the inset table in each figure presents the values of the median<sup>1</sup>,  $\beta$  and  $\chi^2$  (equal to the sum of the square of the errors in this instance) for each curve. Fragility curves for limit states 2 and 3 are not presented in figures 7-11 through 7-16 because components of the grid failed (limit state 4) in the tests following the minor loss of tiles (limit state 1), that is, limit states 2 and 3 were not observed.

Figures 7-41 through 7-64 present the data of figures 7-5 through 7-40 but in a different format. Different scales were used to plot the fragility curves because the magnitude of the spectral acceleration changed substantially as a function of period. The fragility curves in these figures can be used to assess the vulnerability of ceiling systems as a function of size of tiles, the use of retainer clips, the use of compression posts, and the physical condition of grid components.

As can be seen in figures 7-5 through 7-40, the fragility curves corresponding to limit states 1 through 3 do not intersect. Since these curves were developed for different limits states within a sample, these fragility curves are considered to be as dependent (Shinozuka et al. 2000b). When limit states are dependent, the systems in a more severe state of damage constitute a subset of the

---

<sup>1</sup> Median values are reported to two decimal digits in units of *g*.

systems in a state of lesser damage, and the fragilities for specified excitation intensity are always larger for the lesser state of damage than for the more severe condition.

Some of the limit state 4 (grid failure) fragility curves intersect or precede (in terms of demand) or intersect with the curves of limit states 1, 2 and 3 (e.g., configurations 4 and 6). This observation suggests that grid failure it is not dependant on tile failure. Grid components did fail without loss of tiles. However, tile failure can result from grid failure. Based on the tests described in this report, there are intersections of fragility curves for some limit states that should be avoided, for example, limit states 3 (major tile failure) and 4 (grid failure). The performance space beyond the intersection of these curves should be avoided because the simultaneous loss of many tiles and the collapse of large sections of grid could pose a life safety hazard.

For limit states 1 through 3, the least vulnerable ceiling system was the configuration of normal sized tiles with clips (configuration 5) and the most vulnerable systems were the configurations with undersized tiles (configuration 1) and undersized tiles with recycled grid components (configuration 3). Pressure or retainer clips effectively reduced the probabilities of exceeding limit states 1 through 3 by comparison with those systems where clips not were used. The systems with normal sized tiles performed better than the systems with undersized tiles. In Section 6.3 it was not clear whether including the compression post in a ceiling system improves the seismic performance. Based on the information provided in figures 7-41 through 7-64, the addition of the compression post reduces the seismic vulnerability of a ceiling system but the improvements in response are modest.

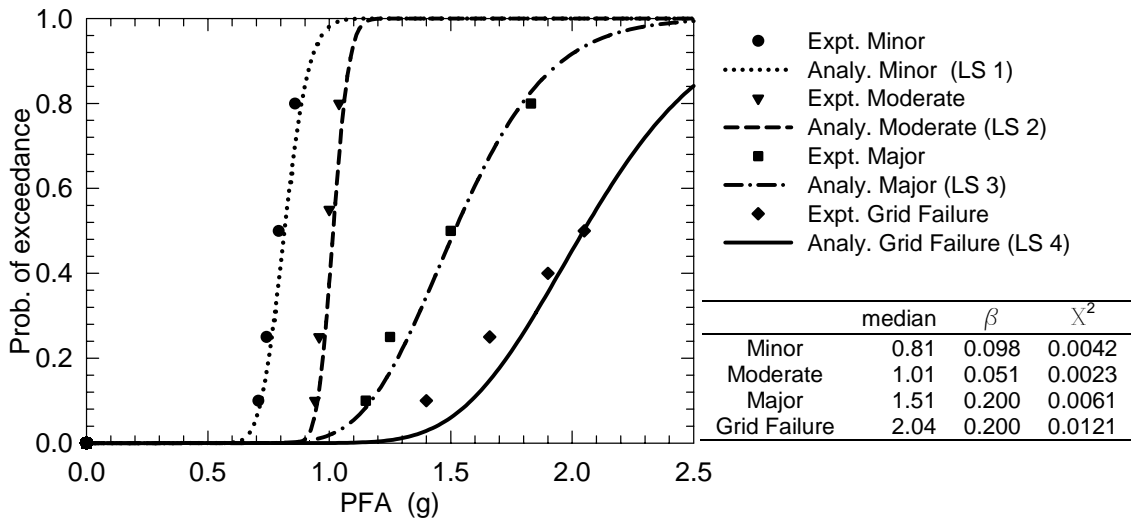


**FIGURE 7-5 Fragility curves for peak floor acceleration, configuration 1: undersized tiles**

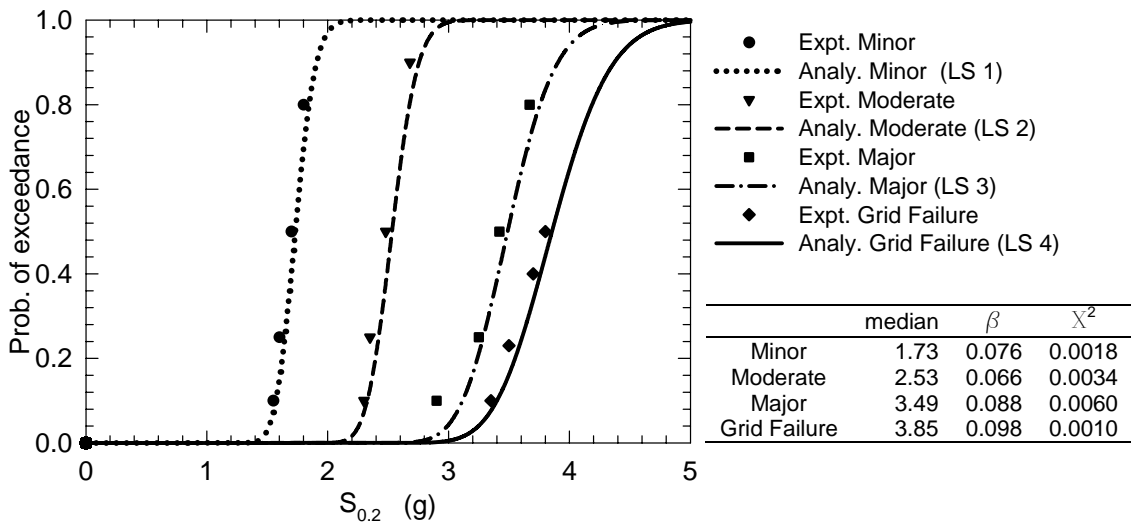


**FIGURE 7-6 Fragility curves for spectral acceleration at 0.2 second, configuration 1: undersized tiles**

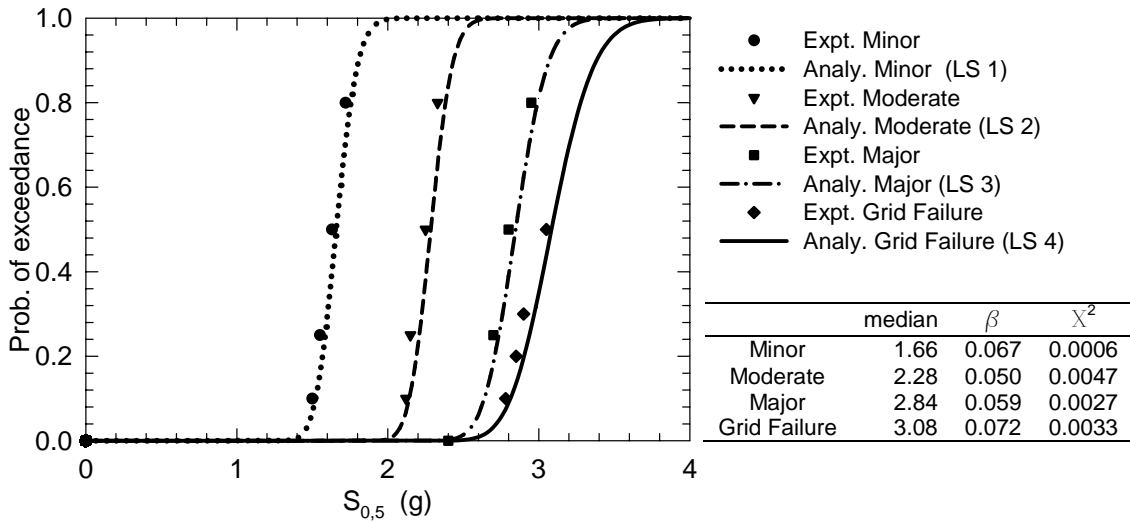


**FIGURE 7-7** Fragility curves for spectral acceleration at 0.5 second, configuration 1: undersized tiles

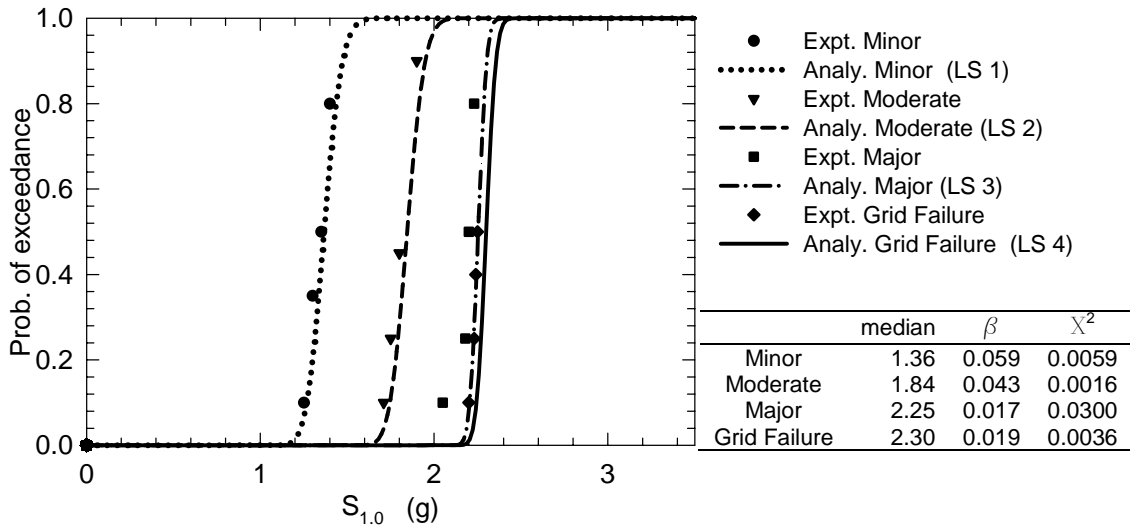


**FIGURE 7-8** Fragility curves for spectral acceleration at 1.0 second, configuration 1: undersized tiles

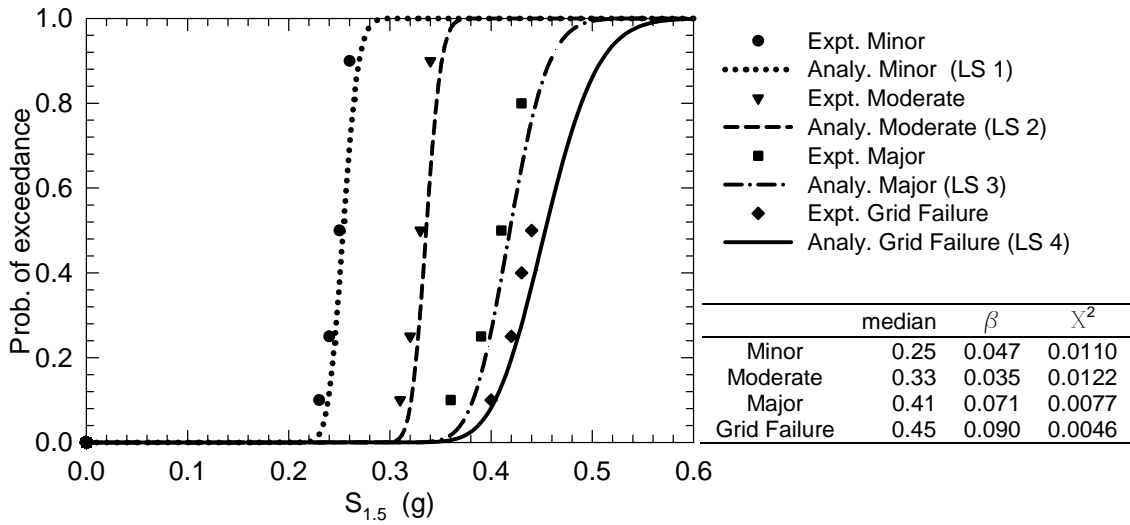


**FIGURE 7-9** Fragility curves for spectral acceleration at 1.5 seconds, configuration 1: undersized tiles

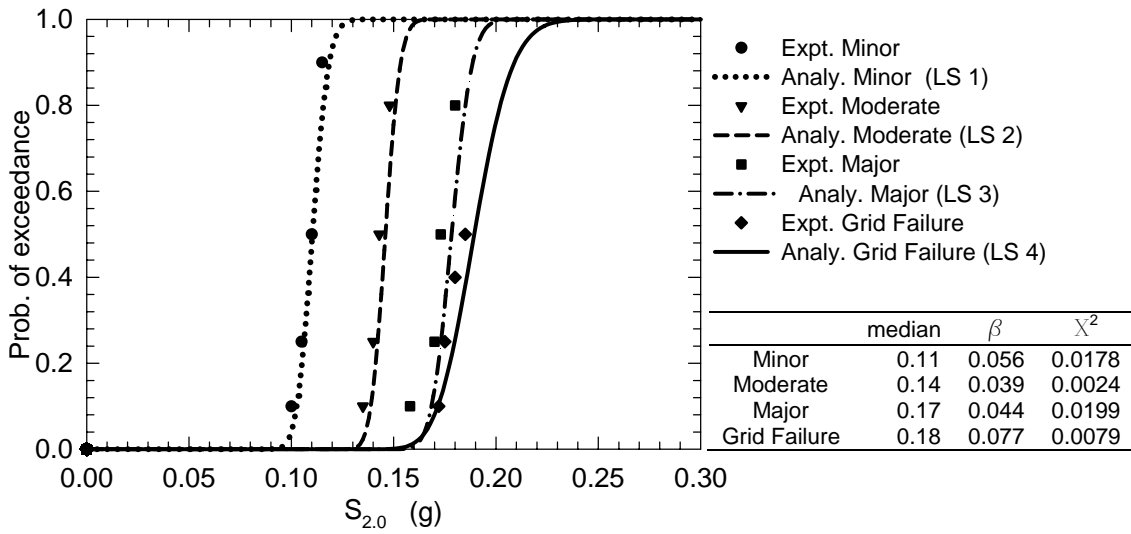


**FIGURE 7-10** Fragility curves for spectral acceleration at 2.0 seconds, configuration 1: undersized tiles

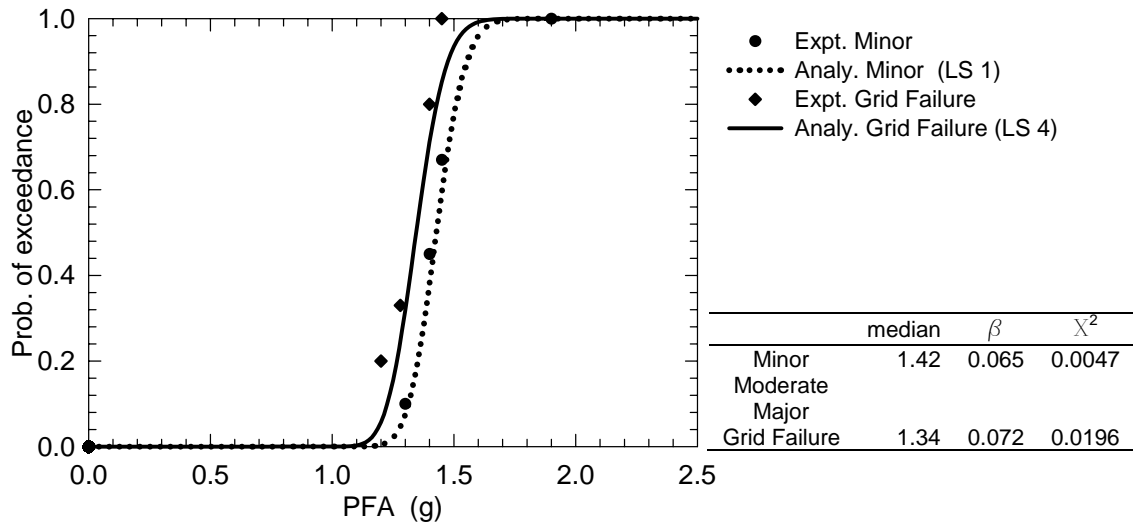


**FIGURE 7-11 Fragility curves for peak floor acceleration, configuration 2: undersized tiles with clips**

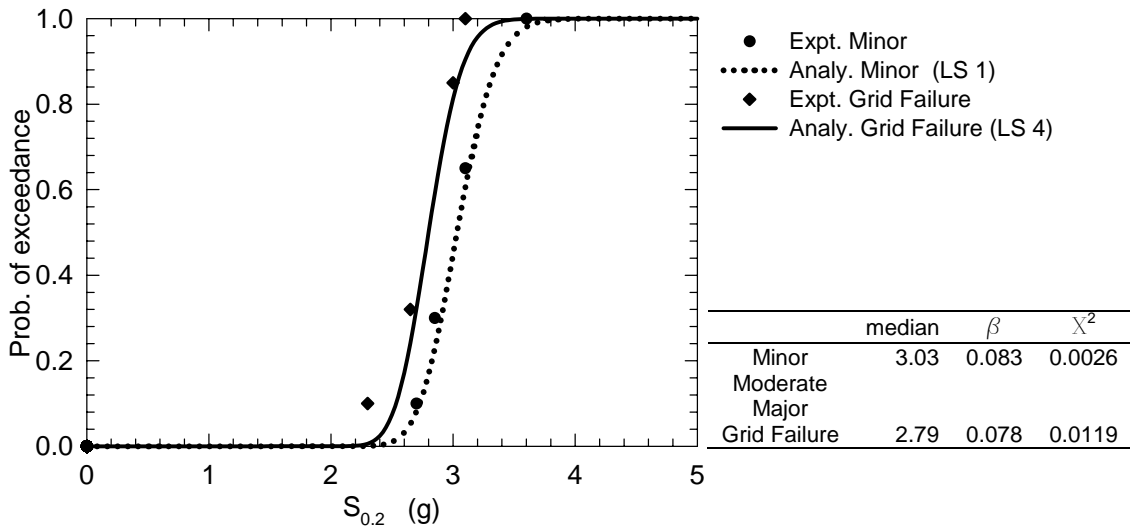


**FIGURE 7-12 Fragility curves for spectral acceleration at 0.2 second, configuration 2: undersized tiles with clips**

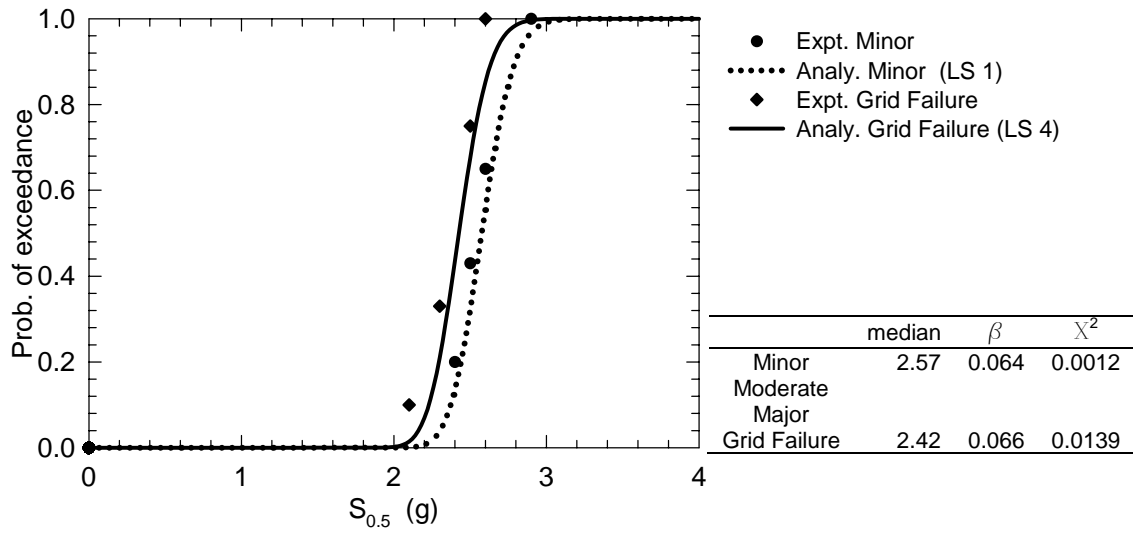


**FIGURE 7-13 Fragility curves for spectral acceleration at 0.5 second, configuration 2: undersized tiles with clips**

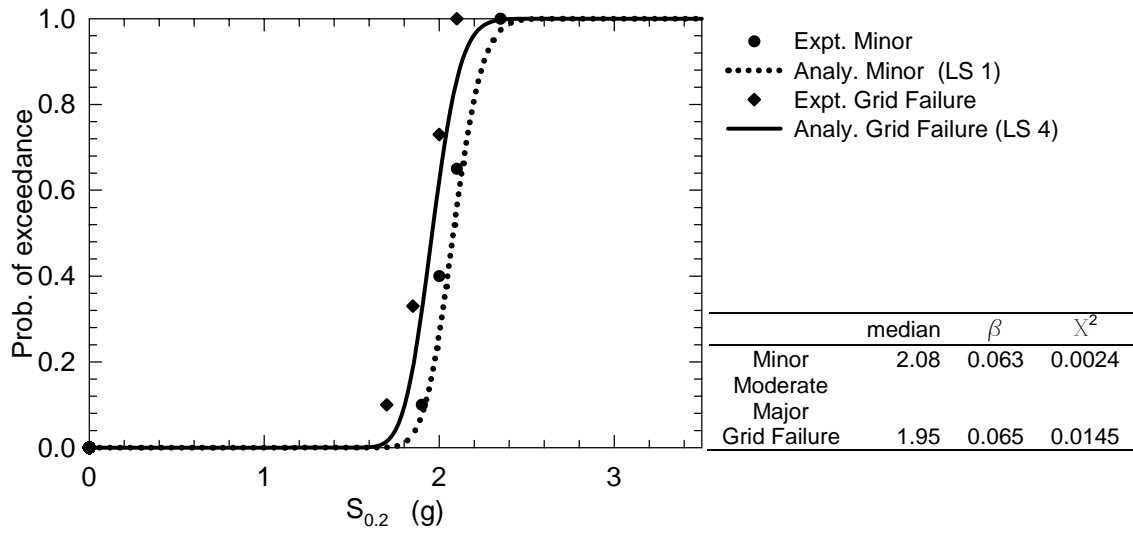


**FIGURE 7-14 Fragility curves for spectral acceleration at 1.0 second, configuration 2: undersized tiles with clips**

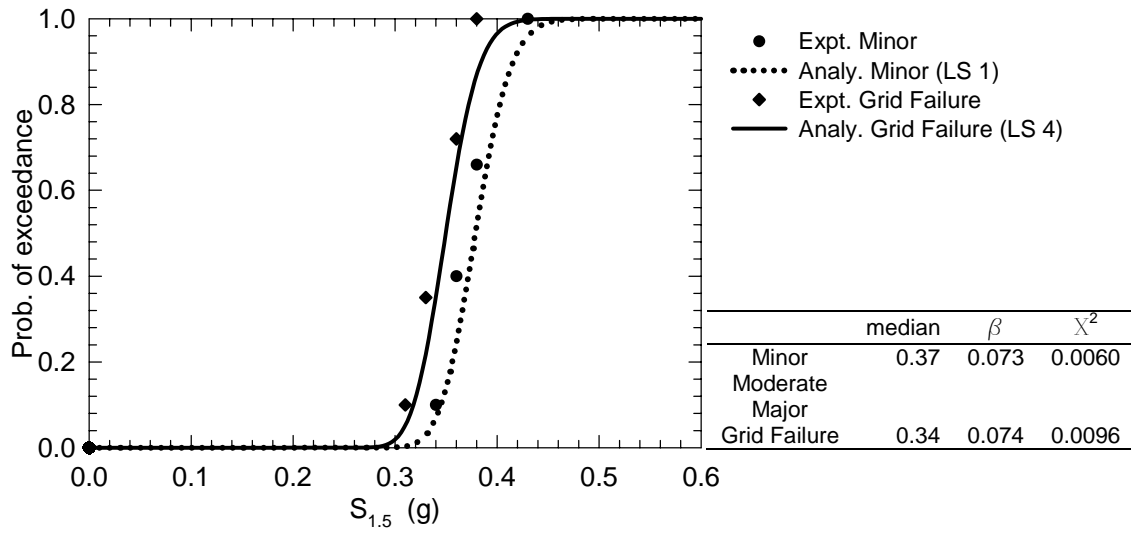


**FIGURE 7-15 Fragility curves for spectral acceleration at 1.5 seconds, configuration 2: undersized tiles with clips**

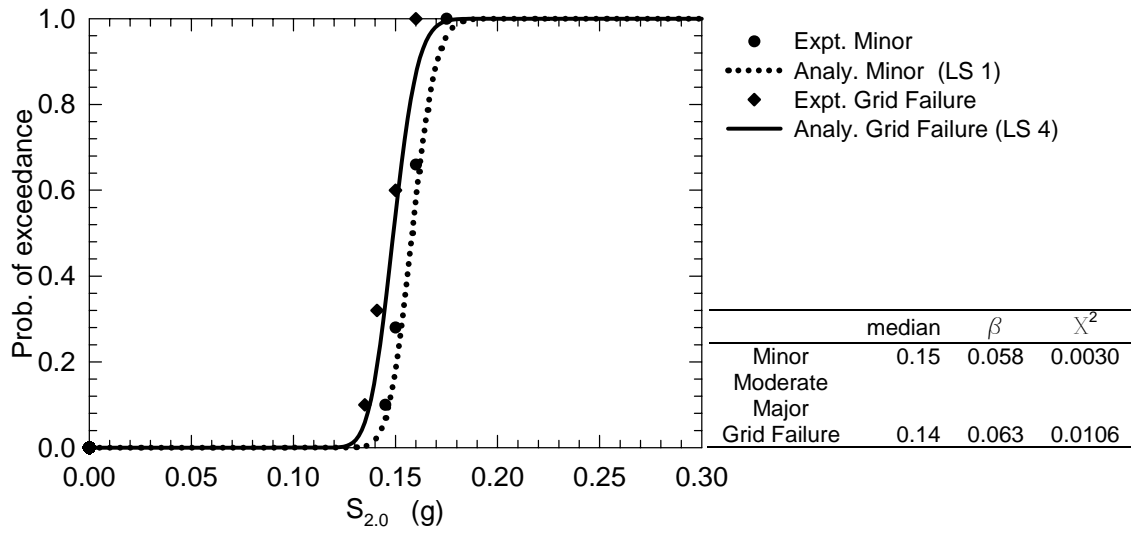


**FIGURE 7-16 Fragility curves for spectral acceleration at 2.0 seconds, configuration 2: undersized tiles with clips**



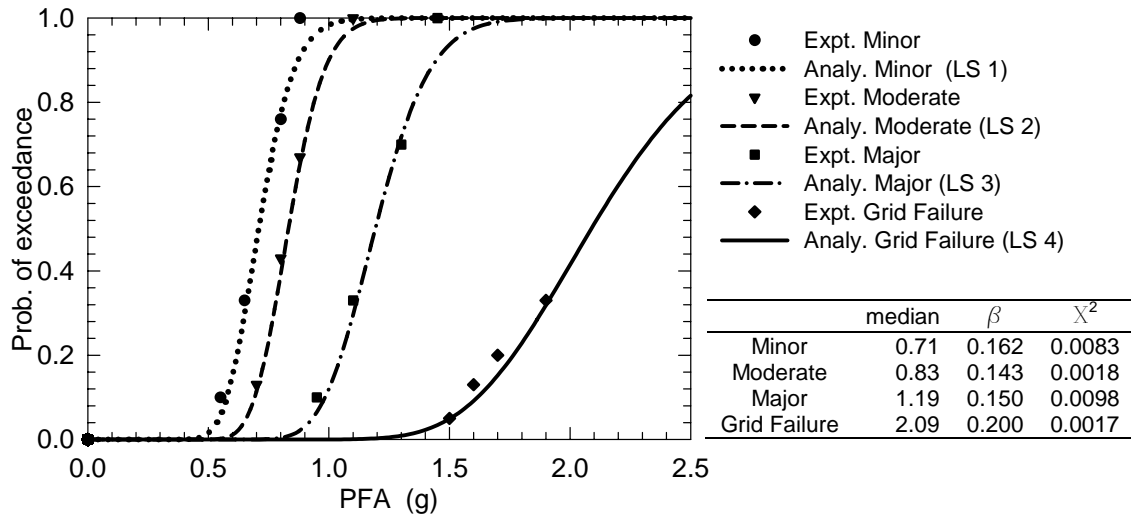


**FIGURE 7-17 Fragility curves for peak floor acceleration, configuration 3: undersized tiles with recycled grid**

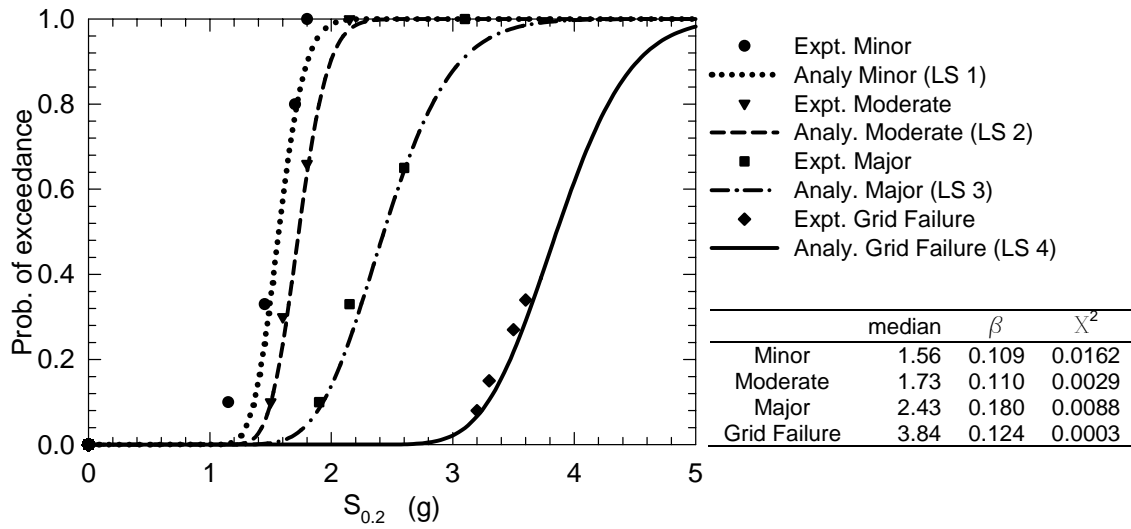


**FIGURE 7-18 Fragility curves for spectral acceleration at 0.2 second, configuration 3: undersized tiles with recycled grid**

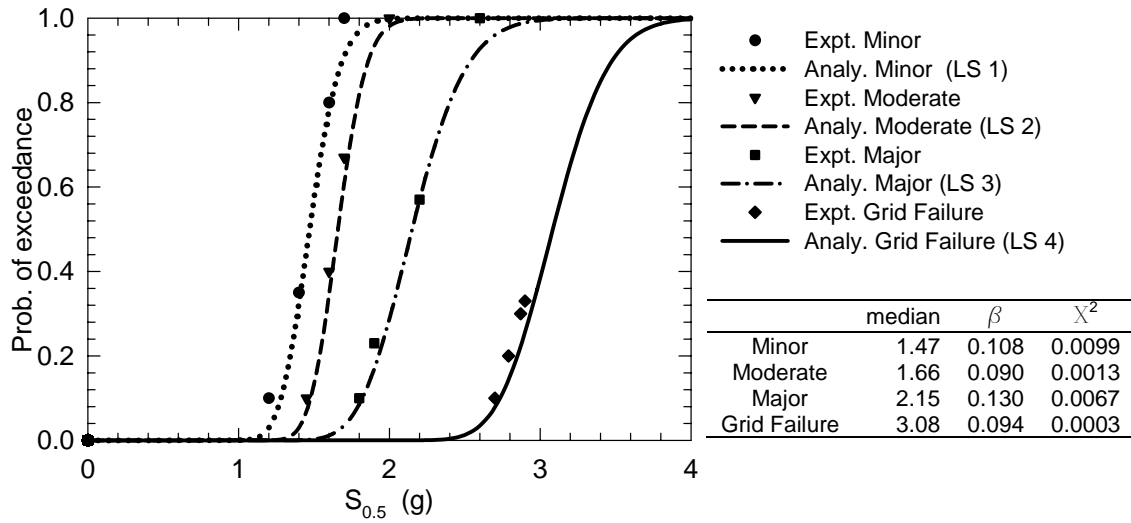


**FIGURE 7-19 Fragility curves for spectral acceleration at 0.5 second, configuration 3: undersized tiles with recycled grid**

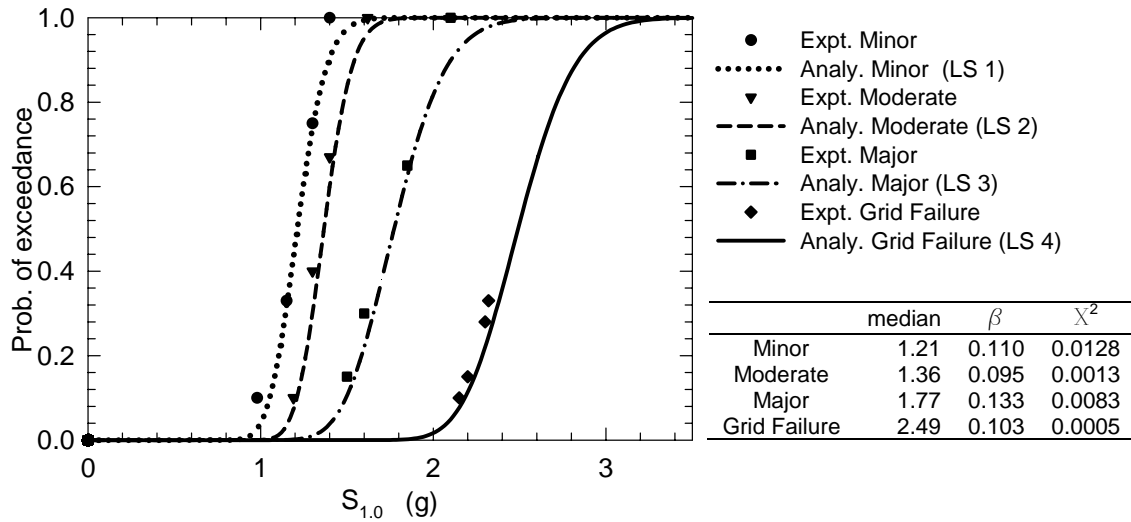


**FIGURE 7-20 Fragility curves for spectral acceleration at 1.0 second, configuration 3: undersized tiles with recycled grid**

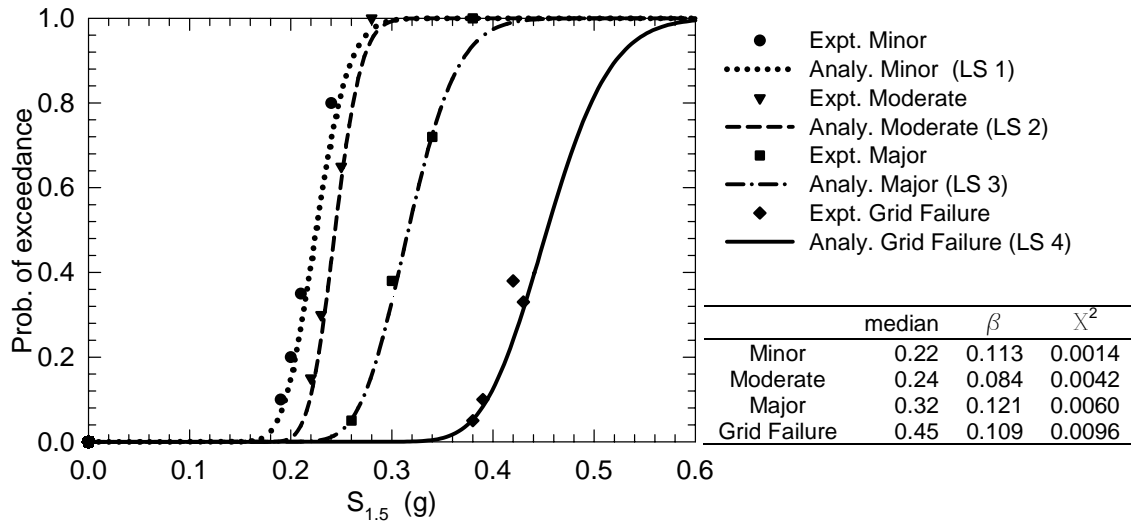


**FIGURE 7-21 Fragility curves for spectral acceleration at 1.5 seconds, configuration 3: undersized tiles with recycled grid**

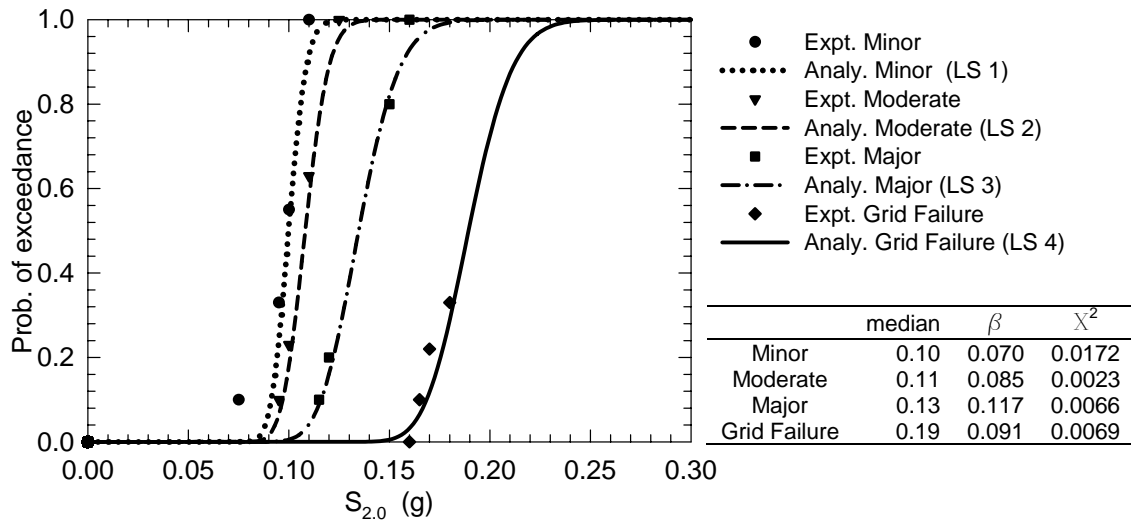


**FIGURE 7-22 Fragility curves for spectral acceleration at 2.0 seconds, configuration 3: undersized tiles with recycled grid**

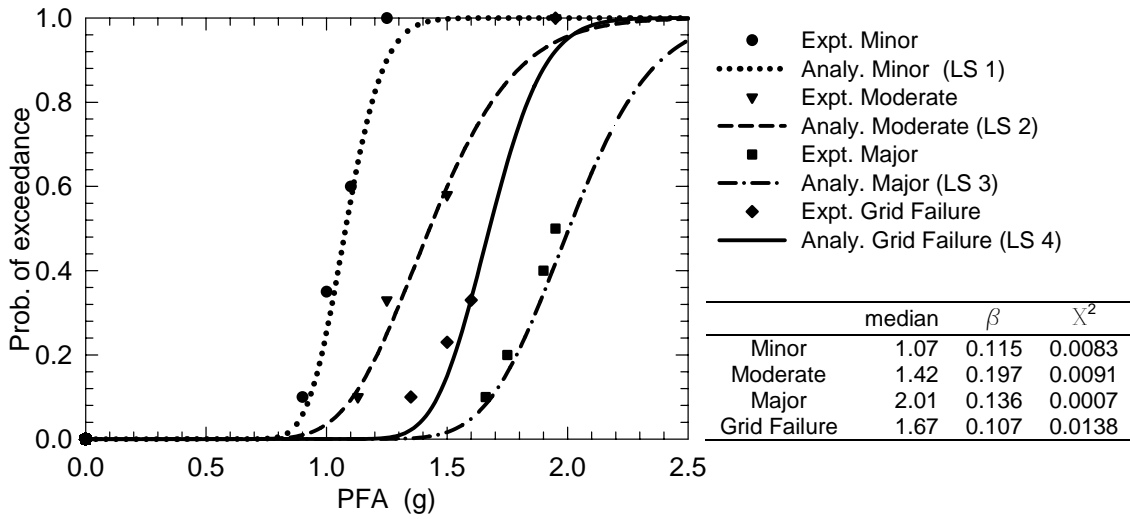


**FIGURE 7-23 Fragility curves for peak floor acceleration, configuration 4: normal sized tiles**

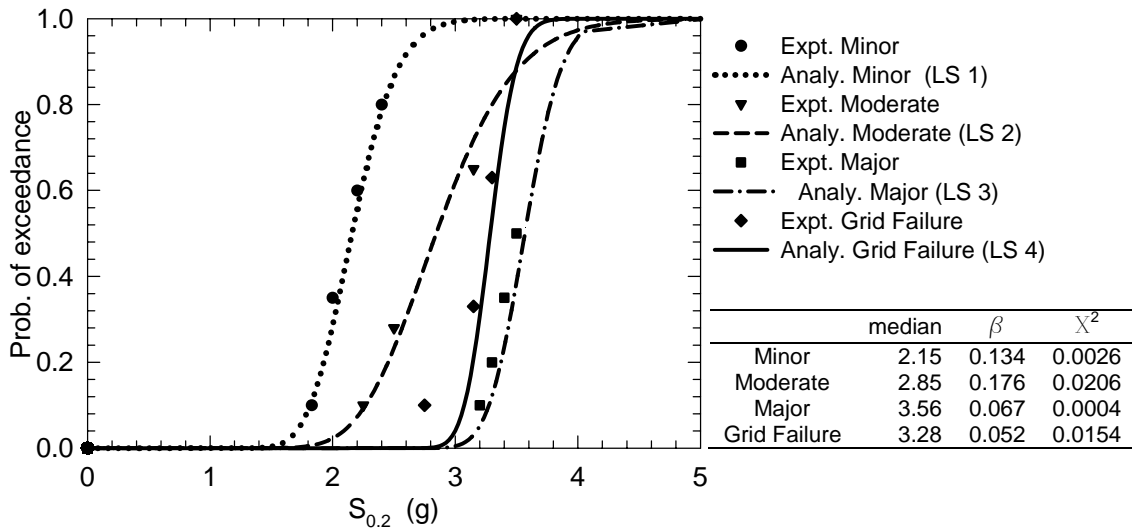


**FIGURE 7-24 Fragility curves for spectral acceleration at 0.2 second, configuration 4: normal sized tiles**

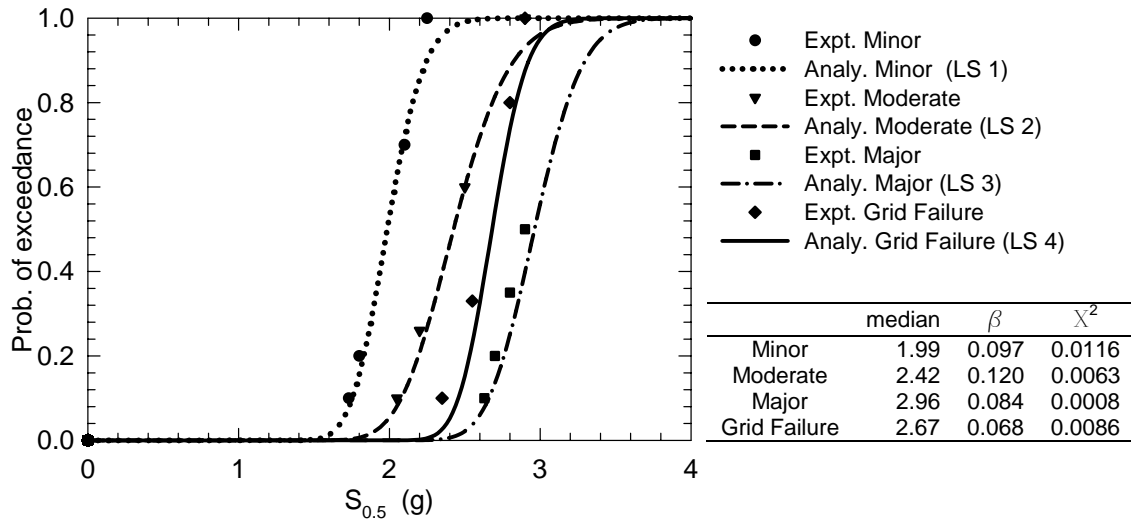


**FIGURE 7-25 Fragility curves for spectral acceleration at 0.5 second, configuration 4: normal sized tiles**

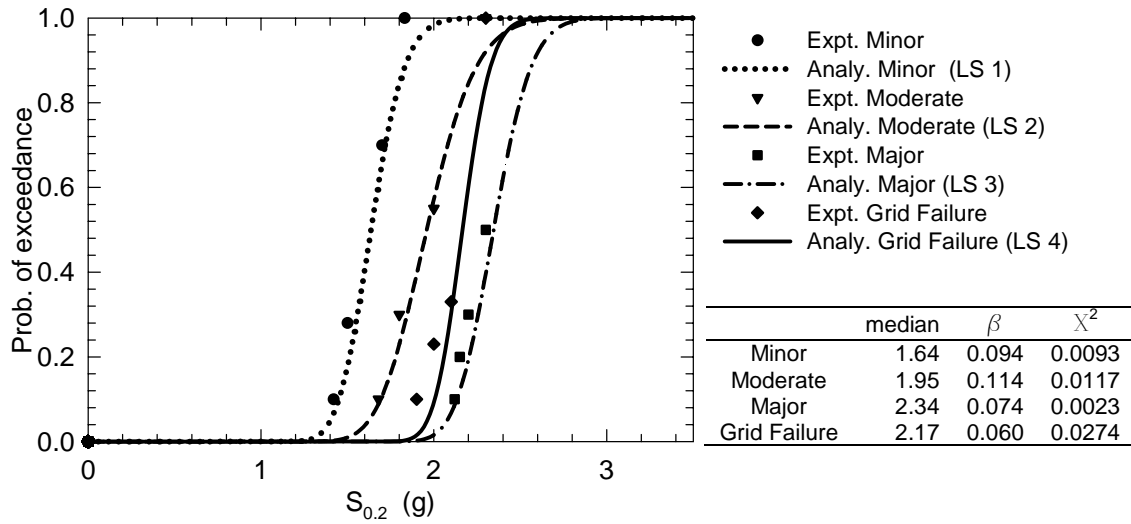


**FIGURE 7-26 Fragility curves for spectral acceleration at 1.0 second, configuration 4: normal sized tiles**

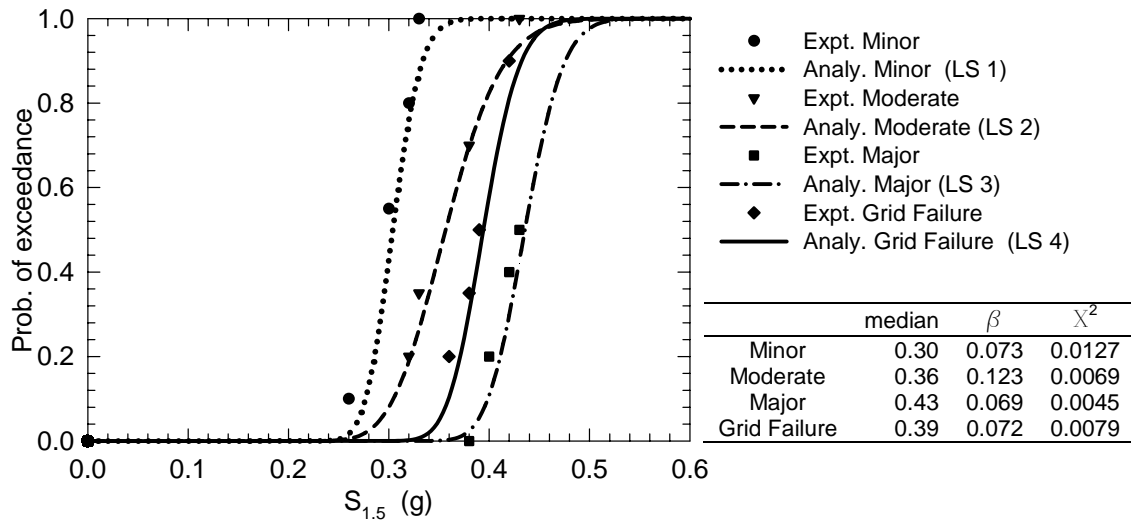


**FIGURE 7-27** Fragility curves for spectral acceleration at 1.5 seconds, configuration 4: normal sized tiles

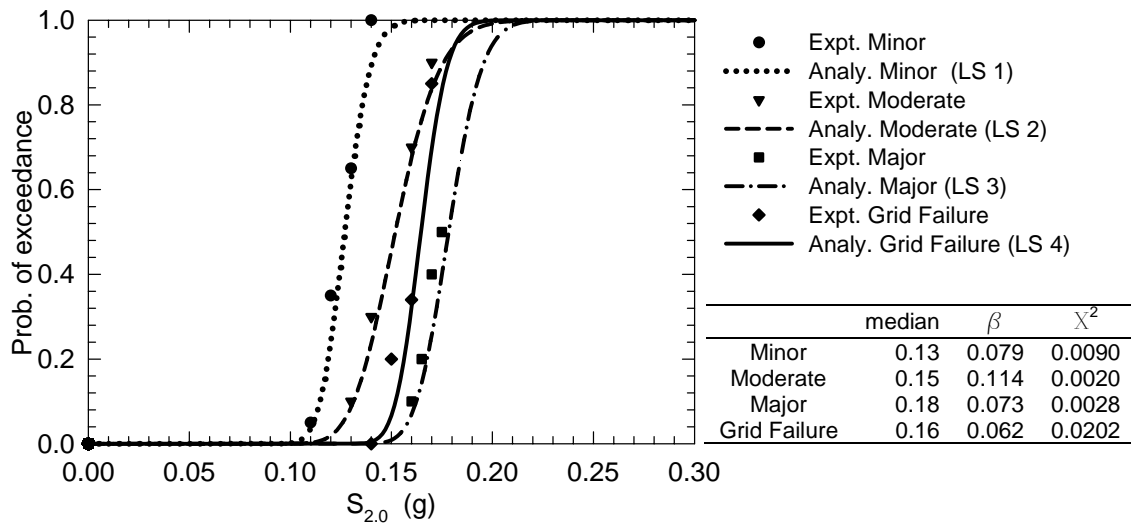


**FIGURE 7-28** Fragility curves for spectral acceleration at 2.0 seconds, configuration 4: normal sized tiles

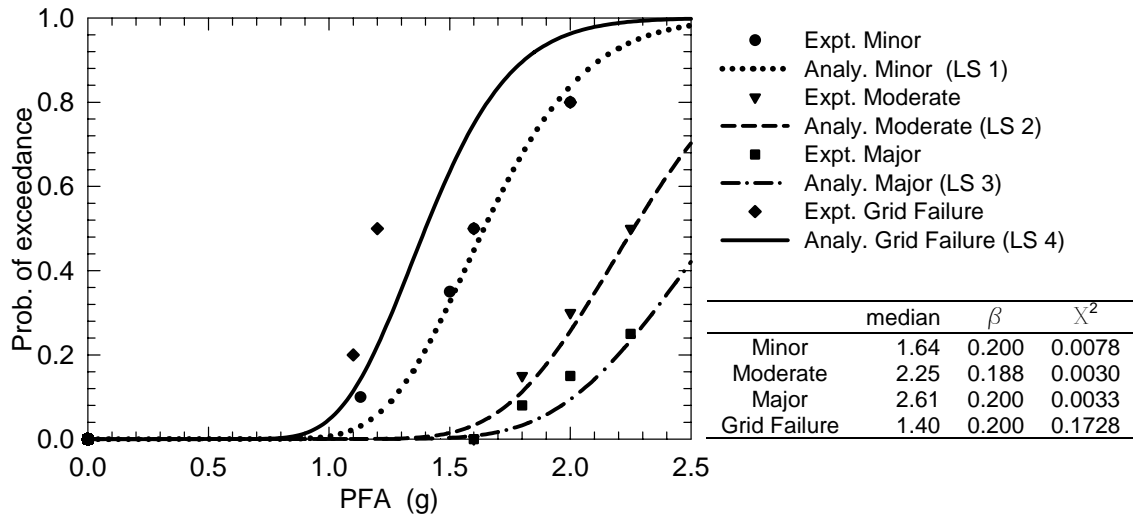


**FIGURE 7-29 Fragility curves for peak floor acceleration, configuration 5: normal sized tiles with clips**

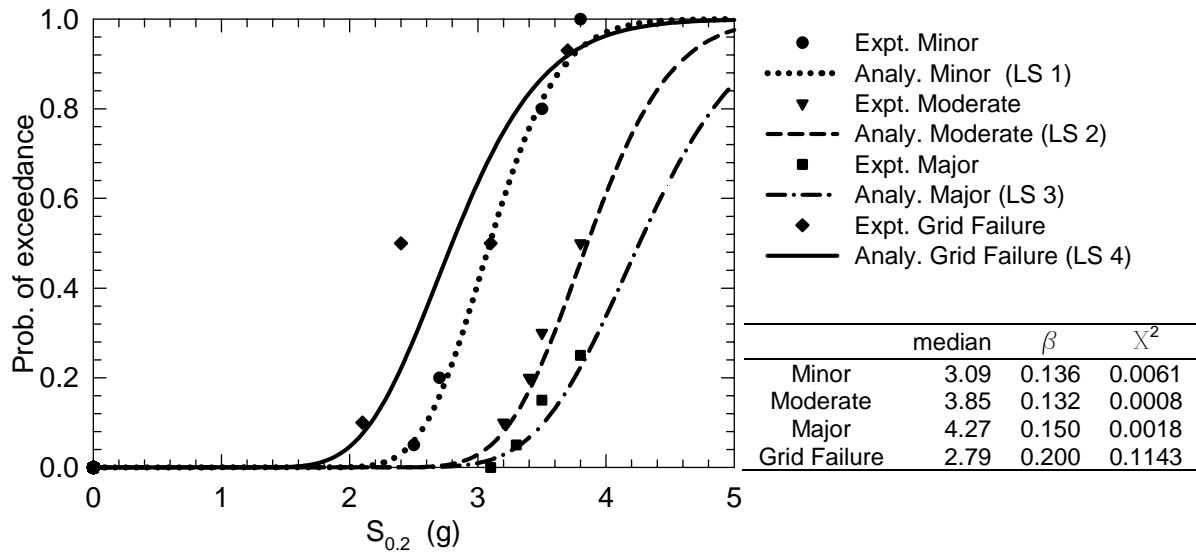


**FIGURE 7-30 Fragility curves for spectral acceleration at 0.2 second, configuration 5: normal sized tiles with clips**

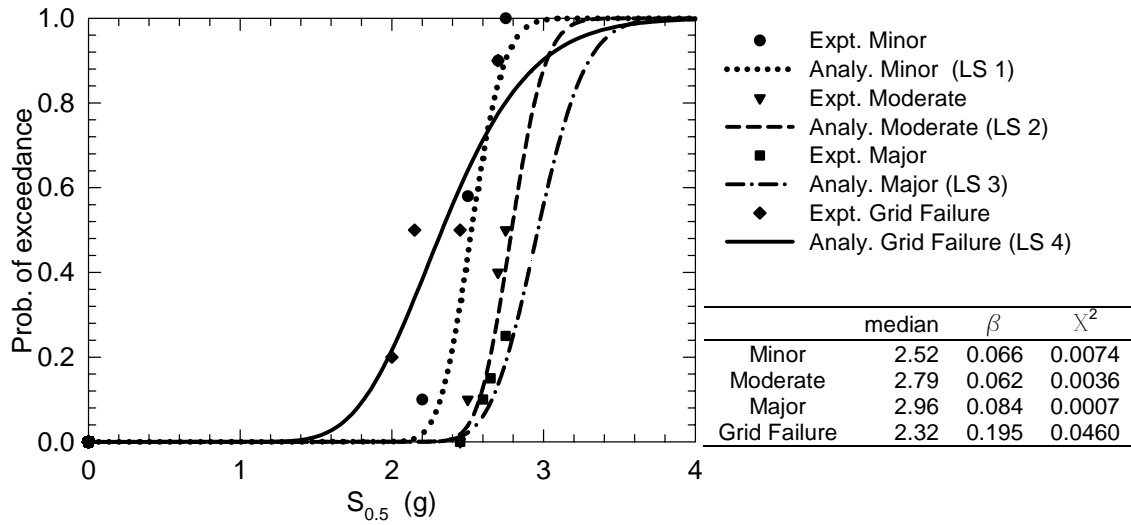


**FIGURE 7-31 Fragility curves for spectral acceleration at 0.5 second, configuration 5: normal sized tiles with clips**

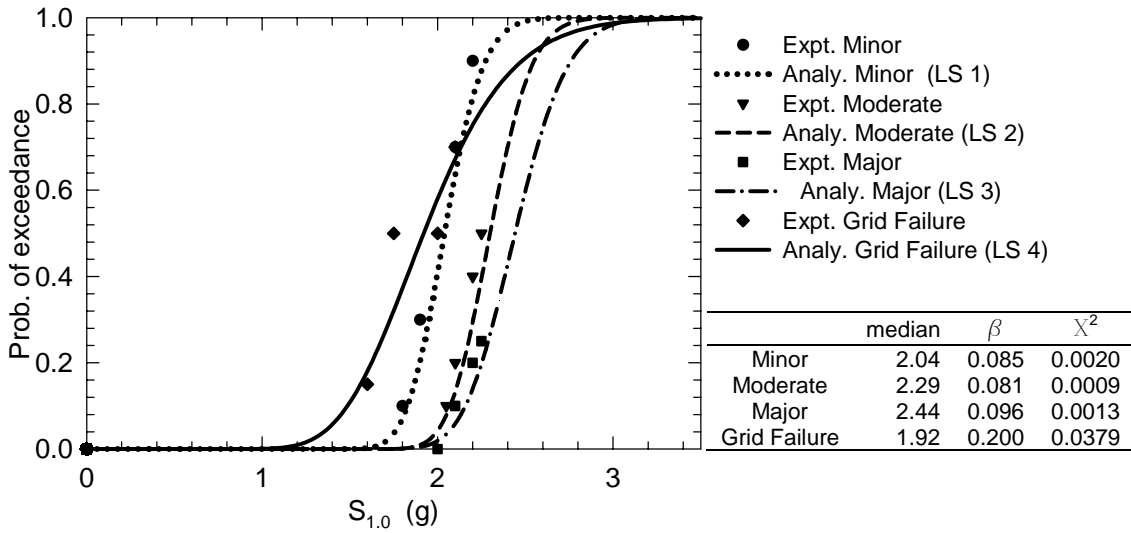


**FIGURE 7-32 Fragility curves for spectral acceleration at 1.0 second, configuration 5: normal sized tiles with clips**



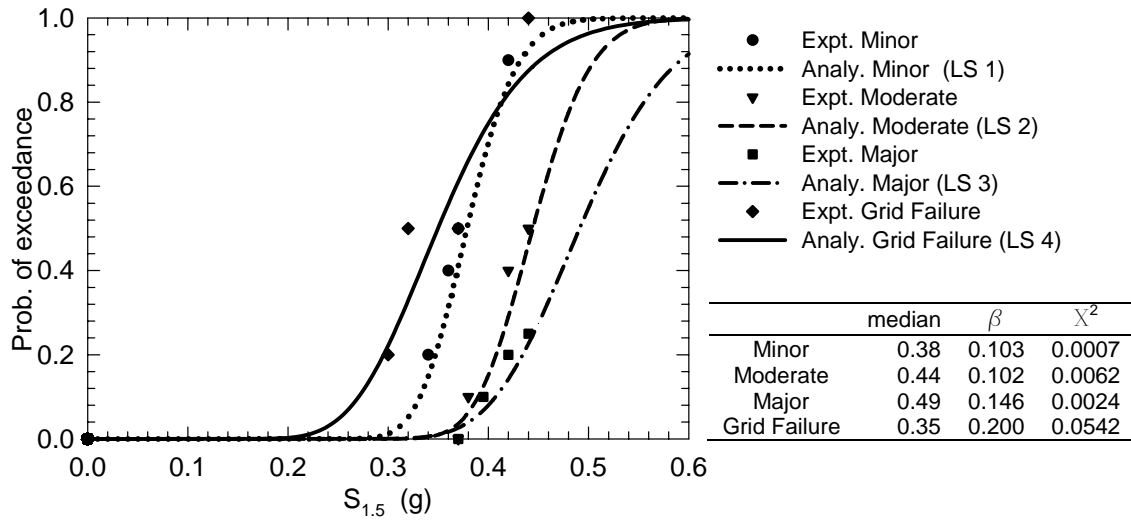


**FIGURE 7-33** Fragility curves for spectral acceleration at 1.5 seconds, configuration 5: normal sized tiles with clips

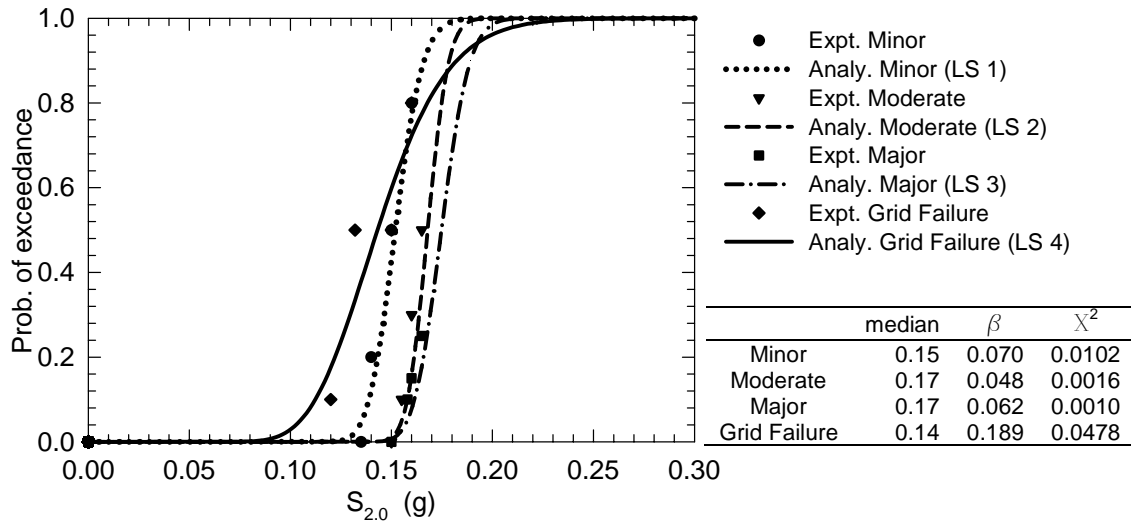


**FIGURE 7-34** Fragility curves for spectral acceleration at 2.0 seconds, configuration 5: normal sized tiles with clips

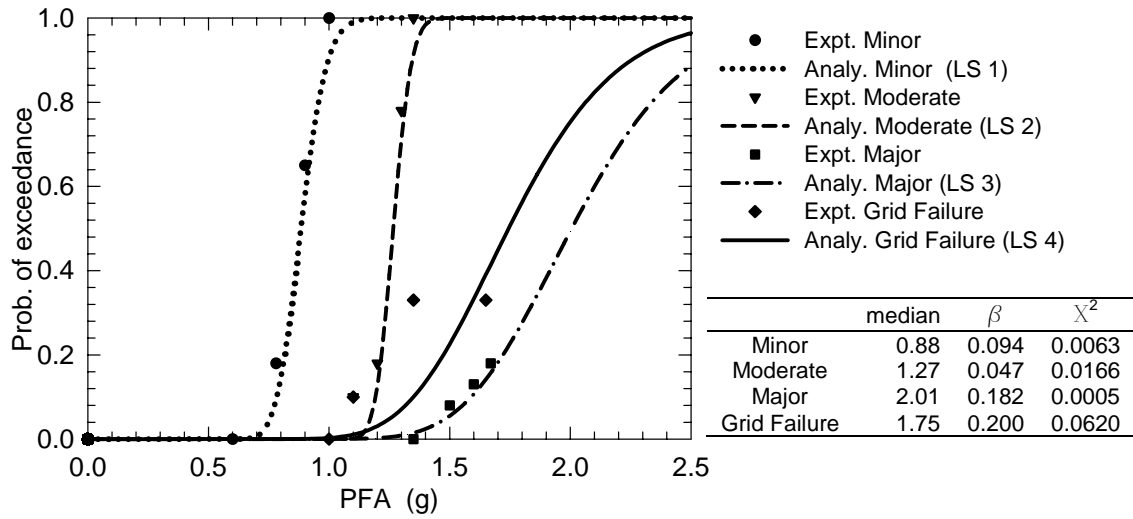


**FIGURE 7-35 Fragility curves for peak floor acceleration, configuration 6: normal sized tiles without post**

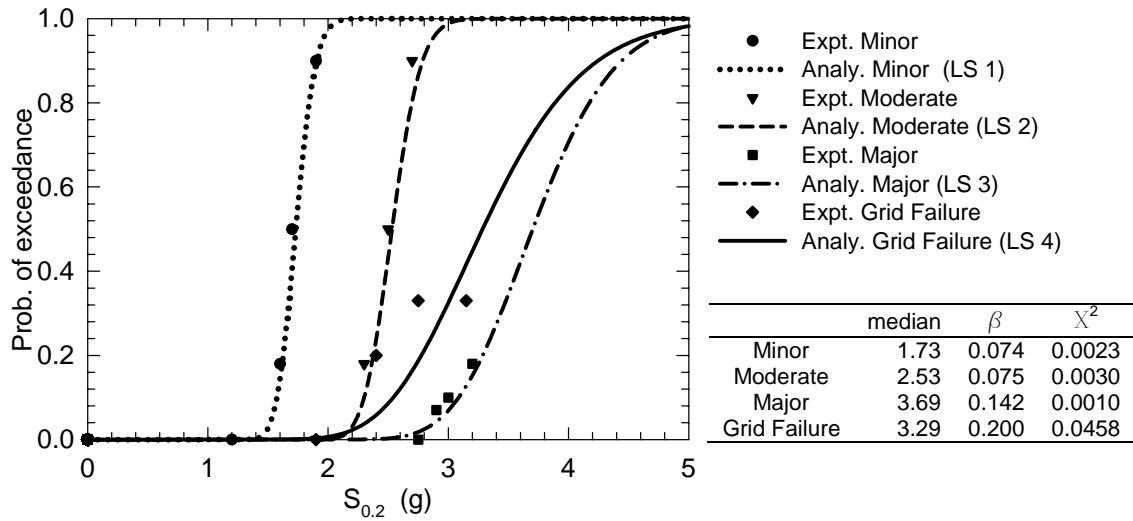


**FIGURE 7-36 Fragility curves for spectral acceleration at 0.2 second, configuration 6: normal sized tiles without post**

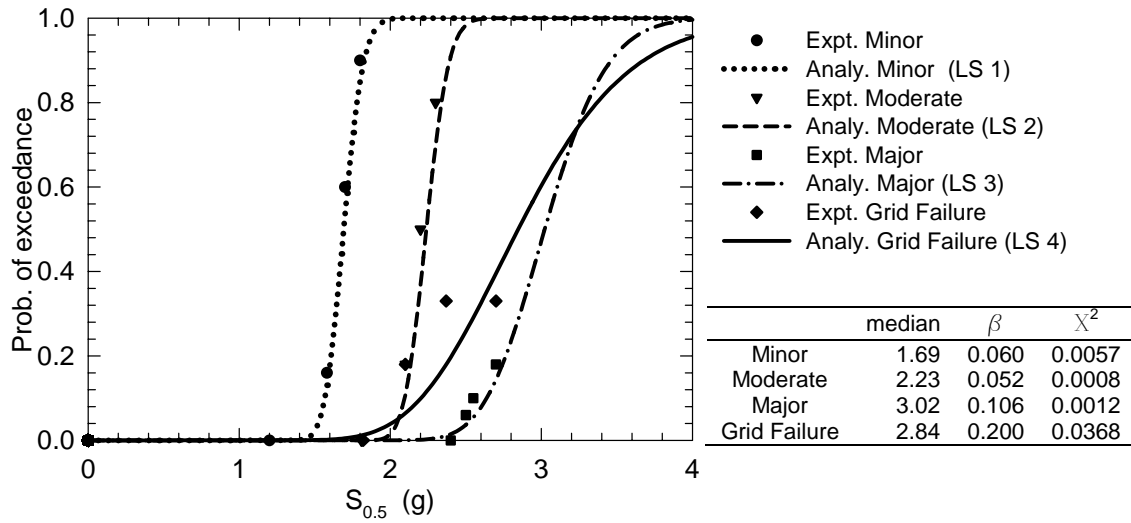


**FIGURE 7-37 Fragility curves for spectral acceleration at 0.5 second, configuration 6: normal sized tiles without post**

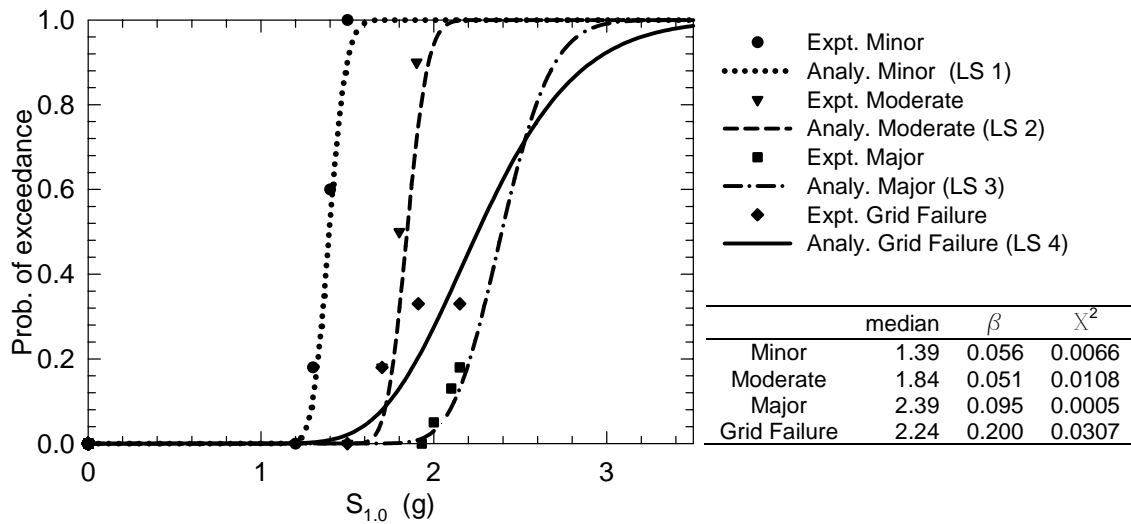


**FIGURE 7-38 Fragility curves for spectral acceleration at 1.0 second, configuration 6: normal sized tiles without post**

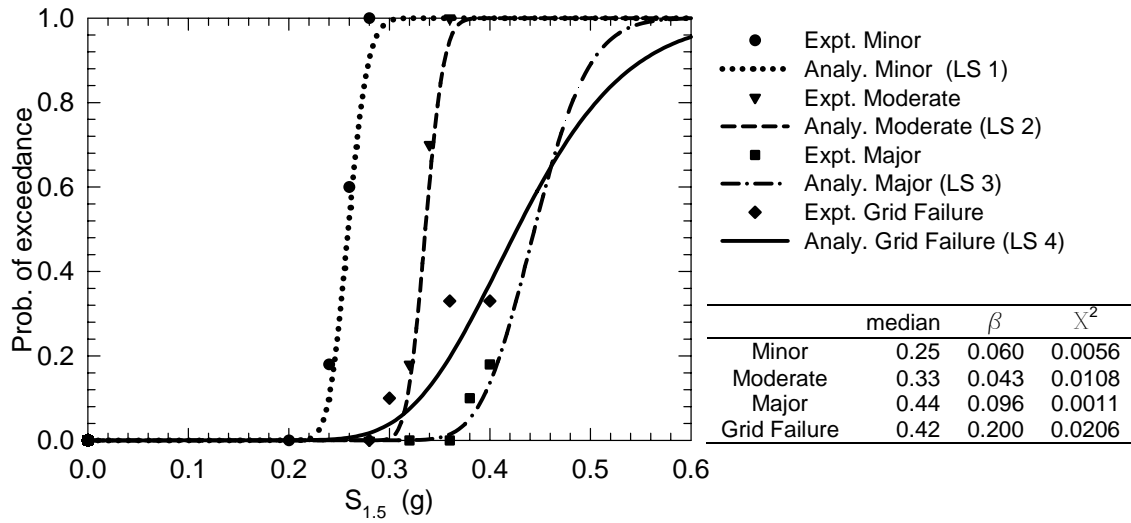


**FIGURE 7-39** Fragility curves for spectral acceleration at 1.5 seconds, configuration 6: normal sized tiles without post

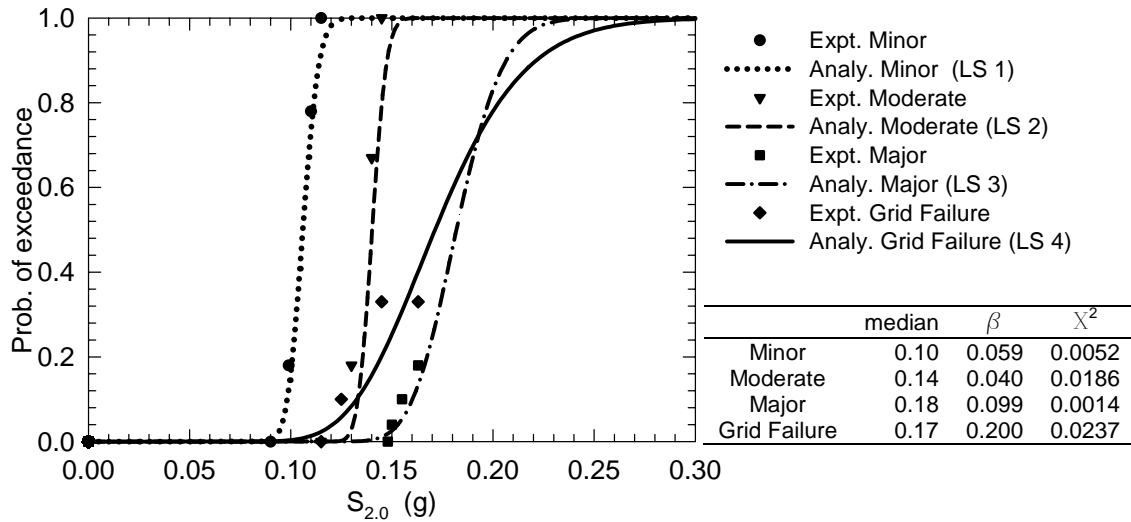
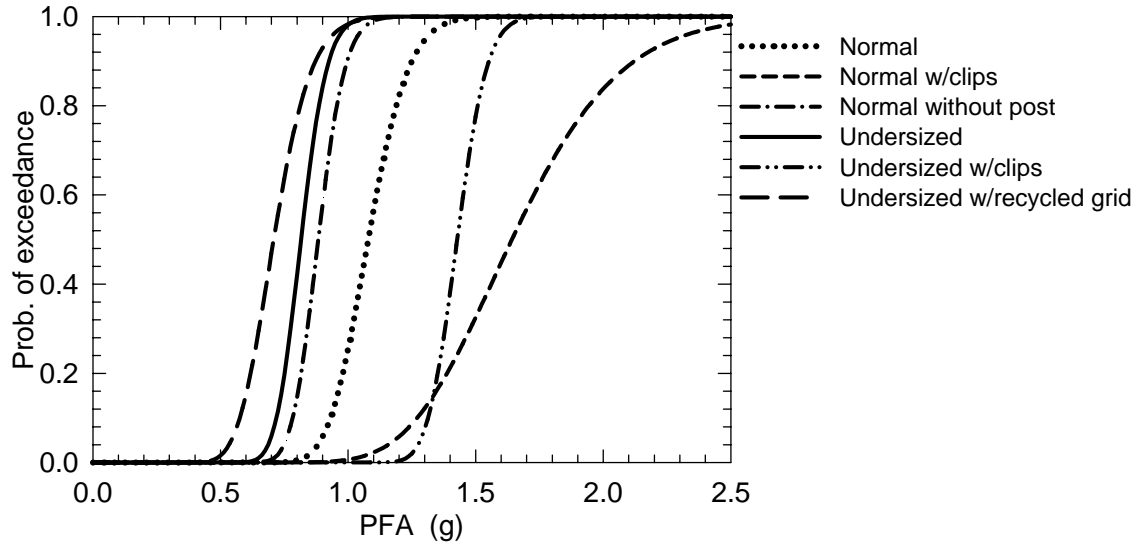
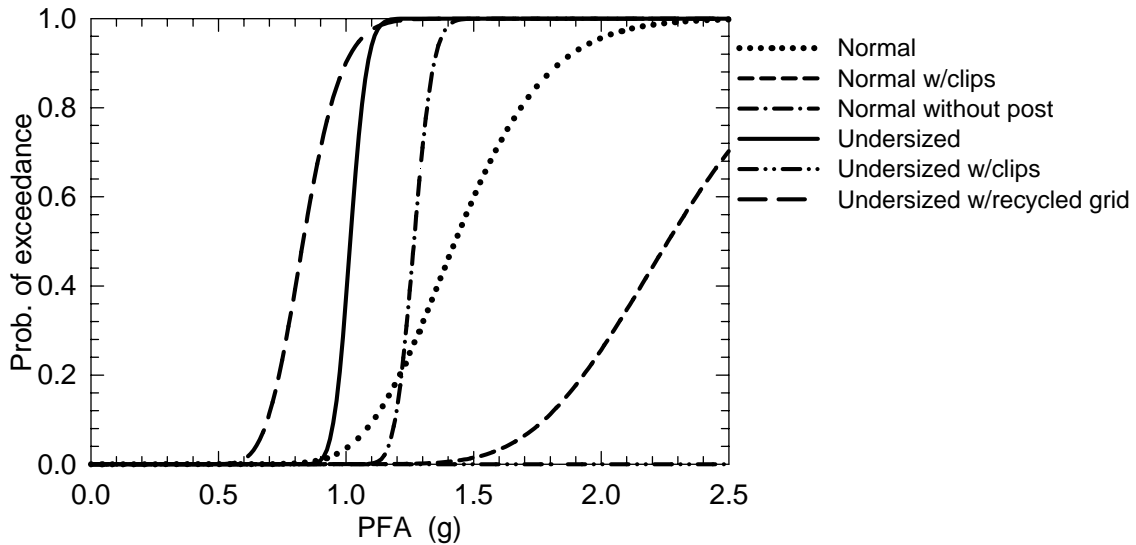


**FIGURE 7-40** Fragility curves for spectral acceleration at 2.0 seconds, configuration 6: normal sized tiles without post



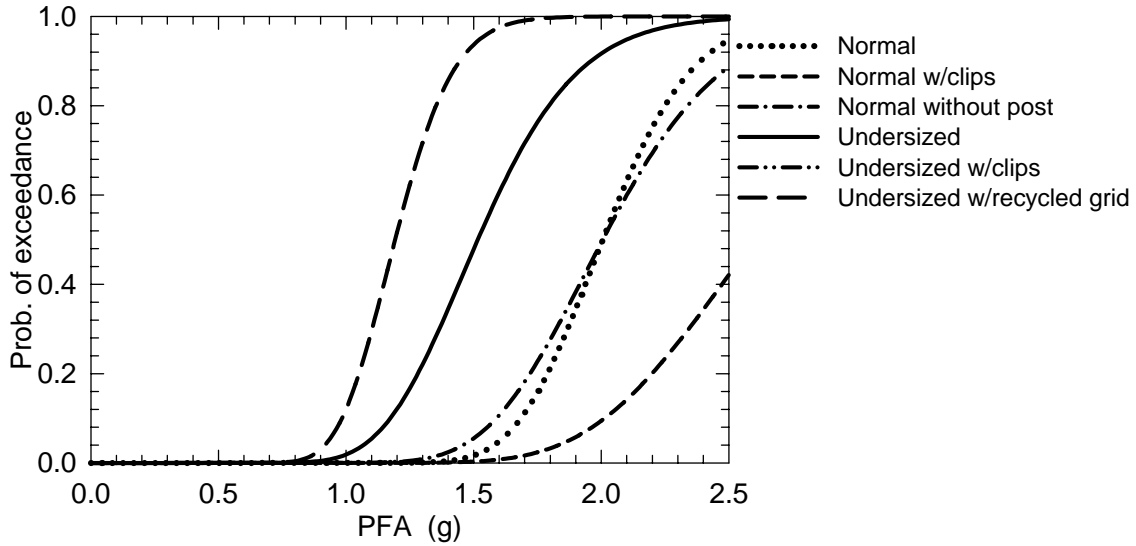
	median	$\beta$
Undersized (C1)	0.81	0.098
Undersized w/clips (C2)	1.42	0.065
Undersized w/recycled grid (C3)	0.71	0.162
Normal (C4)	1.07	0.115
Normal w/clips (C5)	1.64	0.200
Normal without post (C6)	0.88	0.094

**FIGURE 7-41 Fragility curves for peak floor acceleration, limit state 1: minor damage**



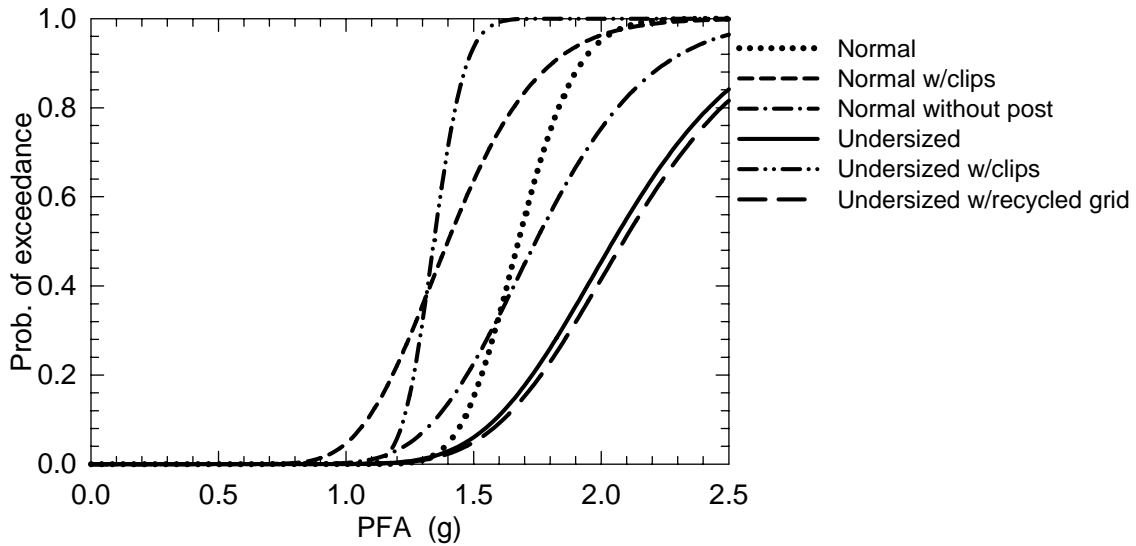
	median	$\beta$
Undersized (C1)	1.01	0.051
Undersized w/clips (C2)	0.83	0.143
Undersized w/recycled grid (C3)	0.83	0.143
Normal (C4)	1.42	0.197
Normal w/clips (C5)	2.25	0.188
Normal without post (C6)	1.27	0.047

**FIGURE 7-42 Fragility curves for peak floor acceleration, limit state 2: moderate damage**



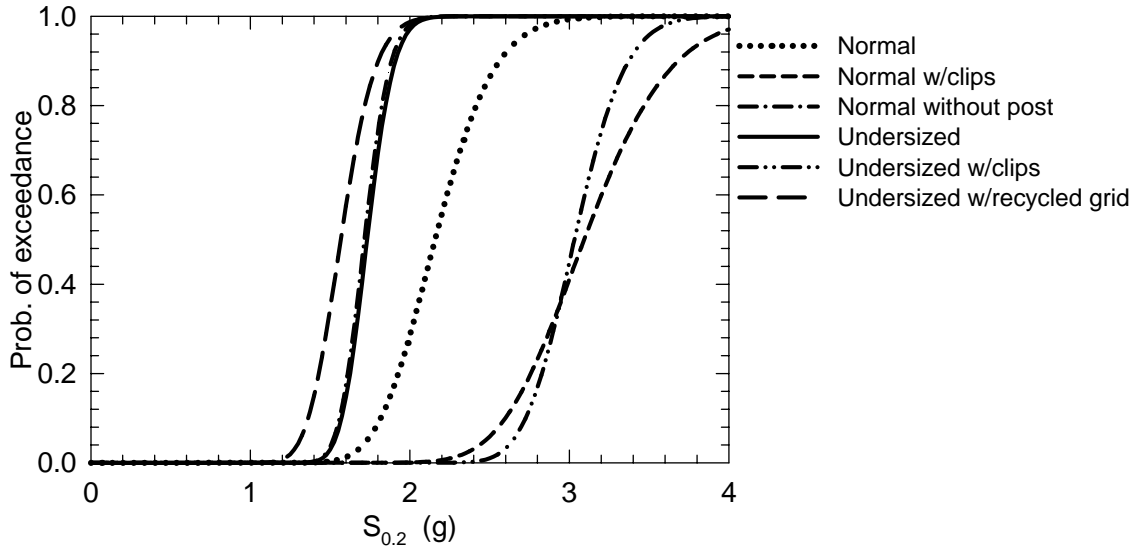
	median	$\beta$
Undersized (C1)	1.51	0.200
Undersized w/clips (C2)	1.19	0.150
Undersized w/recycled grid (C3)	2.01	0.136
Normal (C4)	2.61	0.200
Normal w/clips (C5)	2.01	0.182
Normal without post (C6)		

**FIGURE 7-43 Fragility curves for peak floor acceleration, limit state 3: major damage**



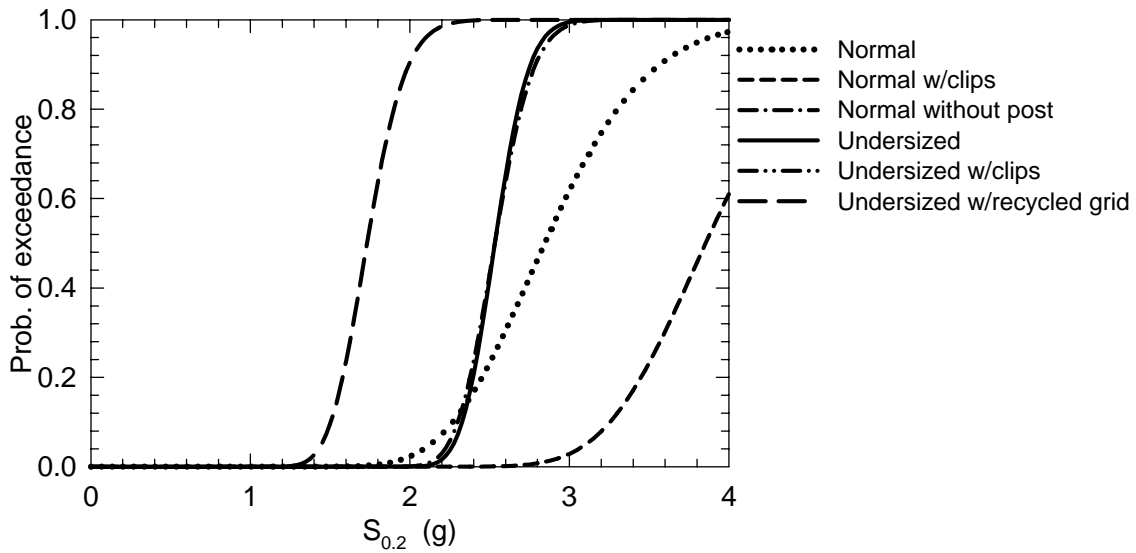
	median	$\beta$
Undersized (C1)	2.04	0.200
Undersized w/clips (C2)	1.34	0.072
Undersized w/recycled grid (C3)	2.09	0.200
Normal (C4)	1.67	0.107
Normal w/clips (C5)	1.40	0.200
Normal without post (C6)	1.75	0.200

**FIGURE 7-44 Fragility curves for peak floor acceleration, limit state 4: grid failure**



	median	$\beta$
Undersized (C1)	1.73	0.076
Undersized w/clips (C2)	3.03	0.083
Undersized w/recycled grid (C3)	1.56	0.109
Normal (C4)	2.15	0.134
Normal w/clips (C5)	3.09	0.136
Normal without post (C6)	1.73	0.074

**FIGURE 7-45 Fragility curves for spectral acceleration at 0.2 second, limit state 1: minor damage**



	median	$\beta$
Undersized (C1)	2.53	0.066
Undersized w/clips (C2)		
Undersized w/recycled grid (C3)	1.73	0.110
Normal (C4)	2.85	0.176
Normal w/clips (C5)	3.85	0.132
Normal without post (C6)	2.53	0.075

**FIGURE 7-46 Fragility curves for spectral acceleration at 0.2 second, limit state 2: moderate damage**

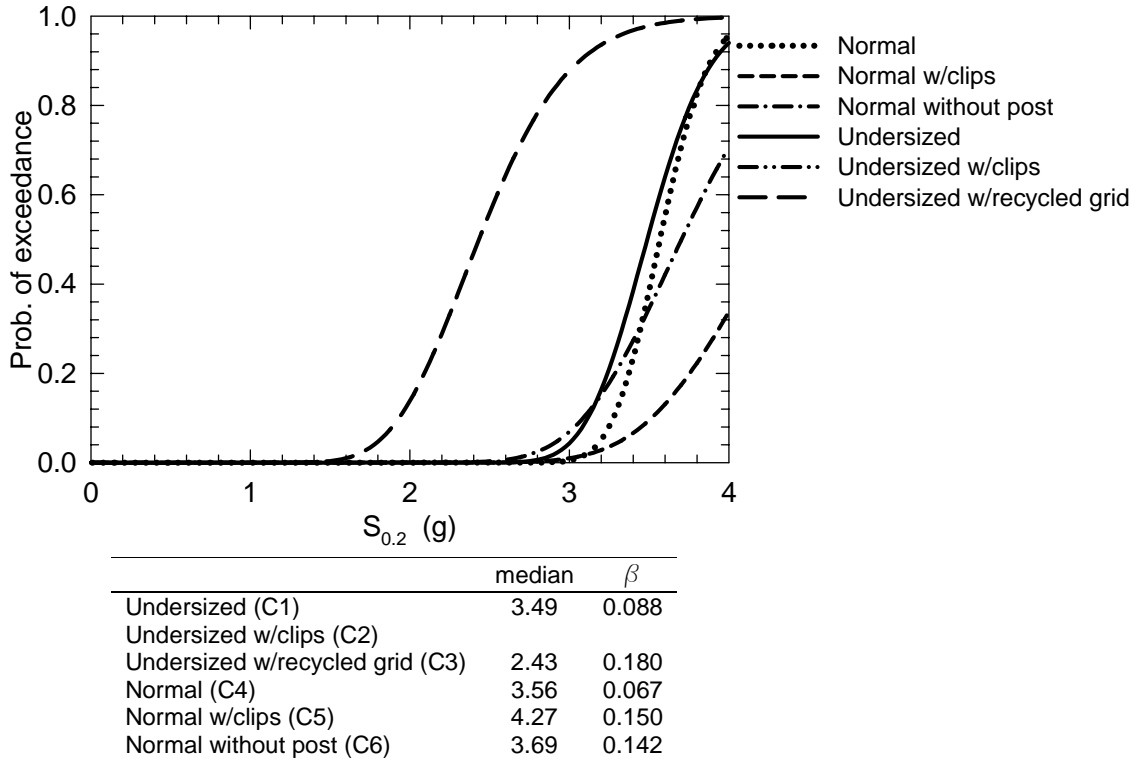


**FIGURE 7-47 Fragility curves for spectral acceleration at 0.2 second, limit state 3: major damage**

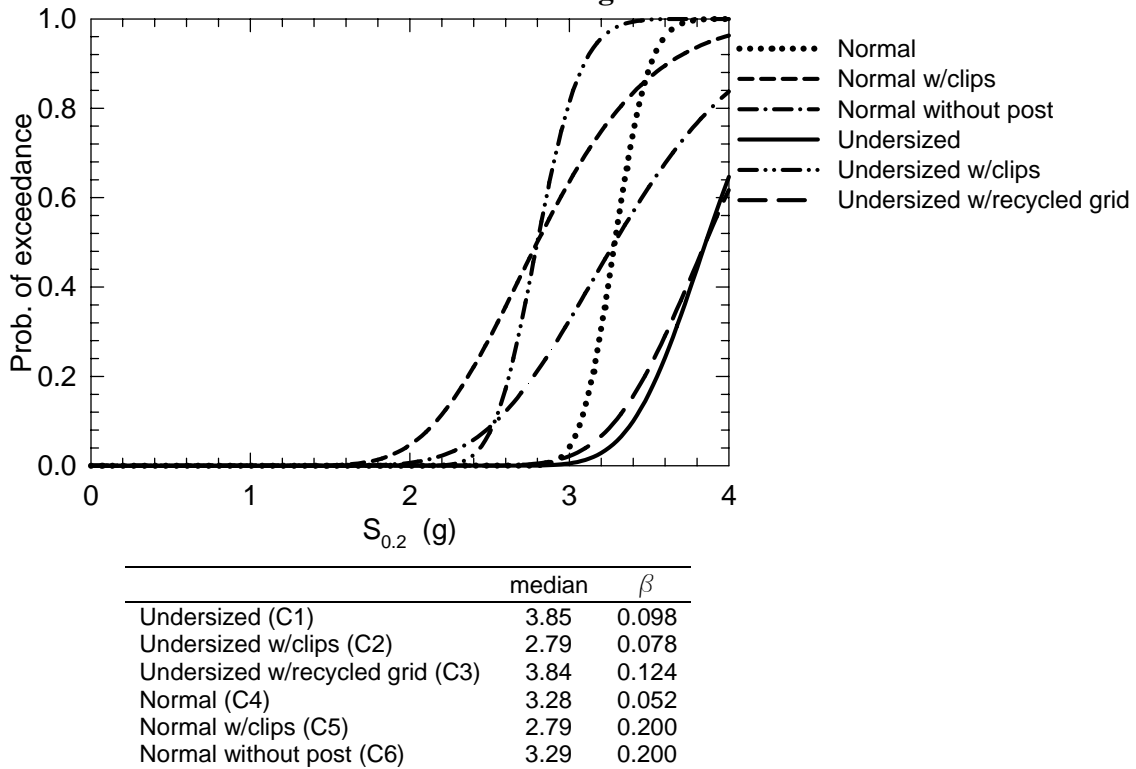
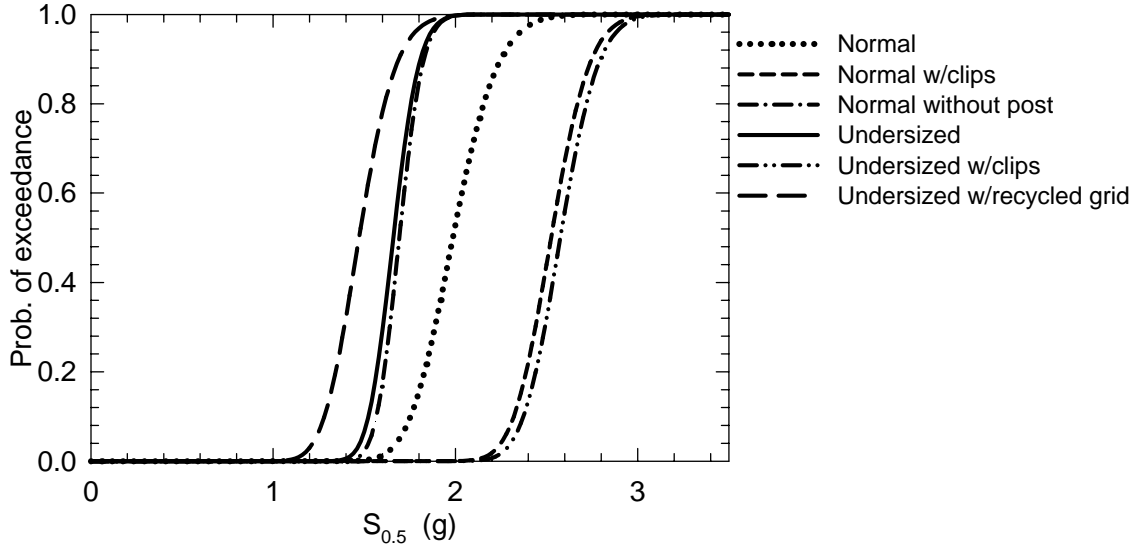


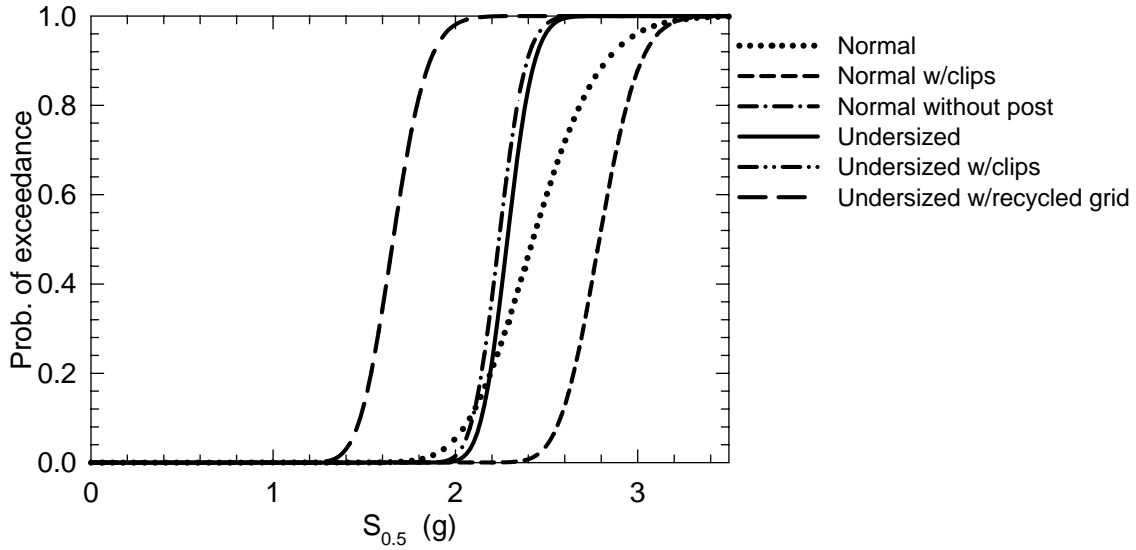
**FIGURE 7-48 Fragility curves for spectral acceleration at 0.2 second, limit state 4: grid failure**





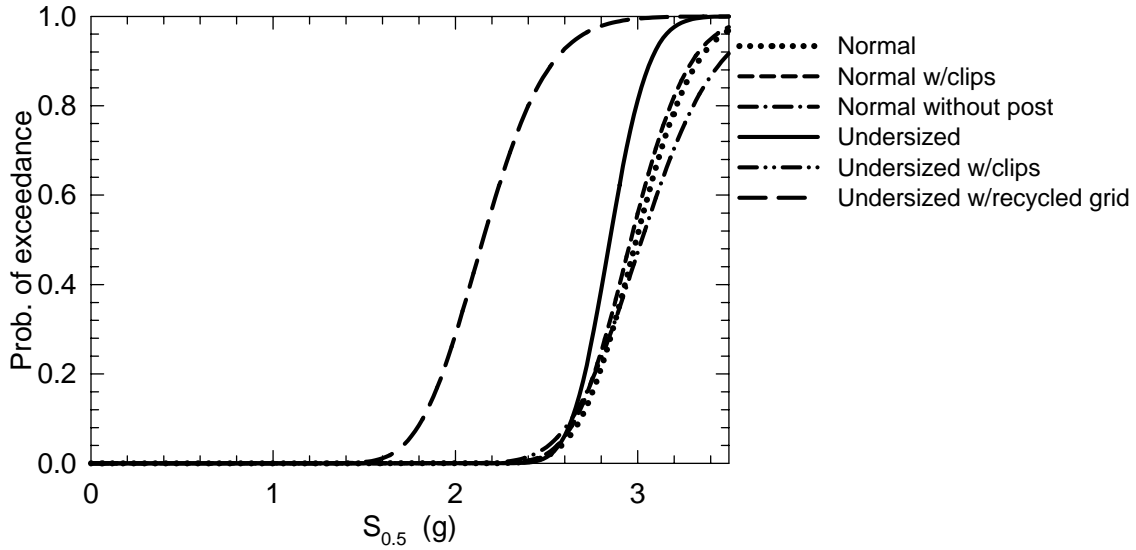
	median	$\beta$
Undersized (C1)	1.66	0.067
Undersized w/clips (C2)	2.57	0.064
Undersized w/recycled grid (C3)	1.47	0.108
Normal (C4)	1.99	0.097
Normal w/clips (C5)	2.52	0.066
Normal without post (C6)	1.69	0.060

**FIGURE 7-49 Fragility curves for spectral acceleration at 0.5 second, limit state 1: minor damage**



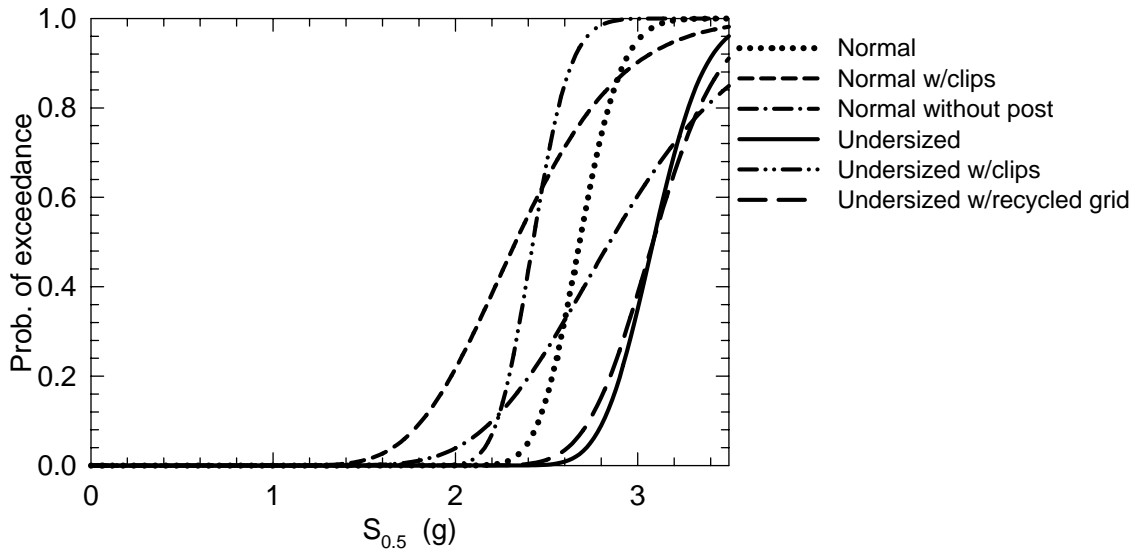
	median	$\beta$
Undersized (C1)	2.28	0.050
Undersized w/clips (C2)		
Undersized w/recycled grid (C3)	1.66	0.090
Normal (C4)	2.42	0.120
Normal w/clips (C5)	2.79	0.062
Normal without post (C6)	2.23	0.052

**FIGURE 7-50 Fragility curves for spectral acceleration at 0.5 second, limit state 2: moderate damage**



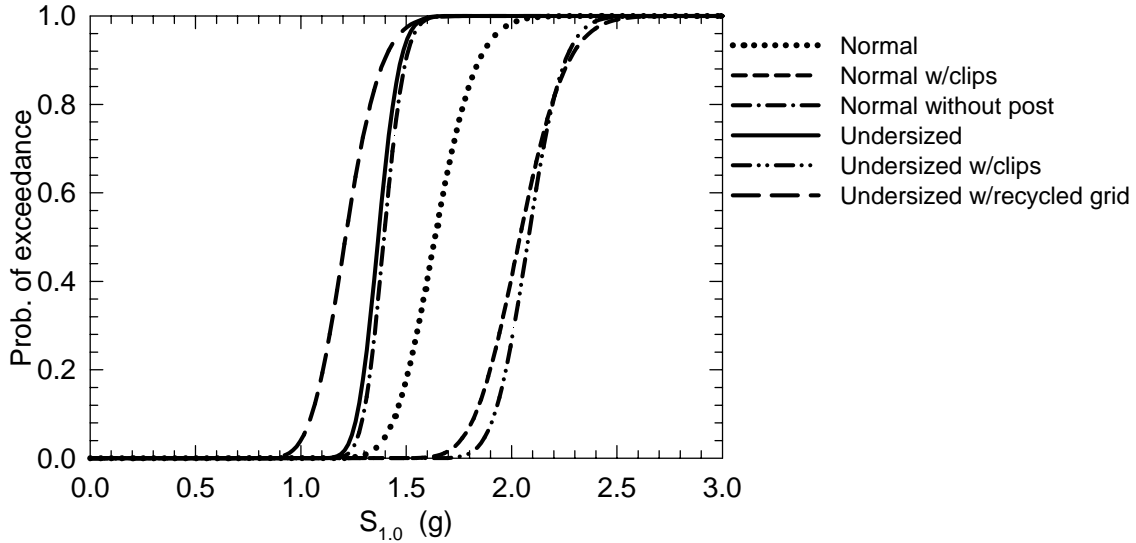
	median	$\beta$
Undersized (C1)	2.84	0.059
Undersized w/clips (C2)		
Undersized w/recycled grid (C3)	2.15	0.130
Normal (C4)	2.96	0.084
Normal w/clips (C5)	2.96	0.084
Normal without post (C6)	3.02	0.106

**FIGURE 7-51 Fragility curves for spectral acceleration at 0.5 second, limit state 3: major damage**



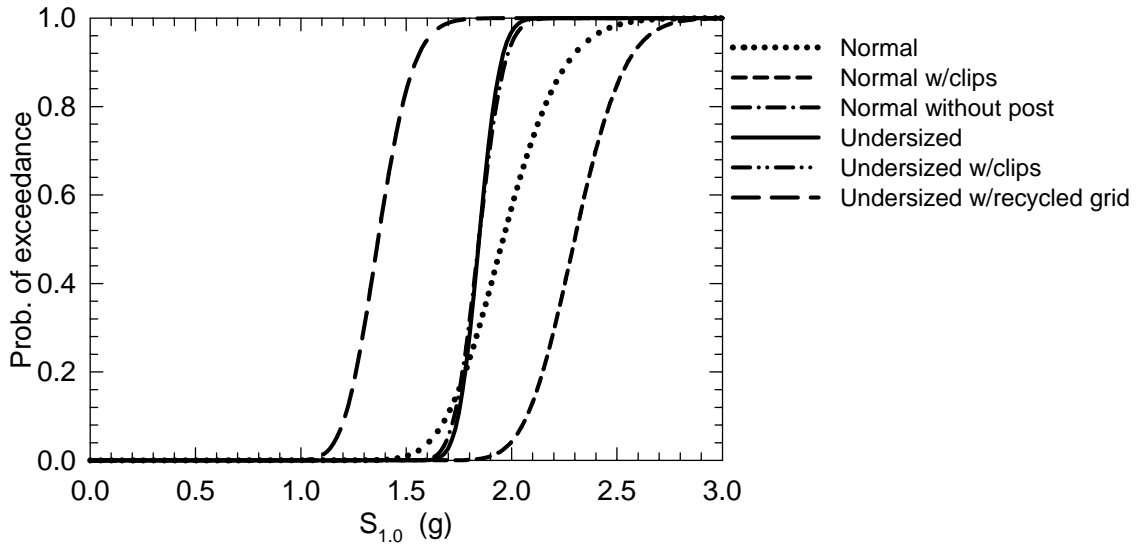
	median	$\beta$
Undersized (C1)	3.08	0.072
Undersized w/clips (C2)	2.42	0.066
Undersized w/recycled grid (C3)	3.08	0.094
Normal (C4)	2.67	0.068
Normal w/clips (C5)	2.32	0.195
Normal without post (C6)	2.84	0.200

**FIGURE 7-52 Fragility curves for spectral acceleration at 0.5 second, limit state 4: grid failure**



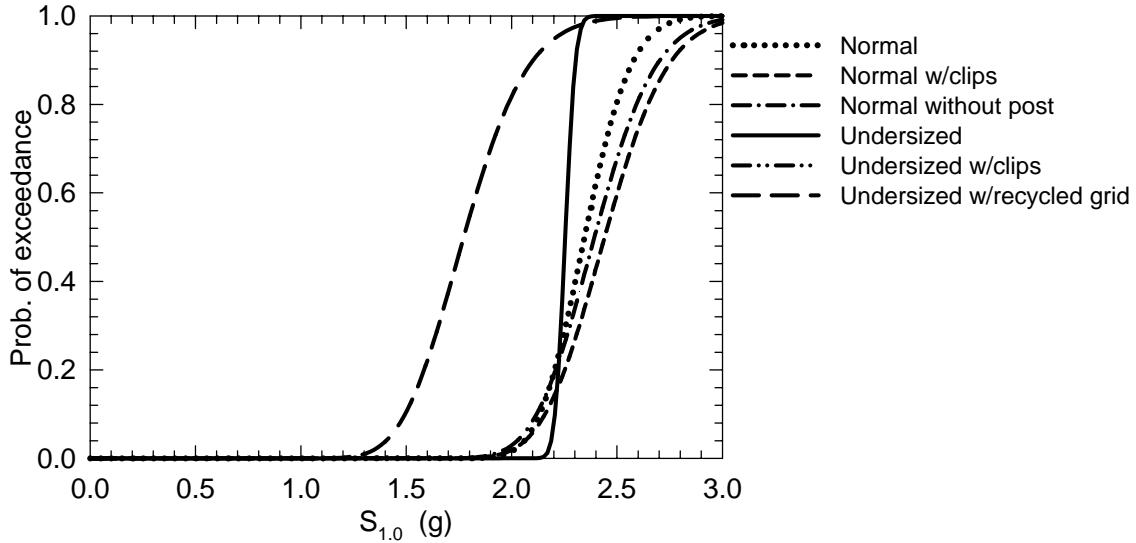
	median	$\beta$
Undersized (C1)	1.36	0.059
Undersized w/clips (C2)	2.08	0.063
Undersized w/recycled grid (C3)	1.21	0.110
Normal (C4)	1.64	0.094
Normal w/clips (C5)	2.04	0.085
Normal without post (C6)	1.39	0.056

**FIGURE 7-53 Fragility curves for spectral acceleration at 1.0 second, limit state 1: minor damage**



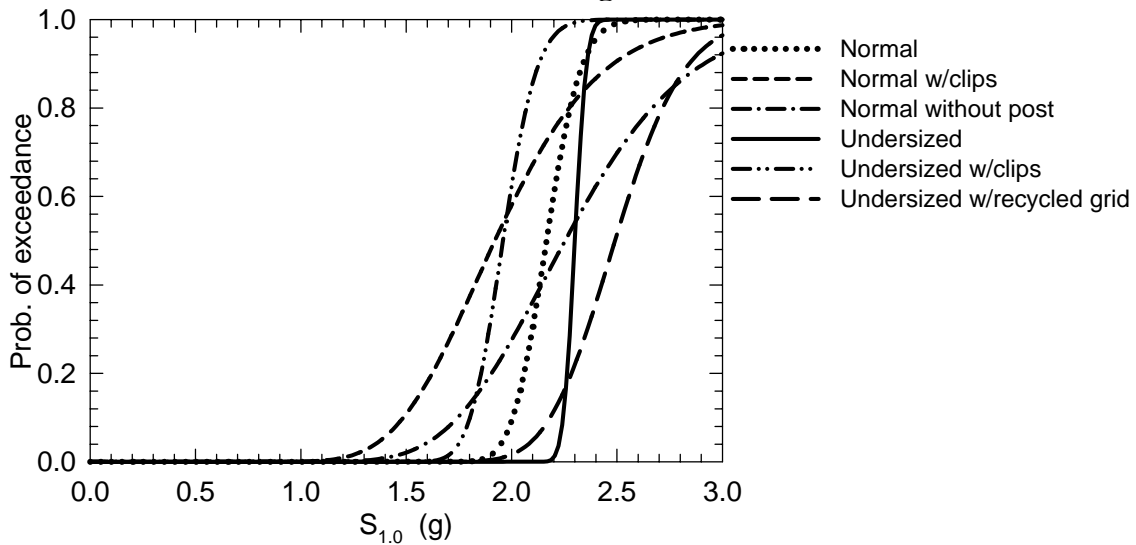
	median	$\beta$
Undersized (C1)	1.84	0.043
Undersized w/clips (C2)	2.29	0.081
Undersized w/recycled grid (C3)	1.36	0.095
Normal (C4)	1.95	0.114
Normal w/clips (C5)	2.29	0.081
Normal without post (C6)	1.84	0.051

**FIGURE 7-54 Fragility curves for spectral acceleration at 1.0 second, limit state 2: moderate damage**



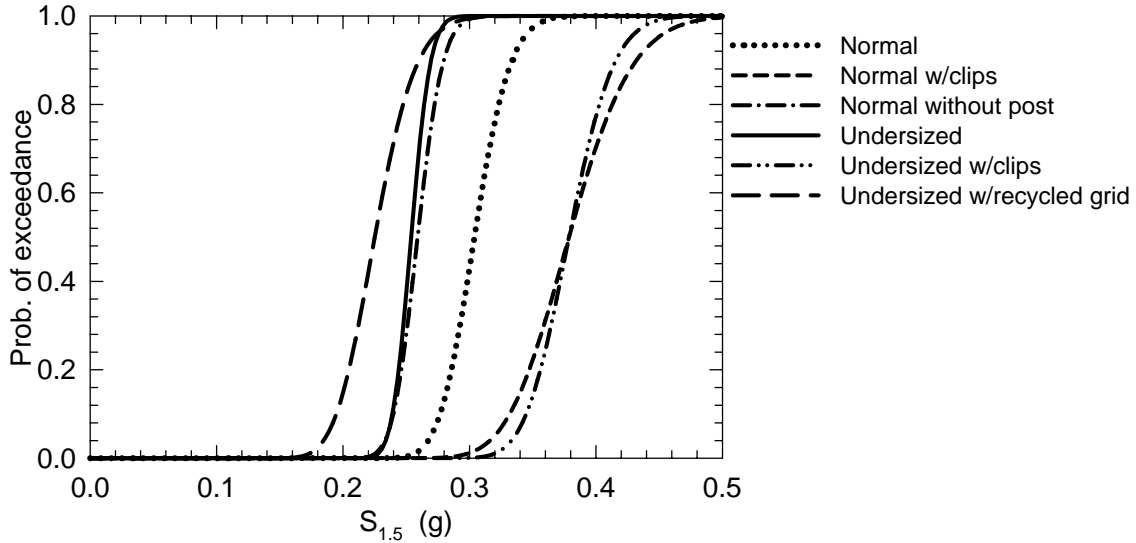
	median	$\beta$
Undersized (C1)	2.25	0.017
Undersized w/clips (C2)		
Undersized w/recycled grid (C3)	1.77	0.133
Normal (C4)	2.34	0.074
Normal w/clips (C5)	2.44	0.096
Normal without post (C6)	2.39	0.095

**FIGURE 7-55 Fragility curves for spectral acceleration at 1.0 second, limit state 3: major damage**



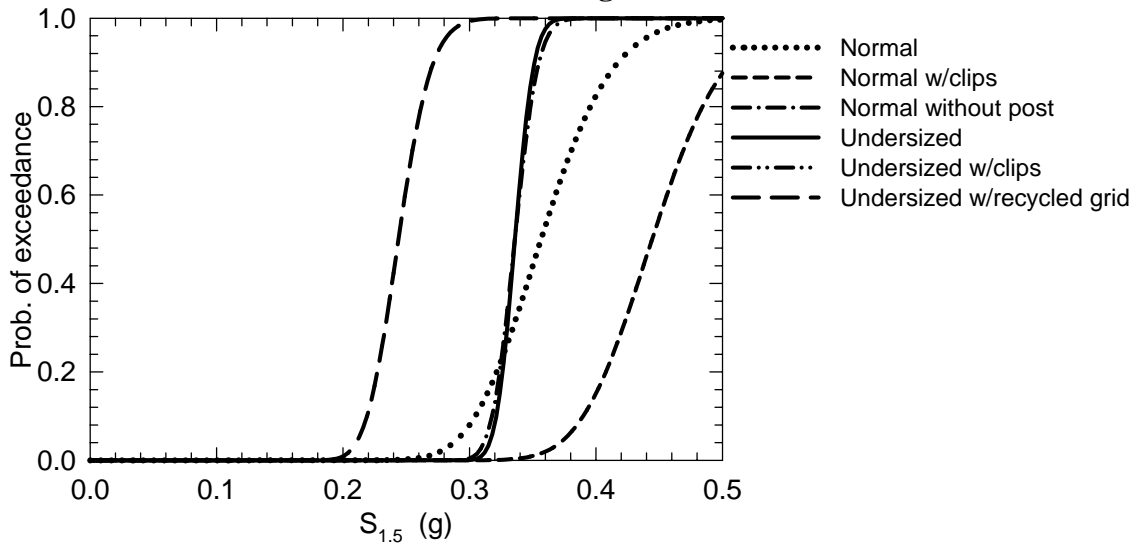
	median	$\beta$
Undersized (C1)	2.30	0.019
Undersized w/clips (C2)	1.95	0.065
Undersized w/recycled grid (C3)	2.49	0.103
Normal (C4)	2.17	0.060
Normal w/clips (C5)	1.92	0.200
Normal without post (C6)	2.24	0.200

**FIGURE 7-56 Fragility curves for spectral acceleration at 1.0 second, limit state 4: grid failure**



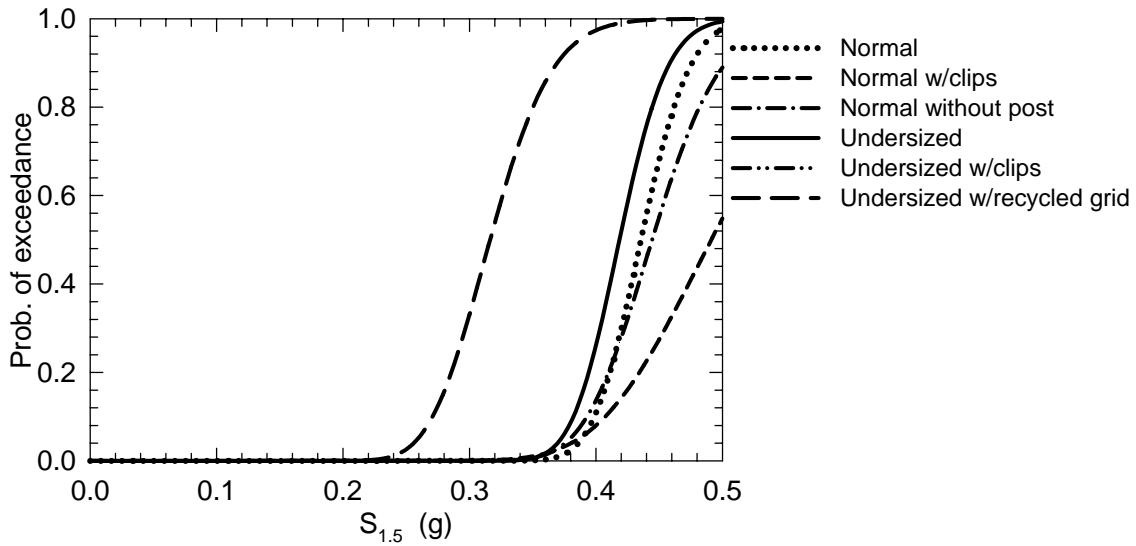
	median	$\beta$
Undersized (C1)	0.25	0.047
Undersized w/clips (C2)	0.37	0.073
Undersized w/recycled grid (C3)	0.22	0.113
Normal (C4)	0.30	0.073
Normal w/clips (C5)	0.38	0.103
Normal without post (C6)	0.25	0.060

**FIGURE 7-57 Fragility curves for spectral acceleration at 1.5 seconds, limit state 1: minor damage**



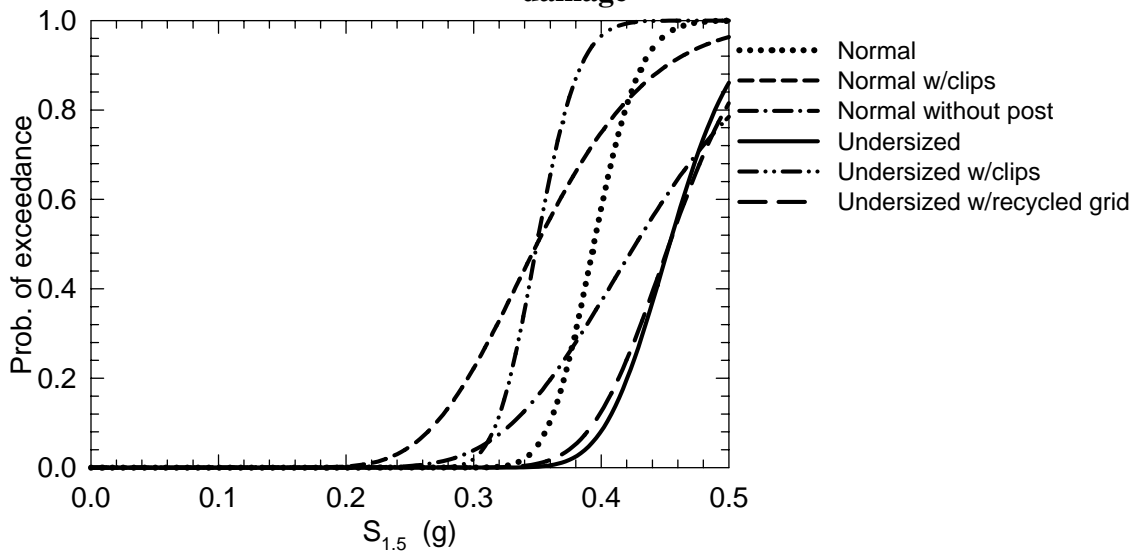
	median	$\beta$
Undersized (C1)	0.33	0.035
Undersized w/clips (C2)	0.24	0.084
Undersized w/recycled grid (C3)	0.24	0.084
Normal (C4)	0.36	0.123
Normal w/clips (C5)	0.44	0.102
Normal without post (C6)	0.33	0.043

**FIGURE 7-58 Fragility curves for spectral acceleration at 1.5 seconds, limit state 2: moderate damage**



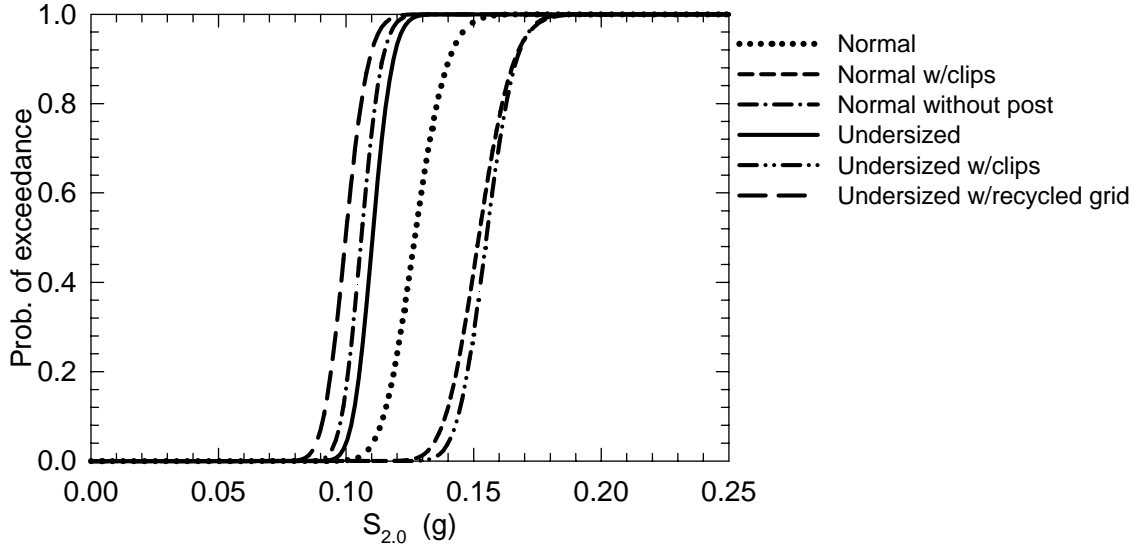
	median	$\beta$
Undersized (C1)	0.41	0.071
Undersized w/clips (C2)		
Undersized w/recycled grid (C3)	0.32	0.121
Normal (C4)	0.43	0.069
Normal w/clips (C5)	0.49	0.146
Normal without post (C6)	0.44	0.096

**FIGURE 7-59** Fragility curves for spectral acceleration at 1.5 seconds, limit state 3: major damage



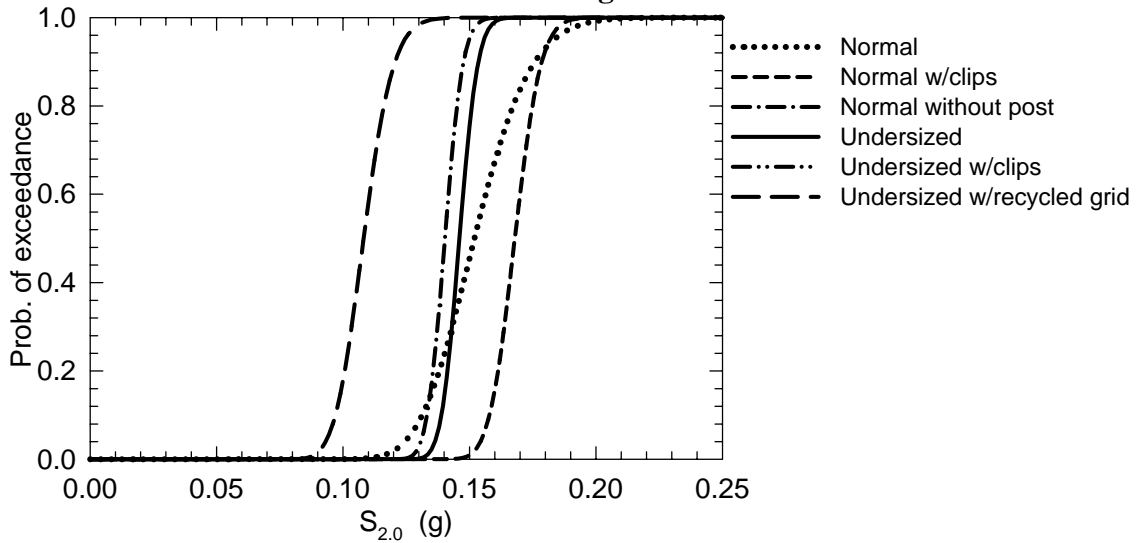
	median	$\beta$
Undersized (C1)	0.45	0.090
Undersized w/clips (C2)	0.34	0.074
Undersized w/recycled grid (C3)	0.45	0.109
Normal (C4)	0.39	0.072
Normal w/clips (C5)	0.35	0.200
Normal without post (C6)	0.42	0.200

**FIGURE 7-60** Fragility curves for spectral acceleration at 1.5 seconds, limit state 4: grid failure



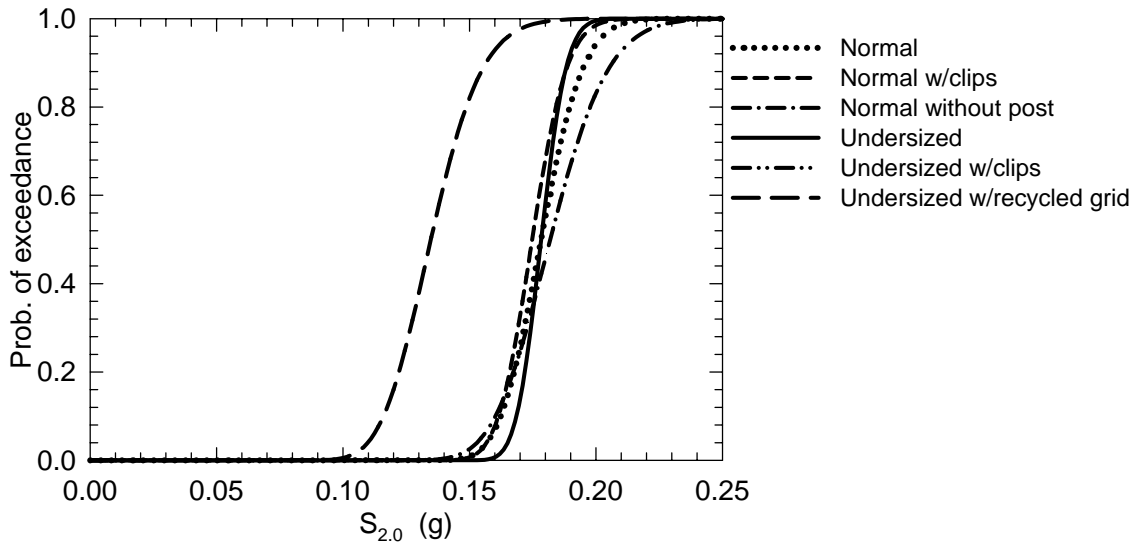
	median	$\beta$
Undersized (C1)	0.11	0.056
Undersized w/clips (C2)	0.15	0.058
Undersized w/recycled grid (C3)	0.10	0.070
Normal (C4)	0.13	0.079
Normal w/clips (C5)	0.15	0.070
Normal without post (C6)	0.10	0.059

**FIGURE 7-61 Fragility curves for spectral acceleration at 2.0 seconds, limit state 1: minor damage**



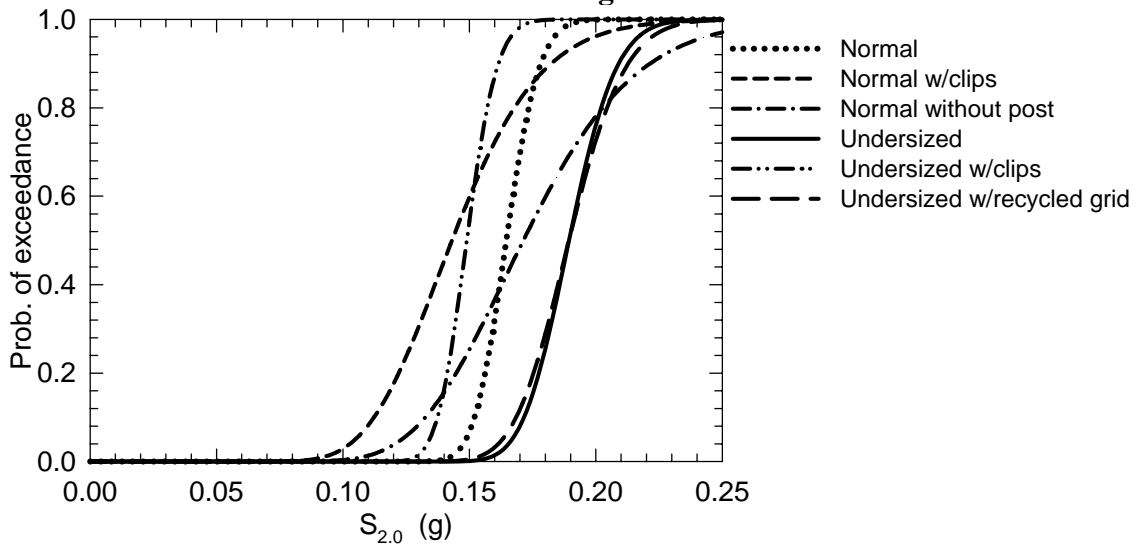
	median	$\beta$
Undersized (C1)	0.14	0.039
Undersized w/clips (C2)	0.11	0.085
Undersized w/recycled grid (C3)	0.15	0.114
Normal (C4)	0.17	0.048
Normal w/clips (C5)	0.14	0.040
Normal without post (C6)	0.14	0.040

**FIGURE 7-62 Fragility curves for spectral acceleration at 2.0 seconds, limit state 2: moderate damage**



	median	$\beta$
Undersized (C1)	0.18	0.044
Undersized w/clips (C2)		
Undersized w/recycled grid (C3)	0.13	0.117
Normal (C4)	0.18	0.073
Normal w/clips (C5)	0.17	0.062
Normal without post (C6)	0.18	0.099

**FIGURE 7-63 Fragility curves for spectral acceleration at 2.0 seconds, limit state 3: major damage**



	median	$\beta$
Undersized (C1)	0.19	0.077
Undersized w/clips (C2)	0.14	0.063
Undersized w/recycled grid (C3)	0.19	0.091
Normal (C4)	0.16	0.062
Normal w/clips (C5)	0.14	0.189
Normal without post (C6)	0.17	0.200

**FIGURE 7-64 Fragility curves for spectral acceleration at 2.0 seconds, limit state 4: grid failure**



## CHAPTER 8

### SUMMARY AND CONCLUSIONS

#### 8.1 Summary

Fragility methods were used in this report to characterize the vulnerability of suspended ceiling systems subjected to earthquake shaking. Since suspended ceiling systems are not amenable to traditional structural analysis, full-scale experimental testing on an earthquake simulator was performed to obtain fragility data. The ceiling systems were composed of tiles and a suspension system. The tiles were installed in the suspension system. The suspension system was hung with wires from the top of a steel test frame. The test frame was mounted on the earthquake simulator.

Four variables that affect the seismic performance of suspended ceiling systems were investigated in this study: (1) the size and weight of tiles, (2) the use of retainer clips, (3) the use of compression posts, and (4) the physical condition of grid components. A total of six configurations were conformed using different combinations of these variables: (1) undersized tiles, (2) undersized tiles with retainer clips, (3) undersized tiles with recycled grid components, (4) normal sized tiles, (5) normal sized tiles with retainer clips and (6) normal sized tiles without the compression post. Configuration 4 meets the requirements of the International Building Code for Seismic Design Categories D, E and F and the CISCA requirements for seismic zones 3 and 4 (CISCA, 1992).

Each configuration was tested multiple times on the earthquake simulator of the Structural Engineering and Earthquake Simulation Laboratory (SEESL) of the University at Buffalo (SUNY) with a testing protocol that included unidirectional (in the horizontal and vertical directions) and combined (horizontal + vertical) earthquake excitations. White noise was used to evaluate the dynamic characteristics of the testing frame and the ceiling systems as part of the testing protocol. The earthquake histories used for testing were generated using the guidelines presented in ICBO AC156, 2000, from ICBO Evaluation Service, Inc. "Acceptance Criteria for Seismic Qualification Testing of Nonstructural Components". The intensity of the earthquake

shaking was characterized by the NEHRP maximum considered earthquake short period spectral acceleration,  $S_S$ . The target values of  $S_S$  ranged between 0.25g and 2.5g.

Four limit states of response that cover most of the performance levels described in the code guidelines for the seismic performance of nonstructural components were defined using physical definitions of damage. Limit states 1 through 3 account for the number (or percentage) of tiles that fell from the suspension grid, whereas the fourth limit state indicates whether failure occurred in the suspension grid. The four limit states were termed as: (1) minor damage, (2) moderate damage, (3) major damage, and (4) grid failure. Data was obtained for every limit state to compare the effect of each configuration on the response of the suspended ceiling systems. The results from the full-scale testing were presented in form of seismic fragility curves.

Two parameters were used to measure the ground motion intensity of the empirically developed fragility curves: peak ground acceleration and the average horizontal spectral accelerations at selected periods. The selected periods represented a broad range that includes most of the in-service conditions of suspended ceiling systems installed in buildings. The fragility curves provided a useful decision-making tool for safety assessment of suspended ceiling systems. The following paragraphs describe the main findings and conclusions of this research project.

## **8.2 Conclusions**

The key conclusions of the fragility study described in this report are:

1. The combined horizontal and vertical motions generally produced more damage in the ceiling system than either of the unidirectional excitations.
2. The most common failure mode of tiles when retention clips were not used was tiles popping out of the grid. If the tiles did not return to the original position on the suspension system, it was very likely for the tiles to rotate and fall to the simulator platform below.

3. The use of retainer clips substantially improved the behavior of the suspended ceiling systems in terms of loss of tiles. However, by retaining the tiles, the use of clips increased the inertial loads on the grid, resulting in grid damage at lower levels of shaking. The loss of tiles in systems with retention clips was due primarily to the failure of grid components.
4. Including recycled cross-tees in the assemblage of the suspended grid substantially increased the number of tiles that fell during the earthquake tests because the locking assembly latches that secured the connection between the cross tees did not lock completely, leaving the mechanical connection between the cross tees slightly loose. The ability to transfer load between adjacent sections of the ceiling grid was therefore compromised by comparison with the systems where only new grid components were used.
5. The effect of a small variation in tile size on the performance of the ceiling systems was considerable in terms of loss of tiles. The number of tiles that fell during the earthquake shaking tests of ceiling systems with undersized or poorly fitting tiles was substantially larger by comparison with the systems equipped with normal sized (snug) tiles.
6. The rivets that attached the main runners and cross tees to the wall molding played a very important role in the seismic performance of the suspended ceiling systems. When a rivet came loose or was destroyed during shaking, the damage in the ceiling systems in terms of loss of tiles was much larger than when all of the rivets were undamaged and the cross tees remained firmly attached to the wall molding.
7. The main beams provided most of the stiffness in the suspension grid in the horizontal and vertical directions. However, the connections between the main beams were substantially more flexible than the main beams. This is clearly reflected in the performance of the ceiling systems in terms of loss of tiles because the first tiles to fall in most of the tests were the tiles located around connections between two main beams. A more effective method of connecting the main beams could be developed to reduce the likelihood of the ceiling failure.

8. The region beyond the intersection of the fragility curves for limits state 3 (major tile failure) and limit state 4 (grid failure) should be avoided because failure of large sections of tiles and grid could pose a life-safety hazard.
  
9. The usefulness of fragility curves was demonstrated when it was not clear from field observations whether including compression posts improved the seismic performance of the suspended ceiling systems. Using the fragility curves, it was clear that including the compression post in suspended ceiling systems improves the seismic performance of the systems in terms of reduced damage to the tiles and grid.

## CHAPTER 9

### REFERENCES

ANCO. (1983). “Seismic Hazard Assessment of Nonstructural Ceiling Components”, NSF Rep. No. CEE-8114155.

ANCO. (1993). “Earthquake Testing of a Suspended Ceiling System”, ANCO Engineers Inc., Culver City, California.

ASTM C635-00. (2000). “Standard Specification for the Manufacture, Performance, and Testing of Metal Suspension Systems for Acoustical Tile and Lay-in Panel Ceilings”, ASTM International, Volume 04.06.

ASTM E580-00. (2000). “Standard Practice for Application of Ceiling Suspension Systems for Acoustical Tile and Lay-in Panels in Areas Requiring Moderate Seismic Restraint”, ASTM International, Volume 04.06.

Badillo, H., Kusumastuti, D., Reinhorn A. M. and Whittaker A. S. (2002). “Testing for Seismic Qualification of Suspended Ceiling Systems, Part I”, Report No. UB CSEE/SEESL-2002-01, State University of New York at Buffalo, Buffalo, New York.

Badillo, H., Whittaker, A. S. and Reinhorn, A. M. (2003a). “Testing for Seismic Qualification of Suspended Ceiling Systems, Part III”, Report No. UB CSEE/SEESL-2003-02, State University of New York at Buffalo, Buffalo, New York.

Badillo, H., Whittaker, A. S. and Reinhorn, A. M. (2003b). “Testing for Seismic Qualification of Suspended Ceiling Systems, Part IV”, Report No. UB CSEE/SEESL-2003-01, State University of New York at Buffalo, Buffalo, New York.

Benuska, L. (1990). “Loma Prieta Earthquake Reconnaissance Report”, Earthquake Spectra, Supplement to Vol. 6, 339–377.

Box, G. E. P., and Tiao, G. C. (1992). “Bayesian Inference in Statistical Analysis”, Addison-Wesley, Reading, Massachusetts.

Bracci, J. M., Reinhorn, A. M. and Mander, J. B. (1992) “Seismic Resistance of Reinforced Concrete Frame Structures Designed Only for Gravity Loads: Part III - Experimental Performance and Analytical Study of a Structural Model” Technical Report NCEER-92-0029, National Center for Earthquake Engineering Research, SUNY/Buffalo.

Ceiling and Interior System Contractors (CISCA). (1992). “Guidelines for Seismic Restraint for Direct-hung Suspended Ceiling Assemblies (zones 3-4)”, 1500 Lincoln Highway, Suite 202, St. Charles, Illinois, 60174.

Cimellaro, G. P., Reinhorn, A. M. and Bruneau, M. (2005). “Resilience of a Health Care Facility,” Proceedings of the Annual Meeting of The Asian Pacific Network of Centers for Earthquake Engineering Research, South Korea.

Clough, R. W. and Penzien, J. (1993). “Dynamics of Structures”, 2nd Edition, McGraw-Hill.

Cornell, C. A., Jalayer, F., Hamburger, R. O. and Foutch, D. A. (2001). “Probabilistic Basis for the 2000 SAC Federal Emergency Management Agency Steel Moment Frame Guidelines”, Journal of Structural Engineering, Vol. 128, No. 4, pp. 526–533.

Der Kiureghian, A. (1999). “A Bayesian Framework For Fragility Assessment”, Proc., 8th Int. Conf. on Applications of Statistics and Probability (ICASP) in Civil Eng. Reliability and Risk Analysis, R.E. Melchers and M. G. Stewart, eds., Vol. 2, 1003–1010.

Ellingwood, B. and Tekie, P. B. (2001). “Fragility Analysis of Concrete Gravity Dams”, Journal of Infrastructure Systems, Vol. 7, No. 2, pp. 41-48.

Federal Emergency Management Agency (FEMA). (2000). “NEHRP Recommended Provisions for Seismic Regulations for New Buildings and Other Structures. Part 1-Provisions, 2000 Edition”, Report No. FEMA 386, Washington D.C.

Hamburger, R. O., Rojahn, C., Moehle, J. P., Bachman, R., Comartin, C. D. and Whittaker, A. S. (2004). “Development of Next-generation Performance-based Earthquake Engineering Design Criteria for Buildings”, Proceedings, 13th World Conference on Earthquake Engineering, Paper 1819, Vancouver, B.C., Canada.

International Conference of Building Officials (ICBO). (2000). “ICBO AC156 Acceptance Criteria for the Seismic Qualification of Nonstructural Components”, ICBO Evaluation Service, Inc., Whittier, California.

International Code Council (ICC). (2000). “International Building Code, 2000 Edition (IBC 2000)”, Falls Church, Virginia.

Kusumastuti, D., Badillo, H., Reinhorn A. M. and Whittaker A. S. (2002). “Testing for Seismic Qualification of Suspended Ceiling Systems, Part II”, Report No. UB CSEE/SEESL-2002-02, State University of New York at Buffalo, Buffalo, New York.

Mathworks, Inc. (1999). “Matlab, The Language of Technical Computing”, Version 5.3 (R11.1). The Mathworks, Inc.

Moehle, J. P. (2003). “A Framework for Performance-based Earthquake Engineering”, Proceedings, Tenth U.S.-Japan Workshop on Improvement of Building Seismic Design and Construction Practices, Report ATC-15-9, Applied Technology Council, Redwood City, California.

MTS Systems Corporation. (1991). “STEX - Seismic Test Execution Software”, MTS Systems Corp., Box 24012, Minneapolis, Minnesota 55424.

- Park, Y-J. and Ang, A. H-S. (1985a). “Mechanistic Seismic Damage Model for Reinforced Concrete”, *Journal of Structural Engineering*, Vol. 111, No. 4, pp. 722-739
- Park, Y-J. and Ang, A. H-S. (1985b). “Seismic Damage Analysis of Reinforced Concrete Buildings”, *Journal of Structural Engineering*, Vol. 111, No. 4, pp. 740-757.
- Reed, J. and Kennedy, R. P. (1994). “Methodology for Developing Seismic Fragilities”, EPRI Report TR-103959, Electric Power research Institute, Palo Alto, California.
- Reinhorn, A. M., Barron-Corvera R. and Ayala, A. G. (2002), “Global Spectral Evaluation of Seismic Fragility of Structures”, *Proceedings of the 7th U.S. National Conference on Earthquake Engineering (7NCEE)*, Vol. 4, pp. 3529-3537.
- Rihal, S. and Granneman, G. (1984). “Experimental Investigation of the Dynamic Behavior of Building Partitions and Suspended Ceilings during Earthquakes”, Report No. ARCE R84-1, California Polytechnic State University, Pomona, California.
- Sasani, M. and Der Kiureghian, A. (2001). “Seismic Fragility of RC Structural Walls: Displacement Approach”, *Journal of Structural Engineering*, Vol. 127, No.2, pp. 219-228.
- Sharpe, R., Kost, G. and Lord, J. (1973). “Behavior Of Structural Systems Under Dynamic Loads”, *Building Practices for Disaster Mitigation, Building Science Series 46*, National Bureau of Standards, 352–394.
- Shinozuka, M., Grigoriu M., Ingrassia, A. R., Billington, S. L., Feenstra, P., Soong T. T., Reinhorn A. M. and Maragakis, E. (2000a). “Development of Fragility Information for Structures and Nonstructural Components”, *MCEER Research Progress and Accomplishments, Volume 1999-2000*, State University of New York at Buffalo, Buffalo, New York, pp. 15-32.
- Shinozuka, M., Feng, M. Q., Lee, J. and Naganuma, T. (2000b). “Statistical Analysis of Fragility Curves”, *Journal of Engineering Mechanics*, Vol. 126, No. 12, pp. 1224–1231
- Singhal, A. and Kiremidjian, A. S. (1996). “Method for Probabilistic Evaluation of Seismic Structural Damage”, *Journal of Structural Engineering*, Vol. 122, No.12, pp. 1459-1467.
- Smith, S. W. (1999). “The Scientist and Engineer's Guide to Digital Signal Processing”, 2nd Edition, California Technical Publishing, San Diego, California.
- International Conference of Building Officials (ICBO). (1991). *Uniform Building Code*, Whittier, California.
- Whittaker, A. S., Fenves, G. L. and Gilani, A. S. J. (2003). “Earthquake Performance of Porcelain Transformer Bushings”, *Earthquake Spectra*, Vol. 19, No. 4.
- Yao, G. C. (2000). “Seismic Performance of Direct Hung Suspended Ceiling Systems”, *Journal of Architectural Engineering*, Vol. 6, No. 1, pp. 6-11.





## **Multidisciplinary Center for Earthquake Engineering Research List of Technical Reports**

The Multidisciplinary Center for Earthquake Engineering Research (MCEER) publishes technical reports on a variety of subjects related to earthquake engineering written by authors funded through MCEER. These reports are available from both MCEER Publications and the National Technical Information Service (NTIS). Requests for reports should be directed to MCEER Publications, Multidisciplinary Center for Earthquake Engineering Research, State University of New York at Buffalo, Red Jacket Quadrangle, Buffalo, New York 14261. Reports can also be requested through NTIS, 5285 Port Royal Road, Springfield, Virginia 22161. NTIS accession numbers are shown in parenthesis, if available.

- NCEER-87-0001 "First-Year Program in Research, Education and Technology Transfer," 3/5/87, (PB88-134275, A04, MF-A01).
- NCEER-87-0002 "Experimental Evaluation of Instantaneous Optimal Algorithms for Structural Control," by R.C. Lin, T.T. Soong and A.M. Reinhorn, 4/20/87, (PB88-134341, A04, MF-A01).
- NCEER-87-0003 "Experimentation Using the Earthquake Simulation Facilities at University at Buffalo," by A.M. Reinhorn and R.L. Ketter, to be published.
- NCEER-87-0004 "The System Characteristics and Performance of a Shaking Table," by J.S. Hwang, K.C. Chang and G.C. Lee, 6/1/87, (PB88-134259, A03, MF-A01). This report is available only through NTIS (see address given above).
- NCEER-87-0005 "A Finite Element Formulation for Nonlinear Viscoplastic Material Using a Q Model," by O. Gyebi and G. Dasgupta, 11/2/87, (PB88-213764, A08, MF-A01).
- NCEER-87-0006 "Symbolic Manipulation Program (SMP) - Algebraic Codes for Two and Three Dimensional Finite Element Formulations," by X. Lee and G. Dasgupta, 11/9/87, (PB88-218522, A05, MF-A01).
- NCEER-87-0007 "Instantaneous Optimal Control Laws for Tall Buildings Under Seismic Excitations," by J.N. Yang, A. Akbarpour and P. Ghaemmaghami, 6/10/87, (PB88-134333, A06, MF-A01). This report is only available through NTIS (see address given above).
- NCEER-87-0008 "IDARC: Inelastic Damage Analysis of Reinforced Concrete Frame - Shear-Wall Structures," by Y.J. Park, A.M. Reinhorn and S.K. Kunnath, 7/20/87, (PB88-134325, A09, MF-A01). This report is only available through NTIS (see address given above).
- NCEER-87-0009 "Liquefaction Potential for New York State: A Preliminary Report on Sites in Manhattan and Buffalo," by M. Budhu, V. Vijayakumar, R.F. Giese and L. Baumgras, 8/31/87, (PB88-163704, A03, MF-A01). This report is available only through NTIS (see address given above).
- NCEER-87-0010 "Vertical and Torsional Vibration of Foundations in Inhomogeneous Media," by A.S. Veletsos and K.W. Dotson, 6/1/87, (PB88-134291, A03, MF-A01). This report is only available through NTIS (see address given above).
- NCEER-87-0011 "Seismic Probabilistic Risk Assessment and Seismic Margins Studies for Nuclear Power Plants," by Howard H.M. Hwang, 6/15/87, (PB88-134267, A03, MF-A01). This report is only available through NTIS (see address given above).
- NCEER-87-0012 "Parametric Studies of Frequency Response of Secondary Systems Under Ground-Acceleration Excitations," by Y. Yong and Y.K. Lin, 6/10/87, (PB88-134309, A03, MF-A01). This report is only available through NTIS (see address given above).
- NCEER-87-0013 "Frequency Response of Secondary Systems Under Seismic Excitation," by J.A. HoLung, J. Cai and Y.K. Lin, 7/31/87, (PB88-134317, A05, MF-A01). This report is only available through NTIS (see address given above).
- NCEER-87-0014 "Modelling Earthquake Ground Motions in Seismically Active Regions Using Parametric Time Series Methods," by G.W. Ellis and A.S. Cakmak, 8/25/87, (PB88-134283, A08, MF-A01). This report is only available through NTIS (see address given above).

- NCEER-87-0015 "Detection and Assessment of Seismic Structural Damage," by E. DiPasquale and A.S. Cakmak, 8/25/87, (PB88-163712, A05, MF-A01). This report is only available through NTIS (see address given above).
- NCEER-87-0016 "Pipeline Experiment at Parkfield, California," by J. Isenberg and E. Richardson, 9/15/87, (PB88-163720, A03, MF-A01). This report is available only through NTIS (see address given above).
- NCEER-87-0017 "Digital Simulation of Seismic Ground Motion," by M. Shinozuka, G. Deodatis and T. Harada, 8/31/87, (PB88-155197, A04, MF-A01). This report is available only through NTIS (see address given above).
- NCEER-87-0018 "Practical Considerations for Structural Control: System Uncertainty, System Time Delay and Truncation of Small Control Forces," J.N. Yang and A. Akbarpour, 8/10/87, (PB88-163738, A08, MF-A01). This report is only available through NTIS (see address given above).
- NCEER-87-0019 "Modal Analysis of Nonclassically Damped Structural Systems Using Canonical Transformation," by J.N. Yang, S. Sarkani and F.X. Long, 9/27/87, (PB88-187851, A04, MF-A01).
- NCEER-87-0020 "A Nonstationary Solution in Random Vibration Theory," by J.R. Red-Horse and P.D. Spanos, 11/3/87, (PB88-163746, A03, MF-A01).
- NCEER-87-0021 "Horizontal Impedances for Radially Inhomogeneous Viscoelastic Soil Layers," by A.S. Veletsos and K.W. Dotson, 10/15/87, (PB88-150859, A04, MF-A01).
- NCEER-87-0022 "Seismic Damage Assessment of Reinforced Concrete Members," by Y.S. Chung, C. Meyer and M. Shinozuka, 10/9/87, (PB88-150867, A05, MF-A01). This report is available only through NTIS (see address given above).
- NCEER-87-0023 "Active Structural Control in Civil Engineering," by T.T. Soong, 11/11/87, (PB88-187778, A03, MF-A01).
- NCEER-87-0024 "Vertical and Torsional Impedances for Radially Inhomogeneous Viscoelastic Soil Layers," by K.W. Dotson and A.S. Veletsos, 12/87, (PB88-187786, A03, MF-A01).
- NCEER-87-0025 "Proceedings from the Symposium on Seismic Hazards, Ground Motions, Soil-Liquefaction and Engineering Practice in Eastern North America," October 20-22, 1987, edited by K.H. Jacob, 12/87, (PB88-188115, A23, MF-A01). This report is available only through NTIS (see address given above).
- NCEER-87-0026 "Report on the Whittier-Narrows, California, Earthquake of October 1, 1987," by J. Pantelic and A. Reinhorn, 11/87, (PB88-187752, A03, MF-A01). This report is available only through NTIS (see address given above).
- NCEER-87-0027 "Design of a Modular Program for Transient Nonlinear Analysis of Large 3-D Building Structures," by S. Srivastav and J.F. Abel, 12/30/87, (PB88-187950, A05, MF-A01). This report is only available through NTIS (see address given above).
- NCEER-87-0028 "Second-Year Program in Research, Education and Technology Transfer," 3/8/88, (PB88-219480, A04, MF-A01).
- NCEER-88-0001 "Workshop on Seismic Computer Analysis and Design of Buildings With Interactive Graphics," by W. McGuire, J.F. Abel and C.H. Conley, 1/18/88, (PB88-187760, A03, MF-A01). This report is only available through NTIS (see address given above).
- NCEER-88-0002 "Optimal Control of Nonlinear Flexible Structures," by J.N. Yang, F.X. Long and D. Wong, 1/22/88, (PB88-213772, A06, MF-A01).
- NCEER-88-0003 "Substructuring Techniques in the Time Domain for Primary-Secondary Structural Systems," by G.D. Manolis and G. Juhn, 2/10/88, (PB88-213780, A04, MF-A01).
- NCEER-88-0004 "Iterative Seismic Analysis of Primary-Secondary Systems," by A. Singhal, L.D. Lutes and P.D. Spanos, 2/23/88, (PB88-213798, A04, MF-A01).

- NCEER-88-0005 "Stochastic Finite Element Expansion for Random Media," by P.D. Spanos and R. Ghanem, 3/14/88, (PB88-213806, A03, MF-A01).
- NCEER-88-0006 "Combining Structural Optimization and Structural Control," by F.Y. Cheng and C.P. Pantelides, 1/10/88, (PB88-213814, A05, MF-A01).
- NCEER-88-0007 "Seismic Performance Assessment of Code-Designed Structures," by H.H-M. Hwang, J-W. Jaw and H-J. Shau, 3/20/88, (PB88-219423, A04, MF-A01). This report is only available through NTIS (see address given above).
- NCEER-88-0008 "Reliability Analysis of Code-Designed Structures Under Natural Hazards," by H.H-M. Hwang, H. Ushiba and M. Shinozuka, 2/29/88, (PB88-229471, A07, MF-A01). This report is only available through NTIS (see address given above).
- NCEER-88-0009 "Seismic Fragility Analysis of Shear Wall Structures," by J-W Jaw and H.H-M. Hwang, 4/30/88, (PB89-102867, A04, MF-A01).
- NCEER-88-0010 "Base Isolation of a Multi-Story Building Under a Harmonic Ground Motion - A Comparison of Performances of Various Systems," by F-G Fan, G. Ahmadi and I.G. Tadjbakhsh, 5/18/88, (PB89-122238, A06, MF-A01). This report is only available through NTIS (see address given above).
- NCEER-88-0011 "Seismic Floor Response Spectra for a Combined System by Green's Functions," by F.M. Lavelle, L.A. Bergman and P.D. Spanos, 5/1/88, (PB89-102875, A03, MF-A01).
- NCEER-88-0012 "A New Solution Technique for Randomly Excited Hysteretic Structures," by G.Q. Cai and Y.K. Lin, 5/16/88, (PB89-102883, A03, MF-A01).
- NCEER-88-0013 "A Study of Radiation Damping and Soil-Structure Interaction Effects in the Centrifuge," by K. Weissman, supervised by J.H. Prevost, 5/24/88, (PB89-144703, A06, MF-A01).
- NCEER-88-0014 "Parameter Identification and Implementation of a Kinematic Plasticity Model for Frictional Soils," by J.H. Prevost and D.V. Griffiths, to be published.
- NCEER-88-0015 "Two- and Three- Dimensional Dynamic Finite Element Analyses of the Long Valley Dam," by D.V. Griffiths and J.H. Prevost, 6/17/88, (PB89-144711, A04, MF-A01).
- NCEER-88-0016 "Damage Assessment of Reinforced Concrete Structures in Eastern United States," by A.M. Reinhorn, M.J. Seidel, S.K. Kunnath and Y.J. Park, 6/15/88, (PB89-122220, A04, MF-A01). This report is only available through NTIS (see address given above).
- NCEER-88-0017 "Dynamic Compliance of Vertically Loaded Strip Foundations in Multilayered Viscoelastic Soils," by S. Ahmad and A.S.M. Israil, 6/17/88, (PB89-102891, A04, MF-A01).
- NCEER-88-0018 "An Experimental Study of Seismic Structural Response With Added Viscoelastic Dampers," by R.C. Lin, Z. Liang, T.T. Soong and R.H. Zhang, 6/30/88, (PB89-122212, A05, MF-A01). This report is available only through NTIS (see address given above).
- NCEER-88-0019 "Experimental Investigation of Primary - Secondary System Interaction," by G.D. Manolis, G. Juhn and A.M. Reinhorn, 5/27/88, (PB89-122204, A04, MF-A01).
- NCEER-88-0020 "A Response Spectrum Approach For Analysis of Nonclassically Damped Structures," by J.N. Yang, S. Sarkani and F.X. Long, 4/22/88, (PB89-102909, A04, MF-A01).
- NCEER-88-0021 "Seismic Interaction of Structures and Soils: Stochastic Approach," by A.S. Veletsos and A.M. Prasad, 7/21/88, (PB89-122196, A04, MF-A01). This report is only available through NTIS (see address given above).
- NCEER-88-0022 "Identification of the Serviceability Limit State and Detection of Seismic Structural Damage," by E. DiPasquale and A.S. Cakmak, 6/15/88, (PB89-122188, A05, MF-A01). This report is available only through NTIS (see address given above).

- NCEER-88-0023 "Multi-Hazard Risk Analysis: Case of a Simple Offshore Structure," by B.K. Bhartia and E.H. Vanmarcke, 7/21/88, (PB89-145213, A05, MF-A01).
- NCEER-88-0024 "Automated Seismic Design of Reinforced Concrete Buildings," by Y.S. Chung, C. Meyer and M. Shinozuka, 7/5/88, (PB89-122170, A06, MF-A01). This report is available only through NTIS (see address given above).
- NCEER-88-0025 "Experimental Study of Active Control of MDOF Structures Under Seismic Excitations," by L.L. Chung, R.C. Lin, T.T. Soong and A.M. Reinhorn, 7/10/88, (PB89-122600, A04, MF-A01).
- NCEER-88-0026 "Earthquake Simulation Tests of a Low-Rise Metal Structure," by J.S. Hwang, K.C. Chang, G.C. Lee and R.L. Ketter, 8/1/88, (PB89-102917, A04, MF-A01).
- NCEER-88-0027 "Systems Study of Urban Response and Reconstruction Due to Catastrophic Earthquakes," by F. Kozin and H.K. Zhou, 9/22/88, (PB90-162348, A04, MF-A01).
- NCEER-88-0028 "Seismic Fragility Analysis of Plane Frame Structures," by H.H-M. Hwang and Y.K. Low, 7/31/88, (PB89-131445, A06, MF-A01).
- NCEER-88-0029 "Response Analysis of Stochastic Structures," by A. Kardara, C. Bucher and M. Shinozuka, 9/22/88, (PB89-174429, A04, MF-A01).
- NCEER-88-0030 "Nonnormal Accelerations Due to Yielding in a Primary Structure," by D.C.K. Chen and L.D. Lutes, 9/19/88, (PB89-131437, A04, MF-A01).
- NCEER-88-0031 "Design Approaches for Soil-Structure Interaction," by A.S. Veletsos, A.M. Prasad and Y. Tang, 12/30/88, (PB89-174437, A03, MF-A01). This report is available only through NTIS (see address given above).
- NCEER-88-0032 "A Re-evaluation of Design Spectra for Seismic Damage Control," by C.J. Turkstra and A.G. Tallin, 11/7/88, (PB89-145221, A05, MF-A01).
- NCEER-88-0033 "The Behavior and Design of Noncontact Lap Splices Subjected to Repeated Inelastic Tensile Loading," by V.E. Sagan, P. Gergely and R.N. White, 12/8/88, (PB89-163737, A08, MF-A01).
- NCEER-88-0034 "Seismic Response of Pile Foundations," by S.M. Mamoon, P.K. Banerjee and S. Ahmad, 11/1/88, (PB89-145239, A04, MF-A01).
- NCEER-88-0035 "Modeling of R/C Building Structures With Flexible Floor Diaphragms (IDARC2)," by A.M. Reinhorn, S.K. Kunnath and N. Panahshahi, 9/7/88, (PB89-207153, A07, MF-A01).
- NCEER-88-0036 "Solution of the Dam-Reservoir Interaction Problem Using a Combination of FEM, BEM with Particular Integrals, Modal Analysis, and Substructuring," by C-S. Tsai, G.C. Lee and R.L. Ketter, 12/31/88, (PB89-207146, A04, MF-A01).
- NCEER-88-0037 "Optimal Placement of Actuators for Structural Control," by F.Y. Cheng and C.P. Pantelides, 8/15/88, (PB89-162846, A05, MF-A01).
- NCEER-88-0038 "Teflon Bearings in Aseismic Base Isolation: Experimental Studies and Mathematical Modeling," by A. Mokha, M.C. Constantinou and A.M. Reinhorn, 12/5/88, (PB89-218457, A10, MF-A01). This report is available only through NTIS (see address given above).
- NCEER-88-0039 "Seismic Behavior of Flat Slab High-Rise Buildings in the New York City Area," by P. Weidlinger and M. Ettouney, 10/15/88, (PB90-145681, A04, MF-A01).
- NCEER-88-0040 "Evaluation of the Earthquake Resistance of Existing Buildings in New York City," by P. Weidlinger and M. Ettouney, 10/15/88, to be published.
- NCEER-88-0041 "Small-Scale Modeling Techniques for Reinforced Concrete Structures Subjected to Seismic Loads," by W. Kim, A. El-Attar and R.N. White, 11/22/88, (PB89-189625, A05, MF-A01).

- NCEER-88-0042 "Modeling Strong Ground Motion from Multiple Event Earthquakes," by G.W. Ellis and A.S. Cakmak, 10/15/88, (PB89-174445, A03, MF-A01).
- NCEER-88-0043 "Nonstationary Models of Seismic Ground Acceleration," by M. Grigoriu, S.E. Ruiz and E. Rosenblueth, 7/15/88, (PB89-189617, A04, MF-A01).
- NCEER-88-0044 "SARCF User's Guide: Seismic Analysis of Reinforced Concrete Frames," by Y.S. Chung, C. Meyer and M. Shinozuka, 11/9/88, (PB89-174452, A08, MF-A01).
- NCEER-88-0045 "First Expert Panel Meeting on Disaster Research and Planning," edited by J. Pantelic and J. Stoyale, 9/15/88, (PB89-174460, A05, MF-A01).
- NCEER-88-0046 "Preliminary Studies of the Effect of Degrading Infill Walls on the Nonlinear Seismic Response of Steel Frames," by C.Z. Chrysostomou, P. Gergely and J.F. Abel, 12/19/88, (PB89-208383, A05, MF-A01).
- NCEER-88-0047 "Reinforced Concrete Frame Component Testing Facility - Design, Construction, Instrumentation and Operation," by S.P. Pessiki, C. Conley, T. Bond, P. Gergely and R.N. White, 12/16/88, (PB89-174478, A04, MF-A01).
- NCEER-89-0001 "Effects of Protective Cushion and Soil Compliancy on the Response of Equipment Within a Seismically Excited Building," by J.A. HoLung, 2/16/89, (PB89-207179, A04, MF-A01).
- NCEER-89-0002 "Statistical Evaluation of Response Modification Factors for Reinforced Concrete Structures," by H.H-M. Hwang and J-W. Jaw, 2/17/89, (PB89-207187, A05, MF-A01).
- NCEER-89-0003 "Hysteretic Columns Under Random Excitation," by G-Q. Cai and Y.K. Lin, 1/9/89, (PB89-196513, A03, MF-A01).
- NCEER-89-0004 "Experimental Study of 'Elephant Foot Bulge' Instability of Thin-Walled Metal Tanks," by Z-H. Jia and R.L. Ketter, 2/22/89, (PB89-207195, A03, MF-A01).
- NCEER-89-0005 "Experiment on Performance of Buried Pipelines Across San Andreas Fault," by J. Isenberg, E. Richardson and T.D. O'Rourke, 3/10/89, (PB89-218440, A04, MF-A01). This report is available only through NTIS (see address given above).
- NCEER-89-0006 "A Knowledge-Based Approach to Structural Design of Earthquake-Resistant Buildings," by M. Subramani, P. Gergely, C.H. Conley, J.F. Abel and A.H. Zaghaw, 1/15/89, (PB89-218465, A06, MF-A01).
- NCEER-89-0007 "Liquefaction Hazards and Their Effects on Buried Pipelines," by T.D. O'Rourke and P.A. Lane, 2/1/89, (PB89-218481, A09, MF-A01).
- NCEER-89-0008 "Fundamentals of System Identification in Structural Dynamics," by H. Imai, C-B. Yun, O. Maruyama and M. Shinozuka, 1/26/89, (PB89-207211, A04, MF-A01).
- NCEER-89-0009 "Effects of the 1985 Michoacan Earthquake on Water Systems and Other Buried Lifelines in Mexico," by A.G. Ayala and M.J. O'Rourke, 3/8/89, (PB89-207229, A06, MF-A01).
- NCEER-89-R010 "NCEER Bibliography of Earthquake Education Materials," by K.E.K. Ross, Second Revision, 9/1/89, (PB90-125352, A05, MF-A01). This report is replaced by NCEER-92-0018.
- NCEER-89-0011 "Inelastic Three-Dimensional Response Analysis of Reinforced Concrete Building Structures (IDARC-3D), Part I - Modeling," by S.K. Kunnath and A.M. Reinhorn, 4/17/89, (PB90-114612, A07, MF-A01). This report is available only through NTIS (see address given above).
- NCEER-89-0012 "Recommended Modifications to ATC-14," by C.D. Poland and J.O. Malley, 4/12/89, (PB90-108648, A15, MF-A01).
- NCEER-89-0013 "Repair and Strengthening of Beam-to-Column Connections Subjected to Earthquake Loading," by M. Corazao and A.J. Durrani, 2/28/89, (PB90-109885, A06, MF-A01).

- NCEER-89-0014 "Program EXKAL2 for Identification of Structural Dynamic Systems," by O. Maruyama, C-B. Yun, M. Hoshiya and M. Shinozuka, 5/19/89, (PB90-109877, A09, MF-A01).
- NCEER-89-0015 "Response of Frames With Bolted Semi-Rigid Connections, Part I - Experimental Study and Analytical Predictions," by P.J. DiCorso, A.M. Reinhorn, J.R. Dickerson, J.B. Radzinski and W.L. Harper, 6/1/89, to be published.
- NCEER-89-0016 "ARMA Monte Carlo Simulation in Probabilistic Structural Analysis," by P.D. Spanos and M.P. Mignolet, 7/10/89, (PB90-109893, A03, MF-A01).
- NCEER-89-P017 "Preliminary Proceedings from the Conference on Disaster Preparedness - The Place of Earthquake Education in Our Schools," Edited by K.E.K. Ross, 6/23/89, (PB90-108606, A03, MF-A01).
- NCEER-89-0017 "Proceedings from the Conference on Disaster Preparedness - The Place of Earthquake Education in Our Schools," Edited by K.E.K. Ross, 12/31/89, (PB90-207895, A012, MF-A02). This report is available only through NTIS (see address given above).
- NCEER-89-0018 "Multidimensional Models of Hysteretic Material Behavior for Vibration Analysis of Shape Memory Energy Absorbing Devices, by E.J. Graesser and F.A. Cozzarelli, 6/7/89, (PB90-164146, A04, MF-A01).
- NCEER-89-0019 "Nonlinear Dynamic Analysis of Three-Dimensional Base Isolated Structures (3D-BASIS)," by S. Nagarajaiah, A.M. Reinhorn and M.C. Constantinou, 8/3/89, (PB90-161936, A06, MF-A01). This report has been replaced by NCEER-93-0011.
- NCEER-89-0020 "Structural Control Considering Time-Rate of Control Forces and Control Rate Constraints," by F.Y. Cheng and C.P. Pantelides, 8/3/89, (PB90-120445, A04, MF-A01).
- NCEER-89-0021 "Subsurface Conditions of Memphis and Shelby County," by K.W. Ng, T-S. Chang and H-H.M. Hwang, 7/26/89, (PB90-120437, A03, MF-A01).
- NCEER-89-0022 "Seismic Wave Propagation Effects on Straight Jointed Buried Pipelines," by K. Elhadi and M.J. O'Rourke, 8/24/89, (PB90-162322, A10, MF-A02).
- NCEER-89-0023 "Workshop on Serviceability Analysis of Water Delivery Systems," edited by M. Grigoriu, 3/6/89, (PB90-127424, A03, MF-A01).
- NCEER-89-0024 "Shaking Table Study of a 1/5 Scale Steel Frame Composed of Tapered Members," by K.C. Chang, J.S. Hwang and G.C. Lee, 9/18/89, (PB90-160169, A04, MF-A01).
- NCEER-89-0025 "DYNA1D: A Computer Program for Nonlinear Seismic Site Response Analysis - Technical Documentation," by Jean H. Prevost, 9/14/89, (PB90-161944, A07, MF-A01). This report is available only through NTIS (see address given above).
- NCEER-89-0026 "1:4 Scale Model Studies of Active Tendon Systems and Active Mass Dampers for Aseismic Protection," by A.M. Reinhorn, T.T. Soong, R.C. Lin, Y.P. Yang, Y. Fukao, H. Abe and M. Nakai, 9/15/89, (PB90-173246, A10, MF-A02). This report is available only through NTIS (see address given above).
- NCEER-89-0027 "Scattering of Waves by Inclusions in a Nonhomogeneous Elastic Half Space Solved by Boundary Element Methods," by P.K. Hadley, A. Askar and A.S. Cakmak, 6/15/89, (PB90-145699, A07, MF-A01).
- NCEER-89-0028 "Statistical Evaluation of Deflection Amplification Factors for Reinforced Concrete Structures," by H.H.M. Hwang, J-W. Jaw and A.L. Ch'ng, 8/31/89, (PB90-164633, A05, MF-A01).
- NCEER-89-0029 "Bedrock Accelerations in Memphis Area Due to Large New Madrid Earthquakes," by H.H.M. Hwang, C.H.S. Chen and G. Yu, 11/7/89, (PB90-162330, A04, MF-A01).
- NCEER-89-0030 "Seismic Behavior and Response Sensitivity of Secondary Structural Systems," by Y.Q. Chen and T.T. Soong, 10/23/89, (PB90-164658, A08, MF-A01).
- NCEER-89-0031 "Random Vibration and Reliability Analysis of Primary-Secondary Structural Systems," by Y. Ibrahim, M. Grigoriu and T.T. Soong, 11/10/89, (PB90-161951, A04, MF-A01).

- NCEER-89-0032 "Proceedings from the Second U.S. - Japan Workshop on Liquefaction, Large Ground Deformation and Their Effects on Lifelines, September 26-29, 1989," Edited by T.D. O'Rourke and M. Hamada, 12/1/89, (PB90-209388, A22, MF-A03).
- NCEER-89-0033 "Deterministic Model for Seismic Damage Evaluation of Reinforced Concrete Structures," by J.M. Bracci, A.M. Reinhorn, J.B. Mander and S.K. Kunnath, 9/27/89, (PB91-108803, A06, MF-A01).
- NCEER-89-0034 "On the Relation Between Local and Global Damage Indices," by E. DiPasquale and A.S. Cakmak, 8/15/89, (PB90-173865, A05, MF-A01).
- NCEER-89-0035 "Cyclic Undrained Behavior of Nonplastic and Low Plasticity Silts," by A.J. Walker and H.E. Stewart, 7/26/89, (PB90-183518, A10, MF-A01).
- NCEER-89-0036 "Liquefaction Potential of Surficial Deposits in the City of Buffalo, New York," by M. Budhu, R. Giese and L. Baumgrass, 1/17/89, (PB90-208455, A04, MF-A01).
- NCEER-89-0037 "A Deterministic Assessment of Effects of Ground Motion Incoherence," by A.S. Veletsos and Y. Tang, 7/15/89, (PB90-164294, A03, MF-A01).
- NCEER-89-0038 "Workshop on Ground Motion Parameters for Seismic Hazard Mapping," July 17-18, 1989, edited by R.V. Whitman, 12/1/89, (PB90-173923, A04, MF-A01).
- NCEER-89-0039 "Seismic Effects on Elevated Transit Lines of the New York City Transit Authority," by C.J. Costantino, C.A. Miller and E. Heymsfield, 12/26/89, (PB90-207887, A06, MF-A01).
- NCEER-89-0040 "Centrifugal Modeling of Dynamic Soil-Structure Interaction," by K. Weissman, Supervised by J.H. Prevost, 5/10/89, (PB90-207879, A07, MF-A01).
- NCEER-89-0041 "Linearized Identification of Buildings With Cores for Seismic Vulnerability Assessment," by I-K. Ho and A.E. Aktan, 11/1/89, (PB90-251943, A07, MF-A01).
- NCEER-90-0001 "Geotechnical and Lifeline Aspects of the October 17, 1989 Loma Prieta Earthquake in San Francisco," by T.D. O'Rourke, H.E. Stewart, F.T. Blackburn and T.S. Dickerman, 1/90, (PB90-208596, A05, MF-A01).
- NCEER-90-0002 "Nonnormal Secondary Response Due to Yielding in a Primary Structure," by D.C.K. Chen and L.D. Lutes, 2/28/90, (PB90-251976, A07, MF-A01).
- NCEER-90-0003 "Earthquake Education Materials for Grades K-12," by K.E.K. Ross, 4/16/90, (PB91-251984, A05, MF-A05). This report has been replaced by NCEER-92-0018.
- NCEER-90-0004 "Catalog of Strong Motion Stations in Eastern North America," by R.W. Busby, 4/3/90, (PB90-251984, A05, MF-A01).
- NCEER-90-0005 "NCEER Strong-Motion Data Base: A User Manual for the GeoBase Release (Version 1.0 for the Sun3)," by P. Friberg and K. Jacob, 3/31/90 (PB90-258062, A04, MF-A01).
- NCEER-90-0006 "Seismic Hazard Along a Crude Oil Pipeline in the Event of an 1811-1812 Type New Madrid Earthquake," by H.H.M. Hwang and C-H.S. Chen, 4/16/90, (PB90-258054, A04, MF-A01).
- NCEER-90-0007 "Site-Specific Response Spectra for Memphis Sheahan Pumping Station," by H.H.M. Hwang and C.S. Lee, 5/15/90, (PB91-108811, A05, MF-A01).
- NCEER-90-0008 "Pilot Study on Seismic Vulnerability of Crude Oil Transmission Systems," by T. Ariman, R. Dobry, M. Grigoriu, F. Kozin, M. O'Rourke, T. O'Rourke and M. Shinozuka, 5/25/90, (PB91-108837, A06, MF-A01).
- NCEER-90-0009 "A Program to Generate Site Dependent Time Histories: EQGEN," by G.W. Ellis, M. Srinivasan and A.S. Cakmak, 1/30/90, (PB91-108829, A04, MF-A01).
- NCEER-90-0010 "Active Isolation for Seismic Protection of Operating Rooms," by M.E. Talbott, Supervised by M. Shinozuka, 6/8/9, (PB91-110205, A05, MF-A01).

- NCEER-90-0011 "Program LINEARID for Identification of Linear Structural Dynamic Systems," by C-B. Yun and M. Shinozuka, 6/25/90, (PB91-110312, A08, MF-A01).
- NCEER-90-0012 "Two-Dimensional Two-Phase Elasto-Plastic Seismic Response of Earth Dams," by A.N. Yiagos, Supervised by J.H. Prevost, 6/20/90, (PB91-110197, A13, MF-A02).
- NCEER-90-0013 "Secondary Systems in Base-Isolated Structures: Experimental Investigation, Stochastic Response and Stochastic Sensitivity," by G.D. Manolis, G. Juhn, M.C. Constantinou and A.M. Reinhorn, 7/1/90, (PB91-110320, A08, MF-A01).
- NCEER-90-0014 "Seismic Behavior of Lightly-Reinforced Concrete Column and Beam-Column Joint Details," by S.P. Pessiki, C.H. Conley, P. Gergely and R.N. White, 8/22/90, (PB91-108795, A11, MF-A02).
- NCEER-90-0015 "Two Hybrid Control Systems for Building Structures Under Strong Earthquakes," by J.N. Yang and A. Danielians, 6/29/90, (PB91-125393, A04, MF-A01).
- NCEER-90-0016 "Instantaneous Optimal Control with Acceleration and Velocity Feedback," by J.N. Yang and Z. Li, 6/29/90, (PB91-125401, A03, MF-A01).
- NCEER-90-0017 "Reconnaissance Report on the Northern Iran Earthquake of June 21, 1990," by M. Mehrain, 10/4/90, (PB91-125377, A03, MF-A01).
- NCEER-90-0018 "Evaluation of Liquefaction Potential in Memphis and Shelby County," by T.S. Chang, P.S. Tang, C.S. Lee and H. Hwang, 8/10/90, (PB91-125427, A09, MF-A01).
- NCEER-90-0019 "Experimental and Analytical Study of a Combined Sliding Disc Bearing and Helical Steel Spring Isolation System," by M.C. Constantinou, A.S. Mokha and A.M. Reinhorn, 10/4/90, (PB91-125385, A06, MF-A01). This report is available only through NTIS (see address given above).
- NCEER-90-0020 "Experimental Study and Analytical Prediction of Earthquake Response of a Sliding Isolation System with a Spherical Surface," by A.S. Mokha, M.C. Constantinou and A.M. Reinhorn, 10/11/90, (PB91-125419, A05, MF-A01).
- NCEER-90-0021 "Dynamic Interaction Factors for Floating Pile Groups," by G. Gazetas, K. Fan, A. Kaynia and E. Kausel, 9/10/90, (PB91-170381, A05, MF-A01).
- NCEER-90-0022 "Evaluation of Seismic Damage Indices for Reinforced Concrete Structures," by S. Rodriguez-Gomez and A.S. Cakmak, 9/30/90, PB91-171322, A06, MF-A01).
- NCEER-90-0023 "Study of Site Response at a Selected Memphis Site," by H. Desai, S. Ahmad, E.S. Gazetas and M.R. Oh, 10/11/90, (PB91-196857, A03, MF-A01).
- NCEER-90-0024 "A User's Guide to Strongmo: Version 1.0 of NCEER's Strong-Motion Data Access Tool for PCs and Terminals," by P.A. Friberg and C.A.T. Susch, 11/15/90, (PB91-171272, A03, MF-A01).
- NCEER-90-0025 "A Three-Dimensional Analytical Study of Spatial Variability of Seismic Ground Motions," by L-L. Hong and A.H.-S. Ang, 10/30/90, (PB91-170399, A09, MF-A01).
- NCEER-90-0026 "MUMOID User's Guide - A Program for the Identification of Modal Parameters," by S. Rodriguez-Gomez and E. DiPasquale, 9/30/90, (PB91-171298, A04, MF-A01).
- NCEER-90-0027 "SARCF-II User's Guide - Seismic Analysis of Reinforced Concrete Frames," by S. Rodriguez-Gomez, Y.S. Chung and C. Meyer, 9/30/90, (PB91-171280, A05, MF-A01).
- NCEER-90-0028 "Viscous Dampers: Testing, Modeling and Application in Vibration and Seismic Isolation," by N. Makris and M.C. Constantinou, 12/20/90 (PB91-190561, A06, MF-A01).
- NCEER-90-0029 "Soil Effects on Earthquake Ground Motions in the Memphis Area," by H. Hwang, C.S. Lee, K.W. Ng and T.S. Chang, 8/2/90, (PB91-190751, A05, MF-A01).



- NCEER-91-0001 "Proceedings from the Third Japan-U.S. Workshop on Earthquake Resistant Design of Lifeline Facilities and Countermeasures for Soil Liquefaction, December 17-19, 1990," edited by T.D. O'Rourke and M. Hamada, 2/1/91, (PB91-179259, A99, MF-A04).
- NCEER-91-0002 "Physical Space Solutions of Non-Proportionally Damped Systems," by M. Tong, Z. Liang and G.C. Lee, 1/15/91, (PB91-179242, A04, MF-A01).
- NCEER-91-0003 "Seismic Response of Single Piles and Pile Groups," by K. Fan and G. Gazetas, 1/10/91, (PB92-174994, A04, MF-A01).
- NCEER-91-0004 "Damping of Structures: Part 1 - Theory of Complex Damping," by Z. Liang and G. Lee, 10/10/91, (PB92-197235, A12, MF-A03).
- NCEER-91-0005 "3D-BASIS - Nonlinear Dynamic Analysis of Three Dimensional Base Isolated Structures: Part II," by S. Nagarajaiah, A.M. Reinhorn and M.C. Constantinou, 2/28/91, (PB91-190553, A07, MF-A01). This report has been replaced by NCEER-93-0011.
- NCEER-91-0006 "A Multidimensional Hysteretic Model for Plasticity Deforming Metals in Energy Absorbing Devices," by E.J. Graesser and F.A. Cozzarelli, 4/9/91, (PB92-108364, A04, MF-A01).
- NCEER-91-0007 "A Framework for Customizable Knowledge-Based Expert Systems with an Application to a KBES for Evaluating the Seismic Resistance of Existing Buildings," by E.G. Ibarra-Anaya and S.J. Fenves, 4/9/91, (PB91-210930, A08, MF-A01).
- NCEER-91-0008 "Nonlinear Analysis of Steel Frames with Semi-Rigid Connections Using the Capacity Spectrum Method," by G.G. Deierlein, S-H. Hsieh, Y-J. Shen and J.F. Abel, 7/2/91, (PB92-113828, A05, MF-A01).
- NCEER-91-0009 "Earthquake Education Materials for Grades K-12," by K.E.K. Ross, 4/30/91, (PB91-212142, A06, MF-A01). This report has been replaced by NCEER-92-0018.
- NCEER-91-0010 "Phase Wave Velocities and Displacement Phase Differences in a Harmonically Oscillating Pile," by N. Makris and G. Gazetas, 7/8/91, (PB92-108356, A04, MF-A01).
- NCEER-91-0011 "Dynamic Characteristics of a Full-Size Five-Story Steel Structure and a 2/5 Scale Model," by K.C. Chang, G.C. Yao, G.C. Lee, D.S. Hao and Y.C. Yeh," 7/2/91, (PB93-116648, A06, MF-A02).
- NCEER-91-0012 "Seismic Response of a 2/5 Scale Steel Structure with Added Viscoelastic Dampers," by K.C. Chang, T.T. Soong, S-T. Oh and M.L. Lai, 5/17/91, (PB92-110816, A05, MF-A01).
- NCEER-91-0013 "Earthquake Response of Retaining Walls; Full-Scale Testing and Computational Modeling," by S. Alampalli and A-W.M. Elgamal, 6/20/91, to be published.
- NCEER-91-0014 "3D-BASIS-M: Nonlinear Dynamic Analysis of Multiple Building Base Isolated Structures," by P.C. Tsopelas, S. Nagarajaiah, M.C. Constantinou and A.M. Reinhorn, 5/28/91, (PB92-113885, A09, MF-A02).
- NCEER-91-0015 "Evaluation of SEAOC Design Requirements for Sliding Isolated Structures," by D. Theodossiou and M.C. Constantinou, 6/10/91, (PB92-114602, A11, MF-A03).
- NCEER-91-0016 "Closed-Loop Modal Testing of a 27-Story Reinforced Concrete Flat Plate-Core Building," by H.R. Somaprasad, T. Toksoy, H. Yoshiyuki and A.E. Aktan, 7/15/91, (PB92-129980, A07, MF-A02).
- NCEER-91-0017 "Shake Table Test of a 1/6 Scale Two-Story Lightly Reinforced Concrete Building," by A.G. El-Attar, R.N. White and P. Gergely, 2/28/91, (PB92-222447, A06, MF-A02).
- NCEER-91-0018 "Shake Table Test of a 1/8 Scale Three-Story Lightly Reinforced Concrete Building," by A.G. El-Attar, R.N. White and P. Gergely, 2/28/91, (PB93-116630, A08, MF-A02).
- NCEER-91-0019 "Transfer Functions for Rigid Rectangular Foundations," by A.S. Veletsos, A.M. Prasad and W.H. Wu, 7/31/91, to be published.

- NCEER-91-0020 "Hybrid Control of Seismic-Excited Nonlinear and Inelastic Structural Systems," by J.N. Yang, Z. Li and A. Daniellians, 8/1/91, (PB92-143171, A06, MF-A02).
- NCEER-91-0021 "The NCEER-91 Earthquake Catalog: Improved Intensity-Based Magnitudes and Recurrence Relations for U.S. Earthquakes East of New Madrid," by L. Seeber and J.G. Armbruster, 8/28/91, (PB92-176742, A06, MF-A02).
- NCEER-91-0022 "Proceedings from the Implementation of Earthquake Planning and Education in Schools: The Need for Change - The Roles of the Changemakers," by K.E.K. Ross and F. Winslow, 7/23/91, (PB92-129998, A12, MF-A03).
- NCEER-91-0023 "A Study of Reliability-Based Criteria for Seismic Design of Reinforced Concrete Frame Buildings," by H.H.M. Hwang and H-M. Hsu, 8/10/91, (PB92-140235, A09, MF-A02).
- NCEER-91-0024 "Experimental Verification of a Number of Structural System Identification Algorithms," by R.G. Ghanem, H. Gavin and M. Shinozuka, 9/18/91, (PB92-176577, A18, MF-A04).
- NCEER-91-0025 "Probabilistic Evaluation of Liquefaction Potential," by H.H.M. Hwang and C.S. Lee," 11/25/91, (PB92-143429, A05, MF-A01).
- NCEER-91-0026 "Instantaneous Optimal Control for Linear, Nonlinear and Hysteretic Structures - Stable Controllers," by J.N. Yang and Z. Li, 11/15/91, (PB92-163807, A04, MF-A01).
- NCEER-91-0027 "Experimental and Theoretical Study of a Sliding Isolation System for Bridges," by M.C. Constantinou, A. Kartoum, A.M. Reinhorn and P. Bradford, 11/15/91, (PB92-176973, A10, MF-A03).
- NCEER-92-0001 "Case Studies of Liquefaction and Lifeline Performance During Past Earthquakes, Volume 1: Japanese Case Studies," Edited by M. Hamada and T. O'Rourke, 2/17/92, (PB92-197243, A18, MF-A04).
- NCEER-92-0002 "Case Studies of Liquefaction and Lifeline Performance During Past Earthquakes, Volume 2: United States Case Studies," Edited by T. O'Rourke and M. Hamada, 2/17/92, (PB92-197250, A20, MF-A04).
- NCEER-92-0003 "Issues in Earthquake Education," Edited by K. Ross, 2/3/92, (PB92-222389, A07, MF-A02).
- NCEER-92-0004 "Proceedings from the First U.S. - Japan Workshop on Earthquake Protective Systems for Bridges," Edited by I.G. Buckle, 2/4/92, (PB94-142239, A99, MF-A06).
- NCEER-92-0005 "Seismic Ground Motion from a Haskell-Type Source in a Multiple-Layered Half-Space," A.P. Theoharis, G. Deodatis and M. Shinozuka, 1/2/92, to be published.
- NCEER-92-0006 "Proceedings from the Site Effects Workshop," Edited by R. Whitman, 2/29/92, (PB92-197201, A04, MF-A01).
- NCEER-92-0007 "Engineering Evaluation of Permanent Ground Deformations Due to Seismically-Induced Liquefaction," by M.H. Baziar, R. Dobry and A-W.M. Elgamal, 3/24/92, (PB92-222421, A13, MF-A03).
- NCEER-92-0008 "A Procedure for the Seismic Evaluation of Buildings in the Central and Eastern United States," by C.D. Poland and J.O. Malley, 4/2/92, (PB92-222439, A20, MF-A04).
- NCEER-92-0009 "Experimental and Analytical Study of a Hybrid Isolation System Using Friction Controllable Sliding Bearings," by M.Q. Feng, S. Fujii and M. Shinozuka, 5/15/92, (PB93-150282, A06, MF-A02).
- NCEER-92-0010 "Seismic Resistance of Slab-Column Connections in Existing Non-Ductile Flat-Plate Buildings," by A.J. Durrani and Y. Du, 5/18/92, (PB93-116812, A06, MF-A02).
- NCEER-92-0011 "The Hysteretic and Dynamic Behavior of Brick Masonry Walls Upgraded by Ferrocement Coatings Under Cyclic Loading and Strong Simulated Ground Motion," by H. Lee and S.P. Prawl, 5/11/92, to be published.
- NCEER-92-0012 "Study of Wire Rope Systems for Seismic Protection of Equipment in Buildings," by G.F. Demetriades, M.C. Constantinou and A.M. Reinhorn, 5/20/92, (PB93-116655, A08, MF-A02).

- NCEER-92-0013 "Shape Memory Structural Dampers: Material Properties, Design and Seismic Testing," by P.R. Witting and F.A. Cozzarelli, 5/26/92, (PB93-116663, A05, MF-A01).
- NCEER-92-0014 "Longitudinal Permanent Ground Deformation Effects on Buried Continuous Pipelines," by M.J. O'Rourke, and C. Nordberg, 6/15/92, (PB93-116671, A08, MF-A02).
- NCEER-92-0015 "A Simulation Method for Stationary Gaussian Random Functions Based on the Sampling Theorem," by M. Grigoriu and S. Balopoulou, 6/11/92, (PB93-127496, A05, MF-A01).
- NCEER-92-0016 "Gravity-Load-Designed Reinforced Concrete Buildings: Seismic Evaluation of Existing Construction and Detailing Strategies for Improved Seismic Resistance," by G.W. Hoffmann, S.K. Kunnath, A.M. Reinhorn and J.B. Mander, 7/15/92, (PB94-142007, A08, MF-A02).
- NCEER-92-0017 "Observations on Water System and Pipeline Performance in the Limón Area of Costa Rica Due to the April 22, 1991 Earthquake," by M. O'Rourke and D. Ballantyne, 6/30/92, (PB93-126811, A06, MF-A02).
- NCEER-92-0018 "Fourth Edition of Earthquake Education Materials for Grades K-12," Edited by K.E.K. Ross, 8/10/92, (PB93-114023, A07, MF-A02).
- NCEER-92-0019 "Proceedings from the Fourth Japan-U.S. Workshop on Earthquake Resistant Design of Lifeline Facilities and Countermeasures for Soil Liquefaction," Edited by M. Hamada and T.D. O'Rourke, 8/12/92, (PB93-163939, A99, MF-E11).
- NCEER-92-0020 "Active Bracing System: A Full Scale Implementation of Active Control," by A.M. Reinhorn, T.T. Soong, R.C. Lin, M.A. Riley, Y.P. Wang, S. Aizawa and M. Higashino, 8/14/92, (PB93-127512, A06, MF-A02).
- NCEER-92-0021 "Empirical Analysis of Horizontal Ground Displacement Generated by Liquefaction-Induced Lateral Spreads," by S.F. Bartlett and T.L. Youd, 8/17/92, (PB93-188241, A06, MF-A02).
- NCEER-92-0022 "IDARC Version 3.0: Inelastic Damage Analysis of Reinforced Concrete Structures," by S.K. Kunnath, A.M. Reinhorn and R.F. Lobo, 8/31/92, (PB93-227502, A07, MF-A02).
- NCEER-92-0023 "A Semi-Empirical Analysis of Strong-Motion Peaks in Terms of Seismic Source, Propagation Path and Local Site Conditions, by M. Kamiyama, M.J. O'Rourke and R. Flores-Berrones, 9/9/92, (PB93-150266, A08, MF-A02).
- NCEER-92-0024 "Seismic Behavior of Reinforced Concrete Frame Structures with Nonductile Details, Part I: Summary of Experimental Findings of Full Scale Beam-Column Joint Tests," by A. Beres, R.N. White and P. Gergely, 9/30/92, (PB93-227783, A05, MF-A01).
- NCEER-92-0025 "Experimental Results of Repaired and Retrofitted Beam-Column Joint Tests in Lightly Reinforced Concrete Frame Buildings," by A. Beres, S. El-Borgi, R.N. White and P. Gergely, 10/29/92, (PB93-227791, A05, MF-A01).
- NCEER-92-0026 "A Generalization of Optimal Control Theory: Linear and Nonlinear Structures," by J.N. Yang, Z. Li and S. Vongchavalitkul, 11/2/92, (PB93-188621, A05, MF-A01).
- NCEER-92-0027 "Seismic Resistance of Reinforced Concrete Frame Structures Designed Only for Gravity Loads: Part I - Design and Properties of a One-Third Scale Model Structure," by J.M. Bracci, A.M. Reinhorn and J.B. Mander, 12/1/92, (PB94-104502, A08, MF-A02).
- NCEER-92-0028 "Seismic Resistance of Reinforced Concrete Frame Structures Designed Only for Gravity Loads: Part II - Experimental Performance of Subassemblages," by L.E. Aycaardi, J.B. Mander and A.M. Reinhorn, 12/1/92, (PB94-104510, A08, MF-A02).
- NCEER-92-0029 "Seismic Resistance of Reinforced Concrete Frame Structures Designed Only for Gravity Loads: Part III - Experimental Performance and Analytical Study of a Structural Model," by J.M. Bracci, A.M. Reinhorn and J.B. Mander, 12/1/92, (PB93-227528, A09, MF-A01).

- NCEER-92-0030 "Evaluation of Seismic Retrofit of Reinforced Concrete Frame Structures: Part I - Experimental Performance of Retrofitted Subassemblages," by D. Choudhuri, J.B. Mander and A.M. Reinhorn, 12/8/92, (PB93-198307, A07, MF-A02).
- NCEER-92-0031 "Evaluation of Seismic Retrofit of Reinforced Concrete Frame Structures: Part II - Experimental Performance and Analytical Study of a Retrofitted Structural Model," by J.M. Bracci, A.M. Reinhorn and J.B. Mander, 12/8/92, (PB93-198315, A09, MF-A03).
- NCEER-92-0032 "Experimental and Analytical Investigation of Seismic Response of Structures with Supplemental Fluid Viscous Dampers," by M.C. Constantinou and M.D. Symans, 12/21/92, (PB93-191435, A10, MF-A03). This report is available only through NTIS (see address given above).
- NCEER-92-0033 "Reconnaissance Report on the Cairo, Egypt Earthquake of October 12, 1992," by M. Khater, 12/23/92, (PB93-188621, A03, MF-A01).
- NCEER-92-0034 "Low-Level Dynamic Characteristics of Four Tall Flat-Plate Buildings in New York City," by H. Gavin, S. Yuan, J. Grossman, E. Pekelis and K. Jacob, 12/28/92, (PB93-188217, A07, MF-A02).
- NCEER-93-0001 "An Experimental Study on the Seismic Performance of Brick-Infilled Steel Frames With and Without Retrofit," by J.B. Mander, B. Nair, K. Wojtkowski and J. Ma, 1/29/93, (PB93-227510, A07, MF-A02).
- NCEER-93-0002 "Social Accounting for Disaster Preparedness and Recovery Planning," by S. Cole, E. Pantoja and V. Razak, 2/22/93, (PB94-142114, A12, MF-A03).
- NCEER-93-0003 "Assessment of 1991 NEHRP Provisions for Nonstructural Components and Recommended Revisions," by T.T. Soong, G. Chen, Z. Wu, R-H. Zhang and M. Grigoriu, 3/1/93, (PB93-188639, A06, MF-A02).
- NCEER-93-0004 "Evaluation of Static and Response Spectrum Analysis Procedures of SEAOC/UBC for Seismic Isolated Structures," by C.W. Winters and M.C. Constantinou, 3/23/93, (PB93-198299, A10, MF-A03).
- NCEER-93-0005 "Earthquakes in the Northeast - Are We Ignoring the Hazard? A Workshop on Earthquake Science and Safety for Educators," edited by K.E.K. Ross, 4/2/93, (PB94-103066, A09, MF-A02).
- NCEER-93-0006 "Inelastic Response of Reinforced Concrete Structures with Viscoelastic Braces," by R.F. Lobo, J.M. Bracci, K.L. Shen, A.M. Reinhorn and T.T. Soong, 4/5/93, (PB93-227486, A05, MF-A02).
- NCEER-93-0007 "Seismic Testing of Installation Methods for Computers and Data Processing Equipment," by K. Kosar, T.T. Soong, K.L. Shen, J.A. HoLung and Y.K. Lin, 4/12/93, (PB93-198299, A07, MF-A02).
- NCEER-93-0008 "Retrofit of Reinforced Concrete Frames Using Added Dampers," by A. Reinhorn, M. Constantinou and C. Li, to be published.
- NCEER-93-0009 "Seismic Behavior and Design Guidelines for Steel Frame Structures with Added Viscoelastic Dampers," by K.C. Chang, M.L. Lai, T.T. Soong, D.S. Hao and Y.C. Yeh, 5/1/93, (PB94-141959, A07, MF-A02).
- NCEER-93-0010 "Seismic Performance of Shear-Critical Reinforced Concrete Bridge Piers," by J.B. Mander, S.M. Waheed, M.T.A. Chaudhary and S.S. Chen, 5/12/93, (PB93-227494, A08, MF-A02).
- NCEER-93-0011 "3D-BASIS-TABS: Computer Program for Nonlinear Dynamic Analysis of Three Dimensional Base Isolated Structures," by S. Nagarajaiah, C. Li, A.M. Reinhorn and M.C. Constantinou, 8/2/93, (PB94-141819, A09, MF-A02).
- NCEER-93-0012 "Effects of Hydrocarbon Spills from an Oil Pipeline Break on Ground Water," by O.J. Helweg and H.H.M. Hwang, 8/3/93, (PB94-141942, A06, MF-A02).
- NCEER-93-0013 "Simplified Procedures for Seismic Design of Nonstructural Components and Assessment of Current Code Provisions," by M.P. Singh, L.E. Suarez, E.E. Matheu and G.O. Maldonado, 8/4/93, (PB94-141827, A09, MF-A02).
- NCEER-93-0014 "An Energy Approach to Seismic Analysis and Design of Secondary Systems," by G. Chen and T.T. Soong, 8/6/93, (PB94-142767, A11, MF-A03).

- NCEER-93-0015 "Proceedings from School Sites: Becoming Prepared for Earthquakes - Commemorating the Third Anniversary of the Loma Prieta Earthquake," Edited by F.E. Winslow and K.E.K. Ross, 8/16/93, (PB94-154275, A16, MF-A02).
- NCEER-93-0016 "Reconnaissance Report of Damage to Historic Monuments in Cairo, Egypt Following the October 12, 1992 Dahshur Earthquake," by D. Sykora, D. Look, G. Croci, E. Karaesmen and E. Karaesmen, 8/19/93, (PB94-142221, A08, MF-A02).
- NCEER-93-0017 "The Island of Guam Earthquake of August 8, 1993," by S.W. Swan and S.K. Harris, 9/30/93, (PB94-141843, A04, MF-A01).
- NCEER-93-0018 "Engineering Aspects of the October 12, 1992 Egyptian Earthquake," by A.W. Elgamal, M. Amer, K. Adalier and A. Abul-Fadl, 10/7/93, (PB94-141983, A05, MF-A01).
- NCEER-93-0019 "Development of an Earthquake Motion Simulator and its Application in Dynamic Centrifuge Testing," by I. Krstelj, Supervised by J.H. Prevost, 10/23/93, (PB94-181773, A-10, MF-A03).
- NCEER-93-0020 "NCEER-Taisei Corporation Research Program on Sliding Seismic Isolation Systems for Bridges: Experimental and Analytical Study of a Friction Pendulum System (FPS)," by M.C. Constantinou, P. Tsopelas, Y-S. Kim and S. Okamoto, 11/1/93, (PB94-142775, A08, MF-A02).
- NCEER-93-0021 "Finite Element Modeling of Elastomeric Seismic Isolation Bearings," by L.J. Billings, Supervised by R. Shepherd, 11/8/93, to be published.
- NCEER-93-0022 "Seismic Vulnerability of Equipment in Critical Facilities: Life-Safety and Operational Consequences," by K. Porter, G.S. Johnson, M.M. Zadeh, C. Scawthorn and S. Eder, 11/24/93, (PB94-181765, A16, MF-A03).
- NCEER-93-0023 "Hokkaido Nansei-oki, Japan Earthquake of July 12, 1993, by P.I. Yanev and C.R. Scawthorn, 12/23/93, (PB94-181500, A07, MF-A01).
- NCEER-94-0001 "An Evaluation of Seismic Serviceability of Water Supply Networks with Application to the San Francisco Auxiliary Water Supply System," by I. Markov, Supervised by M. Grigoriu and T. O'Rourke, 1/21/94, (PB94-204013, A07, MF-A02).
- NCEER-94-0002 "NCEER-Taisei Corporation Research Program on Sliding Seismic Isolation Systems for Bridges: Experimental and Analytical Study of Systems Consisting of Sliding Bearings, Rubber Restoring Force Devices and Fluid Dampers," Volumes I and II, by P. Tsopelas, S. Okamoto, M.C. Constantinou, D. Ozaki and S. Fujii, 2/4/94, (PB94-181740, A09, MF-A02 and PB94-181757, A12, MF-A03).
- NCEER-94-0003 "A Markov Model for Local and Global Damage Indices in Seismic Analysis," by S. Rahman and M. Grigoriu, 2/18/94, (PB94-206000, A12, MF-A03).
- NCEER-94-0004 "Proceedings from the NCEER Workshop on Seismic Response of Masonry Infills," edited by D.P. Abrams, 3/1/94, (PB94-180783, A07, MF-A02).
- NCEER-94-0005 "The Northridge, California Earthquake of January 17, 1994: General Reconnaissance Report," edited by J.D. Goltz, 3/11/94, (PB94-193943, A10, MF-A03).
- NCEER-94-0006 "Seismic Energy Based Fatigue Damage Analysis of Bridge Columns: Part I - Evaluation of Seismic Capacity," by G.A. Chang and J.B. Mander, 3/14/94, (PB94-219185, A11, MF-A03).
- NCEER-94-0007 "Seismic Isolation of Multi-Story Frame Structures Using Spherical Sliding Isolation Systems," by T.M. Al-Hussaini, V.A. Zayas and M.C. Constantinou, 3/17/94, (PB94-193745, A09, MF-A02).
- NCEER-94-0008 "The Northridge, California Earthquake of January 17, 1994: Performance of Highway Bridges," edited by I.G. Buckle, 3/24/94, (PB94-193851, A06, MF-A02).
- NCEER-94-0009 "Proceedings of the Third U.S.-Japan Workshop on Earthquake Protective Systems for Bridges," edited by I.G. Buckle and I. Friedland, 3/31/94, (PB94-195815, A99, MF-A06).

- NCEER-94-0010 "3D-BASIS-ME: Computer Program for Nonlinear Dynamic Analysis of Seismically Isolated Single and Multiple Structures and Liquid Storage Tanks," by P.C. Tsopelas, M.C. Constantinou and A.M. Reinhorn, 4/12/94, (PB94-204922, A09, MF-A02).
- NCEER-94-0011 "The Northridge, California Earthquake of January 17, 1994: Performance of Gas Transmission Pipelines," by T.D. O'Rourke and M.C. Palmer, 5/16/94, (PB94-204989, A05, MF-A01).
- NCEER-94-0012 "Feasibility Study of Replacement Procedures and Earthquake Performance Related to Gas Transmission Pipelines," by T.D. O'Rourke and M.C. Palmer, 5/25/94, (PB94-206638, A09, MF-A02).
- NCEER-94-0013 "Seismic Energy Based Fatigue Damage Analysis of Bridge Columns: Part II - Evaluation of Seismic Demand," by G.A. Chang and J.B. Mander, 6/1/94, (PB95-18106, A08, MF-A02).
- NCEER-94-0014 "NCEER-Taisei Corporation Research Program on Sliding Seismic Isolation Systems for Bridges: Experimental and Analytical Study of a System Consisting of Sliding Bearings and Fluid Restoring Force/Damping Devices," by P. Tsopelas and M.C. Constantinou, 6/13/94, (PB94-219144, A10, MF-A03).
- NCEER-94-0015 "Generation of Hazard-Consistent Fragility Curves for Seismic Loss Estimation Studies," by H. Hwang and J-R. Huo, 6/14/94, (PB95-181996, A09, MF-A02).
- NCEER-94-0016 "Seismic Study of Building Frames with Added Energy-Absorbing Devices," by W.S. Pong, C.S. Tsai and G.C. Lee, 6/20/94, (PB94-219136, A10, A03).
- NCEER-94-0017 "Sliding Mode Control for Seismic-Excited Linear and Nonlinear Civil Engineering Structures," by J. Yang, J. Wu, A. Agrawal and Z. Li, 6/21/94, (PB95-138483, A06, MF-A02).
- NCEER-94-0018 "3D-BASIS-TABS Version 2.0: Computer Program for Nonlinear Dynamic Analysis of Three Dimensional Base Isolated Structures," by A.M. Reinhorn, S. Nagarajaiah, M.C. Constantinou, P. Tsopelas and R. Li, 6/22/94, (PB95-182176, A08, MF-A02).
- NCEER-94-0019 "Proceedings of the International Workshop on Civil Infrastructure Systems: Application of Intelligent Systems and Advanced Materials on Bridge Systems," Edited by G.C. Lee and K.C. Chang, 7/18/94, (PB95-252474, A20, MF-A04).
- NCEER-94-0020 "Study of Seismic Isolation Systems for Computer Floors," by V. Lambrou and M.C. Constantinou, 7/19/94, (PB95-138533, A10, MF-A03).
- NCEER-94-0021 "Proceedings of the U.S.-Italian Workshop on Guidelines for Seismic Evaluation and Rehabilitation of Unreinforced Masonry Buildings," Edited by D.P. Abrams and G.M. Calvi, 7/20/94, (PB95-138749, A13, MF-A03).
- NCEER-94-0022 "NCEER-Taisei Corporation Research Program on Sliding Seismic Isolation Systems for Bridges: Experimental and Analytical Study of a System Consisting of Lubricated PTFE Sliding Bearings and Mild Steel Dampers," by P. Tsopelas and M.C. Constantinou, 7/22/94, (PB95-182184, A08, MF-A02).
- NCEER-94-0023 "Development of Reliability-Based Design Criteria for Buildings Under Seismic Load," by Y.K. Wen, H. Hwang and M. Shinozuka, 8/1/94, (PB95-211934, A08, MF-A02).
- NCEER-94-0024 "Experimental Verification of Acceleration Feedback Control Strategies for an Active Tendon System," by S.J. Dyke, B.F. Spencer, Jr., P. Quast, M.K. Sain, D.C. Kaspari, Jr. and T.T. Soong, 8/29/94, (PB95-212320, A05, MF-A01).
- NCEER-94-0025 "Seismic Retrofitting Manual for Highway Bridges," Edited by I.G. Buckle and I.F. Friedland, published by the Federal Highway Administration (PB95-212676, A15, MF-A03).
- NCEER-94-0026 "Proceedings from the Fifth U.S.-Japan Workshop on Earthquake Resistant Design of Lifeline Facilities and Countermeasures Against Soil Liquefaction," Edited by T.D. O'Rourke and M. Hamada, 11/7/94, (PB95-220802, A99, MF-E08).

- NCEER-95-0001 “Experimental and Analytical Investigation of Seismic Retrofit of Structures with Supplemental Damping: Part I - Fluid Viscous Damping Devices,” by A.M. Reinhorn, C. Li and M.C. Constantinou, 1/3/95, (PB95-266599, A09, MF-A02).
- NCEER-95-0002 “Experimental and Analytical Study of Low-Cycle Fatigue Behavior of Semi-Rigid Top-And-Seat Angle Connections,” by G. Pekcan, J.B. Mander and S.S. Chen, 1/5/95, (PB95-220042, A07, MF-A02).
- NCEER-95-0003 “NCEER-ATC Joint Study on Fragility of Buildings,” by T. Anagnos, C. Rojahn and A.S. Kiremidjian, 1/20/95, (PB95-220026, A06, MF-A02).
- NCEER-95-0004 “Nonlinear Control Algorithms for Peak Response Reduction,” by Z. Wu, T.T. Soong, V. Gattulli and R.C. Lin, 2/16/95, (PB95-220349, A05, MF-A01).
- NCEER-95-0005 “Pipeline Replacement Feasibility Study: A Methodology for Minimizing Seismic and Corrosion Risks to Underground Natural Gas Pipelines,” by R.T. Eguchi, H.A. Seligson and D.G. Honegger, 3/2/95, (PB95-252326, A06, MF-A02).
- NCEER-95-0006 “Evaluation of Seismic Performance of an 11-Story Frame Building During the 1994 Northridge Earthquake,” by F. Naeim, R. DiSulio, K. Benuska, A. Reinhorn and C. Li, to be published.
- NCEER-95-0007 “Prioritization of Bridges for Seismic Retrofitting,” by N. Basöz and A.S. Kiremidjian, 4/24/95, (PB95-252300, A08, MF-A02).
- NCEER-95-0008 “Method for Developing Motion Damage Relationships for Reinforced Concrete Frames,” by A. Singhal and A.S. Kiremidjian, 5/11/95, (PB95-266607, A06, MF-A02).
- NCEER-95-0009 “Experimental and Analytical Investigation of Seismic Retrofit of Structures with Supplemental Damping: Part II - Friction Devices,” by C. Li and A.M. Reinhorn, 7/6/95, (PB96-128087, A11, MF-A03).
- NCEER-95-0010 “Experimental Performance and Analytical Study of a Non-Ductile Reinforced Concrete Frame Structure Retrofitted with Elastomeric Spring Dampers,” by G. Pekcan, J.B. Mander and S.S. Chen, 7/14/95, (PB96-137161, A08, MF-A02).
- NCEER-95-0011 “Development and Experimental Study of Semi-Active Fluid Damping Devices for Seismic Protection of Structures,” by M.D. Symans and M.C. Constantinou, 8/3/95, (PB96-136940, A23, MF-A04).
- NCEER-95-0012 “Real-Time Structural Parameter Modification (RSPM): Development of Innervated Structures,” by Z. Liang, M. Tong and G.C. Lee, 4/11/95, (PB96-137153, A06, MF-A01).
- NCEER-95-0013 “Experimental and Analytical Investigation of Seismic Retrofit of Structures with Supplemental Damping: Part III - Viscous Damping Walls,” by A.M. Reinhorn and C. Li, 10/1/95, (PB96-176409, A11, MF-A03).
- NCEER-95-0014 “Seismic Fragility Analysis of Equipment and Structures in a Memphis Electric Substation,” by J-R. Huo and H.H.M. Hwang, 8/10/95, (PB96-128087, A09, MF-A02).
- NCEER-95-0015 “The Hanshin-Awaji Earthquake of January 17, 1995: Performance of Lifelines,” Edited by M. Shinozuka, 11/3/95, (PB96-176383, A15, MF-A03).
- NCEER-95-0016 “Highway Culvert Performance During Earthquakes,” by T.L. Youd and C.J. Beckman, available as NCEER-96-0015.
- NCEER-95-0017 “The Hanshin-Awaji Earthquake of January 17, 1995: Performance of Highway Bridges,” Edited by I.G. Buckle, 12/1/95, to be published.
- NCEER-95-0018 “Modeling of Masonry Infill Panels for Structural Analysis,” by A.M. Reinhorn, A. Madan, R.E. Valles, Y. Reichmann and J.B. Mander, 12/8/95, (PB97-110886, MF-A01, A06).
- NCEER-95-0019 “Optimal Polynomial Control for Linear and Nonlinear Structures,” by A.K. Agrawal and J.N. Yang, 12/11/95, (PB96-168737, A07, MF-A02).

- NCEER-95-0020 “Retrofit of Non-Ductile Reinforced Concrete Frames Using Friction Dampers,” by R.S. Rao, P. Gergely and R.N. White, 12/22/95, (PB97-133508, A10, MF-A02).
- NCEER-95-0021 “Parametric Results for Seismic Response of Pile-Supported Bridge Bents,” by G. Mylonakis, A. Nikolaou and G. Gazetas, 12/22/95, (PB97-100242, A12, MF-A03).
- NCEER-95-0022 “Kinematic Bending Moments in Seismically Stressed Piles,” by A. Nikolaou, G. Mylonakis and G. Gazetas, 12/23/95, (PB97-113914, MF-A03, A13).
- NCEER-96-0001 “Dynamic Response of Unreinforced Masonry Buildings with Flexible Diaphragms,” by A.C. Costley and D.P. Abrams, 10/10/96, (PB97-133573, MF-A03, A15).
- NCEER-96-0002 “State of the Art Review: Foundations and Retaining Structures,” by I. Po Lam, to be published.
- NCEER-96-0003 “Ductility of Rectangular Reinforced Concrete Bridge Columns with Moderate Confinement,” by N. Wehbe, M. Saiidi, D. Sanders and B. Douglas, 11/7/96, (PB97-133557, A06, MF-A02).
- NCEER-96-0004 “Proceedings of the Long-Span Bridge Seismic Research Workshop,” edited by I.G. Buckle and I.M. Friedland, to be published.
- NCEER-96-0005 “Establish Representative Pier Types for Comprehensive Study: Eastern United States,” by J. Kulicki and Z. Prucz, 5/28/96, (PB98-119217, A07, MF-A02).
- NCEER-96-0006 “Establish Representative Pier Types for Comprehensive Study: Western United States,” by R. Imbsen, R.A. Schamber and T.A. Osterkamp, 5/28/96, (PB98-118607, A07, MF-A02).
- NCEER-96-0007 “Nonlinear Control Techniques for Dynamical Systems with Uncertain Parameters,” by R.G. Ghanem and M.I. Bujakov, 5/27/96, (PB97-100259, A17, MF-A03).
- NCEER-96-0008 “Seismic Evaluation of a 30-Year Old Non-Ductile Highway Bridge Pier and Its Retrofit,” by J.B. Mander, B. Mahmoodzadegan, S. Bhadra and S.S. Chen, 5/31/96, (PB97-110902, MF-A03, A10).
- NCEER-96-0009 “Seismic Performance of a Model Reinforced Concrete Bridge Pier Before and After Retrofit,” by J.B. Mander, J.H. Kim and C.A. Ligozio, 5/31/96, (PB97-110910, MF-A02, A10).
- NCEER-96-0010 “IDARC2D Version 4.0: A Computer Program for the Inelastic Damage Analysis of Buildings,” by R.E. Valles, A.M. Reinhorn, S.K. Kunnath, C. Li and A. Madan, 6/3/96, (PB97-100234, A17, MF-A03).
- NCEER-96-0011 “Estimation of the Economic Impact of Multiple Lifeline Disruption: Memphis Light, Gas and Water Division Case Study,” by S.E. Chang, H.A. Seligson and R.T. Eguchi, 8/16/96, (PB97-133490, A11, MF-A03).
- NCEER-96-0012 “Proceedings from the Sixth Japan-U.S. Workshop on Earthquake Resistant Design of Lifeline Facilities and Countermeasures Against Soil Liquefaction, Edited by M. Hamada and T. O’Rourke, 9/11/96, (PB97-133581, A99, MF-A06).
- NCEER-96-0013 “Chemical Hazards, Mitigation and Preparedness in Areas of High Seismic Risk: A Methodology for Estimating the Risk of Post-Earthquake Hazardous Materials Release,” by H.A. Seligson, R.T. Eguchi, K.J. Tierney and K. Richmond, 11/7/96, (PB97-133565, MF-A02, A08).
- NCEER-96-0014 “Response of Steel Bridge Bearings to Reversed Cyclic Loading,” by J.B. Mander, D-K. Kim, S.S. Chen and G.J. Premus, 11/13/96, (PB97-140735, A12, MF-A03).
- NCEER-96-0015 “Highway Culvert Performance During Past Earthquakes,” by T.L. Youd and C.J. Beckman, 11/25/96, (PB97-133532, A06, MF-A01).
- NCEER-97-0001 “Evaluation, Prevention and Mitigation of Pounding Effects in Building Structures,” by R.E. Valles and A.M. Reinhorn, 2/20/97, (PB97-159552, A14, MF-A03).
- NCEER-97-0002 “Seismic Design Criteria for Bridges and Other Highway Structures,” by C. Rojahn, R. Mayes, D.G. Anderson, J. Clark, J.H. Hom, R.V. Nutt and M.J. O’Rourke, 4/30/97, (PB97-194658, A06, MF-A03).



- NCEER-97-0003 "Proceedings of the U.S.-Italian Workshop on Seismic Evaluation and Retrofit," Edited by D.P. Abrams and G.M. Calvi, 3/19/97, (PB97-194666, A13, MF-A03).
- NCEER-97-0004 "Investigation of Seismic Response of Buildings with Linear and Nonlinear Fluid Viscous Dampers," by A.A. Seleemah and M.C. Constantinou, 5/21/97, (PB98-109002, A15, MF-A03).
- NCEER-97-0005 "Proceedings of the Workshop on Earthquake Engineering Frontiers in Transportation Facilities," edited by G.C. Lee and I.M. Friedland, 8/29/97, (PB98-128911, A25, MR-A04).
- NCEER-97-0006 "Cumulative Seismic Damage of Reinforced Concrete Bridge Piers," by S.K. Kunnath, A. El-Bahy, A. Taylor and W. Stone, 9/2/97, (PB98-108814, A11, MF-A03).
- NCEER-97-0007 "Structural Details to Accommodate Seismic Movements of Highway Bridges and Retaining Walls," by R.A. Imbsen, R.A. Schamber, E. Thorkildsen, A. Kartoum, B.T. Martin, T.N. Rosser and J.M. Kulicki, 9/3/97, (PB98-108996, A09, MF-A02).
- NCEER-97-0008 "A Method for Earthquake Motion-Damage Relationships with Application to Reinforced Concrete Frames," by A. Singhal and A.S. Kiremidjian, 9/10/97, (PB98-108988, A13, MF-A03).
- NCEER-97-0009 "Seismic Analysis and Design of Bridge Abutments Considering Sliding and Rotation," by K. Fishman and R. Richards, Jr., 9/15/97, (PB98-108897, A06, MF-A02).
- NCEER-97-0010 "Proceedings of the FHWA/NCEER Workshop on the National Representation of Seismic Ground Motion for New and Existing Highway Facilities," edited by I.M. Friedland, M.S. Power and R.L. Mayes, 9/22/97, (PB98-128903, A21, MF-A04).
- NCEER-97-0011 "Seismic Analysis for Design or Retrofit of Gravity Bridge Abutments," by K.L. Fishman, R. Richards, Jr. and R.C. Divito, 10/2/97, (PB98-128937, A08, MF-A02).
- NCEER-97-0012 "Evaluation of Simplified Methods of Analysis for Yielding Structures," by P. Tsopelas, M.C. Constantinou, C.A. Kircher and A.S. Whittaker, 10/31/97, (PB98-128929, A10, MF-A03).
- NCEER-97-0013 "Seismic Design of Bridge Columns Based on Control and Repairability of Damage," by C-T. Cheng and J.B. Mander, 12/8/97, (PB98-144249, A11, MF-A03).
- NCEER-97-0014 "Seismic Resistance of Bridge Piers Based on Damage Avoidance Design," by J.B. Mander and C-T. Cheng, 12/10/97, (PB98-144223, A09, MF-A02).
- NCEER-97-0015 "Seismic Response of Nominally Symmetric Systems with Strength Uncertainty," by S. Balopoulou and M. Grigoriu, 12/23/97, (PB98-153422, A11, MF-A03).
- NCEER-97-0016 "Evaluation of Seismic Retrofit Methods for Reinforced Concrete Bridge Columns," by T.J. Wipf, F.W. Klaiber and F.M. Russo, 12/28/97, (PB98-144215, A12, MF-A03).
- NCEER-97-0017 "Seismic Fragility of Existing Conventional Reinforced Concrete Highway Bridges," by C.L. Mullen and A.S. Cakmak, 12/30/97, (PB98-153406, A08, MF-A02).
- NCEER-97-0018 "Loss Assessment of Memphis Buildings," edited by D.P. Abrams and M. Shinozuka, 12/31/97, (PB98-144231, A13, MF-A03).
- NCEER-97-0019 "Seismic Evaluation of Frames with Infill Walls Using Quasi-static Experiments," by K.M. Mosalam, R.N. White and P. Gergely, 12/31/97, (PB98-153455, A07, MF-A02).
- NCEER-97-0020 "Seismic Evaluation of Frames with Infill Walls Using Pseudo-dynamic Experiments," by K.M. Mosalam, R.N. White and P. Gergely, 12/31/97, (PB98-153430, A07, MF-A02).
- NCEER-97-0021 "Computational Strategies for Frames with Infill Walls: Discrete and Smeared Crack Analyses and Seismic Fragility," by K.M. Mosalam, R.N. White and P. Gergely, 12/31/97, (PB98-153414, A10, MF-A02).

- NCEER-97-0022 "Proceedings of the NCEER Workshop on Evaluation of Liquefaction Resistance of Soils," edited by T.L. Youd and I.M. Idriss, 12/31/97, (PB98-155617, A15, MF-A03).
- MCEER-98-0001 "Extraction of Nonlinear Hysteretic Properties of Seismically Isolated Bridges from Quick-Release Field Tests," by Q. Chen, B.M. Douglas, E.M. Maragakis and I.G. Buckle, 5/26/98, (PB99-118838, A06, MF-A01).
- MCEER-98-0002 "Methodologies for Evaluating the Importance of Highway Bridges," by A. Thomas, S. Eshenaur and J. Kulicki, 5/29/98, (PB99-118846, A10, MF-A02).
- MCEER-98-0003 "Capacity Design of Bridge Piers and the Analysis of Overstrength," by J.B. Mander, A. Dutta and P. Goel, 6/1/98, (PB99-118853, A09, MF-A02).
- MCEER-98-0004 "Evaluation of Bridge Damage Data from the Loma Prieta and Northridge, California Earthquakes," by N. Basoz and A. Kiremidjian, 6/2/98, (PB99-118861, A15, MF-A03).
- MCEER-98-0005 "Screening Guide for Rapid Assessment of Liquefaction Hazard at Highway Bridge Sites," by T. L. Youd, 6/16/98, (PB99-118879, A06, not available on microfiche).
- MCEER-98-0006 "Structural Steel and Steel/Concrete Interface Details for Bridges," by P. Ritchie, N. Kaulh and J. Kulicki, 7/13/98, (PB99-118945, A06, MF-A01).
- MCEER-98-0007 "Capacity Design and Fatigue Analysis of Confined Concrete Columns," by A. Dutta and J.B. Mander, 7/14/98, (PB99-118960, A14, MF-A03).
- MCEER-98-0008 "Proceedings of the Workshop on Performance Criteria for Telecommunication Services Under Earthquake Conditions," edited by A.J. Schiff, 7/15/98, (PB99-118952, A08, MF-A02).
- MCEER-98-0009 "Fatigue Analysis of Unconfined Concrete Columns," by J.B. Mander, A. Dutta and J.H. Kim, 9/12/98, (PB99-123655, A10, MF-A02).
- MCEER-98-0010 "Centrifuge Modeling of Cyclic Lateral Response of Pile-Cap Systems and Seat-Type Abutments in Dry Sands," by A.D. Gadre and R. Dobry, 10/2/98, (PB99-123606, A13, MF-A03).
- MCEER-98-0011 "IDARC-BRIDGE: A Computational Platform for Seismic Damage Assessment of Bridge Structures," by A.M. Reinhorn, V. Simeonov, G. Mylonakis and Y. Reichman, 10/2/98, (PB99-162919, A15, MF-A03).
- MCEER-98-0012 "Experimental Investigation of the Dynamic Response of Two Bridges Before and After Retrofitting with Elastomeric Bearings," by D.A. Wendichansky, S.S. Chen and J.B. Mander, 10/2/98, (PB99-162927, A15, MF-A03).
- MCEER-98-0013 "Design Procedures for Hinge Restrainers and Hinge Sear Width for Multiple-Frame Bridges," by R. Des Roches and G.L. Fenves, 11/3/98, (PB99-140477, A13, MF-A03).
- MCEER-98-0014 "Response Modification Factors for Seismically Isolated Bridges," by M.C. Constantinou and J.K. Quarshie, 11/3/98, (PB99-140485, A14, MF-A03).
- MCEER-98-0015 "Proceedings of the U.S.-Italy Workshop on Seismic Protective Systems for Bridges," edited by I.M. Friedland and M.C. Constantinou, 11/3/98, (PB2000-101711, A22, MF-A04).
- MCEER-98-0016 "Appropriate Seismic Reliability for Critical Equipment Systems: Recommendations Based on Regional Analysis of Financial and Life Loss," by K. Porter, C. Scawthorn, C. Taylor and N. Blais, 11/10/98, (PB99-157265, A08, MF-A02).
- MCEER-98-0017 "Proceedings of the U.S. Japan Joint Seminar on Civil Infrastructure Systems Research," edited by M. Shinozuka and A. Rose, 11/12/98, (PB99-156713, A16, MF-A03).
- MCEER-98-0018 "Modeling of Pile Footings and Drilled Shafts for Seismic Design," by I. PoLam, M. Kapuskar and D. Chaudhuri, 12/21/98, (PB99-157257, A09, MF-A02).

- MCEER-99-0001 "Seismic Evaluation of a Masonry Infilled Reinforced Concrete Frame by Pseudodynamic Testing," by S.G. Buonopane and R.N. White, 2/16/99, (PB99-162851, A09, MF-A02).
- MCEER-99-0002 "Response History Analysis of Structures with Seismic Isolation and Energy Dissipation Systems: Verification Examples for Program SAP2000," by J. Scheller and M.C. Constantinou, 2/22/99, (PB99-162869, A08, MF-A02).
- MCEER-99-0003 "Experimental Study on the Seismic Design and Retrofit of Bridge Columns Including Axial Load Effects," by A. Dutta, T. Kokorina and J.B. Mander, 2/22/99, (PB99-162877, A09, MF-A02).
- MCEER-99-0004 "Experimental Study of Bridge Elastomeric and Other Isolation and Energy Dissipation Systems with Emphasis on Uplift Prevention and High Velocity Near-source Seismic Excitation," by A. Kasalanati and M. C. Constantinou, 2/26/99, (PB99-162885, A12, MF-A03).
- MCEER-99-0005 "Truss Modeling of Reinforced Concrete Shear-flexure Behavior," by J.H. Kim and J.B. Mander, 3/8/99, (PB99-163693, A12, MF-A03).
- MCEER-99-0006 "Experimental Investigation and Computational Modeling of Seismic Response of a 1:4 Scale Model Steel Structure with a Load Balancing Supplemental Damping System," by G. Pekcan, J.B. Mander and S.S. Chen, 4/2/99, (PB99-162893, A11, MF-A03).
- MCEER-99-0007 "Effect of Vertical Ground Motions on the Structural Response of Highway Bridges," by M.R. Button, C.J. Cronin and R.L. Mayes, 4/10/99, (PB2000-101411, A10, MF-A03).
- MCEER-99-0008 "Seismic Reliability Assessment of Critical Facilities: A Handbook, Supporting Documentation, and Model Code Provisions," by G.S. Johnson, R.E. Sheppard, M.D. Quilici, S.J. Eder and C.R. Scawthorn, 4/12/99, (PB2000-101701, A18, MF-A04).
- MCEER-99-0009 "Impact Assessment of Selected MCEER Highway Project Research on the Seismic Design of Highway Structures," by C. Rojahn, R. Mayes, D.G. Anderson, J.H. Clark, D'Appolonia Engineering, S. Gloyd and R.V. Nutt, 4/14/99, (PB99-162901, A10, MF-A02).
- MCEER-99-0010 "Site Factors and Site Categories in Seismic Codes," by R. Dobry, R. Ramos and M.S. Power, 7/19/99, (PB2000-101705, A08, MF-A02).
- MCEER-99-0011 "Restrainer Design Procedures for Multi-Span Simply-Supported Bridges," by M.J. Randall, M. Saiidi, E. Maragakis and T. Isakovic, 7/20/99, (PB2000-101702, A10, MF-A02).
- MCEER-99-0012 "Property Modification Factors for Seismic Isolation Bearings," by M.C. Constantinou, P. Tsopelas, A. Kasalanati and E. Wolff, 7/20/99, (PB2000-103387, A11, MF-A03).
- MCEER-99-0013 "Critical Seismic Issues for Existing Steel Bridges," by P. Ritchie, N. Kauh and J. Kulicki, 7/20/99, (PB2000-101697, A09, MF-A02).
- MCEER-99-0014 "Nonstructural Damage Database," by A. Kao, T.T. Soong and A. Vender, 7/24/99, (PB2000-101407, A06, MF-A01).
- MCEER-99-0015 "Guide to Remedial Measures for Liquefaction Mitigation at Existing Highway Bridge Sites," by H.G. Cooke and J. K. Mitchell, 7/26/99, (PB2000-101703, A11, MF-A03).
- MCEER-99-0016 "Proceedings of the MCEER Workshop on Ground Motion Methodologies for the Eastern United States," edited by N. Abrahamson and A. Becker, 8/11/99, (PB2000-103385, A07, MF-A02).
- MCEER-99-0017 "Quindío, Colombia Earthquake of January 25, 1999: Reconnaissance Report," by A.P. Asfura and P.J. Flores, 10/4/99, (PB2000-106893, A06, MF-A01).
- MCEER-99-0018 "Hysteretic Models for Cyclic Behavior of Deteriorating Inelastic Structures," by M.V. Sivaselvan and A.M. Reinhorn, 11/5/99, (PB2000-103386, A08, MF-A02).

- MCEER-99-0019 "Proceedings of the 7<sup>th</sup> U.S.- Japan Workshop on Earthquake Resistant Design of Lifeline Facilities and Countermeasures Against Soil Liquefaction," edited by T.D. O'Rourke, J.P. Bardet and M. Hamada, 11/19/99, (PB2000-103354, A99, MF-A06).
- MCEER-99-0020 "Development of Measurement Capability for Micro-Vibration Evaluations with Application to Chip Fabrication Facilities," by G.C. Lee, Z. Liang, J.W. Song, J.D. Shen and W.C. Liu, 12/1/99, (PB2000-105993, A08, MF-A02).
- MCEER-99-0021 "Design and Retrofit Methodology for Building Structures with Supplemental Energy Dissipating Systems," by G. Pekcan, J.B. Mander and S.S. Chen, 12/31/99, (PB2000-105994, A11, MF-A03).
- MCEER-00-0001 "The Marmara, Turkey Earthquake of August 17, 1999: Reconnaissance Report," edited by C. Scawthorn; with major contributions by M. Bruneau, R. Eguchi, T. Holzer, G. Johnson, J. Mander, J. Mitchell, W. Mitchell, A. Papageorgiou, C. Scaethorn, and G. Webb, 3/23/00, (PB2000-106200, A11, MF-A03).
- MCEER-00-0002 "Proceedings of the MCEER Workshop for Seismic Hazard Mitigation of Health Care Facilities," edited by G.C. Lee, M. Ettouney, M. Grigoriu, J. Hauer and J. Nigg, 3/29/00, (PB2000-106892, A08, MF-A02).
- MCEER-00-0003 "The Chi-Chi, Taiwan Earthquake of September 21, 1999: Reconnaissance Report," edited by G.C. Lee and C.H. Loh, with major contributions by G.C. Lee, M. Bruneau, I.G. Buckle, S.E. Chang, P.J. Flores, T.D. O'Rourke, M. Shinozuka, T.T. Soong, C-H. Loh, K-C. Chang, Z-J. Chen, J-S. Hwang, M-L. Lin, G-Y. Liu, K-C. Tsai, G.C. Yao and C-L. Yen, 4/30/00, (PB2001-100980, A10, MF-A02).
- MCEER-00-0004 "Seismic Retrofit of End-Sway Frames of Steel Deck-Truss Bridges with a Supplemental Tendon System: Experimental and Analytical Investigation," by G. Pekcan, J.B. Mander and S.S. Chen, 7/1/00, (PB2001-100982, A10, MF-A02).
- MCEER-00-0005 "Sliding Fragility of Unrestrained Equipment in Critical Facilities," by W.H. Chong and T.T. Soong, 7/5/00, (PB2001-100983, A08, MF-A02).
- MCEER-00-0006 "Seismic Response of Reinforced Concrete Bridge Pier Walls in the Weak Direction," by N. Abo-Shadi, M. Saiidi and D. Sanders, 7/17/00, (PB2001-100981, A17, MF-A03).
- MCEER-00-0007 "Low-Cycle Fatigue Behavior of Longitudinal Reinforcement in Reinforced Concrete Bridge Columns," by J. Brown and S.K. Kunnath, 7/23/00, (PB2001-104392, A08, MF-A02).
- MCEER-00-0008 "Soil Structure Interaction of Bridges for Seismic Analysis," I. PoLam and H. Law, 9/25/00, (PB2001-105397, A08, MF-A02).
- MCEER-00-0009 "Proceedings of the First MCEER Workshop on Mitigation of Earthquake Disaster by Advanced Technologies (MEDAT-1), edited by M. Shinozuka, D.J. Inman and T.D. O'Rourke, 11/10/00, (PB2001-105399, A14, MF-A03).
- MCEER-00-0010 "Development and Evaluation of Simplified Procedures for Analysis and Design of Buildings with Passive Energy Dissipation Systems," by O.M. Ramirez, M.C. Constantinou, C.A. Kircher, A.S. Whittaker, M.W. Johnson, J.D. Gomez and C. Chrysostomou, 11/16/01, (PB2001-105523, A23, MF-A04).
- MCEER-00-0011 "Dynamic Soil-Foundation-Structure Interaction Analyses of Large Caissons," by C-Y. Chang, C-M. Mok, Z-L. Wang, R. Settgast, F. Waggoner, M.A. Ketchum, H.M. Gonnermann and C-C. Chin, 12/30/00, (PB2001-104373, A07, MF-A02).
- MCEER-00-0012 "Experimental Evaluation of Seismic Performance of Bridge Restrainers," by A.G. Vlassis, E.M. Maragakis and M. Saiid Saiidi, 12/30/00, (PB2001-104354, A09, MF-A02).
- MCEER-00-0013 "Effect of Spatial Variation of Ground Motion on Highway Structures," by M. Shinozuka, V. Saxena and G. Deodatis, 12/31/00, (PB2001-108755, A13, MF-A03).
- MCEER-00-0014 "A Risk-Based Methodology for Assessing the Seismic Performance of Highway Systems," by S.D. Werner, C.E. Taylor, J.E. Moore, II, J.S. Walton and S. Cho, 12/31/00, (PB2001-108756, A14, MF-A03).

- MCEER-01-0001 "Experimental Investigation of P-Delta Effects to Collapse During Earthquakes," by D. Vian and M. Bruneau, 6/25/01, (PB2002-100534, A17, MF-A03).
- MCEER-01-0002 "Proceedings of the Second MCEER Workshop on Mitigation of Earthquake Disaster by Advanced Technologies (MEDAT-2)," edited by M. Bruneau and D.J. Inman, 7/23/01, (PB2002-100434, A16, MF-A03).
- MCEER-01-0003 "Sensitivity Analysis of Dynamic Systems Subjected to Seismic Loads," by C. Roth and M. Grigoriu, 9/18/01, (PB2003-100884, A12, MF-A03).
- MCEER-01-0004 "Overcoming Obstacles to Implementing Earthquake Hazard Mitigation Policies: Stage 1 Report," by D.J. Alesch and W.J. Petak, 12/17/01, (PB2002-107949, A07, MF-A02).
- MCEER-01-0005 "Updating Real-Time Earthquake Loss Estimates: Methods, Problems and Insights," by C.E. Taylor, S.E. Chang and R.T. Eguchi, 12/17/01, (PB2002-107948, A05, MF-A01).
- MCEER-01-0006 "Experimental Investigation and Retrofit of Steel Pile Foundations and Pile Bents Under Cyclic Lateral Loadings," by A. Shama, J. Mander, B. Blabac and S. Chen, 12/31/01, (PB2002-107950, A13, MF-A03).
- MCEER-02-0001 "Assessment of Performance of Bolu Viaduct in the 1999 Duzce Earthquake in Turkey" by P.C. Roussis, M.C. Constantinou, M. Erdik, E. Durukal and M. Dicleli, 5/8/02, (PB2003-100883, A08, MF-A02).
- MCEER-02-0002 "Seismic Behavior of Rail Counterweight Systems of Elevators in Buildings," by M.P. Singh, Rildova and L.E. Suarez, 5/27/02. (PB2003-100882, A11, MF-A03).
- MCEER-02-0003 "Development of Analysis and Design Procedures for Spread Footings," by G. Mylonakis, G. Gazetas, S. Nikolaou and A. Chauncey, 10/02/02, (PB2004-101636, A13, MF-A03, CD-A13).
- MCEER-02-0004 "Bare-Earth Algorithms for Use with SAR and LIDAR Digital Elevation Models," by C.K. Huyck, R.T. Eguchi and B. Houshmand, 10/16/02, (PB2004-101637, A07, CD-A07).
- MCEER-02-0005 "Review of Energy Dissipation of Compression Members in Concentrically Braced Frames," by K.Lee and M. Bruneau, 10/18/02, (PB2004-101638, A10, CD-A10).
- MCEER-03-0001 "Experimental Investigation of Light-Gauge Steel Plate Shear Walls for the Seismic Retrofit of Buildings" by J. Berman and M. Bruneau, 5/2/03, (PB2004-101622, A10, MF-A03, CD-A10).
- MCEER-03-0002 "Statistical Analysis of Fragility Curves," by M. Shinozuka, M.Q. Feng, H. Kim, T. Uzawa and T. Ueda, 6/16/03, (PB2004-101849, A09, CD-A09).
- MCEER-03-0003 "Proceedings of the Eighth U.S.-Japan Workshop on Earthquake Resistant Design of Lifeline Facilities and Countermeasures Against Liquefaction," edited by M. Hamada, J.P. Bardet and T.D. O'Rourke, 6/30/03, (PB2004-104386, A99, CD-A99).
- MCEER-03-0004 "Proceedings of the PRC-US Workshop on Seismic Analysis and Design of Special Bridges," edited by L.C. Fan and G.C. Lee, 7/15/03, (PB2004-104387, A14, CD-A14).
- MCEER-03-0005 "Urban Disaster Recovery: A Framework and Simulation Model," by S.B. Miles and S.E. Chang, 7/25/03, (PB2004-104388, A07, CD-A07).
- MCEER-03-0006 "Behavior of Underground Piping Joints Due to Static and Dynamic Loading," by R.D. Meis, M. Maragakis and R. Siddharthan, 11/17/03, (PB2005-102194, A13, MF-A03, CD-A00).
- MCEER-03-0007 "Seismic Vulnerability of Timber Bridges and Timber Substructures," by A.A. Shama, J.B. Mander, I.M. Friedland and D.R. Allicock, 12/15/03.
- MCEER-04-0001 "Experimental Study of Seismic Isolation Systems with Emphasis on Secondary System Response and Verification of Accuracy of Dynamic Response History Analysis Methods," by E. Wolff and M. Constantinou, 1/16/04 (PB2005-102195, A99, MF-E08, CD-A00).

- MCEER-04-0002 "Tension, Compression and Cyclic Testing of Engineered Cementitious Composite Materials," by K. Kesner and S.L. Billington, 3/1/04, (PB2005-102196, A08, CD-A08).
- MCEER-04-0003 "Cyclic Testing of Braces Laterally Restrained by Steel Studs to Enhance Performance During Earthquakes," by O.C. Celik, J.W. Berman and M. Bruneau, 3/16/04, (PB2005-102197, A13, MF-A03, CD-A00).
- MCEER-04-0004 "Methodologies for Post Earthquake Building Damage Detection Using SAR and Optical Remote Sensing: Application to the August 17, 1999 Marmara, Turkey Earthquake," by C.K. Huyck, B.J. Adams, S. Cho, R.T. Eguchi, B. Mansouri and B. Houshmand, 6/15/04, (PB2005-104888, A10, CD-A00).
- MCEER-04-0005 "Nonlinear Structural Analysis Towards Collapse Simulation: A Dynamical Systems Approach," by M.V. Sivaselvan and A.M. Reinhorn, 6/16/04, (PB2005-104889, A11, MF-A03, CD-A00).
- MCEER-04-0006 "Proceedings of the Second PRC-US Workshop on Seismic Analysis and Design of Special Bridges," edited by G.C. Lee and L.C. Fan, 6/25/04, (PB2005-104890, A16, CD-A00).
- MCEER-04-0007 "Seismic Vulnerability Evaluation of Axially Loaded Steel Built-up Laced Members," by K. Lee and M. Bruneau, 6/30/04, (PB2005-104891, A16, CD-A00).
- MCEER-04-0008 "Evaluation of Accuracy of Simplified Methods of Analysis and Design of Buildings with Damping Systems for Near-Fault and for Soft-Soil Seismic Motions," by E.A. Pavlou and M.C. Constantinou, 8/16/04, (PB2005-104892, A08, MF-A02, CD-A00).
- MCEER-04-0009 "Assessment of Geotechnical Issues in Acute Care Facilities in California," by M. Lew, T.D. O'Rourke, R. Dobry and M. Koch, 9/15/04, (PB2005-104893, A08, CD-A00).
- MCEER-04-0010 "Scissor-Jack-Damper Energy Dissipation System," by A.N. Sigaher-Boyle and M.C. Constantinou, 12/1/04 (PB2005-108221).
- MCEER-04-0011 "Seismic Retrofit of Bridge Steel Truss Piers Using a Controlled Rocking Approach," by M. Pollino and M. Bruneau, 12/20/04.
- MCEER-05-0001 "Experimental and Analytical Studies of Structures Seismically Isolated with an Uplift-Restraint Isolation System," by P.C. Roussis and M.C. Constantinou, 1/10/05 (PB2005-108222).
- MCEER-05-0002 "A Versatile Experimentation Model for Study of Structures Near Collapse Applied to Seismic Evaluation of Irregular Structures," by D. Kusumastuti, A.M. Reinhorn and A. Rutenberg, 3/31/05 (PB2006-101523).
- MCEER-05-0003 "Proceedings of the Third PRC-US Workshop on Seismic Analysis and Design of Special Bridges," edited by L.C. Fan and G.C. Lee, 4/20/05.
- MCEER-05-0004 "Approaches for the Seismic Retrofit of Braced Steel Bridge Piers and Proof-of-Concept Testing of an Eccentrically Braced Frame with Tubular Link," by J.W. Berman and M. Bruneau, 4/21/05 (PB2006-101524).
- MCEER-05-0005 "Simulation of Strong Ground Motions for Seismic Fragility Evaluation of Nonstructural Components in Hospitals," by A. Wanitkorkul and A. Filiatrault, 5/26/05.
- MCEER-05-0006 "Seismic Safety in California Hospitals: Assessing an Attempt to Accelerate the Replacement or Seismic Retrofit of Older Hospital Facilities," by D.J. Alesch, L.A. Arendt and W.J. Petak, 6/6/05.
- MCEER-05-0007 "Development of Seismic Strengthening and Retrofit Strategies for Critical Facilities Using Engineered Cementitious Composite Materials," by K. Kesner and S.L. Billington, 8/29/05.
- MCEER-05-0008 "Experimental and Analytical Studies of Base Isolation Systems for Seismic Protection of Power Transformers," by N. Murota, M.Q. Feng and G-Y. Liu, 9/30/05.
- MCEER-05-0009 "3D-BASIS-ME-MB: Computer Program for Nonlinear Dynamic Analysis of Seismically Isolated Structures," by P.C. Tsopelas, P.C. Roussis, M.C. Constantinou, R. Buchanan and A.M. Reinhorn, 10/3/05.

- MCEER-05-0010 “Steel Plate Shear Walls for Seismic Design and Retrofit of Building Structures,” by D. Vian and M. Bruneau, 12/15/05.
- MCEER-05-0011 “The Performance-Based Design Paradigm,” by M.J. Astrella and A. Whittaker, 12/15/05.
- MCEER-06-0001 “Seismic Fragility of Suspended Ceiling Systems,” H. Badillo-Almaraz, A.S. Whittaker, A.M. Reinhorn and G.P. Cimellaro, 2/4/06.

# MCEER

University at Buffalo, State University of New York  
Red Jacket Quadrangle ■ Buffalo, New York 14261  
Phone: (716) 645-3391 ■ Fax: (716) 645-3399  
E-mail: [mceer@mceermail.buffalo.edu](mailto:mceer@mceermail.buffalo.edu) ■ WWW Site <http://mceer.buffalo.edu>



University at Buffalo *The State University of New York*

ISSN 1520-295X